Title
Hydrodynamics and Water Quality in Rodeo Lagoon, a Hypereutrophic Coastal Lagoon

Author
Cousins, Mary Alice Melugin

Publication Date
2010

Peer reviewed|Thesis/dissertation

Hydrodynamics and Water Quality in Rodeo Lagoon, a Hypereutrophic Coastal Lagoon

by

Mary Alice Melugin Cousins

A dissertation submitted in partial satisfaction of the

requirements for the degree of

Doctor of Philosophy

in

Engineering – Civil and Environmental Engineering

in the

Graduate Division

of the

University of California, Berkeley

Committee in charge:

Professor Mark T. Stacey, Chair
Professor Kara L. Nelson
Professor Thomas M. Powell

Fall 2010

Abstract

Hydrodynamics and Water Quality in Rodeo Lagoon, a Hypereutrophic Coastal Lagoon

by

Mary Alice Melugin Cousins

Doctor of Philosophy in Engineering – Civil and Environmental Engineering

University of California, Berkeley

Professor Mark T. Stacey, Chair

Seasonal variations in vertical density structure, inorganic nutrient concentrations, dissolved oxygen concentrations, and phytoplankton biomass were investigated in a shallow, tidally choked coastal lagoon subject to impaired water quality. Vertical turbulent mixing rates, which govern the distribution of scalars relevant to water quality, were quantified on both seasonal and diurnal time scales. The project site, Rodeo Lagoon, is located in the Golden Gate National Recreation Area, California, and has experienced fish kills and intense algae blooms in recent years.

Monthly measurements collected along a transect of the lagoon from March 2006 to April 2008 show it was strongly stratified by brackish water in winter, when freshwater inputs from the watershed and saltwater inputs from storm surge were both at their largest. The squared buoyancy frequency exceeded 0.5 s^{-2} under these conditions, and the lower layer was typically warmer, depleted in oxygen and enriched in ammonium. In summer, weaker diurnal temperature stratification was the result of strong light absorption in this hypereutrophic lagoon. In fall 2007, hypoxia and potentially toxic levels of ammonium were observed coincident with the seasonal decline in algal biomass.

Wind is the dominant driver of turbulent mixing in Rodeo Lagoon. Although water depths of less than 2.5 m lead to the expectation of rapid vertical mixing, limited fetch and strong density gradients reduce the coupling of wind stress and bottom stress. The vertical turbulent diffusivity is reduced by as much as three orders of magnitude across the pycnocline, and the water column in and below the pycnocline shows active turbulence only intermittently. The annual cycle of salt-based stratification and accompanying reduction in turbulent exchange of nutrients between the sediments and overlying water column inhibit the flushing of nutrients out of the lagoon and contribute to excessive phytoplankton biomass.

for Mom,
for Dave, and
for Elliott

Chapter 1 Introduction ..... - 1 -
1.1 Background ..... - 1 -
1.1.1 Formation of coastal lagoons ..... - 1 -
1.1.2 Productivity and water quality of coastal lagoons ..... - 2 -
1.1.2.1 Nutrient cycling ..... - 3 -
1.1.2.2 Oxygen dynamics ..... - 4 -
1.1.2.3 Cyanobacterial dominance ..... - 5 -
1.1.3 Hydrodynamics of coastal lagoons ..... - 6 -
1.1.3.1 Circulation ..... - 7 -
1.1.3.2 Density stratification ..... - 7 -
1.1.3.3 Turbulent diffusivity, dissipation, and length scales ..... - 8 -
1.1.3.4 Field estimates of turbulent scalar fluxes ..... - 9 -
1.2 Description of field site ..... - 10 -
1.2.1 Physical setting ..... - 10 -
1.2.2 History ..... - 11 -
1.2.3 Bathymetry ..... - 12 -
1.2.4 Biota ..... - 12 -
1.2.5 Water quality ..... - 12 -
1.3 Research questions ..... - 13 -

Chapter 2 Experimental Design ..... - 15 -
2.1 Seasonal monitoring ..... - 16 -
2.1.1 Longitudinal transects ..... - 16 -
2.1.2 Grab samples ..... - 17 -
2.1.3 Meteorology ..... - 18 -
2.1.3.1 Wind stress ..... - 18 -
2.1.3.2 Heat budgets ..... - 20 -
2.1.4 Bathymetry and depth ..... - 22 -
2.2 Hydrodynamics instrumentation ..... - 23 -
2.2.1 Acoustic Doppler Velocimeters ..... - 24 -
2.2.2 Acoustic Doppler Current Profiler ..... - 27 -
2.2.3 Temperature microstructure ..... - 29 -
2.2.4 Moored CTDs ..... - 30 -
2.2.4.1 Density structure ..... - 31 -
2.2.4.2 Potential energy and potential energy anomaly ..... - 32 -
2.3 Summary ..... - 34 -

Chapter 3 Water Quality ..... - 35 -
3.1 Salinity ..... - 35 -
3.2 Temperature ..... - 39 -
3.3 Phytoplankton biomass ..... - 43 -
3.3.1 Seasonal variability ..... - 44 -
3.3.2 Vertical variability ..... - 46 -
3.4 Turbidity ..... - 50 -
3.5 Light extinction ..... - 52 -

3.6 Dissolved oxygen ..... - 54 -
3.6.1 Diurnal variability ..... - 55 -
3.6.2 Seasonal variability ..... - 56 -
3.6.3 Vertical variability ..... - 57 -
3.7 pH ..... - 59 -
3.8 Nutrients ..... - 60 -
3.8.1 Inflows from watershed ..... - 61 -
3.8.2 Nutrients in bottom sediments ..... - 61 -
3.8.3 Lagoon nutrients ..... - 62 -
3.8.3.1 Seasonal variability ..... - 62 -
3.8.3.2 Vertical variability ..... - 64 -
3.9 Summary of water quality observations ..... - 66 -

Chapter 4 Hydrodynamics ..... - 67 -
4.1 Evolution of density structure ..... - 67 -
4.1.1 July 2007: Diurnal temperature stratification ..... - 67 -
4.1.2 January 2008 experiment: Strong salt stratification and internal seiching ..... - 69 -
4.1.3 April 2008 experiment: Mixing and potential energy ..... - 74 -
4.1.4 Summary – density structure ..... - 77 -
4.2 Currents, stresses and shear ..... - 77 -
4.2.1 ADV results: Currents and stresses at the bed ..... - 77 -
4.2.2 ADCP results: Current profiles and shear ..... - 83 -
4.3 Wind waves ..... - 87 -
4.4 Turbulence ..... - 91 -
4.4.1 Analytical methods ..... - 91 -
4.4.1.1 Simple physical scaling ..... - 91 -
4.4.1.2 Turbulent kinetic energy budget ..... - 92 -
4.4.1.3 Temperature microstructure ..... - 94 -
4.4.2 Vertical turbulent diffusivity ..... - 96 -
4.4.2.1 Estimates of diffusivity by various methods ..... - 96 -
4.4.2.2 Evolution of salt field – model vs. observations ..... - 101 -
4.4.3 Turbulent mixing efficiency ..... - 102 -
4.5 Diapycnal mixing ..... - 104 -
4.5.1 Wind mixing efficiency ..... - 104 -
4.5.2 Convective mixing ..... - 106 -
4.6 Summary of hydrodynamics observations ..... - 108 -

Chapter 5 Linkages between hydrodynamics and water quality ..... - 109 -
5.1 Immediate effects of density stratification ..... - 109 -
5.1.1 Nutrient enrichment and phytoplankton ..... - 109 -
5.1.2 Hypoxia ..... - 109 -
5.1.3 Light climate ..... - 110 -
5.1.4 Summary of immediate ecological impacts ..... - 110 -
5.2 Long-term effects of density stratification ..... - 110 -
5.2.1 Residence times ..... - 111 -
5.2.2 Nutrient retention and release ..... - 114 -
5.3 Management implications ..... - 115 -

References ..... **- 117 -**

Appendix A Water Quality Database ..... **- 132 -**

Acknowledgements

My research advisor Mark Stacey, my husband David Briggs, and my colleague Lissa MacVean were all crucial to the success of this project. Each of them provided their own brand of technical and emotional support at every step on my journey, and to each I extent my deepest thanks.

Operating the 11-foot aluminum rowboat in Rodeo Lagoon would have been impossible alone. Fortunately, I had capable assistance from the following field hands: David Briggs, Nate Butler, Stella Cousins, Megan Daniels, Maureen Downing-Kunz, Jeana Drake, Patrick Granvold, Alejandro Guido Zarate, Christy Keenan, Rebecca Leonardson, Sonya Lopez, Lissa MacVean, Mario Magliocco, Maggie McKeon, David Pene, Kristin Robrock, Rudi Schuech, Sarah Silkie, Courtney Siu, Mark Stacey, Joelle Tirindelli, Tristan Toilliez, Wayne Wagner, and Robby Zeller. The participation of Jeana Drake, formerly of the Ed Carpenter lab at Romberg Tiburon Center, was especially helpful and never dull. The assistance of Sarah Silkie in early phases of the project was also notable, beginning with our maiden voyage into the "pea soup" of Rodeo Lagoon in October 2005. Darren Fong of the National Park Service provided inspiration for the research topic, as well as much-appreciated logistical and technical support.

Thanks to Elliott Briggs for providing me with a useful deadline to wrap up field work, and encouraging me to write as quickly as possible. I thank my parents and siblings for expecting much of me, and providing the support to match. Also, I thank the rest of the environmental fluid mechanics research group for providing a rich and peer-supporting academic experience, particularly Katie Lundquist and Megan Daniels. Finally, I thank faculty members Kara Nelson, Thomas Powell, Tina Chow, Jim Hunt, and John Dracup for serving as advisors and exam committee members, reading this dissertation, and encouraging my work.

Funding for this research was provided by the National Science Foundation Graduate Research Fellowship Program, the University of California Chancellor's Opportunity fellowship, the University of California Dissertation-Year fellowship, the University of California Toxic Substances Research and Teaching Program, and the National Park Service.

Chapter 1

Introduction

Rodeo Lagoon, the subject of this dissertation, is a hypereutrophic coastal lagoon located adjacent to the Pacific Ocean in southeastern Marin County, California. It has severe water quality problems that are a typical of eutrophic water bodies, including recurring periods of hypoxia and blooms of toxic cyanobacteria. The underlying causes of eutrophication in Rodeo Lagoon are poorly understood, and this study helps fill a knowledge gap by exploring the connection between lagoon hydrodynamics and water quality. Previous work by others in coastal lagoons with comparable hydrodynamic forcing and water quality problems, as discussed in this section, provides necessary context for discussing these results.

1.1 Background

1.1.1 Formation of coastal lagoons

Coastal lagoons are areas of relatively shallow water that have been sealed off from the ocean by depositional barriers that cover more than 80% of the marine entrance's width (Bird 1994). By definition they have restricted connections to the ocean and long water residence times, so they are typically poorly flushed (Kjerfve and Magill 1989). On a geologic time scale, coastal lagoons are ephemeral features of the landscape; locally, most owe their origin to sea level rise at the end of the last glacial period, between 6,000 and 18,000 years ago (Kjerfve and Magill 1989). Rodeo Lagoon (Fig. 1-1), which fills a valley drowned by sea level rise, is a good example of a coastal lagoon formed by this mechanism (Elder 2001). The lagoon is impounded by a beach berm formed at the coastline, although in Rodeo Lagoon's case the beach berm itself may predate the lagoon and probably formed as a sand dune 8,000–10,000 years ago, before sea level rise (Wakeley 1970). Wave action combined with a local sediment supply, rather than littoral drift, has subsequently maintained the beach berm (Wakeley 1970). In general, high wave energy and a plentiful sand supply are necessary for the formation of "choked" coastal lagoons like Rodeo Lagoon (Kjerfve and Magill 1989).

In Australia, the classification "Intermittently Closed and Open Lake and Lagoon" (ICOLL) is often used to describe this type of wave-dominated estuary with limited tidal connection and seasonally episodic flow regime (Roy et al. 2001; Davis and Koop 2006). The episodic flow regime is a characteristic feature of Mediterranean-climate estuaries, whose watersheds receive nearly all of their annual precipitation in a few wet winter months. Rodeo Lagoon, located in a small catchment with a Mediterranean climate similar to the Australian example, can be classified as an ICOLL. Like the ICOLLs, Rodeo Lagoon is closed off from the ocean by its

beach berm for several months each year, during which time interaction with the ocean is negligible and tidal flushing virtually eliminated. For such systems, including Rodeo Lagoon, the length of time each year that the lagoon outlet remains connected to the ocean is determined by local hydrology; during wet winters, the outlet remains open longer (Hill 1970; Elwany et al. 1998). The outlet at Rodeo Lagoon is formed during and following storms by a combination of wave action from the seaward side and scouring by water impounded behind the beach berm (Hill 1970).

1.1.2 Productivity and water quality of coastal lagoons

Coastal lagoons, like estuaries, are generally highly productive even in their pristine state (McComb 1995). High primary productivity is the result of two major factors: shallow water depths, and large nutrient and organic matter inputs (Razinkovas et al. 2008). The shallowness of coastal lagoons means that most of the water column is in the photic zone, and that there is an increased interaction between the sediment and water column (McComb 1995). However, even though they are naturally productive, coastal lagoons are also vulnerable to further eutrophication and harmful algal blooms caused by anthropogenic factors. In fact, coastal lagoons suffer disproportionately from these problems compared to other types of estuaries, with

Fig. 1-1. Rodeo Beach and Rodeo Lagoon in its typical summer configuration with the outlet closed by the beach berm. Photo taken 09 June 2008 from the bluffs northwest of the lagoon. Also pictured is the pedestrian bridge over the outlet channel, which was the site of some sampling activites discussed in the text.

longer residence times and reduced tidal exchange typically bearing the blame for this degradation (Bricker et al. 2008; Wilson 2008). ICOLLs, in particular, are known to be sensitive to human intervention, with their vulnerability increasing inversely with tidal flushing (Haines et al. 2006; Haines 2008).

1.1.2.1 Nutrient cycling

Nitrogen (N) and Phosphorus (P) are the two most important limiting nutrients for phytoplankton growth; an excess of these nutrients is the cause of eutrophication. These nutrients are needed by phytoplankton at approximately the stoichiometric ratio 16N:1P, or "Redfield ratio;" N or P becomes limiting when the actual ratio varies significantly from this value. It is typical for the ocean to be N-limited, while terrestrial waters are P-limited, although there are numerous exceptions and instances of co-limitation (Harris 1999). Since coastal lagoons represent a transition from terrestrial to coastal conditions, both N and P must be considered as potential limiters.

Phosphorus concentrations in coastal lagoons, as in lakes and estuaries, reflect a mass balance of nutrient inflows, outflows, storage in sediments and biomass, and internal loading from the sediments to the water column (Kalff 2002). Nitrogen has these same mass balance components as well as air-water interactions involving N_2 and ammonia. Direct atmospheric deposition of N is unlikely to be significant in this small water body. For both N and P, inflows and outflows are strongly dependent on watershed inputs and connectivity with the ocean, both of which depend on local hydrology. Meanwhile, storage and internal loading depend on physical processes linking the bed and water column, such as sedimentation, resuspension, and turbulent mixing.

The primary pathway for the permanent storage of N and P is sedimentation, which can be a purely physical process or mediated by benthic organisms (Thornton et al. 1995). Nutrient storage is highly dependent on water residence time, but with different effects for N, which is typically bound up in organic matter, than for P, which is more often in an inorganic form. For N, the relative importance of denitrification in lakes rises with increasing water residence time and decreasing water depth (Kalff 2002). Since the same is true of estuaries (Nixon et al. 1996), lagoons should retain less N as residence times increase. The reverse is true for P: longer residence times generally lead to greater phosphorus retention, at least for lakes with oxygenated hypolimnia, due to the increased time available for sedimentation (Kalff 2002). Confined lagoons tend to accumulate phosphorus in their sediments; unlike nitrogen, which can be permanently removed through denitrification, there is no equivalent removal process for phosphorus (Howard-Williams 1985; Frascari et al. 2002; Badosa et al. 2006).

In coastal lagoons, dissolved inorganic nitrogen tends to be dependent on both inflows and internal recycling, while phosphorus is more dependent on internal recycling process (Badosa et al. 2006). Since lagoons are shallow, there is no deep hypolimnetic sink for accumulated organic matter and sorbed phosphorus. Instead, these materials remain accessible to fuel further productivity through processes known collectivity as internal loading. While microbial activity strongly controls this flux for N, for P internal loading is primarily a physical and chemical process that may be partially mediated by microbial processes. Typically, less than 1% of the total P in the sediments is dissolved; instead, it is sorbed to Fe, Mn, clays, and carbonates, or bound up in organic matter (Boström et al. 1988). Processes that generate release of P in shallow lakes include sediment resuspension, redox conditions that favor Fe reduction, high pH from

primary productivity, and microbial processes (Søndergaard et al. 2003). Redox chemistry is arguably the most important of these. P does not directly participate in redox reactions, but rapid releases of P are observed during reduction of FeOOH (Rozan et al. 2002). In coastal areas, the presence of sulfates in combination with reducing conditions leads to formation of insoluble FeS and FeS_2, eliminating sorption sites for orthophosphate (PO_4^{3-}) and favoring its release compared to a freshwater system. Even within a single estuary, Hartzell et al. (2010) found concentrations of dissolved orthophosphate from sediment cores rising along the estuarine salinity gradient. Temperature is also an important variable in mediating microbial processes; at higher temperatures, increased biological activity leads to a decrease in redox potential, allowing for releases of inorganic P (Gomez et al. 1998). The redox state of the sediments and water column are both important; benthic fluxes of P are greater when the sediments are overlain by waters low in dissolved oxygen (Ingall and Jahnke 1994).

Because of the high availability of phosphorus as outlined above, nitrogen may be limiting in many cases. This is typical of Australian coastal lagoons (Webster and Harris 2004). Nitrate loading comes from the watershed, which in Mediterranean-climate lagoons is confined to the winter wet season, but total nitrogen can be higher in the dry season due to internal loading and accumulation in organic matter over the summer (Badosa et al. 2006). Internal loading of dissolved nitrogen from the sediments into the water column is caused by the microbial degradation of organic N to ammonia.

The potential loss mechanisms for N are outflows, ammonia volatilization, and conversion to N_2 gas via denitrification and anaerobic ammonium oxidation (anammox). In eutrophic marine systems, denitrification can be limited by various factors. Anoxia can cause the nitrification-denitrification cycle to shut down by limiting the first step, which requires oxygen; this means that increasing loads of N and the resultant eutrophication represent an alternative stable state in which losses of N are reduced (Sloth et al. 1995; Webster and Harris 2004). Denitrification can also be inhibited in reduced coastal sediments by the presences of sulfides, perhaps by encouraging the conversion of nitrate to ammonia via the pathway of dissimilatory nitrate reduction to ammonia (DNRA) (Joye and Hollibaugh 1995; An and Gardner 2002). The sulfide-oxidizing bacteria *Beggiatoa*, which is usually found in coastal or marine environments, can also temporarily store nitrate and participate in DNRA (Graco et al. 2001), potentially reducing losses by other mechanisms. In Rodeo Lagoon, a benthic microbial biofilm that detached in November 2006 and formed small (1–5 cm) buoyant globules appeared to be *Beggiatoa* or a similar species, based on its white filamentous appearance. The buoyancy of the globules may have derived from gas vacuoles within the *Beggiatoa* or another species of benthic microbe (D. Nelson pers. comm.).

1.1.2.2 Oxygen dynamics

Oxygen consumption in lakes takes place throughout the water column but is intensified at the sediment-water interface, where bacterial decomposition of accumulated organic matter is greatest (Wetzel 1983). Physical processes, like density stratification and turbulent mixing rates, will then determine when and where this oxygen consumption actually results in an oxygen deficit. Oxygen consumption due to sediment-water interactions can lead to hypoxia at either high or low mixing rates, as described below. Hypoxia is a condition in which dissolved oxygen levels are too low to sustain most animal life, or less than about 2 mg L^{-1} (USGS 2010).

When water circulation stagnates, the atmospheric flux of O_2 is reduced. Mediterranean coastal lagoons are known to suffer from "anoxic crises" during low-wind, warm-weather events (Harzallah and Chapelle 2002). One possible explanation is that anoxia in the sediments of coastal lagoons leads to sulfate reduction of accumulated organic matter; hydrogen sulfide can then diffuse upward and cause hypoxia (Cioffi et al. 1995). Even when energy is available to distribute oxygen through the surface mixed layer, density stratification may cause oxygen depletion in the hypolimnion. This is a well-known phenomenon in deep stratified lakes, where stratification is usually due to seasonal temperature cycling (Wetzel 1983); analogous processes cause oxygen depletion in the salt wedge of stratified estuaries (e.g., Ishikawa et al. 2004). In coastal lagoons, stratification can be due to either temperature or salt, but either way the loss of connection between the lower water column and atmosphere, combined with high sediment oxygen demand, predictably leads to hypoxia (Spooner 2005; Gale et al. 2006). Compared to tidal lagoons, this hypoxia can persist for much longer in ICOLLs and other types of choked lagoons, triggering release of ammonium and orthophosphate from the sediments and directly contributing to algae blooms (Davis and Koop 2006). This type of positive feedback means that stratification can be responsible for a large amount of the interannual variability in productivity. For example, Hearn and Robson (2001) found that winter hypoxia induced by salt stratification in the Harvey estuary was strongly linked to peak chlorophyll-*a* concentrations from spring blooms of *Nodularia*, probably due to release of P from the sediment.

Hypereutrophic waters are vulnerable to diurnal hypoxia due to the cycling of daytime photosynthesis and nighttime respiration, but physical processes add to the problem. Hypereutrophic waters have phytoplankton in such profusion that they also have significant light absorption (Wetzel 1983; Kirk 1983). Some of the light absorbed by phytoplankton is converted to heat, effectively stabilizing the water column (Branco and Torgersen 2009). Since stratification reduces turbulent mixing and reaeration, oxygen depletion ensues (Møller 1996; Conley et al. 2009). This process is somewhat self-limiting, since phytoplankton growth rates are also reduced under lower light.

Alternatively, strong mixing can also lead to anoxia. Wind-driven mixing can resuspend sediment and benthic algae into the water column, bringing along their oxygen demand and thereby causing hypoxia (Carstensen et al. 2007). Resuspension also releases P (Søndergaard et al. 1992), which has a positive feedback on algal growth provided turbidity does not extinguish light to the degree that phytoplankton growth is inhibited (e.g., May et al. 2003 in San Francisco Bay, a turbid estuary). Very high loading rates of P are possible in shallow lakes due to sediment-water column interactions (Søndergaard et al. 2003). In fact, the combination of being shallow and unstratified with periodic wind resuspension and unbalanced oxygen levels is a key characteristic of hypereutrophic ecosystems (Barica and Mur 1980). Wind can also cause upwelling of hypoxic bottom waters, leading to fish kills (Reynolds-Fleming and Luettich 2004).

1.1.2.3 Cyanobacterial dominance

Eutrophic lakes and estuaries can be dominated by cyanobacteria, which are a water quality nuisance if they are toxigenic or form dense scums under bloom conditions (Chorus and Bartram 1999). A variety of factors contribute to the ability of cyanobacteria to out-compete other phytoplankton and macrophytes in eutrophic waters. First, cyanobacteria are more efficient in their use of light. Specifically, they can use photosynthetically active radiation (PAR) over a wider range of wavelengths, giving them a competitive advantage under turbid conditions or

when productivity is already high (Oliver and Ganf 2000). There is also some indication that they are better suited than green algae to make rapid adaptations to the light field, such as would occur under strong mixing in a shallow system (Oliver and Ganf 2000; Schubert et al. 1996; Pilkaityte and Razinkovas 2006). Cyanobacterial dominance can represent a "stable state" since species like *Oscillatoria* thrive under low light but also promote such conditions by causing a higher turbidity per unit of phosphorus than other algae (Scheffer et al. 1997).

Some species of cyanobacteria, such as *Anaebaena* and *Microcystis*, have gas vacuoles that theoretically provide an ability to regulate buoyancy in response to light levels, thus enabling them to travel between zones of high light availability and high nutrient availability (Reynolds et al. 1987). Unfortunately, there is little direct field evidence for such vertical migration actually occurring (Bormans et al. 1999). However, there are numerous studies that show buoyancy-regulating cyanobacteria like *Microcystis* and *Anabaena* thrive when shallow, productive waters experience persistent thermal stratification (Ganf and Oliver 1982; Ibelings et al. 1991; Davis and Koop 2006). Only when the ratio of the mixed layer depth to the photic depth is about equal to one can cyanobacteria dominate; higher ratios are not as conducive to forming blooms (Sherman et al. 1998; Bormans et al. 2004). Other species of cyanobacteria like *Nodularia* also seem to thrive under temperature-stratified conditions (Kanoshina et al. 2003), but this may be more related to their preference for warmer conditions than for stratification per se.

Finally, cyanobacteria thrive in eutrophic waters because of the plentiful supply of phosphorus, which seems to favor their growth for a variety of reasons (Oliver and Ganf 2000). P enrichment has been linked specifically to cyanobacterial blooms in many systems around the globe, with cyanobacteria becoming dominant when N:P ratios are relatively low (< 29, Smith 1983). Although it is logical that nitrogen limitation might favor those species of cyanobacteria that can fix atmospheric N_2 (e.g., *Nodularia*), the correlation with low N:P ratios also extends to non-nitrogen fixing species. Blooms of cyanobacteria at low N:P ratios have been observed in coastal waters of Scandinavia and Australia (Chorus and Bartram 1999) and more specifically in coastal lagoons (e.g., Pilkaityte and Razinkovas 2006). Iron-sulfur cycling may play a supporting role in this trend; in coastal areas, the mutual affinity of Fe and S means that dissolved phosphorus is more freely available and phytoplankton may be Fe-limited (Harris 1999).

1.1.3 Hydrodynamics of coastal lagoons

Some aspects of coastal lagoon hydrodynamics resemble those of lakes, while others more closely resemble estuarine dynamics; both lakes and estuaries are more commonly studied than coastal lagoons, so analogies are helpful. Where a particular lagoon resides on the continuum of lake to estuary depends on its size, outlet configuration, orientation with respect to prevailing winds, bathymetry, mean depth, and local climate (Smith 1994) – or, as Fischer et al. (1979) put it, its "individual personality." Similar to lakes, energy for mixing in coastal lagoons can come from wind forcing or surface heating and cooling; like estuaries, they also experience varying degrees of tidal forcing. Coastal lagoons can behave like well-mixed shallow lakes, though they may act like deep lakes and exhibit a stable two-layer structure. Alternatively, energetic lagoons may exhibit longitudinal density gradients like a well-mixed estuary (Kjerfve and Magill 1989). Salt rather than temperature often causes the density gradients, so the resulting hydrodynamics are closer to that of strongly stratified estuaries than to comparatively weakly stratified lakes.

Since Rodeo Lagoon is shallow, has no tidal action, and alternates between stratified and well-mixed conditions, the following background information will focus on similar systems.

1.1.3.1 Circulation

The tidal connection with the ocean is severely limited in choked lagoons and ICOLLs, so the circulation of water is driven by wind and freshwater runoff, not tides. Winds are usually dominant in causing circulation and mixing, acting via wind-driven currents, set-up and set-down of barotropic pressure gradients, formation of Langmuir cells, and generation of short-period wind waves (Kjerfve and Magill 1989). Hydrology drives the timing of water exchange with the coastal ocean and therefore the salinity, which can vary from fresh to hypersaline depending on the local water balance and location within the lagoon (Smith 1994). Vertical mixing tends to be fast in most shallow lagoons, which can produce a longitudinal salinity gradient from the ocean towards freshwater sources. The resulting baroclinic pressure gradient will drive longitudinal circulation like that classically seen in salt-wedge estuaries, with net upstream flow near the bed balancing net downstream flow in the upper water column (O'Brien 1952; Hansen and Rattray 1965). Differential heating and cooling in areas of different depths, independently or combined with wind-driven circulation, can also lead to baroclinic pressure gradients and drive circulation (Imberger 1985).

The Coriolis effect is important at low Rossby numbers, defined as $R_0 \equiv U(fL)^{-1}$ where L is lagoon width, U is the mean horizontal current speed, and f is the Coriolis parameter $2\omega\sin\phi$ with $\omega = 7.29 \times 10^{-5}$ s^{-1} and ϕ = latitude. Only if $R_0 < 1$, in which case the time period for advection is comparable to the time period for rotation, does the Coriolis effect become significant. The combination of factors producing $R_0 < 1$ are large lagoon size, high latitude, or small current speeds. In Rodeo Lagoon, the maximum horizontal extent is about 1 km, so rotational effects are relevant when velocities are slower than 0.09 m s^{-1}. As shown in §4.2, however, the actual cutoff appears to be about an order of magnitude smaller, as rotational effects in the vertical profile are most evident when velocities approach 0.01 m s^{-1}. This corresponds to conditions with strong stratification or very light winds (roughly, less than 1.5 m s^{-1}). Under well-mixed conditions, the Ekman layer, which is the depth to which wind-driven currents are felt, extends over the whole water column (Chubarenko et al. 2005).

1.1.3.2 Density stratification

As discussed in Chapter 4, the assumption of fast vertical mixing for shallow lagoons is not always a valid one. In extremely turbid or productive environments, strong light attenuation leads to diurnal thermal stratification (Condie and Webster 2002). Furthermore, vertical stratification by salinity is possible if there is insufficient energy available for mixing, such as when the tidal outlet is closed or restricted. The lack of forcing by tides combined with vertical stratification makes lagoon hydrodynamics, at times, more akin to that of lakes rather than estuaries. If density stratification is present, internal waves, basin-wide seiching, and upwelling should be expected to develop under wind forcing. Of course, there are key differences between lagoons and lakes: lagoons tend to be much shallower, while their density gradients may be much larger due to the influence of salinity on density. These attributes can be expressed in nondimensional combinations like the gradient Richardson and Wedderburn numbers. The gradient Richardson number Ri_g compares the magnitude of energy required to overcome density gradients with the energy from velocity shear available for such mixing:

$$Ri_g \equiv \left(\frac{g}{\rho_0}\frac{\partial \rho}{\partial z}\right)\left(\frac{\partial U}{\partial z}\right)^{-2} = \frac{N^2}{(\partial U/\partial z)^2} \sim \frac{\text{buoyancy}}{\text{shear}} \quad (1\text{-}1)$$

where U is the mean horizontal velocity, ρ is the water density at a given depth z, ρ_0 is a constant reference density, and N^2 is the Brunt-Väisälä buoyancy frequency. Only when $Ri_g < 0.25$ is there sufficient kinetic energy available to overcome stabilizing buoyancy forces. The Wedderburn number W, which was developed for lakes with a well-defined surface mixed layer, assumes that wind energy is the main source of turbulence and expresses a balance between surface wind stress and the pressure gradient resulting from the slope of the pycnocline (Thompson and Imberger 1980):

$$W \equiv \frac{g\,\Delta\rho}{\rho_0}\frac{h_1}{u_*^2}\frac{h_1}{L} \quad (1\text{-}2)$$

where h_1 is the depth of the surface layer, L is the basin length, u_* is wind stress, and $\Delta\rho$ is the density jump across the pycnocline. A small Wedderburn number ($W < 1$) indicates upwelling or downwelling is very likely, while larger Wedderburn values (W > 10) indicate a stable lake.

1.1.3.3 Turbulent diffusivity, dissipation, and length scales

The rate at which momentum is distributed through a turbulent flow is proportional to the eddy viscosity, ν_T, and is a property of the flow rather than the fluid itself (Tennekes and Lumley 1972). In one dimension, the eddy viscosity is defined as follows:

$$\nu_T = \frac{\text{flux}}{\text{gradient}} = -\frac{\langle u'w' \rangle}{\partial U / \partial z} \quad (1\text{-}3)$$

where the Reynolds stress component $\langle u'w' \rangle$ is the product of the two fluctuating velocities u' and w', and the brackets indicate a time average. The analogous rate for heat, mass, contaminants and biota rather than momentum has historically been expressed as the scalar diffusivity K_ρ (Barry et al. 2001):

$$K_\rho = \frac{\text{flux}}{\text{gradient}} = \frac{\langle \rho' w' \rangle}{\partial \rho / \partial z} \quad (1\text{-}4)$$

In the definition above, ρ is either density or a generic scalar; brackets indicate a time average of the fluctuating components ρ' and w'; and the velocity w and gradient $\partial/\partial z$ represent the vertical direction, but could be substituted by their horizontal counterparts. K_ρ is an important input to numerical models and is often used as a basis of comparison for mixing rates in different water bodies.

K_ρ is known to be highly variable in time and space, ranging from 10^{-6} to 10^{-4} m^2 s^{-1} in lakes (Imberger and Patterson 1990) to upwards of 10^{-2} m^2 s^{-1} in energetic estuaries (Stacey et al. 1999b). This reflects the natural variability in density profiles and turbulent kinetic energy

available for mixing. In waters with a clearly defined pycnocline, the value of K_ρ across the pycnocline is referred to as a diapycnal diffusivity and is of particular interest since it governs the exchange of scalars between the epilimnion and hypolimnion. Measurements of the interior of stratified lakes show that turbulence levels are typically very weak, with only a small percentage of the water column actively turbulent (Wüest and Lorke 2003). When the water column is not actively turbulent, the concept of a single value of K_ρ for different scalars like heat and salt breaks down, as diffusivity is close to its molecular values – around 10^{-9} m^2 s^{-1} for salt and 10^{-7} m^2 s^{-1} for heat (Kalff 2002).

The turbulent kinetic energy (TKE) equation states that under steady, locally balanced conditions, TKE production by shear is balanced by buoyancy forces and dissipation (Kundu 1990; also see §4.4.1.2 for a more complete development). A stable density profile therefore acts as a sink for turbulent kinetic energy, damping the scale and speed of turbulent motions and inhibiting turbulent mixing. The net result is that K_ρ is reduced in areas with a stable density profile, unless transport of TKE from other areas can compensate for the loss.

The dissipation rate of TKE, ε, is also frequently used as a comparative metric of turbulent mixing among water bodies. Like K_ρ, ε varies over many orders of magnitude, ranging from 10^{-11} m^2 s^{-3} in the ocean and the interior of deep lakes to 10^{-7} to 10^{-3} m^2 s^{-3} in estuaries (Wüest and Lorke 2003; Geyer et al. 2008). Also like K_ρ, ε is typically larger in the surface layer and bottom boundary layer and much reduced in the stratified interior (Wüest and Lorke 2003). Common parameterizations for K_ρ and ε are further discussed in §4.4.

1.1.3.4 Field estimates of turbulent scalar fluxes

The most direct method for estimating diffusive fluxes of the form $\langle \rho' w' \rangle$ is to measure and time-average the instantaneous product of ρ' and w' using a profiling instrument that can simultaneously sample the velocity and scalar fields. However, this can be problematic due the presence of counter-gradient fluxes and contributions from non-turbulent processes like internal waves (e.g., Saggio & Imberger 2001; Etemad-Shahidi & Imberger 2002). Therefore, a more common approach is to calculate K_ρ from ε via one of several methods, most of which also assume that production and dissipation of TKE are in a local balance (see §4.4). Well-known techniques include measuring the velocity shear using a vertical profiling instrument, determining the velocity spectra from a time series collected at a fixed point, or measuring the temperature gradient spectra from a temperature microstructure profiler (Ivey et al. 2008). K_ρ can also be estimated using dye-tracer releases.

Despite the role of stratification and turbulent mixing in regulating water quality, there have been relatively few field studies resolving turbulent mixing rates in highly stratified, low-energy systems such as coastal lagoons. The study of a Mediterranean-climate estuary seasonally blocked by a sand bar by Sharples et al. (2003) is probably most similar to the work described in this dissertation. They quantified turbulent mixing rates using a temperature microstructure profiler in a highly stratified estuary, which had a high-salinity bottom layer during its blocked state, and found that K_ρ within the pycnocline (~2×10^{-6} m^2 s^{-1}) was greatly reduced compared to the surface layer (10^{-5} to 10^{-4} m^2 s^{-1}) and the bottom layer. K_ρ reached its highest values (10^{-3} m^2 s^{-1}) at the bed, which they attributed to internal seiching.

The closest natural analogs to lagoons are strongly stratified tidal estuaries, such as those studied by Peters (1997) and Etemad-Shahidi and Imberger (2002). The latter assessed turbulent microstructure in the Swan River estuary under strongly stratified conditions, and found turbulent events with relatively little vertical mixing despite relatively high dissipation levels. Peters (1997) also found a negligible vertical salt flux in the neap tide halocline of the Hudson River. Similarly, Stevens (2003) found turbulence strongly affected by buoyancy in the pycnocline of an estuarine embayment, with motions governed by internal waves. For the three estuarine studies listed above, the vertical and horizontal scales are much larger than those of the small lagoon discussed here, which provides additional motivation to study this system.

1.2 Description of field site

1.2.1 Physical setting

Rodeo Lagoon is a small coastal lagoon situated perpendicular to the Pacific Ocean within the Marin Headlands division of the Golden Gate National Recreation Area (GGNRA), near Fort Cronkhite and Sausalito, California (Figs. 1-2, 1-3). The lagoon is seasonally connected to the ocean via a channel in its northwest corner, and is a choked, shallow, coastal lagoon according to the classification system of Kjerfve and Magill (Kjerfve and Magill 1989). As mentioned above, the connection to the ocean is intermittently open during the wet season and mostly closed during the dry season. From 1995 to 2005, the lagoon outlet was open an average of 31 days per year, with days in January, February, and March accounting for more than 75% of the total (D. Fong pers. comm.). Freshwater outflow occurs when the outlet is open during the wet season, as does seawater inflow due to large waves associated with winter storms that wash over the beach berm. The lagoon is not tidal, though inflows and outflows are affected by tidal stage to a minor degree.

The local Mediterranean climate features wet winters, dry summers, and summer marine fog. Average annual precipitation in downtown San Francisco is 57 cm, most of which falls from November to March (NOAA/NWS Coop Station 047772, 11 km from Rodeo Lagoon). Vegetation in the watershed is mostly grassland and coastal scrub on the hill slopes with willows and other riparian plants along creek channels. The 11.5 km^2 catchment is divided into two main sub-basins, one home to Gerbode Creek and the other to Rodeo Creek. The two creeks combine in a willow-dominated marsh, then flow into an impoundment immediately upstream of Rodeo Lagoon that is known as Rodeo Lake (F, Fig. 1-3). Rodeo Lake fills a basin that was formerly part of the lagoon before it was impounded by the Army in 1908 to create a fresh water source (Thompson 1979). The subsequent construction of the Bunker Road crossing in 1937 resulted in the current and more complete division of lake and lagoon (Wang 1983; Striplen et al. 2004). Sediment has subsequently filled most of

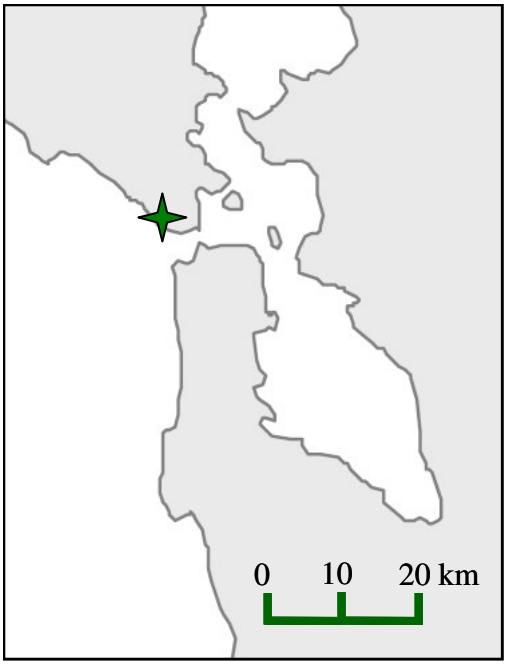

Fig. 1-2. Location of Rodeo Lagoon within the San Francisco Bay Area.

Rodeo Lake to the point where it has very little storage capacity, and functions hydraulically and ecologically as a wetland. For example, it is usually hypoxic, and its pH of about 7 is lower than both its tributary and receiving waters (Silkie 2008). Rodeo Lake spills into Rodeo Lagoon at a weir just to the east of Bunker Road (E, Fig. 1-3; Fig. 4-2).

1.2.2 History

The watershed of Rodeo Lagoon is entirely within the GGNRA and is largely undeveloped, though it has been subject to agricultural and military uses in the past. The watershed was used for dairy farming from the second half of the 19th century until about 1930 (Striplen et al. 2004). The Army began operations in 1901 at Fort Barry, just upstream of Rodeo Lagoon, and maintained a significant presence in the area during World War II. The lagoon and its watershed became the responsibility of the National Park Service when the GGNRA was established in 1972. The most obvious impacts of the watershed's historical use are the reduced size of Rodeo Lagoon due to the road crossing, and increased sediment supply from the construction of roads and trails throughout the watershed, which has resulted in the formation of small deltas at several locations around the lagoon (Striplen et al. 2004). It is perhaps fortunate that Rodeo Lake effectively acts as a settling basin for Rodeo Lagoon, as this has somewhat mitigated the effect of increased sediment load from the watershed on the remaining part of the lagoon.

Past inflows of human and animal waste may have also left a legacy on lagoon ecology. Wastewater from the military base flowed indirectly into Rodeo Lagoon in the early part of 20th century (Striplen et al. 2004). Later, the Army constructed a septic system and leach field that emptied into Rodeo Beach. Because one septic tank was below the high water level of the lagoon, artificial breaching of the beach berm was occasionally necessary to flush the system, demonstrating the hydraulic connectivity that existed with the lagoon (Golden Gate NRA 1992). The septic system was abandoned in 1991 when a pipeline and lift stations to export sewage out of the watershed were constructed (Fong 1997). The only remaining known waste flows into

Fig. 1-3. Rodeo Lagoon and vicinity. (A) Pacific Ocean. (B) Inlet/outlet channel connecting lagoon to ocean. (C) Fort Cronkhite. (D) Rodeo Lagoon. (E) Location of weir connecting lake and lagoon. (F) Rodeo Lake. (G) Rodeo Creek just downstream of its confluence with Gerbode Creek. Background image from October 2003 © Google Earth.

Rodeo Lagoon are from fewer than 20 horses boarding at the Presidio Riding Club Stables (Silkie 2008), and occasional sewer system leaks.

1.2.3 Bathymetry

Most of Rodeo Lagoon resembles a bathtub: the bottom is virtually flat with slopes of less than 1%, while the sides are steep (Fig. 2-6). Where it is flat, the bed is covered with soft, dark, non-cohesive, highly organic sediment (Zembsch 1993; Watson 2006). Non-organic sediments underlie this organic layer (Golden Gate NRA 1992). An exception is the eastern sub-basin of the lagoon, near Rodeo Creek, which is about 0.5 m shallower than the main basin and contains firmer substrate. The lagoon's maximum depth varies seasonally between 1.5 and 2.5 m, with an average surface area of 0.15 km^2.

1.2.4 Biota

The phytoplankton community in Rodeo Lagoon contains both green and blue-green algae. In 2007, the phytoplankton community was dominated by a succession of the cyanobacterium *Nodularia spumigena*, centric diatoms, a second cyanobacterium *Microcystis aeruginosa*, flagellated protozoa, and a combination of chlorophytes and *M. aeruginosa* (Drake 2008). Other phytoplankton which have been found in abundance include the cyanobacteria *Oscillatoria* and *Anabaena*, the flagellated heterotroph *Euglena*, and the chlorophytes *Scenedesmus*, *Oedogonium,* and *Gloeocystis* (Podlech et al. 1993; Codemo et al. 1996; D. Fong pers. comm.; Drake 2008). *N. spumigena*, *M. aeruginosa*, and *Anabaena* are of particular concern because these cyanobacteria are toxigenic under some conditions (Chorus and Bartram 1999); the hepatatoxins nodularin and microcystin have been detected in the lagoon in the past (Martin et al. 2007; D. Fong pers. comm.). Shallow areas of the lagoon are heavily populated by the submerged rooted macrophytes *Stuckenia pectinata* and *Ruppia sp*. in summer and fall, while emergent *Carex* spp., *Scirpus* spp. and *Typha latifolia* are present along the shoreline (Swenson 1994; D. Fong pers. comm.)

The lagoon is home to several species of fish, including threespine stickleback (*Gasterosteus aculeatus*), prickly sculpin (*Cottus asper*) and the federally endangered tidewater goby (*Eucyclogobius newberryi*) (Wang 1983; Fong 1997), for which Rodeo Lagoon is designated Critical Habitat (*Federal Register* 2008). It also provides habitat for many species of birds, including the brown pelican (*Pelecanus occidentalis*), which was recently delisted from the federal endangered species list (*Federal Register* 2009). Rodeo Lake, a freshwater body, provides habitat for the federally threatened California red-legged frog (*Rana aurora daytonii*) (Fong 1997). A group of river otters (*Lontra canadensis*) also inhabits the lagoon, and was observed preying on brown pelicans in dramatic fashion during the course of this field study.

1.2.5 Water quality

Rodeo Lagoon can be classified as a hypereutrophic ecosystem (Barica and Mur 1980), with extremely high productivity, large fluctuations in dissolved oxygen (DO), and limited water circulation. The phytoplankton biomass peak, which occurs in late summer, produced chlorophyll *a* (Chl *a*) concentrations in excess of 1000 $\mu g\ L^{-1}$ in 2007, with basin-wide hypoxia driven by decomposition following several weeks thereafter. Large fish kills have been observed in 1993, 1996, 2001, 2005, 2006, and 2007, with partial fish kills in other years (D. Fong pers. comm.). Hypoxia and high pH, rather than un-ionized ammonia, temperature, salinity, or turbidity, are though to be responsible for these kills (Martin et al. 2007).

Water quality sampling over the past few decades has been intermittent and mostly consisted of surface grab samples. Nonetheless, a few robust seasonal trends emerge. Madej (1989), Leach et al. (1997), Beutel (1998), and Silkie (2008) all found that lagoon salinity is higher in the summer and fall than in the winter or spring, which is consistent with the winter peak in freshwater inflow. Summer pH levels greater than 9 have been observed in the lagoon since at least 1988 (Madej 1989; Podlech et al. 1993; Silkie 2008). The summer pH is consistently higher than the winter pH, presumably due to the lagoon's high productivity and negligible summertime rainfall (Madej 1989; Leach et al. 1997; Beutel 1998; Silkie 2008). Low DO has been consistently observed in summer and fall, although super-saturated values are also common when a phytoplankton bloom is underway (Podlech et al. 1993; Codemo et al. 1996; SFBRWQCB 2008; Silkie 2008). Salinity gradually decreases over time in some summers (e.g., Podlech et al. 1993) and gradually increases in others (e.g., 1995, D. Fong pers. comm.), probably reflecting year-to-year changes in the ratio of inflow to evaporation after the lagoon outlet closes for the season.

Salinity can vary over depth as well as in time, but this spatial variability has been less well studied because it is difficult to observe from shore-based equipment. A seasonal variation in the salinity structure has been known since at least 1995, when National Park Service staff collected salinity profiles over several seasons that showed strong stratification in January and March and a well-mixed salinity profile from July to October (D. Fong pers. comm.). Waljeski and Williams (2004) conducted a salinity survey in summer and found mild stratification (3.2 psu throughout most of the water column vs. 8.5 psu very near the bed) which could have been a remnant of winter density stratification.

The lagoon has been analyzed for nutrient content several times beginning in 1989, but the only clear trend is that the lagoon is enriched in both N and P, and is susceptible to events with high ammonia. For example, a 1992 study (BioSystems Analysis 1993) found plentiful orthophosphate and ammonium but no nitrate or nitrite; the sediments were particularly rich in ammonium. The atomic N:P ratio was 14:1, but neither N nor P was low enough to be limiting. The study concluded that nitrification was somehow suppressed, probably by a lack of oxygen, but that denitrification was rapid. Similarly, a year-long sampling effort by Silkie (2008) found a mean orthophosphate level of 0.08 mg/L as P and a mean ammonia level of 0.14 mg/L as N , but did not detect nitrate in the lagoon. The atomic N:P ratio in soluble nutrients was 7:1, indicating that if there were a nutrient limitation it would be due to nitrogen, but again there was no direct evidence of this limit applying. A nutrient enrichment study in summer 2006 found evidence of co-limitation by N and P (Silkie 2008).

1.3 Research questions

Rodeo Lagoon's recent water quality problems, combined with preliminary observations of the intermittent density stratification, motivated this joint study of lagoon water quality and hydrodynamics. Using the experimental approach outlined in §2, my research project was designed to address the following knowledge gaps:

Question 1. How long does salt-based density stratification persist in Rodeo Lagoon, and what variables control its persistence?

The salinity field has a characteristic annual cycle that is presented in the chapter on water quality (§3, particularly §3.1). Salt-based density stratification as quantified by the buoyancy frequency N^2 is discussed throughout the chapter on hydrodynamics (§4), but particularly in §4.1 and §4.4.

Question 2. What effects does this density stratification have on lagoon hydrodynamics, in particular turbulent mixing?

In §4, I present detailed observations of the way that seasonal, salt-based density stratification in Rodeo Lagoon modifies turbulence, currents, bed stresses, velocity shear, and scalar diffusivity.

Question 3. What effects does this density stratification have on lagoon water quality, at both short and long time scales?

In §5, I discuss how density stratification, by drastically reducing turbulent mixing and bed stresses in winter, ultimately leads to degraded water quality. This degradation is readily observed when the lagoon is salt-stratified, but it also contributes to the lagoon's hypereutrophic status, even though production is highest in summer when stratification is typically absent.

Chapter 2

Experimental Design

My research approach combined continuous monitoring of water quality on a weekly to monthly basis with three intensive hydrodynamics experiments lasting several weeks each (Fig. 2-1). Water quality monitoring was aimed at resolving seasonal changes in temperature, salinity, density gradients, dissolved oxygen, nutrient concentrations, and phytoplankton biomass and speciation. Such variables have been measured previously in Rodeo Lagoon, but not on a systematic basis over this length of time. The hydrodynamics experiments, meanwhile, were focused on resolving the response of lagoon currents and turbulent mixing rates to external forcing under various seasonal conditions. These external energy sources, like wind stress, diurnal heating and cooling, and freshwater inflow, tend to vary on rapid time scales (hours to days) as well as seasonally. Combining the two types of monitoring ensured that the hydrodynamics data captured the range of lagoon conditions over an annual cycle.

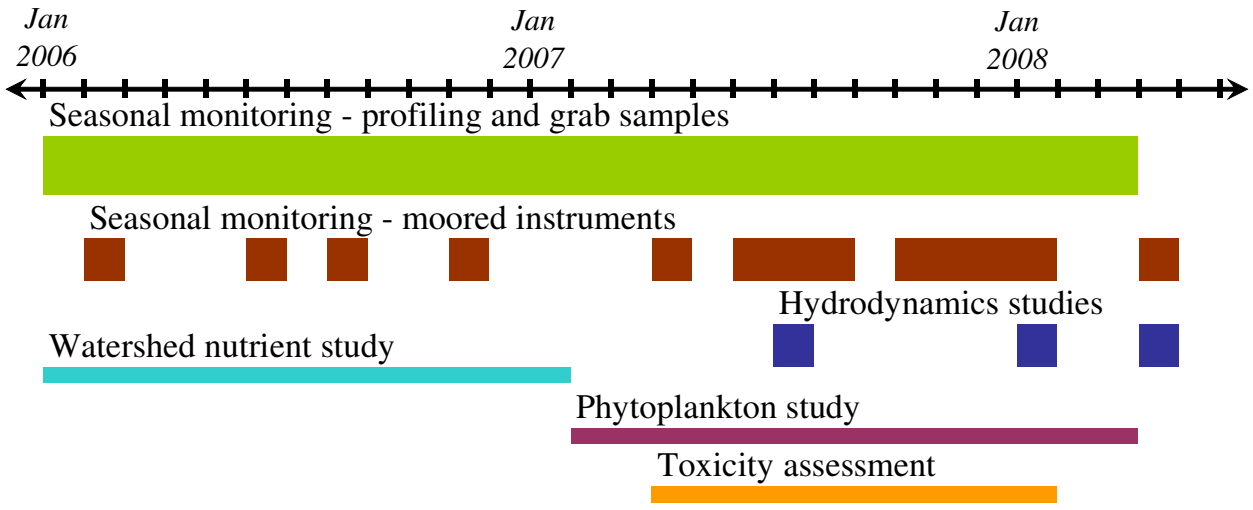

Fig. 2-1. Timeline of research activities, including seasonal monitoring via water quality grab samples and longitudinal transects (green), seasonal monitoring via moored CTDs (brown), and three hydrodynamics experiments involving ADVs, microstructure profiling, and an ADCP (blue). Also shown are collaborative work led by others, including a watershed nutrient study by S. Silkie (aqua, Silkie 2008), a phytoplankton monitoring study by J. Drake (purple, Drake 2008) and a toxicity assessment by A. Guido Zarate (orange, Drake et al. *in press*).

2.1 Seasonal monitoring

2.1.1 Longitudinal transects

I monitored seasonal changes in water quality and water column structure over a two-year period, from March 2006 to April 2008, using a variety of methods. Approximately monthly, I collected fifteen vertical profiles on a longitudinal transect with a Sea-Bird 19+ SEACAT (Sea-Bird Electronics) equipped with temperature, conductivity, depth, and oxygen channels (Fig. 2-2). Temperature and conductivity are used to calculate salinity in practical salinity units (psu). The oxygen sensor is of the polarographic membrane type (SBE 43, Sea-Bird Electronics). The instrument package also included sensors for chlorophyll-*a* (Chl *a*) fluorescence and turbidity (SCUFA, Turner Designs) and photosynthetically active radiation, or PAR (LI-193SA, LI-COR). The PAR sensor detects light in the wavelength band of 400–700 nm. The spherical design of the sensor used in this study means that PAR is reported as single scalar quantity rather than as the vector quantity downwelling PAR, which is another frequently reported type of light measurement.

In most cases, profiling data collected with the Sea-Bird instrument package are reported as averages from 5-cm depth bins, but there are several exceptions. PAR data was transformed into a light extinction value using unbinned data (§3.5). Also, the detailed profiles of Chl *a* fluorescence, turbidity, and dissolved oxygen shown in Figs. 3-9, 3-12, and 3-18 required the use of unbinned data.

The profiling stations used to create the longitudinal transect are listed below in Table 2-1. Station #1 corresponds to the west end of the lagoon at the pedestrian bridge, and Station #15 to the east end of the lagoon at the Bunker Road bridge, which is very near the inflow from Rodeo Creek via Rodeo Lake (Fig. 2-2).

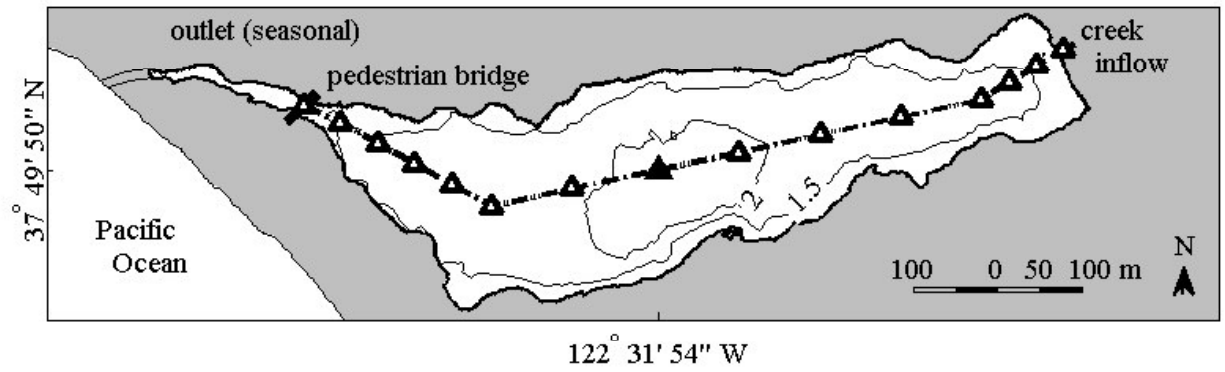

Fig. 2-2. Location of Rodeo Lagoon. The approximate center of the lagoon, where moored instruments were placed during the experiments, is shown by a filled black triangle. The dashed line and open triangles indicate the position of the longitudinal transect used for profiling, from the west end at the pedestrian bridge to the east end at the Bunker Road bridge and inflow weir. Contour lines indicate depths of 1.5 m and 2 m at the time of the bathymetric survey.

Station No.	Northing	Easting	Description
1	37.83132	-122.53647	pedestrian bridge / west end
2	37.83114	-122.53598	
3	37.83092	-122.53546	
4	37.83070	-122.53497	
5	37.83048	-122.53446	
6	37.83024	-122.53391	
7	37.83043	-122.53281	
8	37.83064	-122.53164	lagoon center
9	37.83082	-122.53056	
10	37.83102	-122.52944	
11	37.83120	-122.52835	
12	37.83139	-122.52725	
13	37.83158	-122.52687	
14	37.83176	-122.52649	
15	37.83193	-122.52613	Bunker Road bridge / east end

Table 2-1. Locations of stations used for vertical profiling.

2.1.2 Grab samples

Throughout the same time period as the longitudinal transects but with greater frequency in 2007, I collected grab samples for laboratory analysis of nutrient, Chl *a* content, and phytoplankton species identification. While collecting grab samples, I concurrently took measurements with a handheld oxygen, conductivity, salinity, and temperature system (YSI-85, YSI). The oxygen sensor of this instrument also uses a polarographic membrane, a similar technology to the oxygen sensor on the Sea-Bird CTD used for longitudinal profiling.

Sediment samples for pore water analysis were collected using the pneumatic coring device described in Nelson and Jiménez (2000) . The cores were taken from the top 15 cm of sediment. Pore water samples were obtained by centrifuge extraction and filtration of sediment samples.

Samples for nutrient content analysis were collected in acid-washed containers and passed through 0.7-μm glass fiber filters prior to storage and analysis. Concentrations of orthophosphate and nitrate + nitrite were determined colorimetrically using a Bran and Luebbe AutoAnalyzer II (Whitledge et al. 1981). Ammonium ($NH_4^+ + NH_3$) was determined using the phenol–hypochlorite method of Solorzano (1969). The detection limit for all three classes of nutrients is 0.05 μM.

I measured Chl *a* concentrations, a proxy for biomass, using visible spectrophotometry for grab samples collected in 2006 and early 2007 (Arar 1997). Grab samples from 2007 were analyzed by J. Drake using fluorescence (Holm-Hansen and Riemann 1978; Arar and G.B. Collins 1997). Duplicate samples were analyzed by both methods to ensure data continuity. From grab samples preserved in acid Lugol's solution, J. Drake also identified and quantified cells greater than 1 μm in diameter using light microscopy (Booth 1993; Drake 2008).

Hydrogen ion concentration was measured to the nearest 0.1 pH unit using an Oakton pHTestr 2 with automatic temperature compensation. The unit was field-calibrated during each sampling day.

2.1.3 Meteorology

To monitor wind forcing, during the January 2008 and April 2008 experiments I installed an anemometer (Model #05106, RM Young) on the north bank of the lagoon about 2 m above the water surface. In addition, information about wind forcing is available from National Oceanic and Atmospheric Administration (NOAA) station 9414290, located 5.6 km from Rodeo Lagoon at the southern end of the Golden Gate (37° 48.4' N, 122° 27.9' W) and referred to here as the Golden Gate weather station. Both data sources provide wind speed and direction data on a 6-minute interval; hourly averages during the three hydrodynamics experiments are shown in Fig. 2-3.

Rainfall data are from the National Weather Service's Cooperative Station 047772 in downtown San Francisco, about 11 km from the field site (Fig. 2-4). Significant wave height data for the Pacific Ocean are from NOAA buoy 46026, located 27 km off shore from the lagoon (Fig. 2-4). Solar radiation data was provided by the San Francisco Public Utilities Commission, which operates a solar monitoring station located in northwestern San Francisco, 7 km from the field site.

Local meteorological conditions are relevant because they are manifested as energy fluxes across the lagoon surface via wind stress and heat exchange. As I describe in the sections below, these fluxes are straightforward to estimate by combining some commonly available meteorological data like wind speed, air temperature, and relative humidity with empirical parameters from the literature.

2.1.3.1 Wind stress

I converted wind speed to a surface wind friction velocity, u^*_{wind}, using a drag coefficient, C_D, to relate wind speed and wind stress:

$$u*_{wind} = \sqrt{\frac{\tau_{surface}}{\rho_w}} = \sqrt{\frac{\rho_{air} C_D U_{wind}^{\ 2}}{\rho_w}} = \sqrt{\frac{\rho_{air} C_D}{\rho_w}} U_{wind} \qquad (2\text{-}1)$$

To estimate C_D, I applied the formula of Yelland and Taylor (1996), which has a minimum value of C_D at 6 m s^{-1}:

$$C_D = 1\times10^{-3} \cdot (0.29 + 3.1 U_{wind}^{-1} + 7.7 U_{wind}^{-2}) \quad \text{for } U_{wind} < 6 \text{ m s}^{-1} \qquad (2\text{-}2a)$$

$$C_D = 1\times10^{-3} \cdot (0.60 + 0.07 U_{wind}) \quad \text{for } U_{wind} > 6 \text{ m s}^{-1} \qquad (2\text{-}2b)$$

Most of the observed wind speeds were less than 6 m s^{-1}. The results presented in §4 are not very sensitive to the functional form of C_D. In fact, for the mixing efficiency discussion of §4.5.1, C_D was set to 1×10^{-3} to allow for a direct comparison of my observations with other studies that used a constant value of C_D.

Since the purpose of computing u^*_{wind} is to compare it to hourly hydrodynamics data from the ADVs and ADCP, I also created hourly averages of u^*_{wind}. For comparison with temperature

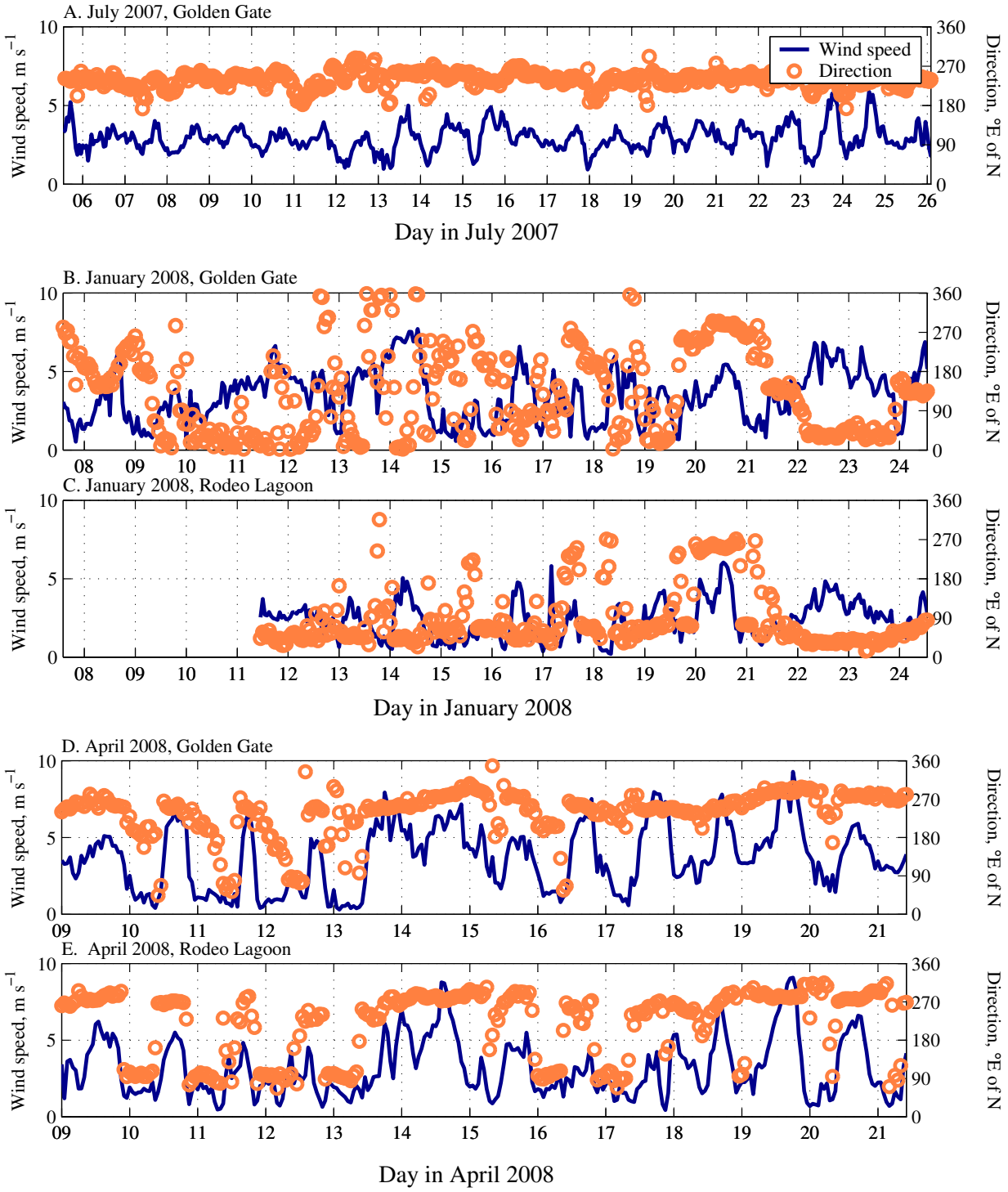

Fig. 2-3. Wind speed (blue line, left axis, m s^{-1}) and direction (orange circles, right axis, degrees east of North) at the Golden Gate weather station (**A**, **B**, **D**) and Rodeo Lagoon (**C**, **E**) in July 2007 (**A**), January 2008 (**B, C**), and April 2008 (**D, E**).

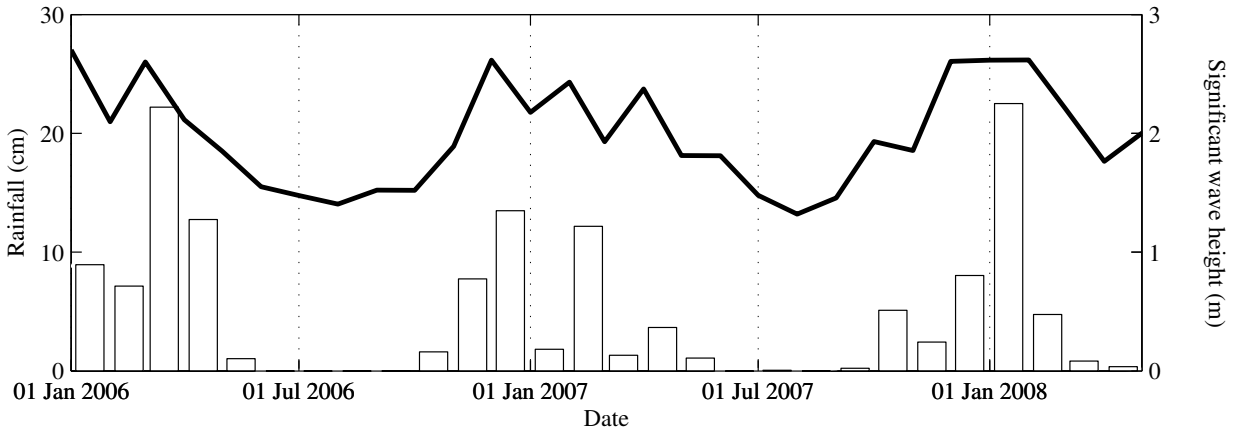

Fig. 2-4. Inflows to the lagoon are from ocean waves and rainfall. Shown here are significant wave height from a NOAA ocean buoy 46026 (solid line, right axis), presented as a monthly average, and total monthly rainfall at NWS co-op station 047772 in downtown San Francisco (bars, left axis).

microstructure data, I averaged wind velocities over the entire time period that microstructure profiling took place on each day of sampling, also including the hour preceding sampling.

The wind speed U_{wind} comes either from the Golden Gate weather station or from the anemometer that was temporarily deployed on the north shore of Rodeo Lagoon during the January 2008 and April 2008 experiments. Since that anemometer was only 2 m above the water surface, the wind speed was adjusted according to the ratio

$$\frac{U_{wind}(z = 10\,\mathrm{m})}{U_{wind}(z = 2\,\mathrm{m})} = \frac{\ln(10\,\mathrm{m}) - \ln(z_0)}{\ln(2\,\mathrm{m}) - \ln(z_0)} \qquad (2\text{-}3)$$

where for $C_D = 1\times10^{-3}$ the roughness height z_0 is calculated as $z_0 = (10\text{ m})/\exp(k/C_D^{1/2}) = 3.2\times10^{-5}$ m. The ratio of adjustment is a modest 1.15, but it has the advantage of producing a wind record that has the temporal variability of the Rodeo Lagoon site with a magnitude that is comparable to the Golden Gate data. This distinction is important because the temporal variability of observed mixing is significantly better correlated with the Rodeo Lagoon wind record than the Golden Gate wind record (*see* §4.4.2 and §4.5.1). For the Golden Gate anemometer, which is located 10 m above the surface, no adjustment is necessary.

2.1.3.2 Heat budgets

Heat fluxes influence the stability and potential energy budget of the water column and can be estimated by constructing a simple heat budget using standard meteorological formulae. For the April 2008 experiment and more crudely for all of 2007, I estimated the net heat transfer rate of the surface mixed layer, H_{net} [W m^{-2}], using estimates of shortwave radiation, longwave radiation, latent heat transfer, and sensible heat transfer:

$$H_{net} = H_{shortwave} + H_{longwave} + H_{latent} + H_{sensible} \qquad (2\text{-}4)$$

Each of these terms is discussed in greater detail below and has units [W m^{-2}].

Shortwave radiation
The estimate of shortwave radiation, $H_{shortwave}$, comes from radiation data for northwestern San Francisco. Shortwave radiation was adjusted for surface albedo according to the formula of Henderson-Sellers (1986), assuming a cloudiness of 5-50% since no data were available.

Longwave radiation
As shown in the equation below (TVA 1972; Fischer et al. 1979), $H_{longwave}$ is the sum of longwave radiation from the atmosphere into the lagoon, less longwave radiation from the lagoon towards the atmosphere:

$$H_{longwave} = (5.18\times10^{-13}(1+0.17C^2)(273+T_{air})^6) - (0.972*5.67\times10^{-8}(273+T_{water})^4) \quad (2\text{-}5)$$

For the April 2008 model, the air temperature in °C, T_{air}, comes from the weather station mounted at the lagoon's north shore, while the water temperature in °C, T_{water}, comes from a CTD at the lagoon's center. C is the cloudiness fraction, but since no data were available, this was set to zero as a way of calibrating the April 2008 model, which has too much heat gain compared to the observations. For the 2007 annual heat budget, T_{air} comes from the Golden Gate weather station while T_{water} comes from the model's previous time step.

Latent and sensible heat fluxes
Although latent and sensible heat fluxes are a significantly smaller portion of the heat budget than longwave and shortwave radiation, they are included for completeness and were calculated according to the method of Friehe and Schmitt (1976):

$$H_{latent} = -C_L\rho_{air}L_wU_{wind}(SH_{sat} - SH) \quad (2\text{-}6)$$
$$H_{sensible} = -C_S\rho_{air}C_{p,air}U_{wind}(T_{water}-T_{air}) \quad (2\text{-}7)$$

In the formulae above, C_L and C_S are constants that depend on the "stability index" $U_{wind}(T_{water}-T_{air})$, with U_{wind} in units [m s^{-1}] and temperature in °C. $C_{p,air}$ is the specific heat of air (1.012×10^3 J kg^{-1} $°C^{-1}$). SH is the specific humidity (mass of water vapor per unit mass of air) calculated using air temperature and relative humidity data from the lagoon weather station, combined with atmospheric pressure data from the Golden Gate weather station. The latent (evaporative) heat flux is the smallest component of the heat budget; since the local weather has a strong marine influence, humidities were high and evaporation was correspondingly low.

In addition to the surface fluxes discussed above, other possible contributions to the heat budget of the surface mixed layer include (a) entrainment of the warmer, salty water below the pycnocline, (b) inflows, and (c) outflows. The annual heat budget for 2007 does not include entrainment, and inflows and outflows were set equal to one another at ½ of the monthly rainfall rate multiplied by watershed area. The temperature of inflows was set to the local air temperature in the annual heat budget.

For the April 2008 heat budget, the contribution of entrainment was calculated by combining a smoothed version of the observed change in pycnocline location dh/dt (Fig. 2-10; §2.2.2) with temperature data from surface and bottom CTDs. Independent estimates of inflow and outflow

are not available, so outflow was roughly estimated as the change in lagoon volume over time. This term is probably the largest source of error in the heat budget since it ignores the heat budget contribution of creek inflow, which is generally several degrees cooler than the lagoon itself.

The heat budget model for the surface mixed layer was validated by comparing the observed surface water temperature with one calculated by explicit forward integration of the following formula, which includes terms for surface fluxes, entrainment, and outflow:

$$\frac{dT_{water}}{dt} = \frac{H_{net}}{\rho_w C_p \Delta h_{mix}} + \frac{dh}{dt}\frac{(T_{water,bottom} - T_{water,surface})}{\Delta h_{mix}} - \frac{Q_{outflow} T_{water,surface}}{V} \qquad (2\text{-}8)$$

C_p is the specific heat of water (4.1×10^3 J kg^{-1} °C^{-1}) and V is lagoon volume.

For April 2008, the model was initialized with the observed water temperature and run with a time step of 1 hour for a total of 478 time steps (20 days). For the annual heat budget, the model was initialized with the observed water temperature and run with a time step of 1 day for a total of 365 time steps (1 year).

2.1.4 Bathymetry and depth

A continuously logging Druck pressure sensor located at the east end of the lagoon provided a depth record spanning the period December 2005 to June 2008 at a recording interval of 15 minutes, with only a few gaps for instrument service and following a severe storm in January 2008. A similar pressure sensor was also located in the lake. The depth records for both lake and lagoon are shown in Fig. 2-5. Conversion of pressure data to elevation relative to mean sea level (MSL) is from a June 2007 survey to benchmark K481, which is located beside Bunker Rd. near Field Rd, combined with MSL data from NOAA station 9414290. The June 2007 survey indicated that a maximum reading of 9.99′ on the manual gage near the Bunker Rd. bridge (Shaw

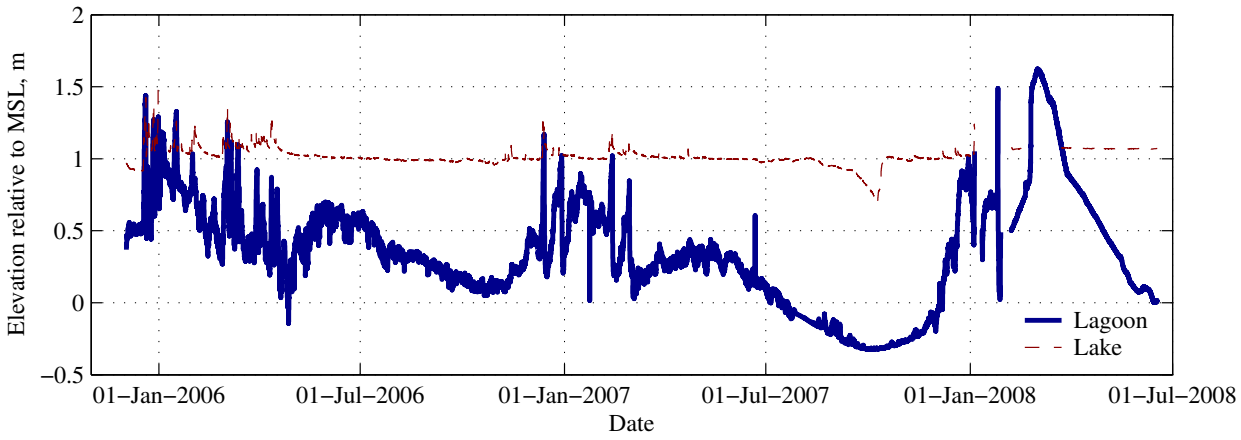

Fig. 2-5. Elevation of the surface of Rodeo Lagoon (solid blue line) and Rodeo Lake (dashed red line), December 2005 to June 2008, relative to mean sea level (MSL). Raw data is from a Druck pressure sensor, courtesy of National Park Service, and was calibrated for sensor drift with visual observations collected approximately weekly.

2005) corresponds to 2.20 m in NAVD 88 and 1.23 m above MSL.

I completed a bathymetric survey of the lagoon in April 2008 using a 1200-kHz ADCP and completed a perimeter survey in June 2008, the combined results of which are shown in Fig. 2-6. I then combined the depth record from the pressure sensor with the bathymetry to derive a volume-depth relationship for use in flushing time calculations (§5.2.1). The relatively low water level at the time of the two surveys necessitated a small extrapolation of the known bathymetry to calculate volume at higher water levels.

2.2 Hydrodynamics instrumentation

To understand lagoon hydrodynamics over time scales within each season, I conducted three detailed experiments in July 2007, January 2008, and April 2008, when the lagoon was well-mixed in terms of salt, stratified by salt, and transitioning between the two, respectively. The experimental setup included two types of instruments that sense fluid motion (§2.2.1–2), a temperature microstructure profiler useful for inferring turbulent mixing rates (§2.2.3), and moored instruments that record information about density structure (§2.2.4).

Although there is some net flow through the lagoon when the outlet is open under wet weather conditions, this flow is not fast enough to be a significant source of momentum to the system. Inflows of saltwater are rare and also too slow to add much momentum, except perhaps in the outlet channel itself. The instrumentation is therefore configured to capture wind forcing and vertical momentum fluxes in a way that might allow an explanation of the linkages between the two. The hypothesis that there should be a connection between bottom stress and wind stress is based on the observation that there is very little other external forcing acting on the system.

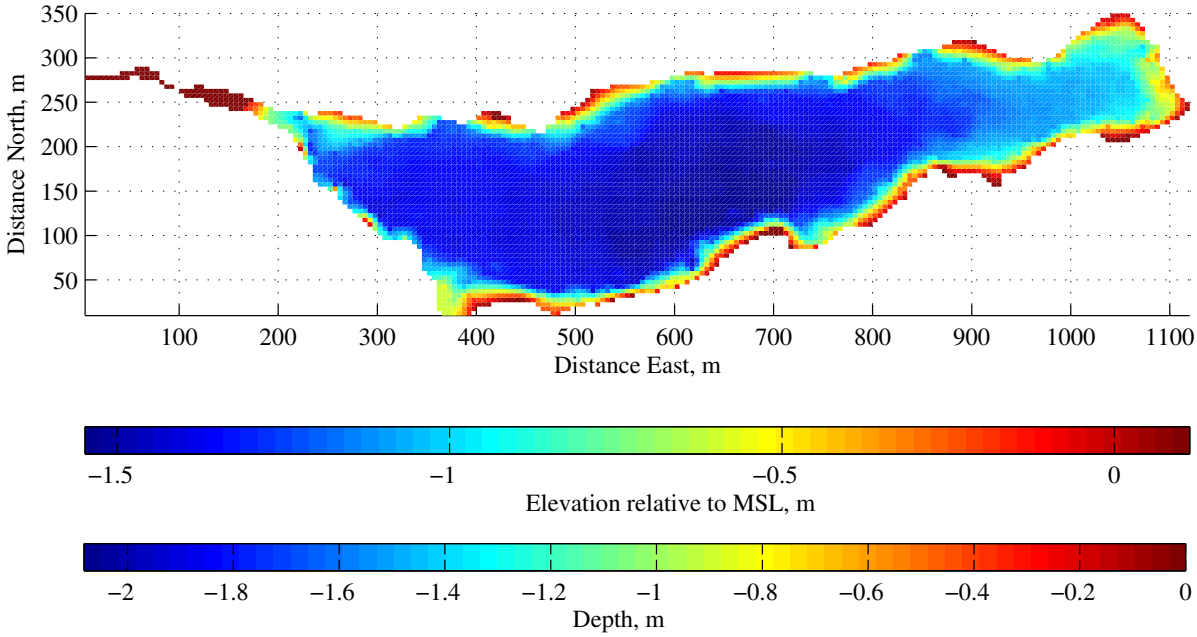

Fig. 2-6. Bathymetry of Rodeo Lagoon from surveys in April and June 2008, shown both as elevation relative to mean sea level (MSL) and as depth below the surface in April 2008.

2.2.1 Acoustic Doppler Velocimeters

In each of the three experiments, I deployed a pair of Nortek Vector acoustic Doppler velocimeter (ADV) in the middle of the lagoon (Fig. 2-2, 37.83064ºN, 122.53164ºW). The ADVs were located with a sampling volume 10 and 20 cm above the bed, respectively. Because these ADVs were located quite close to the bottom boundary, the data provide information about bottom stresses experienced under different wind and stratification conditions. The instruments were separated horizontally by 40 cm and mounted on a PVC sawhorse-type frame, as shown in Fig. 2-7. Although PVC is less rigid than a welded metal frame, its lighter weight allowed for deployment from the boat without a winch.

The ADVs sampled at 16 Hz for 6 minutes every hour, for a total of 5760 samples per burst. Because the lagoon is typically a very low-energy environment, I used the lowest velocity range setting, which can resolve horizontal velocities up to 0.05 m $s^{-1}$and vertical velocities up to 0.02 m s^{-1}. This setting produced some data errors under windy conditions, when wave orbital velocities exceeded that threshold. Nortek Vectors are equipped with compass and tilt sensors so that the absolute orientation of the probe is known, but instrument compass performance was compromised by magnetic interference, so only the tilt is known accurately.

In addition to the data quality issues at high velocities and compass errors that are mentioned above, I encountered the following instrument problems:

- In January 2008, only two of three beams on the lower ADV (10 cm from the bed)

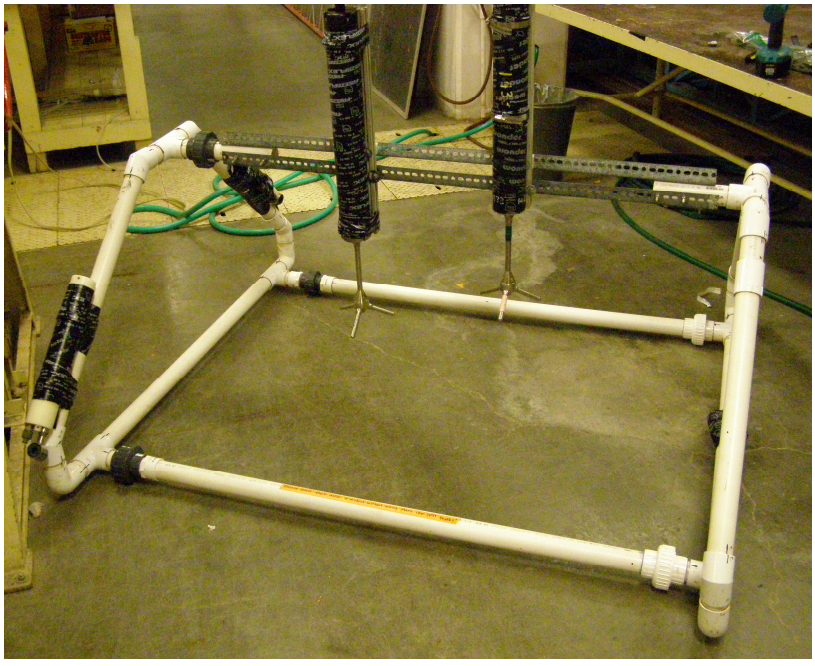

Fig. 2-7. Configuration of downward-looking Nortek ADVs on a PVC frame. The ADV sampling volumes are separated vertically by 10 cm and horizontally by 40 cm. Two CTDs (RBR Ltd.) with sampling volumes vertically coincident with the ADV sampling volumes are mounted on the left side of the frame..

operated correctly, so the data from this instrument is not included here.

- In April 2008, quiescent conditions and/or a low concentration of backscattering particles led to an unacceptably low signal-to-noise ratio at the beginning of the deployment. This poor-quality data has been removed from the record.

ADV data can be processed two ways, depending on the time scale of interest. Data from within each burst sheds light on short time-scale processes like turbulence and waves, while burst-averaged data (1 sample h^{-1}) corresponds to processes operating on diurnal or synoptic time scales. This section describes some of the basic calculations that I used to investigate the evidence for these processes in the ADV data. Processes that act on a time scale of several minutes to several hours, such as surface and internal seiching, are not well resolved by the ADV data due to experiment design.

Prior to any other processing, I first rotated the raw ADV data into a principal horizontal axis (u), a secondary horizontal axis (v), and vertical axis (w) using the formula

$$\theta_p = \frac{1}{2}\tan^{-1}\left[\frac{2\overline{u_1' u_2'}}{\overline{u_1'^2} - \overline{u_2'^2}}\right] \qquad (2\text{-}9)$$

where θ_p is the angle of the major principal axis relative to the instrument's coordinate system (Emery and Thomson 2001). The velocity fluctuations u'_1 and u'_2 come from the horizontal velocities prior to rotation, calculated as $u_1' = u_1 - \overline{u_1}$ where $\overline{u_1}$ is the time average over the entire data set. As previously noted, I do not know the compass heading that corresponds to the principal axis.

I will use the notation $u' = u - U$ to refer to the velocities after rotation into principal axes, where u is the instantaneous velocity along the principal horizontal axis, U is the average velocity over each six-minute burst, and u' is the fluctuation from the burst average.

Before calculating burst averages and fluctuating velocities within each burst, I first removed some suspect data points from the record. All three velocity components (u, v, and w) were removed from a burst if either instantaneous horizontal velocity measurement differed by more than 0.03 m/s from the median burst value. The remaining data points were used to calculate U and u'. Then, I used the fluctuating velocities to calculate the three components of the burst-averaged Reynolds stress tensor, $\tau_{1,3} = -\rho\overline{u'w'}$, $\tau_{2,3} = -\rho\overline{v'w'}$, and $\tau_{1,2} = -\rho\overline{u'v'}$. The turbulent transfer of momentum from horizontal to vertical is represented by a bed stress that that is the vector sum of two of these Reynolds stress components:

$$\tau_{bed} = \left((\tau_{1,3})^2 + (\tau_{2,3})^2\right)^{1/2} \qquad (2\text{-}10)$$

The third component, $\tau_{1,2}$, is a horizontal momentum flux that is not directly relevant here. Assuming the ADV is sensing the bottom boundary layer, the scaling $\tau_{bed} = \rho(u^*_{bed})^2$ can be used to translate the Reynolds stress into a shear velocity. Thus,

$$u^*_{bed} = \left(\left(\overline{u'w'}\right)^2 + \left(\overline{v'w'}\right)^2 \right)^{1/4} \quad (2\text{-}11)$$

An alternative method of calculating Reynolds stresses was developed by Shaw and Trowbridge (2001) specifically to remove interference from waves; they define the turbulent shear stress as

$$u^*_{cov} = \tfrac{1}{2}\,\text{covariance}(\Delta U, \Delta W) \quad (2\text{-}12)$$

where U and W are total (not fluctuating) velocities at two closely spaced locations – in this case, the upper and lower ADVs.

To look at trends in the burst-averaged data on time scales of hours to days, I applied some simple spectral analysis techniques. This analysis used Welch's averaged, modified periodogram method to calculate the power spectral density, with block averaging and a block size of 64 data points (~2.7 days) and smoothing with a Hamming window of 50% overlap.

In addition to averaging over the hourly bursts, I also looked within each burst for evidence of shorter time-scale processes like wind waves and turbulent mixing. For spectral analysis of u' and cospectral analysis of u' and w' within a burst, I used detrended raw data (no suspect data points removed) so as to have a continuous time record. I then used the spectral power of u' to estimate dissipation by identifying the inertial subrange and applying Kolmogorov's law. This method uses the following formulae:

$$E_{uu}(k) = C\varepsilon^{2/3}K^{-5/3} \quad (2\text{-}13)$$

where $E_{uu}(k)$ is the wave number power spectra in the inertial subrange, C is a constant equal to 0.5, ε is dissipation, and K is the wave number (Nezu and Nakagawa 1993). The power spectra is converted from time to space by applying the frozen turbulence hypothesis, $E(k) = U/(2\pi)\,S_{uu}(f)$, where $S_{uu}(f)$ is the power spectral density in frequency space. Eq. 2-13 can then be rearranged to solve for the intercept of the best-fit line through the inertial subrange, y_0, which is related to dissipation ε by the formula

$$\varepsilon = \left[\frac{10^{y_0}}{C} \left(\frac{2\pi}{U} \right)^{2/3} \right]^{3/2} \quad (2\text{-}14)$$

This dissipation value can be used to estimate a shear velocity in the bottom boundary layer via the relationship below, where z_{sensor} is the distance of the sensor to the bottom boundary (0.2 m):

$$u^*_{dissipation} = (\varepsilon\,\kappa\,z_{sensor})^{1/3} \quad (2\text{-}15)$$

The method above requires a definition of the spectral band for the inertial subrange of the velocity spectra being analyzed. I defined the inertial subrange as beginning at 0.1 Hz, since the maximum size of turbulent eddies is constrained by z_{sensor}. Dividing a typical average velocity by this length scale, the minimum frequency becomes U/z_{sensor} = (0.02 m/s)/(0.2 m) = 0.1 Hz (Talke 2005). I defined the maximum frequency of the inertial subrange as either 1 Hz, 1.3 Hz, or 2 Hz, depending on the location of the noise floor in each burst and whether or not waves were present. Before fitting a regression line to slope of the power spectra, I removed points in the wind wave band (0.6 – 1.3 Hz) if a prominent wave peak appeared in this range. This wave filtering applied only to a fraction of bursts (e.g., 114 of 494 for July 2007). A set slope of –5/3 was not enforced, but dissipation values were not used if the slope varied outside of the range –0.9 to –2.4, or if the r^2 value of the fit was less than 0.7. These criteria resulted in a loss of many data points, particularly for low-energy bursts in January and April 2008, where over half the burst spectral density diagrams did not show a clear inertial subrange.

2.2.2 Acoustic Doppler Current Profiler

For the April 2008 experiment only, I deployed an Acoustic Doppler Current Profiler (ADCP) near the center of the lagoon (Fig. 2-2). The RD Instruments Workhorse Monitor 1200-kHz broadband ADCP operated in "Mode 11," a pulse-to-pulse coherent mode intended to produce low-noise velocities in low-flow situations where fine vertical resolution is desired (RD Instruments 2003). It was mounted on a flat metal plate looking upwards into the water column, as shown in Fig. 2-8. This configuration was also attempted in the July 2007 and January 2008 experiments, but no data was successfully collected.

The ADCP sampled continuously for 8 minutes every hour at 2.5 Hz, which was the instrument's maximum possible ping rate for the depth of about 2 m. The vertical cell spacing was 0.05 m,

Fig. 2-8. Approximate deployment configuration for the RDI 1200-kHz ADCP in April 2008, mounted upward-looking on a flat plate. The battery pack orientation differed from that shown here.

and the first bin of ADCP data was discarded to allow for proper blanking distance. Since the ADCP and mounting plate are together 21 cm tall, the first observed velocities are 0.36 m above the bed. Pressure sensor data from the ADCP was used to eliminate any spurious information collected above the actual water surface.

ADCP data was collected in instrument (XYZ) coordinates with no averaging while the "variance method" of Stacey et al. (1999a) uses velocity data collected in beam coordinates, so a transformation from instrument to beam coordinates was required. The formula is $X = \boldsymbol{T}b$, where X are the four velocities in instrument coordinates (u, v, w, and error velocity), b are the four beam velocities (u_1, u_2, u_3, and u_4), and $\boldsymbol{T}$ is the transformation matrix:

$\boldsymbol{T}$ = [a –a 0 0; 0 0 –a a; b b b b; d d –d –d] (2-16)
where a = 1/(2 sin θ), b = 1/(4 cos θ) and d = (a/$\sqrt{2}$)

$\theta = 20°$ in eqs. 2-16 and 2-17 due to the configuration of the ADCP sensor head.

The velocity uncertainty for a single ping as reported by instrument software was 0.0134 m s^{-1}, but since I averaged velocities over 1200 pings (2.5 Hz * 8 min * 60 seconds min^{-1}), the uncertainty for the burst-averaged velocity U is considerably lower. Fugate and Chant (2005) estimated the instrument noise from a similarly configured ADCP as the difference between the variance at lag = 0 s and the autocovariance at the smallest lag (0.4 s in this case). Applying this method to my data, the instrument noise ranges from approximately $1–3\times10^{-5}$ m s^{-1}, or about two orders of magnitude lower than the observed mean velocities. Thus, I can be certain that the average velocities are well above the instrument noise floor.

I used the method of Stacey et al. (1999a) to calculate Reynolds stresses according to the following formulae:

$$u'w' = \frac{\overline{(u_4')^2} - \overline{(u_3')^2}}{4\sin\theta\cos\theta} \quad \text{and} \quad v'w' = \frac{\overline{(u_1')^2} - \overline{(u_2')^2}}{4\sin\theta\cos\theta} \tag{2-17}$$

Mean shear can be defined either as a gradient in the mean velocity profile, $\partial U/\partial z$, or as a time average of instantaneous velocity gradients, $\langle \partial u/\partial z \rangle$. By the second definition, there is also strong shear very near the surface, but this is probably due to surface waves rather than mean shear. Therefore, the first definition is applied here.

Shear is of interest here because shear production is one of two source terms in the turbulent kinetic energy budget. Total shear production, which represents the conversion of mean kinetic energy into turbulent kinetic energy (Kundu 1990), is the sum of its two lateral components:

$$P = -\overline{u'w'}\frac{\partial U}{\partial z} - \overline{v'w'}\frac{\partial V}{\partial z} \tag{2-18}$$

Analysis of the ADCP data to identify wind waves used Welch's averaged, modified periodogram method to calculate the power spectral density. This method uses smoothing via a Hamming window of 150 data points (6.25 days) with 50% overlap between windows.

2.2.3 Temperature microstructure

I deployed a Self-Contained Autonomous MicroProfiler (SCAMP, Precision Measurement Engineering; Head 1983) to measure temperature microstructure in the lagoon on multiple days during each experiment. On each day, I collected between 30 and 62 profiles in the main lagoon basin (Table 2-2). These measurements provide the only record of turbulent mixing parameters throughout the water column during all three experiments in July 2007, January 2008, and April 2008. This is because ADV measurements are spatially limited to the bottom boundary, while ADCP data is only available for April 2008. In addition to providing a way to estimate turbulent mixing rates, the microstructure profiling provides detailed information about stratification in the lagoon that is not well-resolved by other types of CTD casts.

Rodeo Lagoon is among the most shallow water bodies ever sampled with this microstructure profiler, which required adaptations for handling the instrument. The SCAMP was used in downward profiling mode and was lowered through the water column on a rigid pole at approximately 10 cm s^{-1} rather than drifting on a tethered line, which is the more typical mode of operation (Fig. 2-9). I ensured a smooth descent at the appropriate velocity by marking the pole in 10-cm sections and lowering one section per second. The pole apparatus was used to ensure

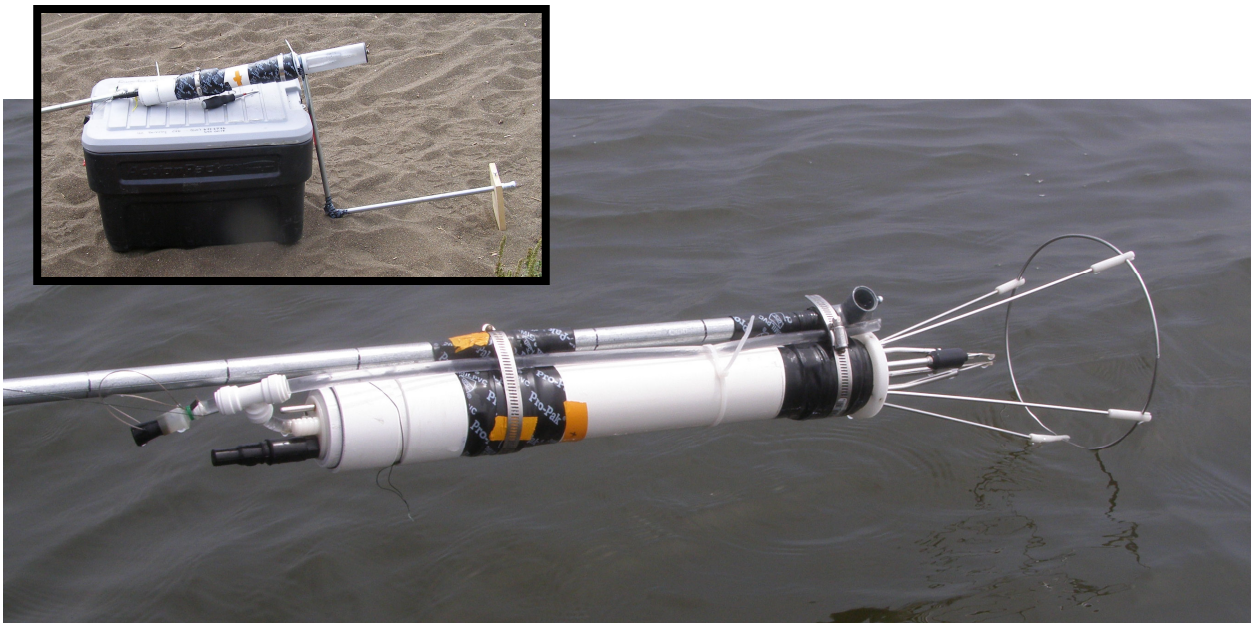

Fig. 2-9. The SCAMP was mounted to a rigid pole for deployment in the very shallow water of Rodeo Lagoon. 10-cm increments are marked on the pole that was used to aid in lowering the instrument at the proper velocity (10 cm s^{-2}). Flexible tubing was used to extend the pressure sensor. Top left, the instrument is shown with its protective wood plate attachment, which was used on three days of sampling. The orientation used for profiling is 90° clockwise of the orientation shown here.

.

that the instrument's delicate end sensors would not be damaged by contact with soft sediments at the bottom of the lagoon, while at the same time allowing the instrument to be used relatively close to the bed.

Using small flexible tubing, I extended the pressure sensor from the top of the instrument to the sensor end so as to allow data collection nearer to the surface than would otherwise be possible: the instrument is about 0.7 m in length, and the water column was less than 2 m deep during sampling in July 2007 (Fig. 2-9). I also used a small (14 cm x 19 cm) wood plate, offset from the sensor tip by about 30 cm vertically and 55 cm horizontally, to protect the instrument in July 2007 and on the first ten profiles collected on 15 January 2008.

The instrument's sampling rate of 100 Hz combined with a drop velocity of 10 cm/s leads to a spatial resolution of about 1 mm. All profiles were trimmed to include only the data collected when the instrument was traveling downward at approximately 10 cm s^{-1} because Taylor's "frozen turbulence" hypothesis does not apply at low velocities.

Table 2-2 lists the days that I collected SCAMP profiles. As noted below, I also collected longitudinal transects similar to those collected with the Sea-Bird instrument package on 16 January, 21 January, and 17 April 2008 (Fig. 2-2). For the purposes of the temperature microstructure analysis, the "center" of the lagoon is defined as all profiles conducted at stations 5 through 11, as listed in Table 2-1.

Date	Stratified by salt	Number of profiles collected near lagoon center	Other activities
11 Jul 2007	No	32	
18 Jul 2007	No	60	
15 Jan 2008	Yes	39	
16 Jan 2008	Yes	43	Long. transect
17 Jan 2008	Yes	42	Long. transect
18 Jan 2008	Yes	62	
14 Apr 2008	Yes	30	
17 Apr 2008	Yes	47	Long. transect

Table 2-2. Settings for SCAMP data collection and processing.

Because of the small size of the boat used for profiling, the SCAMP was used in its autonomous mode. In this mode, data could not be monitored in real time, which made it somewhat difficult to optimize the temperature gradient gain settings.

2.2.4 Moored CTDs

Moored conductivity-temperature-depth sensors (CTDs) (XR-420, RBR), logging every 30 minutes, were placed near the center of the lagoon for most of April through December 2007, collecting data near the surface and bottom on a total of 195 days (Fig. 2-1). In addition, the Sea-Bird 19+ package described in §2.1.1 was moored near the center for 27 days in November 2006.

During the January 2008 experiment, I also deployed near the lagoon center a vertical array of 15 thermistors (SBE 39, Sea-Bird Electronics) sampling every 90 seconds, as well as four additional moored CTDs (SBE 37, Sea-Bird Electronics).

Data from the moored CTDs were combined to provide information about the evolution of the density structure in space and time, as described below.

2.2.4.1 Density structure

Calculating the squared buoyancy frequency, N^2, requires two or more point estimates of density in the water column to define $\partial\rho/\partial z$. In some cases, only the minimum two points are available; in others, as for the SCAMP, hundreds of points are available to define N^2. N^2 is an input variable for some calculations (e.g., K_ρ) and a basis for comparison with other hydrodynamic variables (e.g., u^*_{bed}). The particulars of the calculation in each case were subject to data availability, as described below.

For the comparison in §4.2.1 with hourly estimates of u^*_{bed} and $u^*_{wind,}$ I calculated hourly values of N^2 using just two point values of density, one near the surface and one near the bottom. Density data are derived from the moored CTDs located at the center of the lagoon during each experiment.

$N^2(z,t)$ is a critical component in the calculations of $K_\rho(z,t)$ of §4.4.2. For these calculations, which are for the April 2008 experiment only, I needed a record of $N^2(z,t)$ with temporal and spatial resolution comparable to the ADCP data, which has 5-cm bins and one-hour bursts. Since the moored CTDs alone do not provide this spatial resolution, I constructed a record of $N^2(z,t)$ that combines the moored CTD data with information from higher-resolution profiles conducted on 20 March 2008 (Sea-Bird 19+), 14 April 2008 (SCAMP), and 17 April 2008 (SCAMP). These profiles were used to design typical shape functions for $\rho(z)$ and $N^2(z)$ near the pycnocline.

For the times between these higher-resolution profiles, I inferred the actual location of the pycnocline using the acoustic backscatter signal (also called beam intensity) from the ADCP. The sharp density interface of the pycnocline coincided with a local maximum in the ADCP acoustic backscatter signal (Fig 2-10). Although I will not speculate as to the exact method by which the pycnocline produced this peak in acoustic backscatter, others have reported acoustic peaks near density interfaces as a result of enhanced temperature microstructure (e.g., Moum et al. 2003), and double-diffusive microstructure (Lavery and Ross 2007). Regardless of the physical mechanism, the use of acoustic backscatter maxima as a proxy for pycnocline is a common technique, particularly in strongly stratified flows (Farmer and J.D. Smith 1980; Valle-Levinson et al. 2001).

Even in the comparatively well-mixed surface layer, which is defined by its lack of a vertical salinity gradient, mild temperature gradients are present such that $N^2(z)$ is typically greater than zero in April 2008. For times when the top two CTDs indicated a temperature difference consistent with a positive value of N^2 in the surface layer, I used this N^2 value. At times early in the record when there were not two CTDs in the surface layer, $N^2(z,t)$ was set to match a diurnally varying average based on the days later in the experiment for which a surface layer

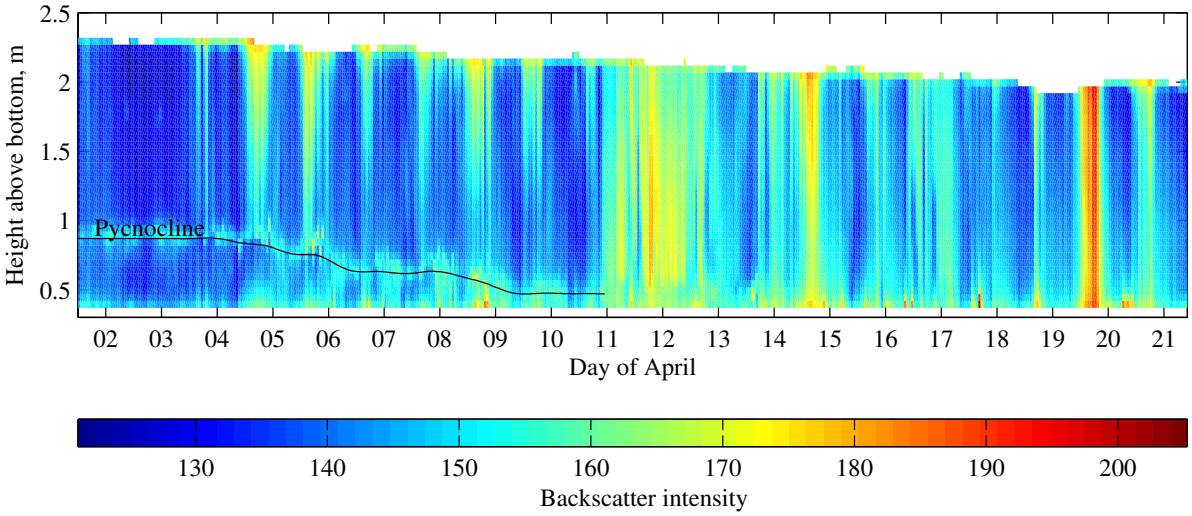

Fig. 2-10. Backscatter from the ADCP in April 2008 was used to infer the location of the pycnocline as it is gradually eroded from above. Backscatter data are the average from all four beams for each burst, with the average mean profile removed.

value of N^2 was available. For times, usually at night, when CTDs in the surface layer indicated an inverse temperature gradient, N^2 was se to 1×10^{-5} s^{-2}; as reported by Jonas et al. (2003), mild stratification can persist in lakes, despite intense cooling. This N^2 value is also approximately equal to the detection limit of temperature differences between the two surface CTDs.

2.2.4.2 Potential energy and potential energy anomaly

Potential energy (*PE*) per unit area of the water column is defined as

$$PE = \int_0^h \rho g z dz = \left(\int_0^{h_0} \rho_S g z dz \right) + \left(\int_0^{h_0} \rho_T g z dz \right) + \left(\int_0^{h(t)} \rho_0 g z dz \right) \quad (2\text{-}19)$$

In the equation above, ρ_S is the density as it reflects time variations in salinity only (i.e., assuming depth and temperature are constant), while ρ_T is the density as it reflects time variations in temperature only (i.e., assuming depth and salinity are constant). The last term includes the contribution of depth changes to *PE*. Total water depth is represented by either a constant h_0 or the time-variable $h(t)$, and z is positive upwards so that z=0 at the bed. In a similar vein, Simpson (1981) defined the potential energy anomaly ϕ:

$$\phi = \frac{1}{h} \int_0^h (\overline{\rho} - \rho) g z \mathrm{d}z \quad (2\text{-}20)$$

where $\overline{\rho}$ is the depth-averaged density. ϕ represents the work per volume required to completely mix the water column.

The chief interest here is changes in PE or ϕ that represent irreversible, diapycnal mixing of salt. PE and ϕ are also strongly influenced by changes in depth and temperature, but these effects can be separated out, as shown below.

$$\frac{\mathrm{d}PE}{\mathrm{d}t} = \frac{\partial}{\partial t}\left(\int_0^h \rho\, g\, z\, dz\right) = \left(\int_0^{h_0} \left.\frac{\partial \rho}{\partial t}\right|_S g\, z\, dz\right) + \left(\int_0^{h_0} \left.\frac{\partial \rho}{\partial t}\right|_T g\, z\, dz\right) + \frac{\partial}{\partial t}\left(\int_0^{h(t)} \rho_0\, g\, z\, dz\right) \qquad (2\text{-}21)$$

where h_0 is the initial depth. The first term represents changes in PE due to salt fluxes (S); the second term, changes in PE due to temperature fluxes (T); and the third term, changes in PE due to depth. Assuming that $\overline{\rho}$ does not substantially change over time, the time derivatives of PE and ϕ are closely related: $\mathrm{d}PE/\mathrm{d}t = -\,h\,\mathrm{d}\phi/\mathrm{d}t$. I continue to use both notations in the discussion below, since both appear in the literature; for example, $\mathrm{d}PE/\mathrm{d}t$ under the name P_{pot} is used in a study of lakes by Wüest et al. (2000), while Burchard et al. (2008) reviewed the calculation of $\mathrm{d}\phi/\mathrm{d}t$ in various estuaries.

The change in potential energy due to the diapycnal mixing of salt, which appears as the first term on the right hand side of eq. 2-21, will be referred to as $\mathrm{d}PE_S/\mathrm{d}t$ for convenience in the discussion below.

For the April 2008 mixing event, I calculated the three terms in eq. 2-21 using the same CTD data used in calculating N^2, with the integrals discretized as a summation of three layers of differing density. The surface layer makes the largest contribution to PE and ϕ, so these summed quantities are not sensitive to the precise location of the interface or even to the density of the lower layer. Because of the weighted contribution of the surface layer density to $\mathrm{d}PE_S/\mathrm{d}t$, it is closely related to the buoyancy flux across the pycnocline into the surface layer, which is defined as:

$$B = \frac{g\,\Delta h_{mix}}{\rho_0}\frac{\partial \rho}{\partial t} \qquad (2\text{-}22)$$

where Δh_{mix} is the depth of the surface mixed layer ($\Delta h_{mix} = h\text{-}h_{pyc}$, with h_{pyc} the height of the pycnocline from the bed). In other words,

$$\frac{\mathrm{d}PE_S}{\mathrm{d}t} = \frac{1}{2}\rho_0 B\left(\frac{h^2 - {h_{pyc}}^2}{\Delta h_{mix}}\right) = \frac{1}{2}\rho_0 B\overline{h} \qquad (2\text{-}23)$$

where $\overline{h}$ is the mean height of the surface mixed layer above the bed.

The instantaneous definitions of PE_S and $\mathrm{d}PE_S/\mathrm{d}t$ are "noisy" in that they are not purely a reflection of irreversible diapycnal mixing. Instead, there are periods where PE_S increases, then subsequently decreases over several hours, which I assume is a baroclinic adjustment to wind forcing (see Fig. 4-11B). Therefore, the reported values have been windowed over 12 hours, from 0700h to 1900h and 1900h to 0700h PDT. The windowing corresponds to periods of either

heating (day) or cooling (night). Although some periods of negative dPE_S/dt remain even after the windowing, the approach is simple and captures quite well the periods of rapid mixing, which are of greatest interest.

2.3 Summary

This chapter describes the field collection methods and preliminary analysis techniques that I used for the data presented in subsequent chapters. Chapter 3 focuses on water quality and is primarily concerned with data from the longitudinal transects (§2.1.1), grab samples (§2.1.2), and to a lesser extent the moored CTDs (§2.2.4.1). Chapter 4 focuses on hydrodynamics (§2.2) and its meteorological forcing (§2.1.3), but these topics are inseparable from the density dynamics described in §2.2.4.1 and §2.2.4.2. Bathymetry and depth information is used throughout the text, but particularly in Chapter 5 with respect to water residence time.

Chapter 3

Water Quality

Recurring fish kills in Rodeo Lagoon over the past few decades motivate the continued study of lagoon water quality and the factors governing its variability. The water quality parameters that have an immediate effect on fish mortality are dissolved oxygen concentrations, un-ionized ammonium, and possibly high temperatures (Martin et al. 2007). Cyanobacterial toxins are also a potential concern for fish mortality, but are outside the scope of this study; a study conducted collaboratively with this one found that microcystin congeners were present in the lagoon in fall 2007, but at concentrations below any established toxicity levels (Drake et al. *in press*).

The water quality parameters that affect fish morbidity and mortality are themselves dependent on a host of other water quality variables, which necessitates taking a broader view of the problem. In fact, during the period of observation (2006-08), phytoplankton biomass and vertical density stratification were the two most important water quality indicators in Rodeo Lagoon. These two parameters exerted a great deal of control on the other water quality variables monitored in this study, which include temperature, turbidity, light availability, dissolved oxygen, pH, and nutrients. Dissolved oxygen is depleted mainly as a result of phytoplankton respiration and decay, so the variables that impact algal growth – namely, light and nutrients – must also be of concern. Turbidity is a relatively less important water quality variable in this context, since it is unlikely to cause fish mortality, but is included because of its effect on the light climate. pH is included because it influences un-ionized ammonia concentrations and internal phosphate loading. A complete database of grab sample water quality can be found in Appendix A.

The two "master variables" of phytoplankton biomass and vertical density stratification are not completely independent of one another, but they are separated temporally: phytoplankton biomass fluctuated most in summer, while vertical density stratification was limited to winter and spring.

3.1 Salinity

Throughout the wet season, it was typical for a lens of brackish water to be present at the bottom of the lagoon (Fig. 3-1), creating very strong vertical gradients in salinity and density that subsequently allowed gradients in temperature, oxygen, and other water quality variables to develop. Steep salinity gradients of 15 psu over less than 30 cm were typical, corresponding to $0.1 < N^2 < 1.0\ s^{-2}$. In contrast to this very strong vertical stratification, in the horizontal direction salinity tended to be homogeneous, with the exception of a small zone (< 100 m lateral extent) of fresher water created by the mixing of inflow from Rodeo Creek. For reference, the salinity of

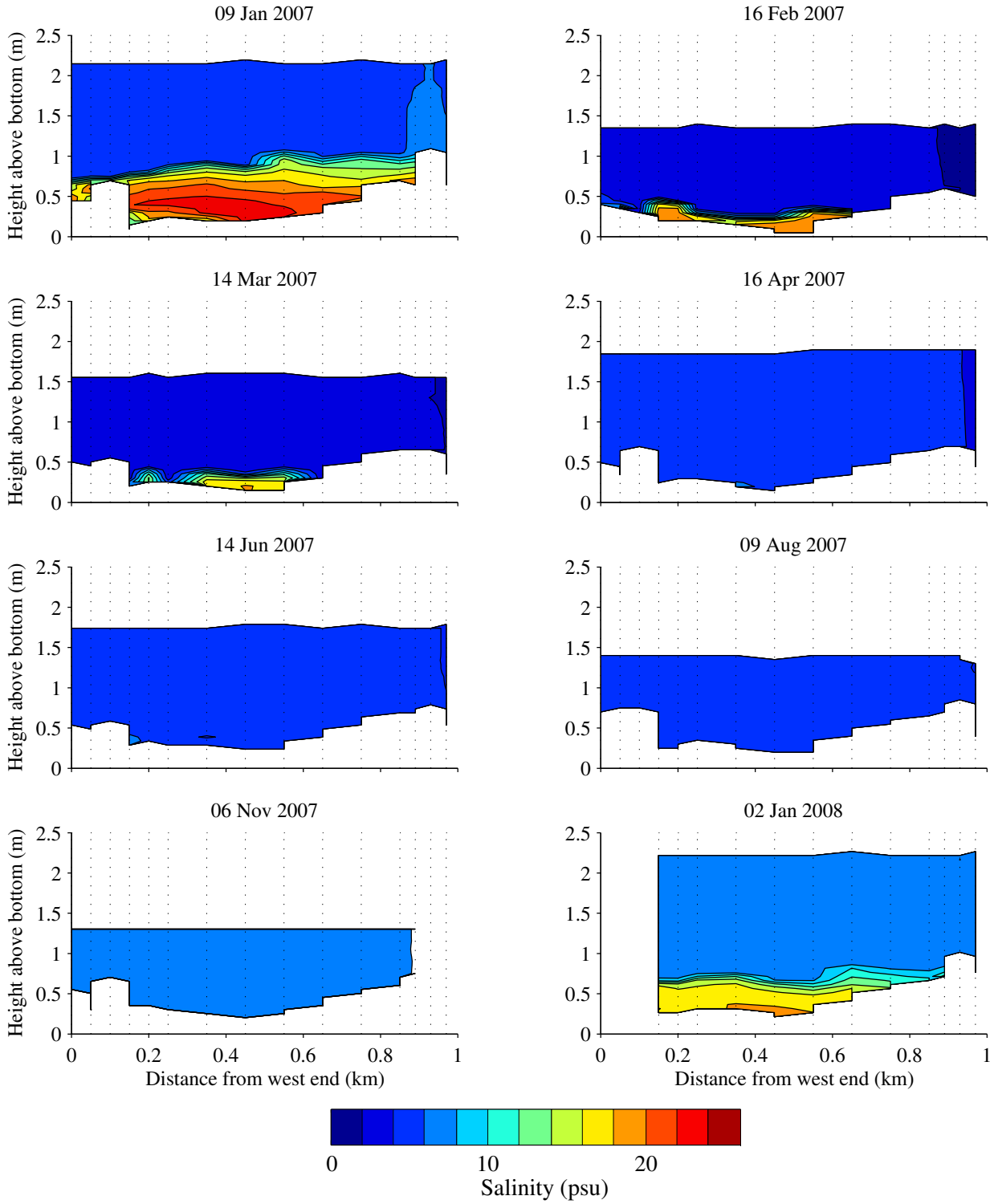

Fig. 3-1. Cross-sections of salinity structure in 2007. Salinity (psu) is from a series of 15 Sea-Bird 19+ profiles collected on each day, as marked. Locations of vertical profiles are indicated by dotted grid lines. Distance along the lagoon's long axis from the pedestrian bridge at the west end (see Fig. 2-2) is indicated by external tick marks.

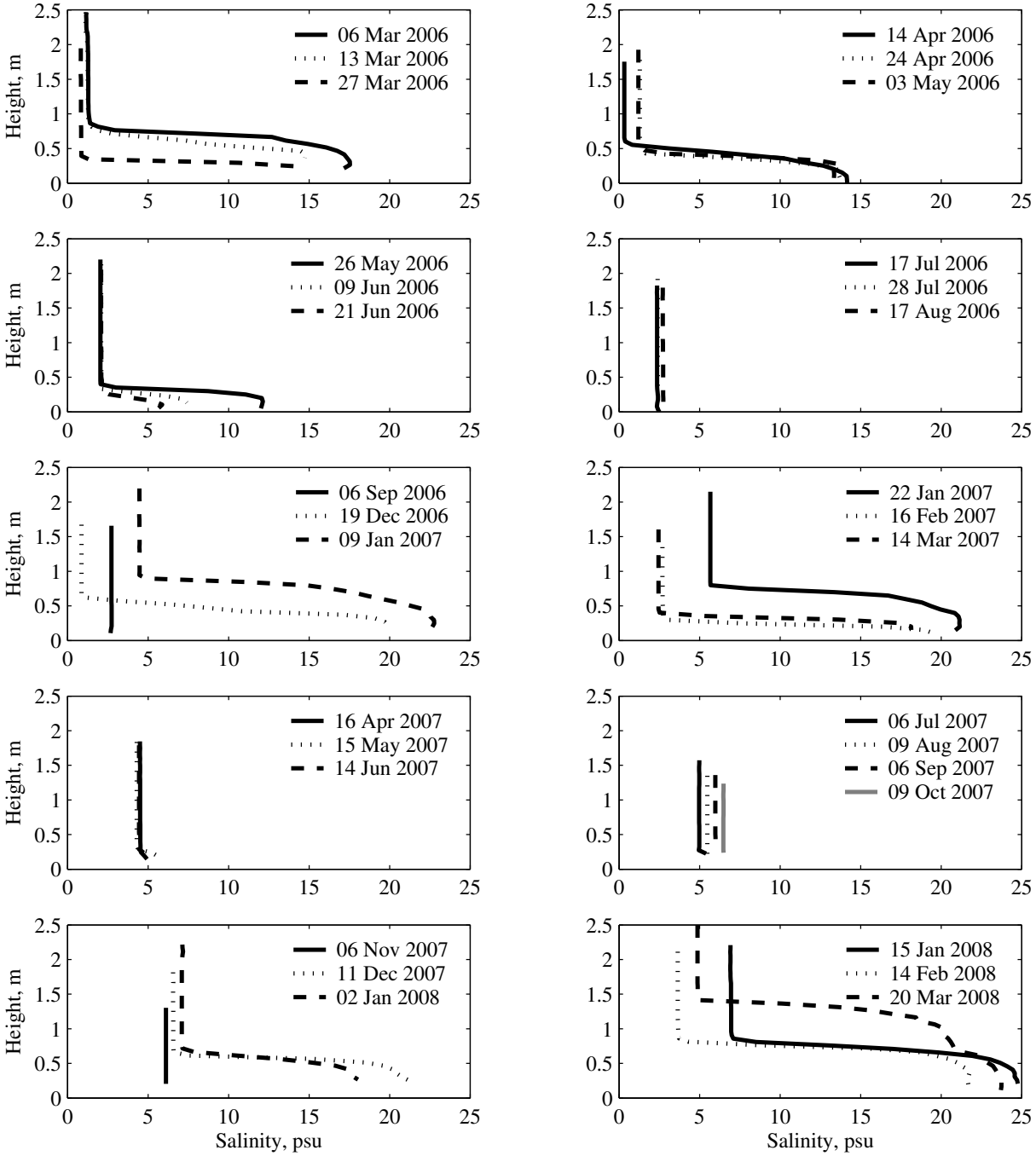

Fig. 3-2. Vertical profiles of salinity structure from March 2006 to March 2008. Salinity (psu) is from Sea-Bird 19+ profiles collected at the lagoon center station on each day, as marked. The center station is 0.45 km from the west end (Figs. 2-2, 3-1).

inflow into the lagoon from Rodeo Lake was always 0.2 psu or less, while the ocean salinity is 35 psu.

Vertical salinity structure near the center of the lagoon, which is representative of most of the main basin, showed pronounced seasonal variability as the brackish layer was formed and eroded (Figs. 3-2, 3-3). Saltwater was able to enter the lagoon during the winter because of the passage of storms over the adjacent Pacific Ocean, which has two related effects (Fig. 2-4). First, these storms generate ocean waves high enough to overtop the beach berm. Second, rainfall associated with winter storms fills the lagoon and hydrostatic pressure then forges an outlet channel through the beach. The presence of well-defined outlet channel reduces distance and height barriers for saltwater to reach the main basin of the lagoon. In the winter of 2006-07, the depth and salinity records suggest that the lagoon was open for the first time of the season in the week of 13 December 2006. In the winter of 2007-08, the lagoon was open for the first time the week of 4 December 2007.

Once brackish water enters, it is retained in the lagoon by the beach berm and a sill located between the main basin and the outlet channel, rather than flowing out. The result was a two-layer density structure of brackish water overlain by fresher water. The most pronounced versions of this vertical structure are shown in profiles collected on 06 March 2006, 09 January 2007, 22 January 2007, and 11 December 2007 through 20 March 2008 (Fig. 3-2).

As the wet season comes to an end, typically in late winter and spring, the outlet closes and the brackish layer slowly mixes into the overlying water column, with new inflows of salt water occurring only intermittently. During this transition interval, the brackish layer decreases both in volume and salinity. Examples of profiles collected during this transition are those from 24 April 2006 through 17 July 2006, and from 16 April 2007 through 06 July 2007. In all these profiles, the brackish layer was less than 0.25 m thick and shrinking over time (Fig. 3-2).

By the arrival of the dry season in early summer, the outlet channel is typically closed, and no further significant inflows of salt water occur, allowing the water column to become well-mixed in terms of salinity (Fig. 3-2, 28 July 2006 to 06 September 2006 and 09 August 2007 to 06

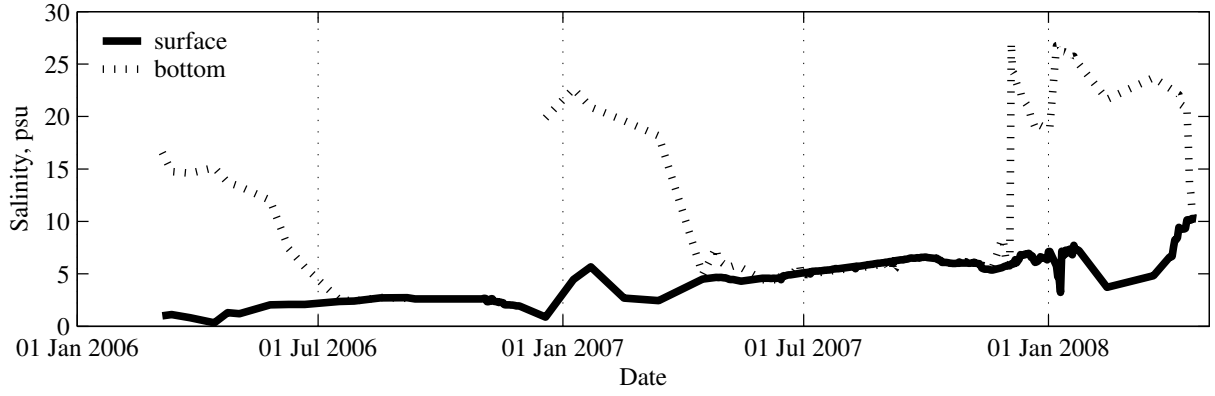

Fig. 3-3. Seasonal evolution of salinity near the surface (solid line) and bottom (dashed line) of the lagoon. Included are data from moored instruments (RBR XR-420 or Sea-Bird 19+) as well as point measurements (Sea-Bird 19+ or YSI 85).

November 2007). With a closed outlet and only limited creek inflow (< 5 L s^{-1}), salinity gradually increased throughout the dry seasons of summer and fall as evaporation exceeded freshwater renewal (Fig. 3-3). This slow increase in salinity was naturally more pronounced in dry years, such as 2007, than in wetter ones like 2006 due to lower creek inflows. Beginning immediately with the arrival of winter storms, this annual cycle of stratification by brackish water repeats itself.

3.2 Temperature

The annual cycle of spring and summer heating and fall cooling is clearly visible in the temperature record of the lagoon (Fig. 3-4). For most of each year, the lagoon was considerably warmer than either the local air temperature, the ocean (which accounts for small inflows in winter), or the lake upstream. The exception to this rule occurs under wet conditions (Fig. 2-4) when lake and lagoon temperatures nearly converged and both were colder than the local air temperature (see, e.g., December and January 2007 in Fig. 3-4). Cold creek inflows, combined with short winter residence times in the lagoon (see Chapter 5) presumably are responsible for this trend.

In summer, net heating was a result of long water residence times combined with solar heating. The simplified annual heat budget shown in Fig. 3-5A indicates that the two main components of the heat budget were shortwave and longwave radiative heat fluxes; latent and sensible heat fluxes played a comparatively minor role. Likewise, heat losses associated with inflows and outflows were not significant; they reduced summer temperatures by only an estimated 2–3°C. Rodeo Lake is shallower than the lagoon and receives similar radiative forcing, so its much cooler summer temperatures (Fig. 3-4) must have been a product of shorter residence times and less efficient light absorption.

Salt stratification controlled the density structure during the winter and early spring, allowing inverse temperature stratification to develop (Fig. 3-6A,B). The lower, insulated brackish layer

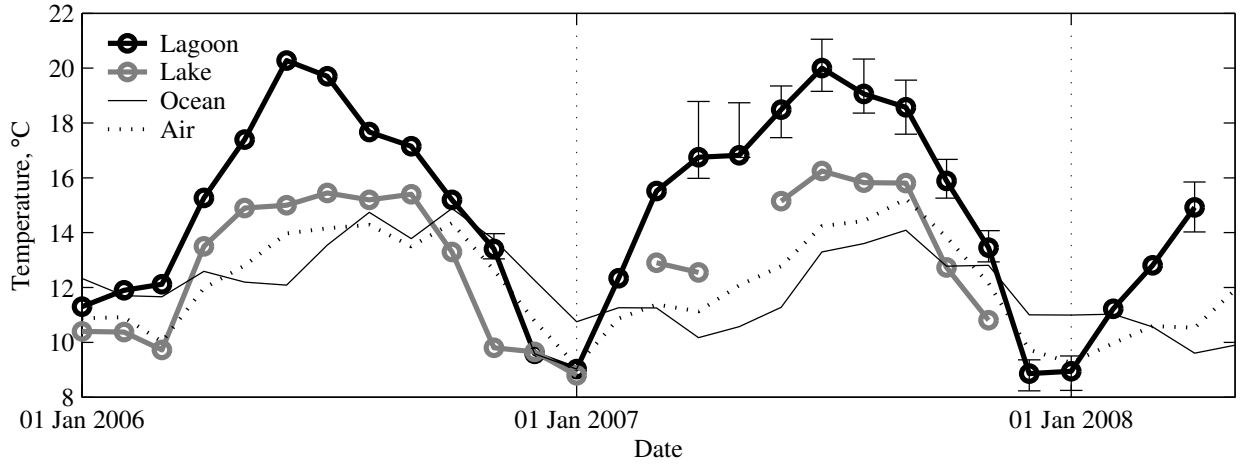

Fig. 3-4. Monthly averaged water temperatures near the surface of Rodeo Lagoon, as well as the lake immediately upstream of the lagoon, the adjacent Pacific Ocean (from ocean buoy 46026), and air temperature at the Golden Gate (NOAA station 9414290). Error bars on lagoon temperatures indicate the diurnal maxima and minima, averaged monthly.

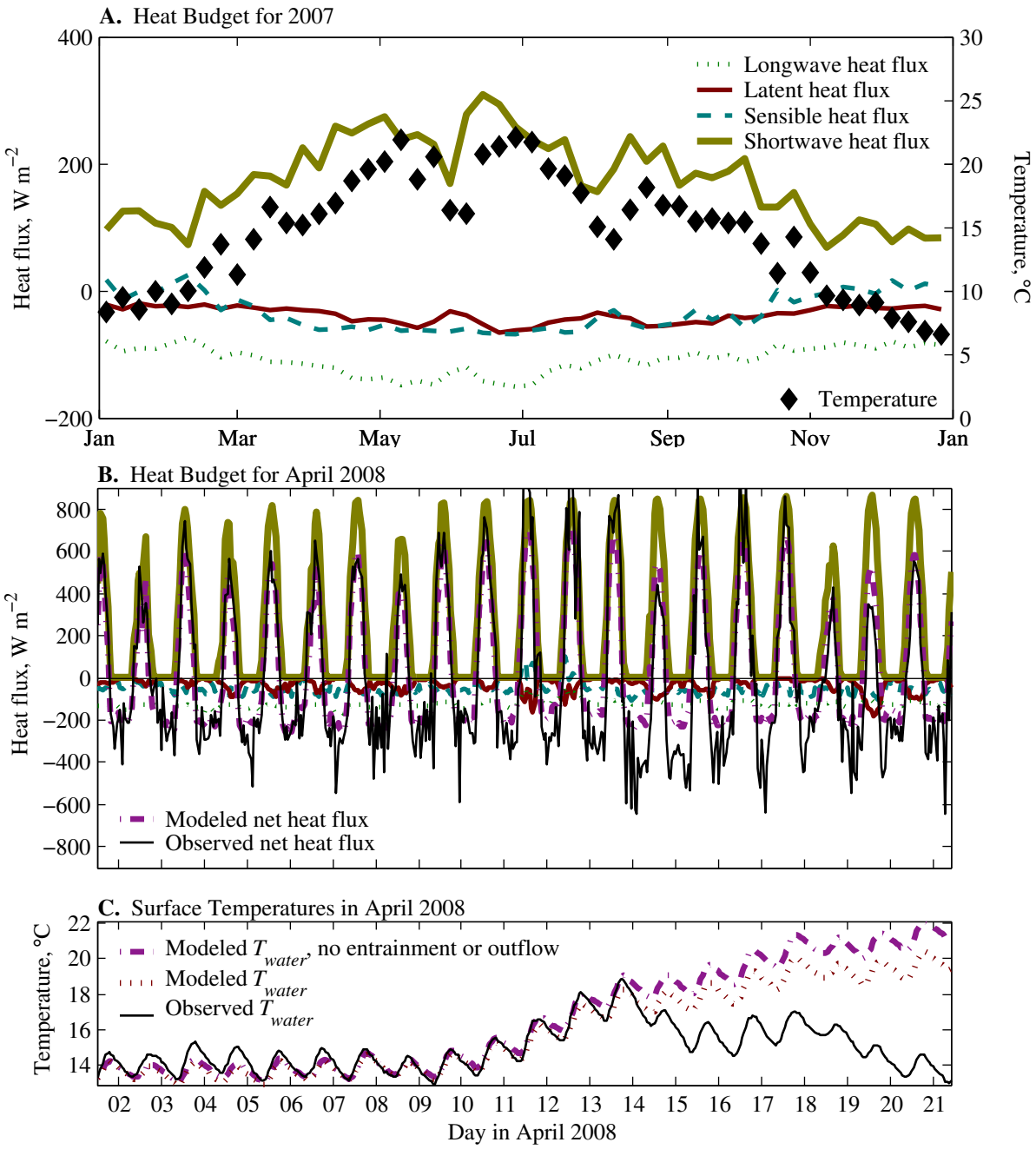

Fig. 3-5. (**A**) Heat budget for 2007 (lines, left axis) and resulting modeled lagoon temperature (black diamonds, right axis). All quantities were calculated on a daily time step, but are shown as weekly averages. (**B**) Hourly heat budget for April 2008. The modeled net heat flux (purple dot-dashed line) is the sum of longwave, latent, sensible, and shortwave heat fluxes, which are shown here with the same symbols as in panel A. The observed net heat flux (solid black line) is calculated as $(dT_{water}/dt)\cdot\rho_w C_p \Delta h_{mix}$. (**C**) Surface temperatures in April 2008 from observations (solid black line), and from the heat budgets including entrainment and outflows (red dotted line) and neglecting entrainment and outflows (purple dot-dashed line). Heat budget calculations for panels A, B, and C are discussed in §2.1.3.2.

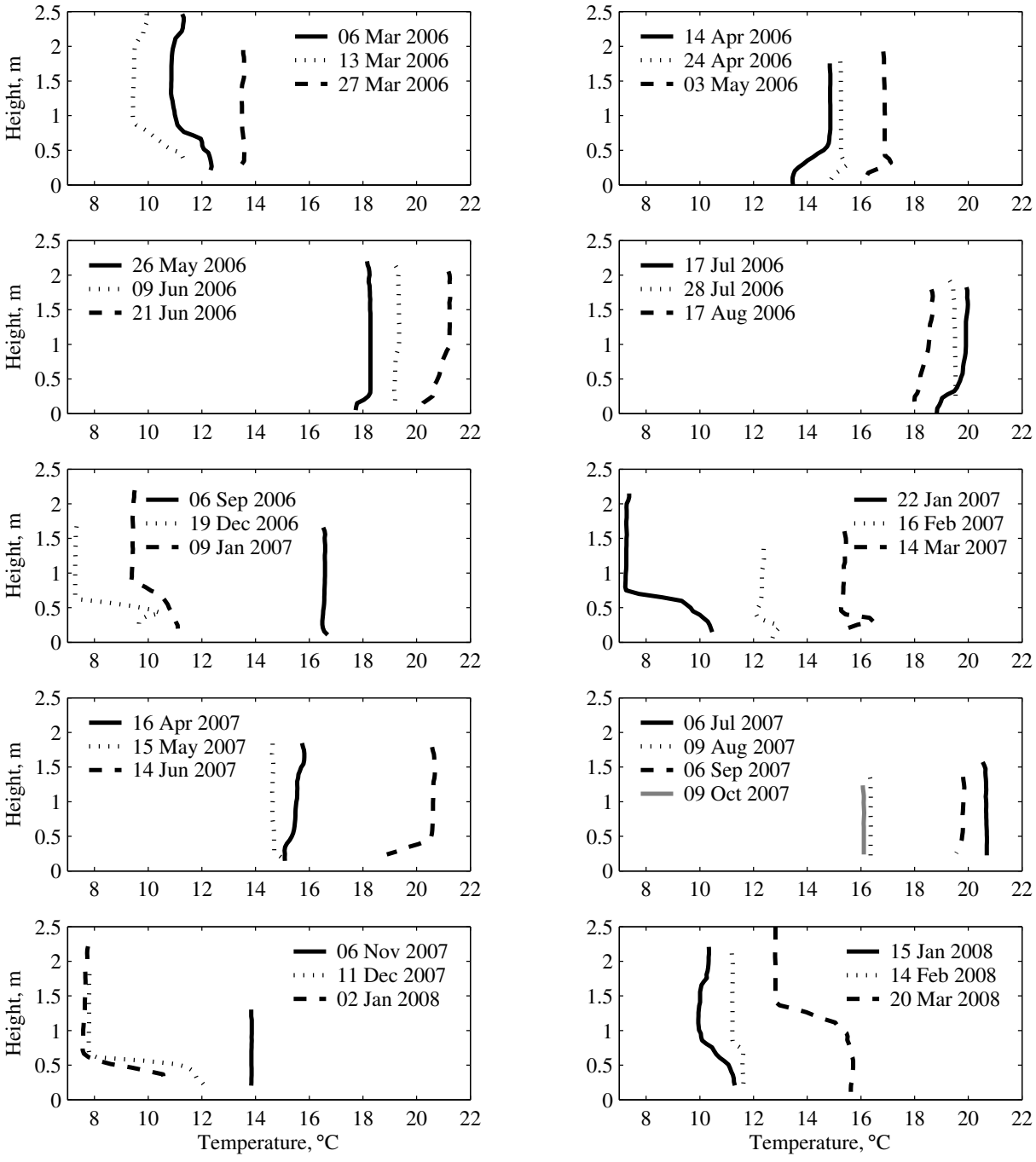

Fig. 3-6. Temperature profiles collected from March 2006 to March 2008 with a Sea-Bird 19+ CTD.

was often warmer than the overlying fresh water, and did not display strong diurnal temperature variations. Although ocean inflows originate at a higher temperature (Fig. 3-4), the vertical temperature gradients in the lagoon would have soon homogenized if they were not maintained by some physical forcing. The factors responsible must include some combination of anaerobic degradation in the sediments, absorption of solar radiation by the very dark-colored sediments, and insulation from radiative losses by the surface layer.

The lagoon showed pronounced diurnal variability both in the surface temperature and in the vertical temperature structure. The diurnal variability in surface temperatures was typically 2–4°C (error bars in Fig. 3-4). The diurnal temperature range clearly reflects local weather forcing; foggy periods in summer are manifested as muted variability of the diurnal temperature record (Fig 3-7). In winter, the actively mixing surface layer, which mostly consisted of cold inflows from the watershed, displayed diurnal temperature variability extending down to the top of the pycnocline (Fig. 4-9), but there was almost no diurnal temperature variability in the salty layer itself.

I constructed an hourly heat budget for the surface layer in April 2008, during which time there are more detailed observations for comparison than for the annual heat budget (Fig. 3-5B,C).

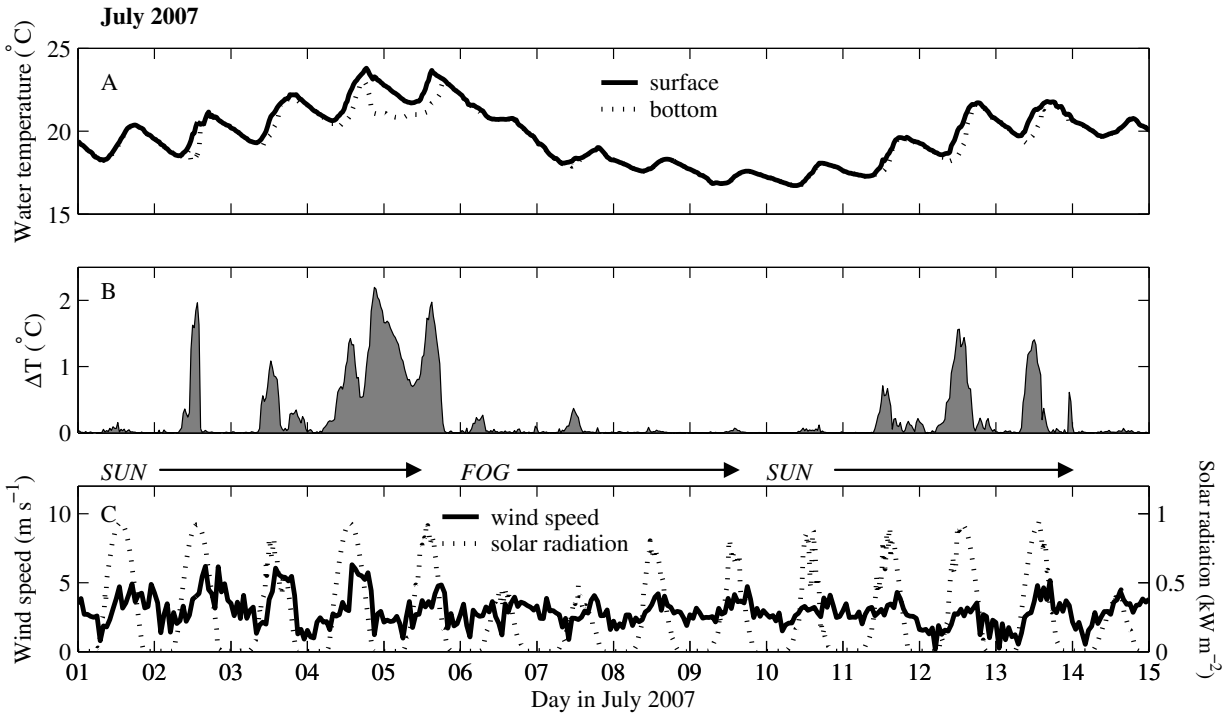

Fig. 3-7. Diurnal fluctuations in (**A**) temperature and (**B**) temperature gradients under uniform salinity conditions in July 2007. Data were collected at the lagoon center station with moored RBR XR-420 CTDs located near the surface (solid line, A) and bottom (dashed line, A), which was about 1.35 deep at the time. (**C**) Meterological forcing includes wind (solid line) and solar radiation (dashed line). Wind data are from the Golden Gate weather station. Periods of fog indicated above (C) correspond to reduced solar radiation and, in some cases, reduced wind speed.

This heat budget includes the diurnal cycle of heating and cooling, which is important for convective mixing. The model seems to have performed reasonably well given the lack of tuneable parameters other than sky cloudiness fraction (eq. 2-5), which was unknown and set to 0 as a way of slightly increasing longwave radiation. The diurnal temperature swing is slightly underestimated (Fig. 3-5C), indicating that both the heating and cooling terms are too small. The model captures quite well the heating that occurred from 10 April to 14 April 2008, though it does not reproduce the subsequent cooling very well (Fig. 3-5C). Overall, the heat budget seems accurate enough for the purposes needed here, which is merely to conduct a scaling comparison of convective cooling and wind forcing (§4.5.2).

Vertical temperature gradients also developed throughout the year in response to diurnal forcing by solar radiation and wind (Fig 3-7C). Sunny days are often windier at Rodeo Lagoon due to sea breeze development, but solar radiation was still sufficient to cause stratification. Temperature stratification during the 2007 dry season, when the lagoon had uniform salinity, commonly reached values as high as 2ºC over a vertical distance of only 1.1 m, corresponding to $N^2 = 5 \times 10^{-3}$ s^{-2} (Fig. 3-7B); the peak value in June 2007 was even higher at $N^2 = 9 \times 10^{-3}$ s^{-2}. Such N^2 values are several orders of magnitude smaller than the density gradients produced by salinity, but occur when there is no salinity structure and are still large enough to have potential significance for phytoplankton growth, particularly for buoyancy-regulating cyanobacteria like the *Microcystis aeruginosa* found here (Sherman and Webster 1994).

The ease with which this very shallow water column achieved strong vertical temperature stratification is due to a combination of two factors: limited energy input for mixing (see §4), and very strong light absorption (see §3.5).

3.3 Phytoplankton biomass

Phytoplankton biomass as represented by Chl *a* concentration varied dramatically over time (Fig. 3-8), and to a lesser extent over the water column. As discussed below, strong vertical gradients in Chl *a* were limited to periods of salt stratification (Fig. 3-9). The vertical distribution of phytoplankton biomass, $B(z,t)$, can be modeled mathematically using the following differential equation (Cloern 1991):

$$\frac{\partial B}{\partial t} = (\mu - r - G)B - \frac{\partial}{\partial z}(w_s B) + \frac{\partial}{\partial z}(K_\rho \frac{\partial B}{\partial z}) \qquad (3\text{-}1)$$

In the equation above, μ is the light-dependent specific growth rate, r is the specific respiration rate, G is the loss rate to zooplankton grazing, w_s is the sinking speed of phytoplankton, and K_ρ is the vertical scalar diffusivity. Contributions to net growth may be grouped into one constant, $\mu_{net} = (\mu - r - G)$. Depending on the relative balance of terms in eq. 3-1, the dominant mode of variability may be in time (§3.3.1) or space (§3.3.2).

A term of the form $-U(\partial B/\partial x)$ may be added to eq. 3-1 to represent advection, but since both velocities (§4.2) and horizontal gradients in Chl *a* (Drake 2008) were small, this term was likely negligible except during winter wet weather, when losses due to flushing would have been significant. Indeed, Chl *a* reached its minimum values at this time of year (Fig. 3-8A).

Chl *a* was measured using laboratory extractions of biomass (§2.1.2) and *in situ* fluorescence (§2.1.1). Lagoon-averaged *in situ* Chl *a* fluorescence as measured with the SCUFA (Fig. 3-8A, open diamonds) somewhat tracked the trend of Chl *a* biomass. The *in situ* Chl *a* fluorescence is only properly reported after calibrating with biomass, and a priori these cannot be assumed to track one another. Under peak biomass conditions the SCUFA sensor voltage reached its maximum value (100 relative fluorescence units, or RFU) a problem which contributes to the mismatch between *in situ* Chl *a* fluorescence and laboratory-extracted Chl *a* concentrations. Even if *in situ* Chl *a* fluorescence cannot be used as a reliable marker of seasonal trends, however, it does reveal interesting spatial trends in the phytoplankton population for any given sampling day, when the fluorescence-biomass relationship of the phytoplankton is assumed to follow a linear relationship. These spatial trends are discussed below in §3.3.2, and data in Fig. 3-9 are a combination of *in situ* fluorescence calibrated by laboratory extractions via a least-squares fit.

I have not corrected the *in situ* Chl *a* fluorescence data for photoinhibition, the process in which bright solar radiation suppresses photosynthesis near the surface (Vincent et al. 1984; Long et al. 1994). The lack of consistent near-surface minima in the Chl *a* profiles, the high levels of light extinction in the water column, and lack of a diurnal signal in the *in-situ* fluorescence data from November 2006 are the basis for this assumption (Hambrook Berkman and Canova 2007).

3.3.1 Seasonal variability

Rodeo Lagoon is a hypereutrophic system with a phytoplankton biomass peak in late summer, when little surface inflow occurs and the lagoon is well-mixed in terms of salt. The scalar diffusivity is sufficiently large at this time of year (see §4.4.2) that strong vertical gradients in Chl *a* do not develop. In both 2006 and 2007, the summer dry season lasted from May to October; during this time, the lagoon acted as a closed system with virtually no loss of phytoplankton due to flushing. Phytoplankton that sink to the bottom can be resuspended into the photic zone within a day by turbulent diffusion, since the observed K_ρ value of ~3×10^{-5} m^2 s^{-1} and a water depth of 1.5 m correspond to a characteristic time for diffusion of 21 hours ($t \sim h^2/K_\rho$). During well-mixed summer conditions, therefore, the balance in eq. 3-1 is between unsteadiness and net growth, reflecting a changing seasonal balance among growth, respiration, and grazing.

The peak observed Chl *a* concentration in summer 2006 was 257 μg L^{-1} in late July, although the actual concentration could have been even higher – the sampling regimen was admittedly rather sparse. The peak Chl *a* concentration in summer 2007, when weekly samples were collected, reached an astonishingly high 1043 μg L^{-1} in late August (Fig. 3-8A, black squares). These Chl *a* concentrations are an order of magnitude higher than the Chl *a* criterion for hypereutrophic status, which is about 100 μg L^{-1} (Vollenweider and Kerekes 1982).

Under well-mixed conditions and neglecting any fluxes at the bed, eq. 3-1 can be depth-averaged to produce an equation for first-order growth:

$$\frac{d\overline{B}}{dt} = \mu_{net}\overline{B} \qquad (3\text{-}2)$$

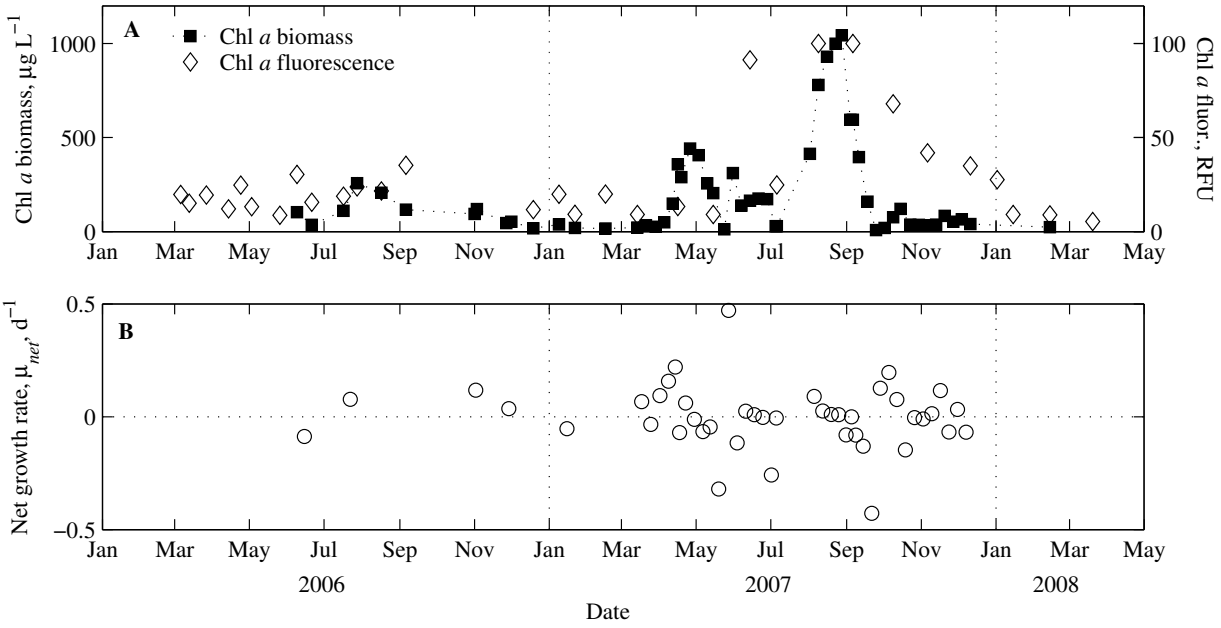

Fig. 3-8. (**A**) Chl *a* biomass (µg L^{-1}, left axis) and uncalibrated fluorescence (relative fluorescence units or RFU, right axis). Biomass values are from laboratory extractions, while fluorescence is a near-surface, lagoon-wide average from the *in-situ* fluorometer (SCUFA) attached to the Sea-Bird 19+ CTD. The uncalibrated Chl *a* fluorescence is pinned to the maximum value of 100 RFU in August and September 2007. (**B**) First-order net growth rate μ_{net} (d^{-1}) calculated from data in panel A using eq. 3-2.

The net growth rate can then be estimated using the Chl *a* data as follows (Cloern 1991):

$$\mu_{\text{net}} = \ln\left(\frac{\overline{B}_j}{\overline{B}_{j-1}}\right) \Big/ \Delta t \qquad (3\text{-}3)$$

where B_j is the mean Chl *a* concentration at the lagoon center station on date *j*, and Δt is the time interval between sampling dates *j-1* and *j*. Data were only used if $\Delta t \leq 14$ days, and μ_{net} ranged from -0.5 d^{-1} to 0.5 d^{-1} over the period of observation (Fig. 3-8B). The exact balance of growth, respiration, and grazing is unknown since these processes were not measured independently. These values are in within the range found in other estuarine systems; for example, Cloern (1991) reported a net growth rate of 0.1–0.25 d^{-1} for South San Francisco Bay, while Robson and Hamilton (2003) reported a maximum net growth rate of 0.35 d^{-1} for *M. aeruginosa* in an Australian estuary. Sustained peak values of μ_{net} in 2007 corresponded to rapid growth of two species of cyanobacteria, *N. spumigena* in April and *M. aeruginosa* in late September (Fig. 3-8B, Drake 2008). The maximum value of μ_{net} in late May 2007 occurred during a rapid population shift from dominance by the cyanobacteria *N. spumigena* to dominance by centric diatoms (Drake 2008). Minima in μ_{net} were associated with this same population shift, as well as shifts from centric diatoms to chlorophytes in early July 2007 and a shift from flagellated protozoa to *M. aeruginosa* in late September 2007 (Drake 2008). Theoretically, the specific growth rate μ should depend jointly on light and nutrient availability, both of which vary seasonally and in

response to phytoplankton biomass, as discussed in §3.5 and §3.8. Indeed, the late August biomass peak of 2007 seems to have resulted from a combination of light and nitrogen limitations, since light extinction reached a maximum (Fig. 3-14) and dissolved nitrogen reached a local minimum (Fig. 3-20) near the time of the Chl *a* peak. Thus, while total biomass was somewhat controlled by the availability of light and nutrients, the seasonal variation in μ_{net} also clearly reflected competition among different species of phytoplankton.

3.3.2 Vertical variability

The observed Chl *a* profiles typically showed an increase with depth under salt-stratified conditions, compared to more uniform structure when the lagoon was well-mixed by salt (Fig. 3-9). When present, the distinctive vertical layering closely reflected the salinity structure, which is consistent with both of the proposed explanations for vertical variability presented above. For example, most of the profiles collected in winter showed a thin layer of elevated Chl *a* just above the pycnocline (19 December 2006, 09 January 2007, 22 January 2007, 16 February 2007). In late spring and early summer, the trend was for elevated Chl *a* very near the bed, coincident with remnants of elevated salinity, although benthic algae could also have been responsible (09 June 2006, 21 June 2006, 15 May 2007, 06 July 2007). In late summer and fall, the vertical distributions of Chl *a* were fairly uniform, as were the salinity distributions (28 July 2006, 17 August 2006, 06 September 2006, 09 October 2007, and 06 November 2007). Several of the vertical profiles are variations on this theme, like that of 11 December 2007 and 14 March 2007, when Chl *a* was elevated both directly above and everywhere below the pycnocline.

The vertical variability in winter and spring (Fig. 3-9) is surprising given the lagoon depth is only about 2 m, and can be attributed to at least two causes (Condie and Bormans 1997):

(**a**) Nutrient supply from the organic-rich bottom sediments. This mechanism acts by increasing the specific phytoplankton growth rate $\mu(z)$ near the bed or pycnocline, where nutrients are more available compared to the surface. The surface maximum in light availability is also expressed through $\mu(z)$, and the product of light and nutrient supply can create a *Chl a* maximum at depth.

(**b**) Gravitational settling of cells. Large values of either the settling velocity w_s or its vertical gradient $\partial w_s/\partial z$ may be responsible (eq. 3-1). When the water column has a surface mixed layer underlain by strong density stratification, the combination of settling and stratification can create a biomass maximum in the pycnocline even if the settling velocity w_s is constant with depth (Condie and Bormans 1997). Furthermore, if w_s is lower beneath the pycnocline, as would be expected due to the increased water density, biomass can accumulate at the top of the pycnocline (e.g., MacIntyre et al. 1995). In either case, density stratification reduces turbulent mixing rates at the bed and prevents settled biomass from being resuspended into the upper water column.

To distinguish between mechanisms (a) and (b) for the available data from Rodeo Lagoon, an estimate of w_s is needed. The settling velocity w_s was not explicitly measured here, but typical settling velocities are on the order of 0.1 to 1.0 m d^{-1} (Burns and Rosa 1980). Significantly larger values have also been observed; for example, settling rates of 30 m d^{-1} were reported for the resting stage of *Chaetoceros* (Passow 1991), a diatom similar to one that dominated Rodeo Lagoon in spring 2007. Also, some phytoplankton like the *M. aeruginosa* found here in summer 2007 can be buoyant with a rising velocity as large as 10 m d^{-1} (Sherman and Webster 1994). A

few profiles in Fig. 3-9 showed a gradual increase in Chl *a* over depth that can be used to roughly estimate the settling rate. Assuming that diffusion and settling were in balance and net growth was small by comparison, an estimate of the settling velocity can be obtained by equating the last two terms of eq. 3-1:

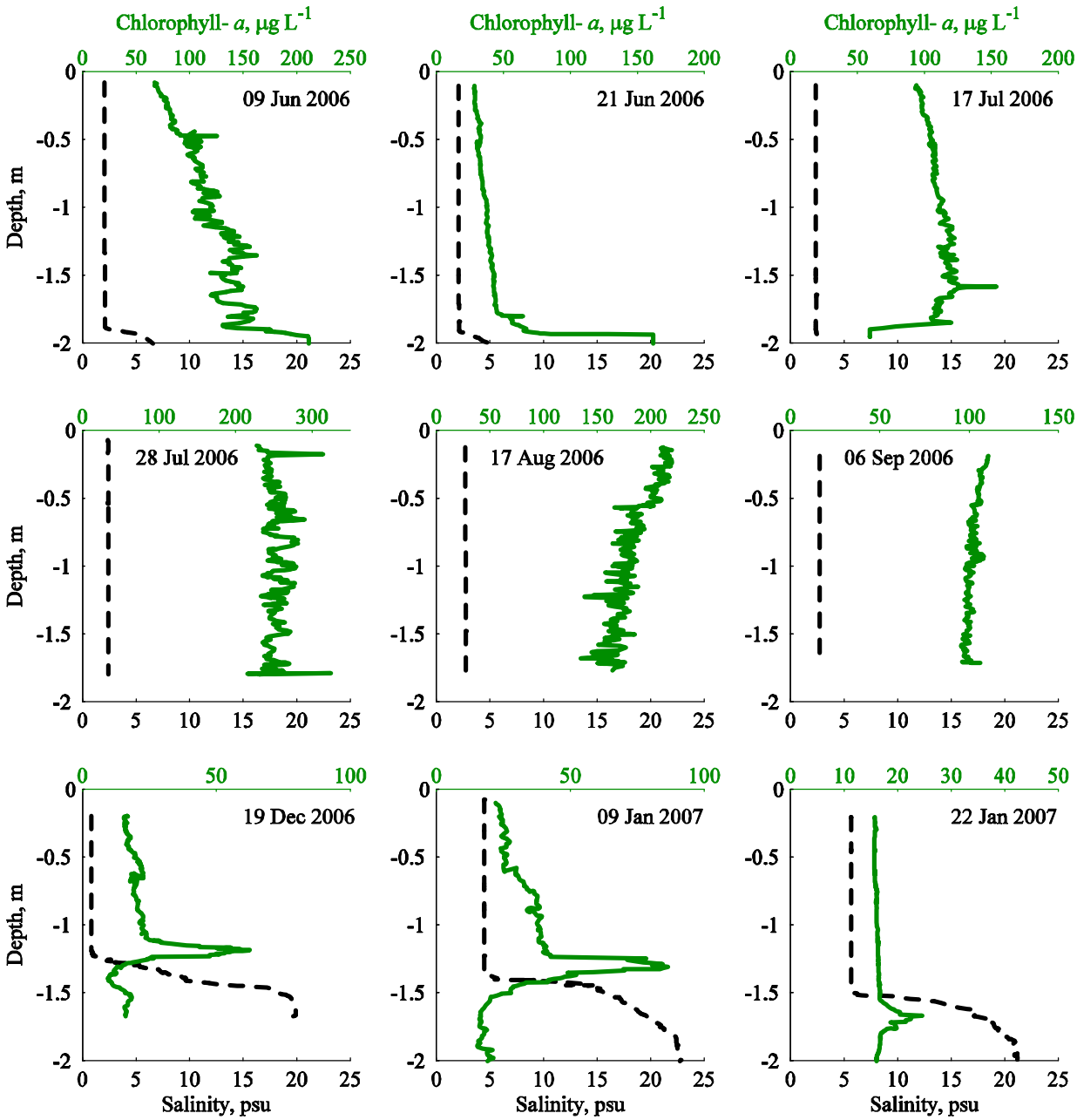

Fig. 3-9A. Vertical profiles of Chl *a* biomass (µg L^{-1}, green line, top axis) and salinity (psu, black dashed line, bottom axis). Chla *a* biomass was calculated by calibrating in-situ fluorescence profiles with point values from grab samples analyzed in the laboratory.

$$w_s = \frac{1}{B} K_\rho \frac{\partial B}{\partial z} \qquad (3\text{-}4)$$

Applying this formula to observations within 1 m of the surface from 09 June 2006, 21 June 2006, 17 July 2006, 09 January 2007, 14 June 2007, and 06 July 2007 (Fig. 3-9) produces a estimate of w_s = 1.5 m d^{-1} for $K_\rho = 3\times10^{-5}$ m^2 s^{-1}, which is in line with typical values.

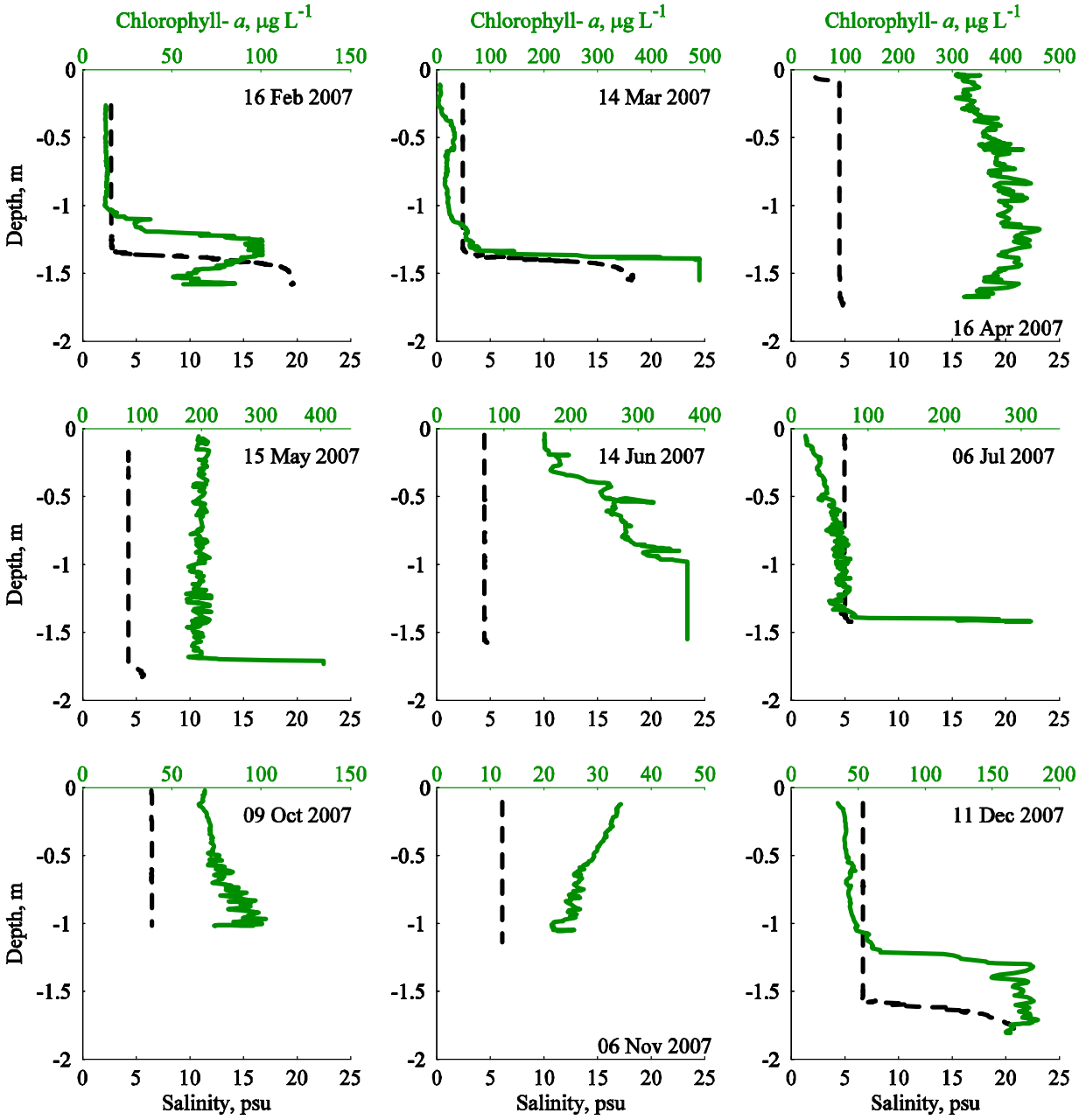

Fig. 3-9B. More vertical profiles of Chl *a* biomass (µg L^{-1}, green line, top axis) and salinity (psu, black dashed line, bottom axis). Chla *a* biomass was calculated by calibrating in-situ fluorescence profiles with point values from grab samples analyzed in the laboratory.

If the same settling rate of 1.5 m d^{-1} applied in and below and the pycnocline, where $K_\rho < 1\times10^{-6}$ m^2 s^{-1}, then settling should have been fast compared to diffusion (Peclet number > 10, where Pe $=h \cdot w_s/K_\rho$ and h = depth). This makes it nearly impossible for settled particles to escape the lower layer by diffusing upwards. Further, the ratio of net growth to settling ($\mu_{net} \cdot h/w_s$) is less than 1 even for the maximum observed net growth rate of 0.5 d^{-1}, which implies that local growth was not responsible for the biomass peaks observed near the bed in Fig. 3-9. For the profiles with a pronounced biomass maximum at the top of the pycnocline (19 December 2006, 09 January 2007, 22 January 2007, 16 February 2007, Fig. 3-9), it seems likely that a change in the gravitational settling rate at the pycnocline is responsible for the shape. An approximate speed for forming such a layer by differential settling is

$$w_{convergence} = \tfrac{1}{2}(w_{s1} - w_{s2}) \qquad (3\text{-}5)$$

where w_{s1} is the settling velocity in the upper mixed layer and w_{s2} is a slower settling velocity in the lower layer. Settling velocity is a function of the excess density of phytoplankton compared to the water density, $\Delta\rho_{excess}$, which ranges from 100–300 kg/m^3 for diatoms; other species have similar values (Eppley et al. 1967; MacIntyre et al. 1995):

$$w_{s1} = \left(k\,\Delta\rho_{excess}\right)^{1/2} \qquad (3\text{-}6)$$

Combining eqs. 3-5 and 3-6 and assuming that in the lower layer $\Delta\rho_{excess}$ is reduced by the density difference across the pycnocline, $\Delta\rho_{pyc}$, gives:

$$w_{convergence} = \frac{1}{2}\left[w_{s1} - \left(\frac{w_{s1}^{\,2}}{\Delta\rho_{excess}} (\Delta\rho_{excess} - \Delta\rho_{pyc}) \right)^{1/2} \right] \qquad (3\text{-}7)$$

On the dates that a thin layer above the pycnocline was observed, $\Delta\rho_{pyc}$ exceeded 10 kg m^{-3} (Fig.

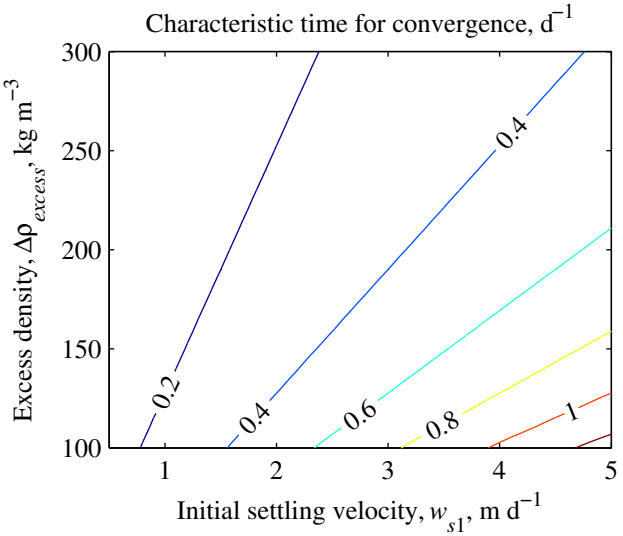

Fig. 3-10. Characteristic time for convergence of biomass due to differential settling across the pycnocline, calculated from eq. 3-7 using a range of values for the initial settling velocities w_{s1} and excess density $\Delta\rho_{excess}$. Shown here is $w_{convergence}/L$, where L is a layer depth of 0.1 m.

3-2). Results from eq. 3-7 for a range of initial settling velocities and excess densities are shown in Fig. 3-10. The net growth rate rarely exceeded 0.2 d^{-1}, which is smaller than most of the values of $w_{convergence}/L$ in Fig. 3-10 . Since the characteristic time for biomass convergence by settling is faster than the net growth rate, then, it seems probable that mechanism (b), specifically a vertical gradient in the settling rate, is responsible for the distinct Chl a peaks at the top of the pycnocline.

In conclusion, phytoplankton biomass varied seasonally as a succession of different species competed for the available light and nutrients. Throughout the summer, when peak biomass values were observed, the phytoplankton distribution was relatively uniform over the water column. However, when the lagoon was stratified by salt in winter and spring, phytoplankton were retained in and below the pycnocline by the effects of gravitational settling combined with density stratification. Table 3-1 lists some of the rates that govern these processes, all of which appear in eq. 3-1.

Parameter	**μ_{net}, net growth rate**	**w_s, settling velocity**	**K_ρ, turbulent diffusivity**
Value	-0.5 to 0.5 d^{-1}	0.5 to 5 m d^{-1}	1×10^{-5} to 1×10^{-4} in surface mixed layer < 1×10^{-6} below pycnocline
Notes	See Fig. 3-8B	Depends on value of K_ρ in surface layer	See Fig. 4-26, §4.4.2 for more detail
Comparison with published values	Within range	Conservatively low	Highly variable due to strong stratification
References	Cloern (1991); Robson and Hamilton (2003); Huisman et al. (2005)	Burns and Rosa (1980); Passow (1991); Sherman and Webster (1994)	Fischer et al. (1979)

Table 3-1. Factors governing phytoplankton biomass growth rates, as listed in eq. 3-1.

3.4 Turbidity

Turbidity, defined here in nephelometric turbidity units (NTU) or the ability to scatter light, is an indication of the concentration of small particles like phytoplankton and sediment. Unfortunately, turbidity measurements offer no good way to distinguish *between* these two types of scatterers, which would be of greater interest. Lagoon-averaged turbidity was highest during times of wet weather, particularly the very wet spring 2006, as well as during peaks in Chl *a* biomass (Figs. 3-11, 3-14).

In the absence of vertical salinity gradients, turbidity and Chl *a* were nearly uniform over the water column. When salinity stratification occurred during the winter months, the usual trend was for turbidity and Chl *a* to show similar vertical variability, regardless of the shape of that profile. For example, on 22 January 2007, turbidity and Chl *a* peaks were both evident within the pycnocline, while on 14 February 2008 turbidity and Chl *a* were larger in the surface layer but smaller in the salty lower layer (see Fig. 3-12A, B). In a few unusual cases, however, the

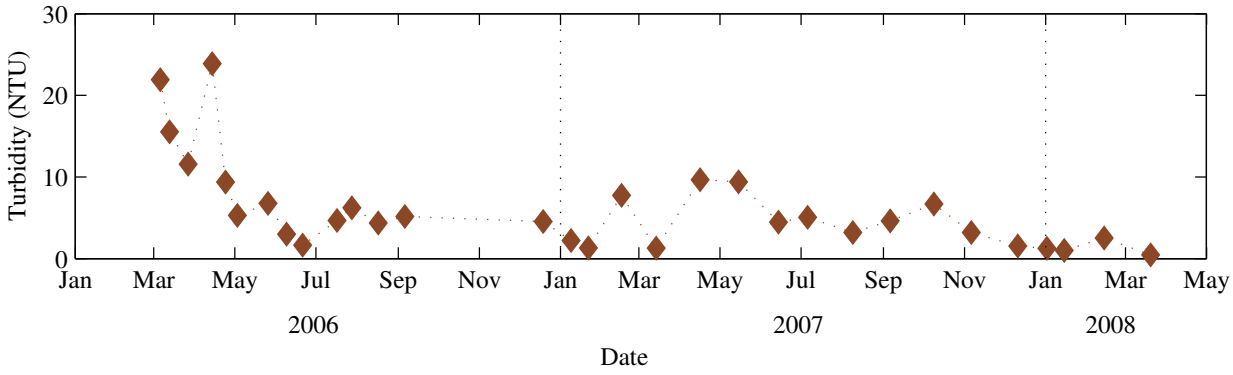

Fig. 3-11. Turbidity in nephelometric turbidity units (NTU). Each point is a lagoon-wide average taken from the longitudinal transect of Sea-Bird 19+ CTD casts.

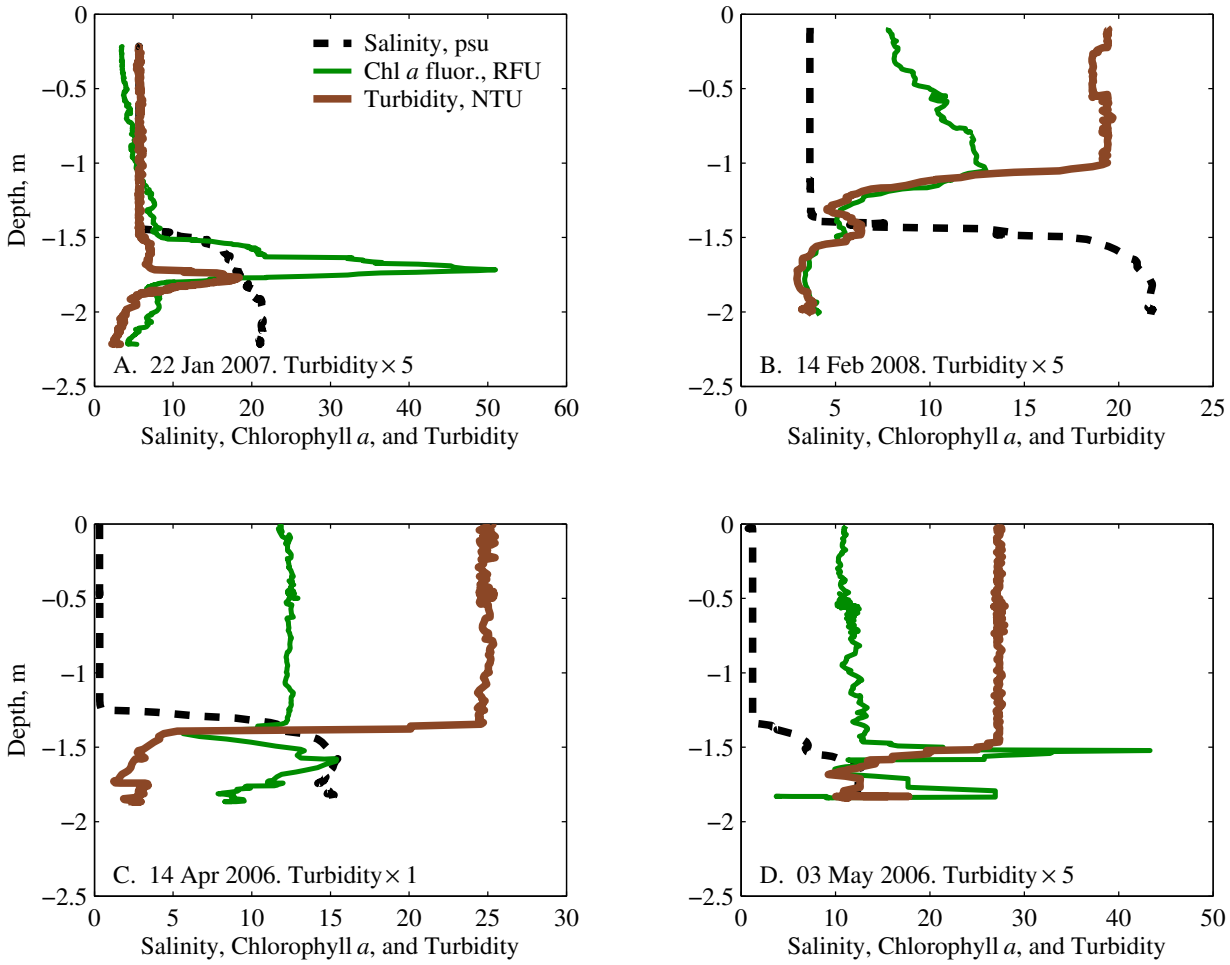

Fig. 3-12. Vertical profiles of salinity (psu), uncalibrated Chl *a* fluoresence (relative fluorescence units, RFU), and turbidity (nephelometric turbidity units, NTU) on (**A**) 22 Jan 2007, (**B**) 14 Feb 2008, (**C**) 14 April 2006, and (**D**) 03 May 2006. Data are from Sea-Bird 19+ CTD casts and are not binned. Turbidity values are multiplied by 5 in panels A, B, and D.

turbidity profile differed from the Chl *a* profile. In April and May 2006, for example, turbidity was greatly reduced in the lower salty layer, but Chl *a* was not (Fig. 3-12C, D). In both of these spring 2006 profiles, there seems to be evidence for reduced turbidity in the salty layer, regardless of the Chl *a* trend. There are two possible explanations for this trend: (a) coagulation and settling of fine particles is more rapid in salt water, and (b) the main source of sediment is from freshwater inflows, so if the particles were slow to settle they would logically be found in the surface layer.

Within the surface layer, it appears that Chl *a* was the main contributor to turbidity, rather than inorganic turbidity being a source of noise in the Chl *a* data. This interference is often a concern in calibrating Chl *a* fluorescence with biomass extractions (Turner Designs 2004), but did not cause problems here.

I measured turbidity at shorter time scales using moored instruments in summer 2006 (SCUFA, Turner Designs) as well as summer 2007, January 2008, and April 2008 (OBS-3, D&A). The ADVs moored 10 and 20 cm from the bed during the hydrodynamics experiments also provide an uncalibrated estimate of suspended sediment concentration through their measurement of acoustic backscatter intensity (Kawanisi and Yokosi 1997). In all cases, I expected to see evidence of sediment resuspension by wind on short time scales, but none of the data mentioned above contained such a signal. For example, in July 2007, when the lagoon was vertically well-mixed, the correlation between wind stress and acoustic backscatter intensity was less than $r^2 = 0.05$. This poor correlation is consistent with the observation that Chl *a*, **not** sediment resuspended from the bed, was the main driver of turbidity.

3.5 Light extinction

The extremely high values of phytoplankton biomass in the lagoon result in efficient absorption of light, quantified here as the scalar quantity Photosynthetically Active Radiation (PAR). Theoretically, PAR (*I*) should decrease exponentially with depth, as follows:

$$I = I_0 e^{-k_e z} \tag{3-8}$$

where I_0 is the value of PAR just below the surface, z is the depth from the surface, and k_e is a light extinction coefficient. I calculated one representative value of k_e for each longitudinal transect by averaging the results of log-linear fits to each of fourteen profiles of $I(z)$; profiles of $I(z)$ at the far eastern end of the lagoon were excluded due to the strong influence of creek inflow. Near-surface values of *I,* which tended to have an even larger exponential rate of decrease, were excluded from the least-squares fits (Kirk 1983), and values of k_e from poor least-squares fits were likewise excluded from the averaging.

The values of k_e in Rodeo Lagoon varied from 1.2–8.6 m^{-1}, with a mean of 3.8 m^{-1} (Fig. 3-13A). Values of k_e typically exceeded 2 m^{-1} in summer, which is equivalent to a Secchi disk transparency of less than 1 m. These values are consistent with other eutrophic shallow lakes (Kalff 2002; Van Duin et al. 2001) and are one indicator of hypereutrophic status (Vollenweider and Kerekes 1982; Kalff 2002). However, taken alone they are not sufficient to define trophic status, since inorganic particles and dissolved organic matter can also absorb light. For example, light extinction in nearby San Francisco Bay is equally high due to turbidity from suspended

particulate matter (Cloern 1987). Though already high, these estimates of k_e for Rodeo Lagoon may in fact be an underestimate, since the method combines light extinction across the PAR wavelength band into one value rather than using a spectrally weighted approach (Kirk 1983; Van Duin et al. 2001)

Another way of quantifying light extinction is through the photic depth, z_p, at which PAR reaches 1% of its near-surface value. The photic depth is calculated as $z_p = (\ln 100)/k_e$ rather than established using the original $I(z)$ profile. Fig. 3-13B shows the result of this calculation, as well as the lagoon total depth and mixed-layer depth, z_{mix}, for reference. Light availability can limit phytoplankton growth to the point of net negative productivity, with rates of respiration rates exceeding photosynthesis, when the ratio of mixing depth to photic depth (z_{mix}:z_p) exceeds 2–5 (Talling 1971; Cloern 1987). The precise cutoff depends on phytoplankton respiration rates and other factors. In Rodeo Lagoon, the ratio z_{mix}:z_p approached this criteria only during the first

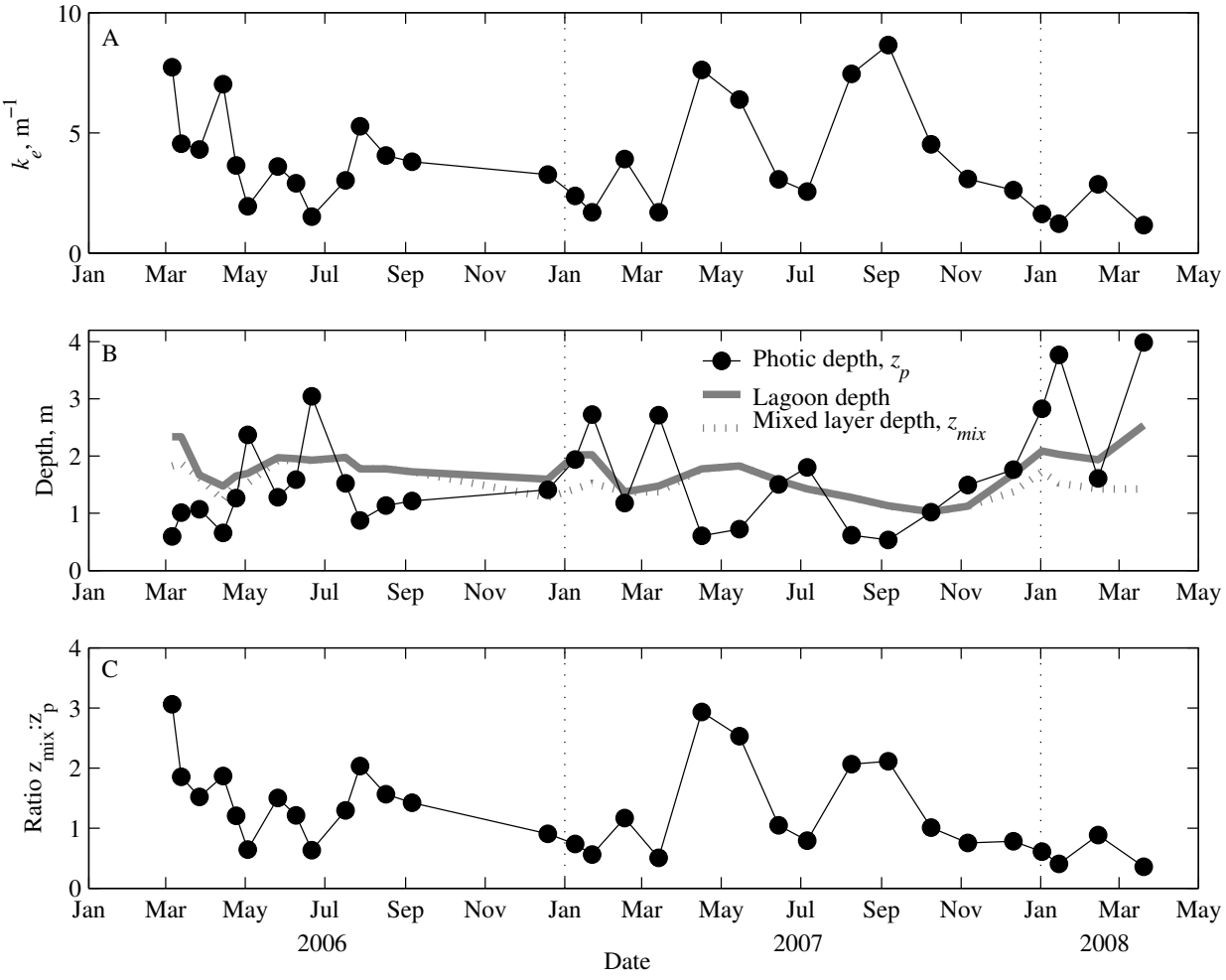

Fig. 3-13. (**A**) Light extinction coefficient, k_e (m^{-1}), averaged over a longitudinal transect of the lagoon. (**B**) Photic depth z_p (m), defined as $z_p = (\ln 100)/k_e$, total water depth near the lagoon center (m), and depth of the upper mixed layer, z_{mix} (m). z_{mix} differs from the total depth only when the lagoon is stratified by salt. (**C**) Ratio of mixed layer depth z_{mix} to photic depth z_p.

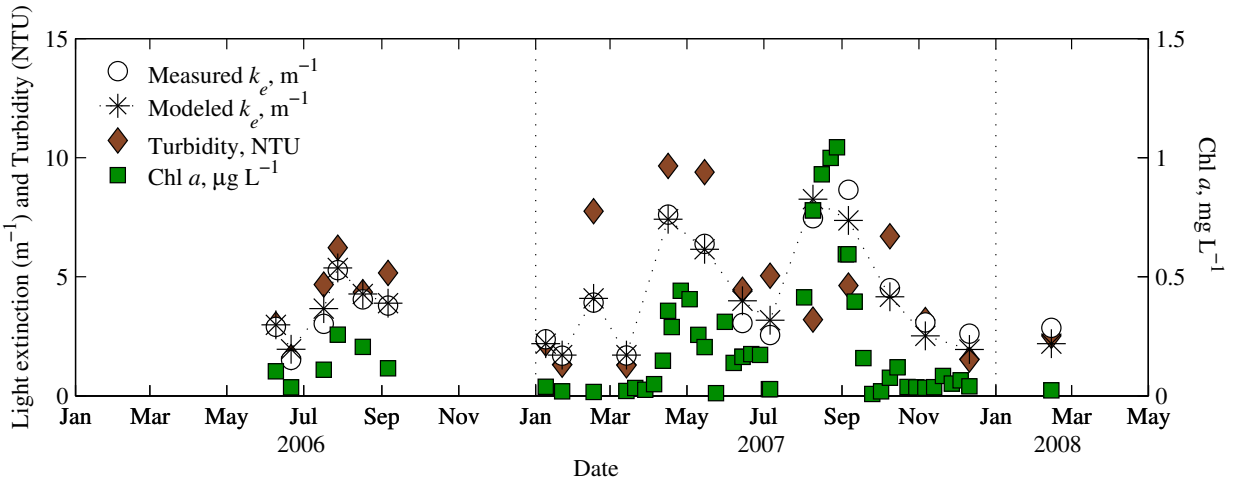

Fig. 3-14. Results of a multiple regression of the light extinction coefficients, k_e (m^{-1}) on turbidity (NTU) and Chl *a* biomass (mg L^{-1}). Observations of k_e are shown in circles, while model results are shown in stars. Only concurrent data used in the multiple regression is shown here; for full data sets, refer to Figs. 3-8, 3-10, and 3-12.

biomass peak of summer 2007, which featured a bloom of *Nodularia spumigena*, and under very wet weather in March 2006, when inputs of suspended particles from the watershed were at a high level (Fig. 3-13C). Thus, while low light availability may have slowed productivity to some extent, it only did so when Chl *a* levels were already very high.

A multiple regression of observed light extinction coefficients k_e on surface Chl *a* concentrations and turbidity reveals a strong correlation among the variables, with surface Chl *a* alone explaining 73% of the variance in k_e and the two variables together explaining 93% of the variance (Fig. 3-14). The seasonal variability of k_e is consistent with phytoplankton self-shading, which peaks in summer, combined with inputs of fine particles suspended in wet season inflows, which both scatter and absorb light. Turbidity alone explains 41% of the variance in k_e, largely because of the contribution of these fine particles in the wet season (Fig. 3-11, early 2006). Although in other shallow systems wind-driven sediment resuspension contributes to turbidity and light absorption on shorter (~diurnal) time scales (Van Duin 2001), the lack of light absorption data at short time scales precludes such analysis here. However, since turbidity did not show a strong dependence on wind stress, it is highly unlikely that light absorption would.

As previously discussed, the net result of this strong light absorption was a predictable pattern of sunny days rapidly producing a stable water column, which persisted throughout the afternoon and occasionally longer than 24 hours (e.g., 04 Jul 2007 - 06 Jul 2007, Fig. 3-7).

3.6 Dissolved oxygen

Dissolved oxygen concentrations varied considerably – from super-saturated to virtually anoxic – on diurnal and seasonal time scales and from the top to bottom of the water column, particularly when the lagoon was salt-stratified. This section explores each of these modes of variability.

Dissolved oxygen concentrations, [*DO*], reflect a balance of photosynthesis *P*, respiration *R*, and diffusive vertical mixing governed by a scalar diffusivity K_ρ.

$$\frac{\partial[DO]}{\partial t} = P - R + \frac{\partial}{\partial z}\left(K_\rho \frac{\partial[DO]}{\partial z} \right) \tag{3-9}$$

Surface aeration and sediment oxygen demand can be incorporated as flux boundary conditions on eq. 3-9. When the lagoon is well-mixed by salt, it is appropriate to depth-average eq. 3-9, replacing the flux boundary conditions with terms to explicitly represent sediment oxygen demand *S*, and transfer across the air-water interface. Interfacial gas transfer is governed by the difference between $\left[\overline{DO}\right]$ and its saturated value $[DO]_{sat}$, an interfacial mass transfer coefficient *K* with units [length time^{-1}] which varies with wind speed, and the area *A* and volume *V* of the lagoon (Chapra 1997):

$$\frac{\partial\left[\overline{DO}\right]}{\partial t} = P - R - S + \frac{KA}{V}\left([DO]_{sat} - [\overline{DO}]\right) \tag{3-10}$$

In eqs. 3-9 and 3-10, *P* varies diurnally, whereas *R* and *S* vary seasonally with lagoon biomass.

3.6.1 Diurnal variability

Dissolved oxygen concentrations vary diurnally because of the dependence of $[DO]_{sat}$ on temperature and because of photosynthesis. At times of high biomass concentrations, increased rates of photosynthesis produce correspondingly large diurnal fluctuations in [*DO*]. Measuring rates of photosynthesis is outside the scope of this study (see Drake 2008), but I did record an example of the diurnal variability in [*DO*] during a near-surface moored deployment of the CTD equipped with an O_2 sensor in November 2006 (Fig. 3-15). Dissolved oxygen fluctuated

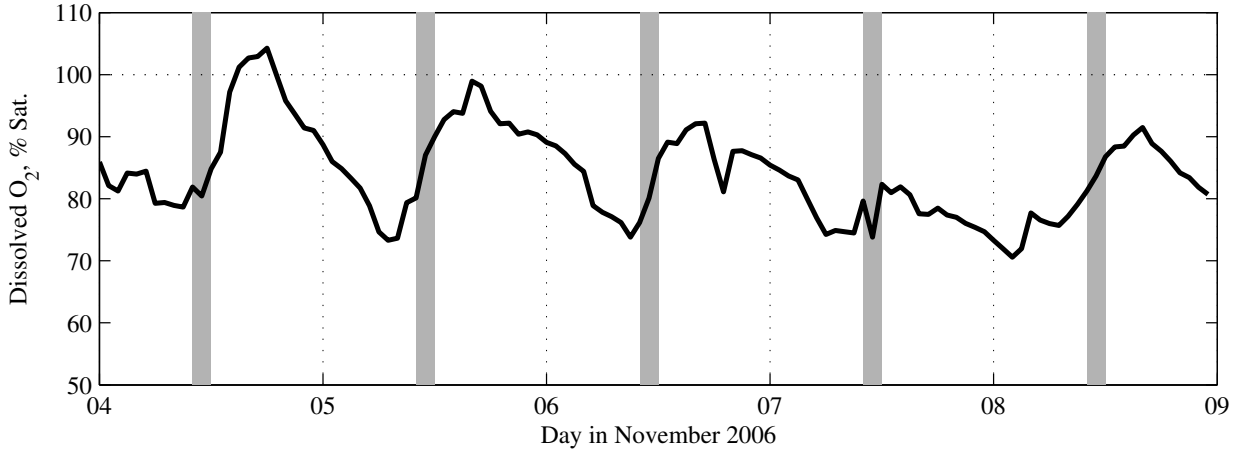

Fig. 3-15. Diurnal fluctuations in the dissolved oxygen concentration, expressed as a percentage of the saturated value. Data was collected with a Sea-Bird 19+ CTD moored 1.2 m beneath the surface of the lagoon in November 2006. The shaded regions correspond to 10:00 – 12:00, the window during which I took most of the water quality measurements discussed in this chapter.

between about 75% of saturation at the diurnal minimum just after sunrise (7:00–9:00) to nearly saturated values in the late afternoon (16:00-18:00). At the time, the Chl *a* concentration was about 100 μg L^{-1} – on the low end for Rodeo Lagoon, but high by any other standards. At other times of the year, when Chl *a* concentrations were typically much higher, the diurnal fluctuation in dissolved oxygen was presumably even larger.

3.6.2 Seasonal variability

Dissolved oxygen in the surface layer varies seasonally with the rate of change of phytoplankton biomass. Following eq. 3-9, if diurnally averaged photosynthesis *P* exceeds respiration *R*, as during an increase in biomass, the water column will gain [*DO*], and vice versa. Unfortunately, the seasonal trend is somewhat obscured by the superposed diurnal variability. It is notable that I collected most of the longitudinal transects data closer to the diurnal minima (10:00–12:00, shaded regions, Fig. 3-15) than the diurnal maxima. There is also a significant difference in the dissolved oxygen values measured by the grab samples and the CTD (Fig. 3-16A, B). The grab samples were always taken within 0.25 m of the true surface and bottom of the water column, and sometimes even closer. Meanwhile, the so-called "surface" and "bottom" values measured *in situ* by the profiling CTD were actually collected 0.7–1 m from the surface and within 0.3 m of the bottom. Furthermore, the CTD's oxygen sensor is susceptible to error when the dissolved oxygen, temperature or descent speed are rapidly varying, since the membrane does not have time to come to equilibrium; by contrast, the sensor for the grab samples was always allowed to come to equilibrium before recording the value. It is therefore not surprising that the grab samples show lower dissolved oxygen near the bed compared to the profiling CTD data, reflecting the fact that the grab samples were closer to the organic-rich sediments, which are an oxygen sink. The surface grab samples frequently indicate substantial super-saturation of dissolved oxygen (up to 150% in July 2007, Fig. 3-15B), which might reflect a slight mis-calibration of the instrument, although these high values are consistent with previous work (Silkie 2008).

Despite these difficulties, some seasonal trends emerge (Fig. 3-16A,B). In winter and spring, surface dissolved oxygen concentrations were typically close to 100% saturation. In the summer, things get more interesting. Supersaturated dissolved oxygen conditions in the surface layer, like those observed in spring and early summer 2007, were associated temporally with peaks in phytoplankton biomass and its rate of increase, while hypoxic conditions immediately followed declines in phytoplankton biomass. Specifically, the hypoxia in August and September 2007 (shaded regions, Fig. 3-16A, B) probably resulted from a die-off of a large bloom of the centric diatom *Chaetoceros muelleri* var. *muelleri* and the cyanobacterium *M. aeruginosa,* combined with a proliferation of mixotrophic flagellated protozoa (Drake 2008). The only documented fish kill in 2007 occurred during this period, in the week of 06 August.

As Fig. 3-16C shows, inflow from the lake/wetland complex was typically hypoxic or even anoxic in summer; dissolved oxygen levels approach saturation only during periods of sustained wet weather. Dissolved oxygen levels in the lagoon were therefore lower in areas dominated by lake inflow, which corresponds to the area within about 80 m of the lake overflow weir at the east end of the lagoon. To make matters worse, the east end of the lagoon is downwind of the daytime sea breeze, so surface scums of phytoplankton and other organic debris tend to accumulate there, increasing the oxygen demand and making the eastern end of the lagoon particularly vulnerable to hypoxia. Alas, this is one of numerous examples demonstrating that

the Bunker Road bridge at the east end of the lagoon is *not* representative of the lagoon as a whole, as Silkie (2008) previously noted, despite being a convenient sampling location used in several previous studies.

3.6.3 Vertical variability

Vertical profiles of dissolved oxygen (Fig. 3-17) typically showed hypoxia in the lower salty layer, when one is present. Although this trend is by far the dominant one, salt-based stratification and hypoxia also each occurred without the other. For example, on 02 January 2008 (Fig. 3-18A), oxygen levels and Chl *a* fluorescence were both slightly elevated in the lower

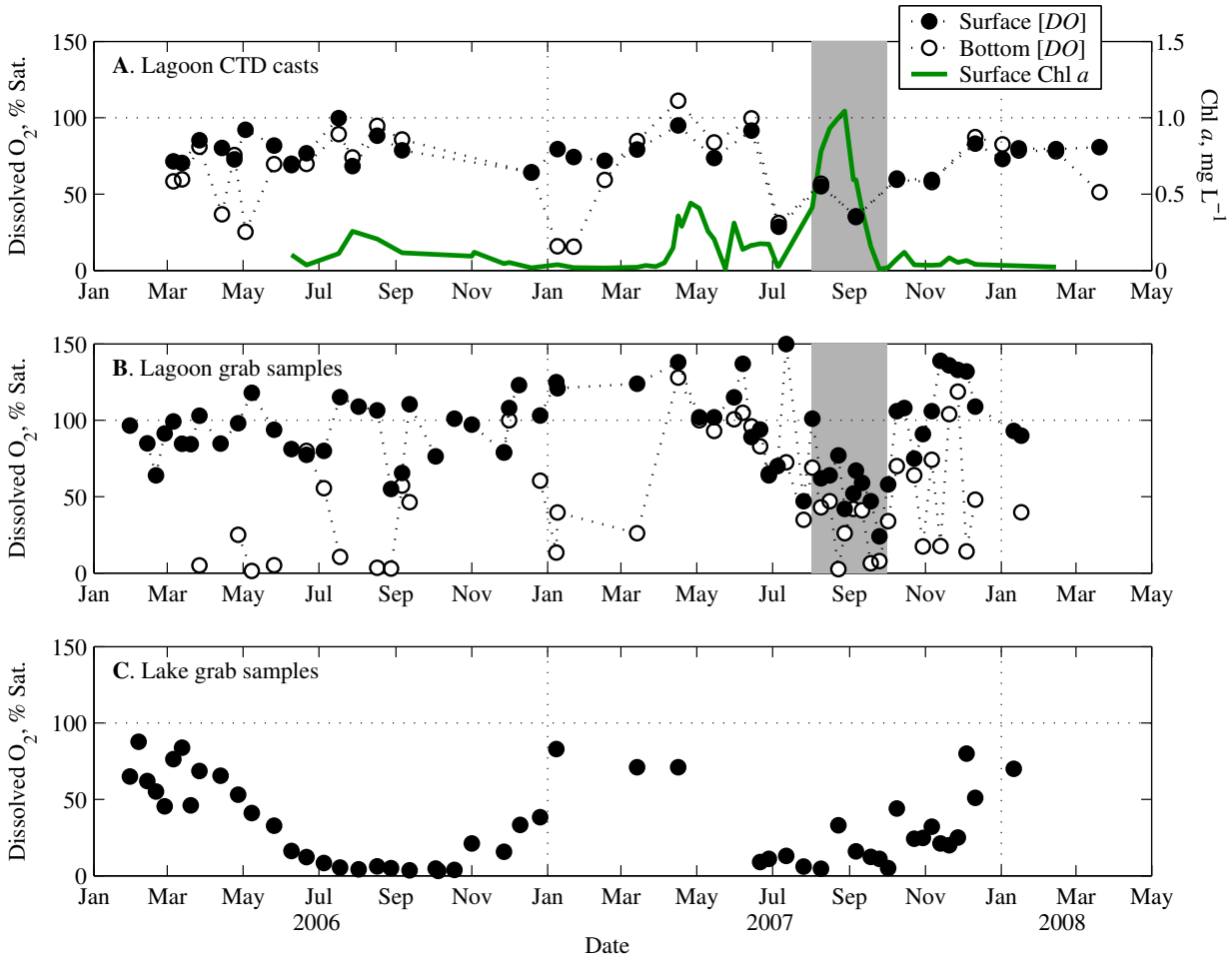

Fig. 3-16. Dissolved oxygen concentrations [*DO*] as a percentage of the saturated value. (**A**) "Surface" values of [*DO*] correspond to 0.7–1 m below the surface, while "bottom" [*DO*] corresponds to the region within 0.3 m of the bottom. Data are taken from lagoon profiles collected with a CTD and Sea-Bird 43 oxygen sensor; for reference, Chl *a* biomass is also shown on the right axis. The shaded region in (A) and (B) corresponds to the annual [*DO*] minimum of August and September 2007, which occurred with the decline in biomass. (**B**) Surface and bottom [*DO*] in lagoon grab samples analyzed with a YSI-85 oxygen meter. Both types of grab samples were taken within 0.25 of the true surface or bottom near the lagoon center station. (**C**) Lake surface grab samples analyzed for [*DO*] with a YSI-85 oxygen meter.

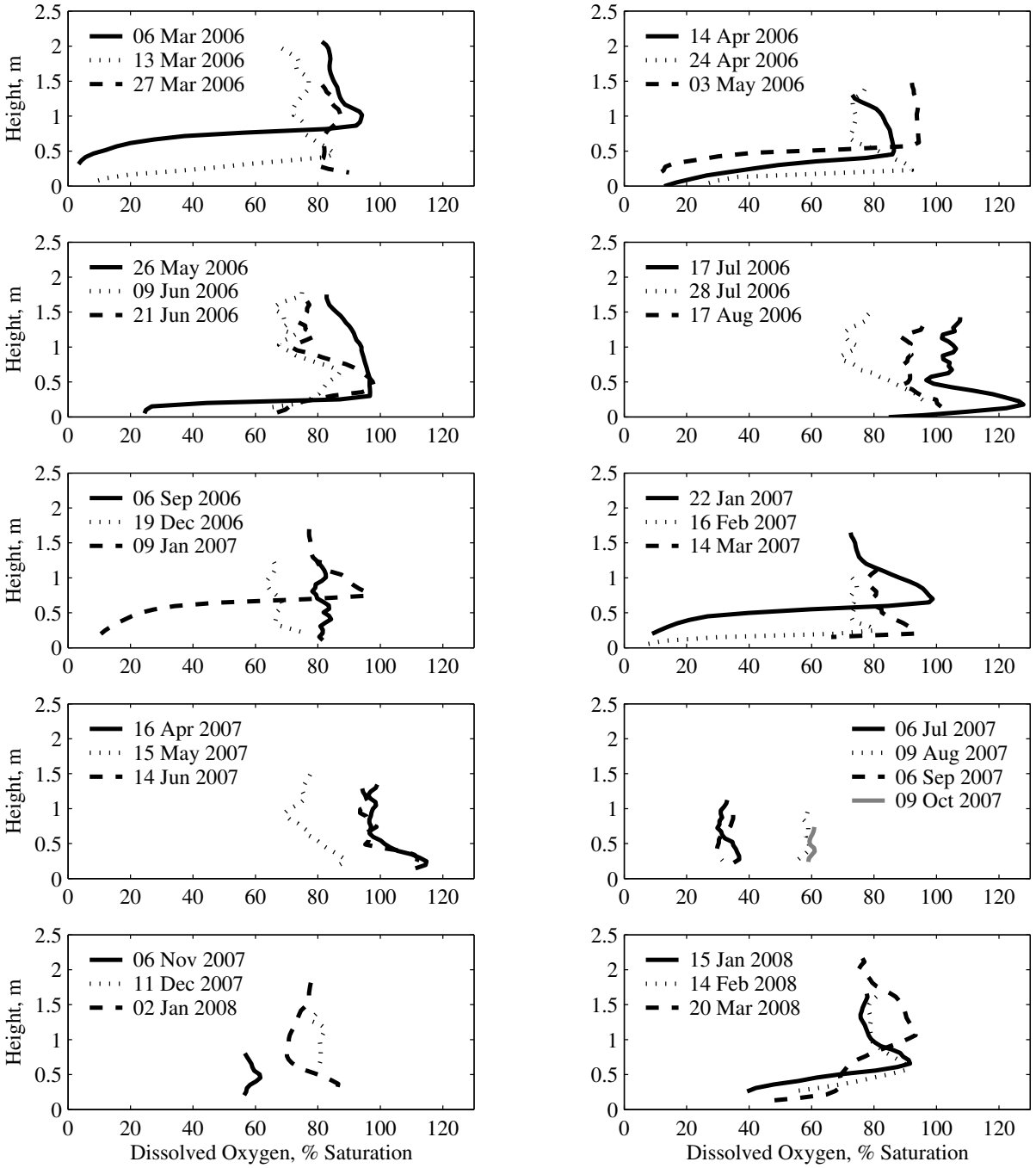

Fig. 3-17. Dissolved oxygen profiles collected from March 2006 to March 2008 with a Sea-Bird 19+ CTD equipped with a Sea-Bird 43 oxygen sensor. No data are available within 0.6 m of the surface because of equipment limitations.

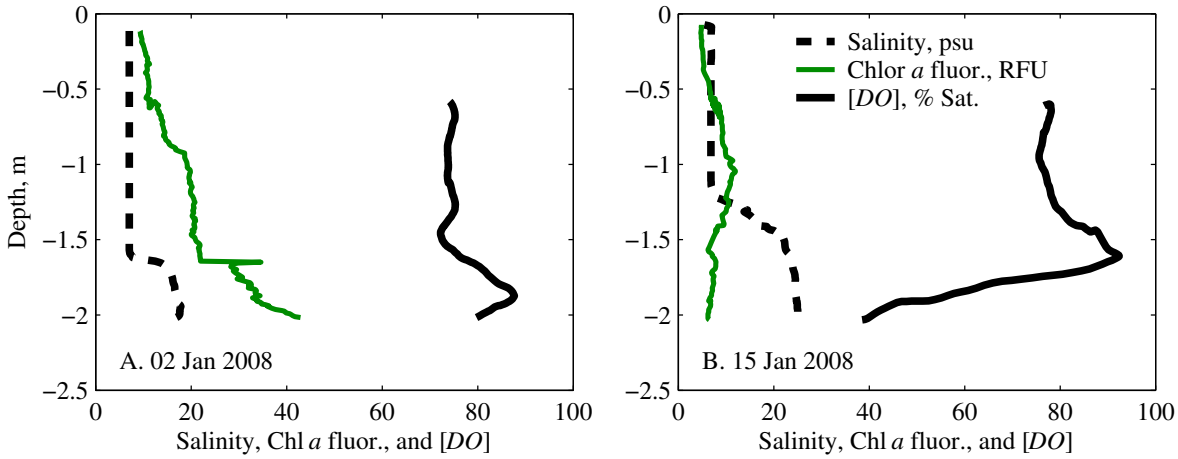

Fig. 3-18. Vertical profiles of salinity (psu), uncalibrated Chl *a* fluorescence (relative fluorescence units, RFU), and dissolved oxygen ([*DO*], % of saturated concentration) on (**A**) 02 Jan 2008 and (**B**) 15 Jan 2008. Data are from Sea-Bird 19+ CTD casts and are not binned. In (**A**), elevated Chl *a* in the lower salty layer appears to be responsible for the higher oxygen levels. However, (**B**) represents the more common pattern, with a Chl *a* maxima above the pycnocline and oxygen deficit below.

salty layer, so there was apparently enough oxygen being added by phytoplankton resident in this layer to offset any benthic oxygen demand. A similar pattern was in place on 15 May 2007 and 11 December 2007 (Fig. 3-17). By contrast, profiles collected on 15 January 2008 (Fig. 3-18B) show the more typical vertical pattern, with hypoxia in the lower salty layer and a Chl *a* peak above the pycnocline rather than near the bed.

There are plenty of examples of hypoxia occurring when the lagoon is well-mixed; as discussed above, this tends to occur under peak biomass summer concentrations such as those observed in July and September 2007 (Fig. 3-17). By contrast, biomass was considerably lower in summer 2006, and I did not collect any transects that were fully hypoxic like those in summer 2007.

In summary, dissolved oxygen levels respond to salt-based stratification of the lagoon, but the presence of a salty layer at the bottom does not completely guarantee that hypoxia will develop, since elevated phytoplankton biomass capable of adding dissolved oxygen was sometimes found in this lower salty layer (see §3.3.2). Also, hypoxia frequently develops in summer when the water column is well-mixed.

3.7 pH

The seasonal trend in pH clearly shows a relationship with both primary productivity and its rate of increase (Fig. 3-19). Like most natural waters, the pH in Rodeo Lagoon is assumed to be dominated by the carbonate buffering system; indeed, Rodeo Lagoon water quality data from Drake (2008) show the expected strong linkage between dissolved inorganic carbon and pH. In this context, primary productivity raises pH by taking up CO_2, while respiration and decomposition lower pH by producing CO_2. Since dissolved oxygen also responds to the

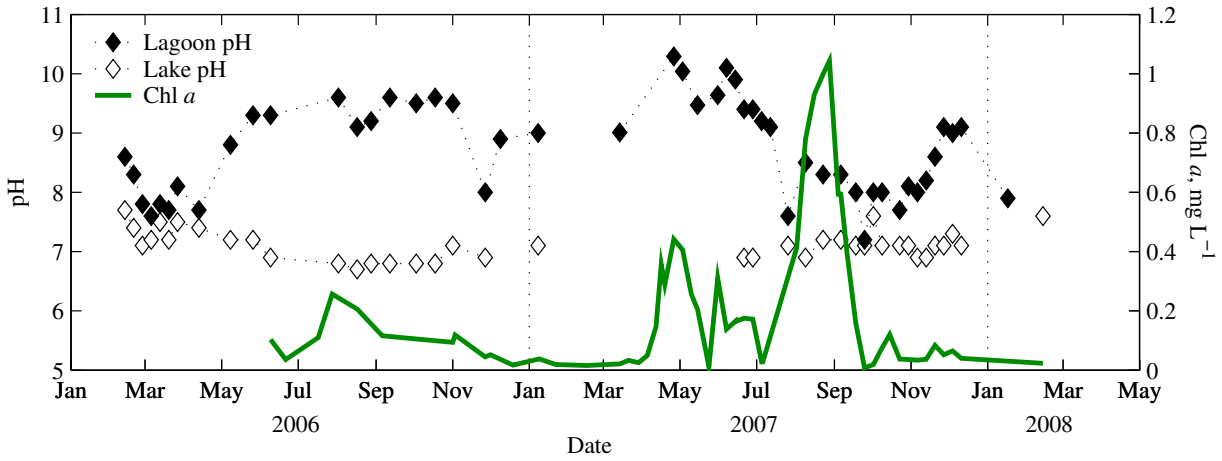

Fig. 3-19. pH of surface grab samples from Rodeo Lagoon and the lake upstream (left axis). Chl *a* biomass (mg L^{-1}, right axis) is also shown for reference. Some 2006 pH data were previously reported in Silkie (2008).

relative balance of primary productivity and respiration, it is not surprising that pH and dissolved oxygen show similar seasonal trends (Figs. 3-16B, 3-19).

In summer 2006, the lagoon pH remained high, exceeding 9.0 for most of the summer (Fig. 3-19). No precipitous crashes in phytoplankton biomass were observed, and the lagoon had episodic oxygen deficits but was not hypoxic. Two brief periods of reduced pH on 17–28 August and 27 November coincided with oxygen deficits and declining biomass concentration, although in the August case the oxygen deficit appears to have lagged the reduced pH by about a week. By contrast, pH was much more variable in summer 2007, exceeding 10.0 during the first biomass peak in April, then falling as low as 7.2 during the September rapid biomass decline. In fact, pH was relatively low for all of August and September, corresponding to a sustained period of oxygen depletion. The atypically low pH value of 7.6 recorded on 26 July 2007 also coincided with an oxygen deficit (surface [*DO*] = 47% of saturation). Although total Chl *a* biomass was increasing at the time, a pronounced population shift from centric diatoms to *M. aeruginosa* and flagellated protozoa was underway (Drake 2008).

In summer, the pH of the lagoon depends primarily on internal lagoon processes like those mentioned above, not the pH of its tributary waters. The pH of ocean water is relatively constant at about 8.1 (Buck and Folger 2009), and the pH of the upstream lake/wetland was typically close to 7, with slightly higher values under wet weather (Fig. 3-19). Of course, under wet weather conditions, the lake and lagoon pH values converge, as both become dominated by inflows from the creek.

3.8 Nutrients

Nutrient availability was monitored by analyzing grab samples for ammonium, nitrate + nitrite, and orthophosphate (§2.1.2). In the lagoon, variability in these three dissolved inorganic nutrients primarily reflected three processes: internal loading from the bottom sediments, phytoplankton uptake, and remineralization. As discussed in the sections below, internal loading

is assumed to be important because of the lack of significant nutrient loading from the watershed combined with observations of nutrient enrichment near and within the bed. Meanwhile, phytoplankton uptake and remineralization appear to be important based on the timing of peaks in inorganic nutrients compared to those of Chl *a*.

3.8.1 Inflows from watershed

Inflows from the lake (Fig. 3-20, red triangles) were only a minor contribution to the dissolved nutrient pool in summer 2007, as the volumetric inflow rates were low (< 5 L s^{-1}) and concentrations were typically lower than those already found in the lagoon (Fig. 3-20). This trend is consistent with a 2006 study of watershed nutrient fluxes, which found that total nitrogen and total phosphorus concentrations in the lagoon peaked during the summer dry season, when they also exceeded those at sites sampled upstream (Silkie 2008). Of course, nutrients are also transported from the watershed via the lake in the form of suspended organic matter, which is not reflected in the dissolved nutrient analysis discussed here.

Lake inflows contained much higher concentrations of dissolved nutrients in winter than in summer. This was particularly true for nitrogen, whose primary inorganic components are ammonium and nitrate + nitrite (referred to hereafter as nitrate). Lake concentrations of nitrate were slightly elevated, for example, in the February 2007 and January 2008 samples (Fig. 3-20B). For orthophosphate, the wet season was the only time when inflow concentrations were comparable to those already in the lagoon (Fig. 3-20C). The elevated lagoon nutrient levels observed in summer were in excess of that assumed to be due to the concentration of nutrients by summer evaporation, which means that some mechanism other than inflows must have been responsible.

3.8.2 Nutrients in bottom sediments

In the deepest parts of the lagoon, the bottom sediments are shiny, black, cohesive, and extremely fine-grained, indicating a content that is primarily reduced organic matter. This organic matter has a considerable oxygen demand, as evidenced by the oxygen deficit that quickly forms when the water column is stratified. When the overlying water column becomes anoxic, the flux of both ammonium and orthophosphate into the water column can correspondingly increase, although on slightly different theoretical grounds. For ammonium, any fluxes from the bed are converted to nitrate at the sediment-water interface as long as oxygen is present, but this conversion is halted in the absence of oxygen (Webster and Harris 2004) and sulfides (Joye and Hollibaugh 1995). For phosphate, the releases are presumed to be linked to Fe reduction, as explained in Chapter 1.

Pore water concentrations indicated nutrient-replete conditions. Concentrations of orthophosphate in July 2007, for example, were 65 μmol L^{-1} in sediment pore water, compared to <0.05 μmol L^{-1} in the water column. In January 2008, when the water column was salt-stratified, pore water concentrations of orthophosphate, ammonium, and nitrate + nitrite were 22.5 μmol L^{-1}, 70.0 μmol L^{-1}, and 0.4 μmol L^{-1}, respectively, compared to near-bottom values of 0.1 μmol L^{-1}, 25.5 μmol L^{-1}, and 8.8 μmol L^{-1}. In other words, the pore water was slightly enriched in ammonium, and extremely enriched in orthophosphate. Although by no means a complete data set, these pore water sample results are consistent with the hypothesis that the sediments are acting as a nutrient reservoir, particularly for phosphorus.

3.8.3 Lagoon nutrients

3.8.3.1 Seasonal variability

Concentrations of orthophosphate, ammonium, and nitrate in lagoon surface water each showed a pronounced seasonal peak in 2007, but the timing of the peaks differed, as discussed in the sections below.

Nitrogen

The major seasonal pattern in ammonium was its dramatic increase in fall 2007 as the summer phytoplankton population declined (Fig. 3-20A). Chl *a* peaked on 28 August, while ammonium peaked on 2 October. Over this five week-period, a dramatic shift in lagoon water quality occurred: Chl *a* values fell from 1044 to 19 μg L^{-1}, while ammonium rose ten-fold from about 20 to 200 μMol L^{-1}. The coordinated timing of these events is strong evidence that mineralization of organic matter is responsible for the ammonium peak.

Concentrations of ammonium remained quite high through December 2007. Meanwhile, nitrate lagged ammonium by about a month, beginning to rise only in October 2007 and peaking on 11 December (Fig. 3-20B). Together, these two trends are an indication that nitrification, which is the conversion of ammonia to nitrate that subsequently allows denitrification to proceed, was inhibited. Sulfide inhibition of nitrification is common in marine sediments (Joye and Hollibaugh 1995), and it is likely that Rodeo Lagoon sediments contain sufficient sulfides to have this effect. A lack of dissolved oxygen near the bed may have also contributed to the slow conversion of ammonia to nitrate. Finally, the large size of the organic matter pool being mineralized, which also included senescing macrophytes, may have also contributed to the prolonged peak in ammonium.

Although barely visible in Fig. 3-20A, ammonium levels were also elevated following the Chl *a* peak in late April 2007. However, this ammonium was presumably recycled back into phytoplankton biomass, which increased in June, July, and August 2007.

Ammonium levels were high enough during the fall 2007 peak to be a potential toxicity concern. The thirty-day chronic criterion ranges from 166–297 μMol L^{-1} for freshwater with fish early life stages present, no mussels present, temperatures below 20°C, and pH range of 8–7.5 (US EPA 2009). Grab samples from the west end of the lagoon, which had a more extended ammonium peak than the center station, exceeded this criterion in October and November 2007 (Fig. 3-20A).

Phosphorus

Inorganic phosphorus concentrations did not reflect phytoplankton dynamics as closely as did inorganic nitrogen. There was a gradual draw-down in orthophosphate in spring 2007 that might reflect phytoplankton uptake, but there was no peak in the fall caused by mineralization (Fig. 3-20C). Instead, the seasonal pattern of orthophosphate reflects benthic fluxes that increase under hypoxic conditions. Specifically, orthophosphate and dissolved oxygen from 2007 are inversely correlated ($r^2 = 0.4$) and show opposite seasonal trends (Figs. 3-20C, 3-16B). By contrast, there is little evidence for high-pH events releasing phosphorus. Even though dissolved oxygen and pH observations are weakly related ($r^2 = 0.17$), the relationship between pH and orthophosphate was even weaker ($r^2 = 0.04$) and not in the expected the direction. However, there could have been releases in summer 2006, when pH was significantly higher than in summer 2007.

The peak level of orthophosphate in the lagoon was 45 μg L^{-1}, while the mean over the summer 2007 growing season was about 12 μg L^{-1}. These levels are on the low end for a hypereutrophic system (Vollenweider and Kerekes 1982).

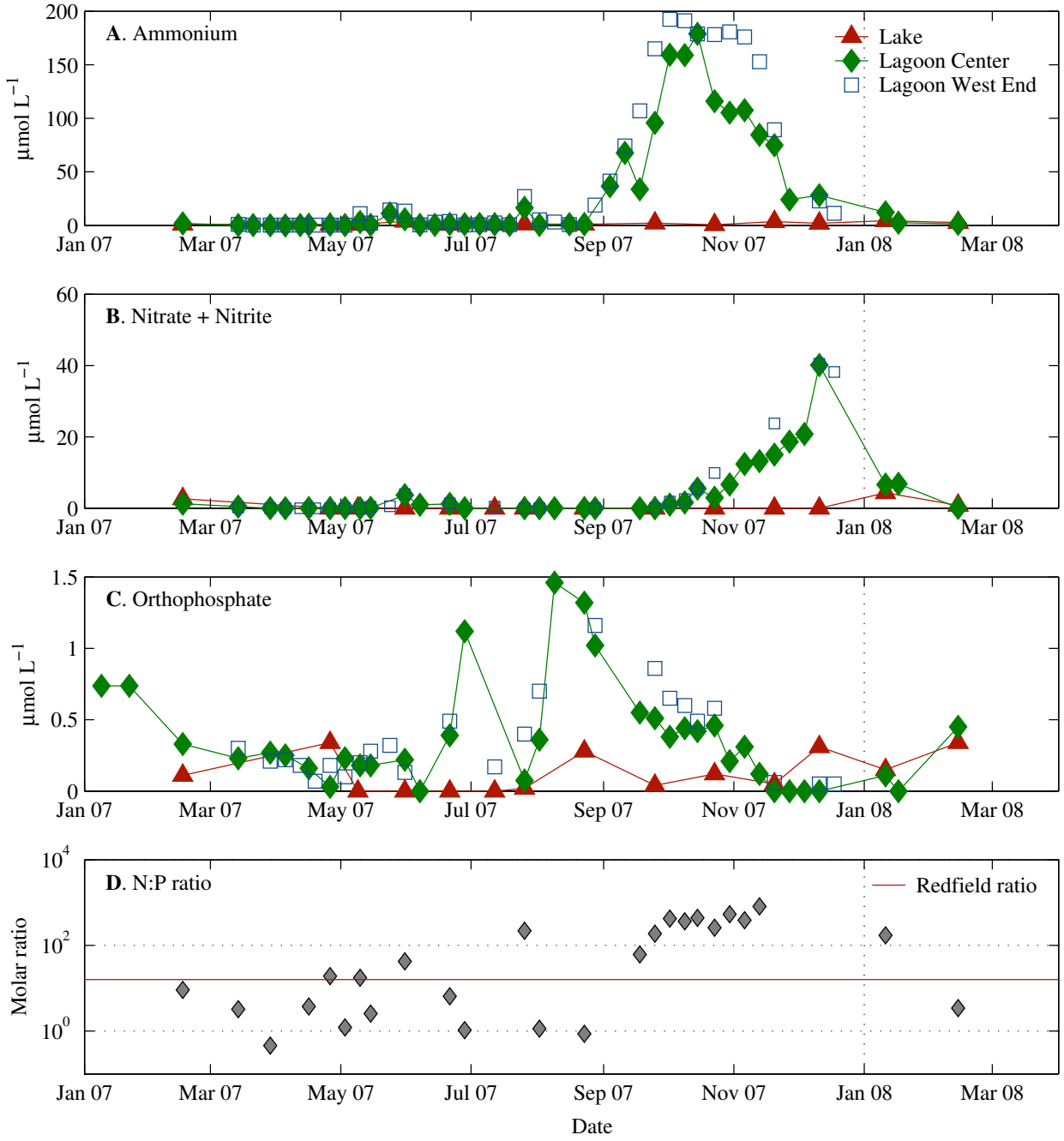

Fig. 3-20. Concentrations of (**A**) ammonium, (**B**), nitrate + nitrite, and (**C**) orthophosphate in grab samples (µmol L^{-1}) from Rodeo Lake (red triangles), the center station of Rodeo Lagoon (green diamonds), and the west end of Rodeo Lagoon (open blue squares). (**D**) Molar N:P ratio, defined using molar concentrations of (ammonium + nitrate + nitrite)/orthophosphate. The theoretical Redfield ratio of N:P=16 is also shown for reference (red line).

N:P ratios

Molar N:P ratios to compare to the Redfield ratio of 16 were approximated as ($[NH_4^+]$ + $[NO_3^-]$ + $[NO_2^-]$)/($[PO_4^{3-}]$). The N:P ratio increased dramatically through 2007, reaching levels orders of magnitude larger than the Redfield ratio during the prolonged ammonium peak from September to November (Fig. 3-20D). Although phosphorus was the more limiting nutrient at this time, it was not drawn down in a way that is consistent with true phosphorus limitation. The surface layer of the lagoon was comparatively nitrogen-limited in the spring and summer, with most N:P ratios below 16. Drake (2008) hypothesized that nitrogen fixation by *N. spumigena* and its subsequent re-mineralization may have been responsible for the shift from away from N limitation in late May 2007.

3.8.3.2 Vertical variability

When salt stratification was present, dissolved nutrient concentrations were typically higher in the lower brackish layer (Table 3-2). The adjacent Pacific Ocean has comparatively low nutrient concentrations (Wilkerson et al. 2002), so the sea water itself cannot be responsible. This trend, which is particularly strong for ammonium, is not surprising considering the high organic content of the bottom sediments. The dates with higher salinity and nutrient concentrations in the lower layer are highlighted in gray in Table 3-2. Nitrate, which is not shown in Table 3-2, did not show the same pronounced vertical layering (see Appendix A).

The federal toxicity criteria for continuous concentrations of total ammonia in saltwater ranges from 82–376 μMol L^{-1} for a salinity of 10 psu, a pH range of 7.5–8, and temperature range of 10-15°C (US EPA 1989). Bottom layer ammonia concentrations in winter 2007 were squarely in this range, indicating a potential for toxicity to aquatic organisms.

Date	Depth, m	Salinity, psu	Orthophosphate, µMol L^{-1}	Ammonium, µMol L^{-1}
17 Aug 2006	0	3	1.89	10.7
	0.5	3	0.95	8.6
	1	3	1.79	10.0
	1.5	3	2.21	13.6
	1.65	3	2.53	11.4
06 Sep 2006	0	3	1.19	9.3
	0.5	3	1.11	8.9
	1	3	1.00	7.8
	1.5	3	1.05	7.8
	1.8	3	1.00	11.4
01 Nov 2006	0	3	2.11	2.9
	0.5	3	1.16	4.3
	1.5	3	1.53	5.0
09 Jan 2007	0	3	0.74	
	0.5	3	0.13	0.8
	1	3	0.06	0.5
	1.5	12	4.12	25.3
	2	16	23.68	264.3
22 Jan 2007	0	5	0.74	

	2.05	18	17.84	
16 Feb 2007	0	3	0.33	1.8
	1.3	17	24.51	178.9
14 Mar 2007	0	2	0.23	0.3
	1.4	15	24.44	140.6
26 Apr 2007	0	5	0.03	0.6
	1.45	4	0.12	
31 May 2007	0	4	0.22	5.7
	1.4	4	0.05	8.2
21 Jun 2007	0	4	0.39	1.3
	1.25	5	0.17	13.8
26 Jul 2007	0	5	0.08	16.4
	0.5	5	0.10	14.4
	1	5	0.18	16.0
	1.25	5	0.02	18.4
23 Aug 2007	0	5	1.32	1.1
	0.9	5	1.34	1.5
25 Sep 2007	0	6	0.51	95.8
	0.75	6	0.43	104.6
23 Oct 2007	0	6	0.46	116.0
	0.85	6	0.52	83.4
20 Nov 2007	0	5	not detected	74.9
	1	5	not detected	41.1
11 Dec 2007	0	6	not detected	28.1
	1.35	19	0.03	80.1
11 Jan 2008	0	5	0.11	12.2
	0.5	5	0.04	6.7
	1	11	not detected	18.6
	1.5	18	0.36	25.7
	2	19	0.25	32.4
17 Jan 2008	0	7	not detected	2.5
	0.5	7	0.04	
	1	7	not detected	
	1.2	12	0.12	
	1.4	15	not detected	
	1.6	18	not detected	
	1.8	19	0.02	
	2	22	0.06	79.4
14 Feb 2008	0	4	0.45	1.4
	1	4	0.25	10.1
	1.5	22	0.24	53.2

Table 3-2. Nutrient concentrations over the vertical extent of the water column. Blank indicates that no data are available, while results below the detection limit are listed as "not detected."

3.9 Summary of water quality observations

From 2006 to 2008, there were two main modes of variability in the water quality of Rodeo Lagoon: salt stratification forced vertical variations in winter, while phytoplankton imposed a seasonal variability in summer. Both types of variability were associated with serious deteriorations in dissolved oxygen and other parameters relevant to fish survival.

Vertical density stratification by salt had a cascading effect on all of the other water quality variables studied here, resulting in a bottom layer that was typically saltier, warmer, hypoxic, and enriched in nutrients. As discussed in Chapters 4 and 5, this density stratification resulted in greatly reduced turbulent mixing rates, which explains why atmospheric oxygen could not reach the lower brackish layer. Unless a significant phytoplankton population was present, dissolved oxygen was rapidly depleted. Under these definitely hypoxic and probably sulfide-rich conditions, the bottom sediments could more easily release inorganic nutrients like ammonium and orthophosphate into the lower brackish layer. Temperatures in the lower layer also rose as the overlying fresh water acted as an insulator.

In the summer, vertical density stratification was absent, and the phytoplankton population density itself appeared to be the most important water quality variable. In this hypereutrophic system, large diurnal variations in dissolved oxygen were apparent. Phytoplankton absorbed significant amounts of light, nearly limiting their own growth at the times of the greatest biomass. This produced a stable water column, and diurnal density stratification by temperature was present on an intermittent basis. In fall 2007, when phytoplankton biomass began to decline, dissolved oxygen was quickly depleted and ammonium levels rose as nitrification was apparently suppressed.

Chapter 4

Hydrodynamics

Rodeo Lagoon is a small water body with no tidal connection to the ocean, so the hydrodynamic forcing – that is, the driver of currents and mixing – is limited to a few factors: wind, diurnal heating and cooling, and inflows of fresh and salt water. This chapter describes how these forces govern the interaction of salt and fresh water at time scales ranging from hours to months. The interaction of salt and fresh water is interesting in its own right, but also has implications for nutrient transport that are discussed in Chapter 5. In this chapter, I also present observations on processes like wind waves that have less immediate impact on scalar mixing, but are nonetheless important in understanding the hydrodynamics of the lagoon.

The observations in this chapter are based on hydrodynamics experiments that provided raw data in various forms, like instantaneous velocities, temperature microstructure, and density profiles. The low-level analysis used to condense this raw data into information about mean currents and stresses can be found in Chapter 2. Subsequent processing of the data to reach conclusions about turbulent mixing rates and mixing efficiency is found within this chapter. A summary of the data sources used for each topic is shown in Fig. 4-1.

4.1 Evolution of density structure

Fluid motion in Rodeo Lagoon is best understood in the context of the density structure. Chapter 3 presented some information about the seasonally recurring salt-based stratification, but this chapter provides further details about the density structure as it pertains to currents and turbulence (see §4.2–4.5). The three hydrodynamics experiments of July 2007, January 2008, and April 2008 had markedly different density dynamics at work, as presented in the three sub-sections below. The July 2007 experiment was notable for well-mixed salinity conditions with diurnal temperature stratification; the January 2008 experiment was notable for very strong salt stratification and internal seiching, and April 2008 was notable for the turbulent mixing that marked the transition from salt stratified to well-mixed conditions.

4.1.1 July 2007: Diurnal temperature stratification

The experiment of 06 July 2007 to 26 July 2007 took place under typical dry summer conditions: the outlet was closed, inflows from the weir were very low (Fig. 4-2), and the weather alternated between coastal fog and sunny with sea breezes. The lagoon was well-mixed in terms of salt, as the outlet had been closed since early May. Observations from 2006-2008 and previous seasonal monitoring by others (Silkie 2008; D. Fong pers. comm.) suggest that this is a "typical" summer condition; after the dry season begins, the outlet closes and the remaining salt eventually reaches a uniform distribution in the water column. Despite the lack of salinity gradients, the strong light

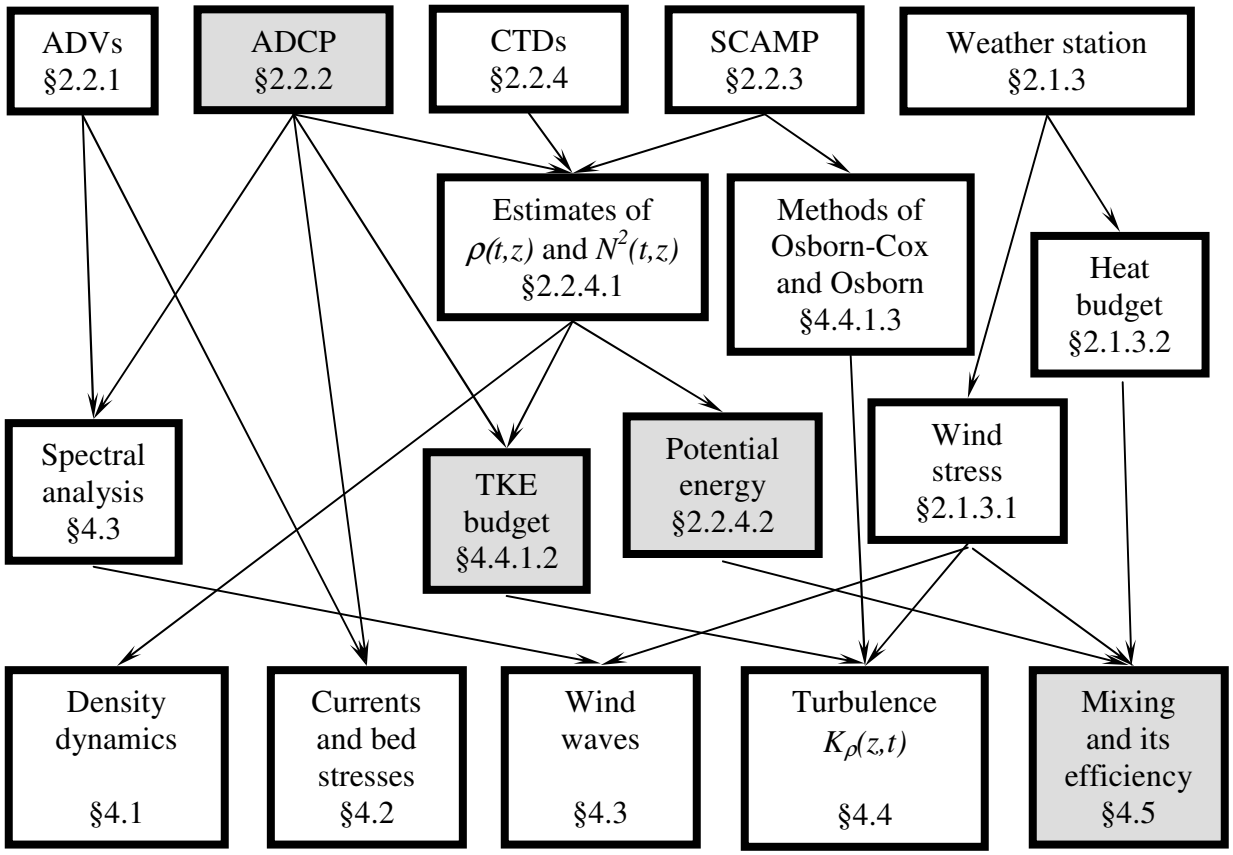

Fig. 4-1. I used several types of analysis to transform the raw data from the ADVs, an ADCP, CTDs, SCAMP, and weather stations into conclusions about hydrodynamics in Rodeo Lagoon. This figure indicates where to find descriptions of the instrumentation setup, analysis methods, and results. The shaded boxes denote data analysis that pertains to April 2008 only; unshaded boxes pertain to all three hydrodynamics experiments.

Fig. 4-2. The photo on the left from 12 July 2007 shows the lagoon outlet in its closed state. The photo on the right from 06 July 2007 shows the weir that separates lagoon from the freshwater wetland/lake upstream; the is almost no spillage over the weir due to the dry summer climate that prevailed during the July 2007 experiment.

absorption in the water column made diurnal temperature stratification relatively common during the July 2007 experiment (§3.5, Fig. 3-7). The lagoon is quite shallow – less than 1.5 m deep in July 2007 – so even though absolute temperature differences from surface to bed are only 1–2°C, N^2 is moderately high ($N^2 = 5 \times 10^{-3}$ s^{-2}).

Observations with three different types of CTDs at the lagoon center station on the calm and sunny day of 18 July 2008 provide an example of this diurnal temperature stratification (Fig. 4-3). Over the course of about three hours, the lagoon warmed by about 1°C, as shown both by the sequential SCAMP profiles and the moored CTDs. However, the moored CTDs, which were only at the surface and bottom, are unable to provide information about the vertical structure of the temperature profile (Fig. 4-3C). The fine structure was even somewhat difficult to observe with a larger pumped CTD like the Sea-Bird 19+ that I used for seasonal monitoring (Fig. 4-3B). The SCAMP, by contrast, has considerably higher vertical resolution than the 4-Hz Sea-Bird even on the slowest of its three thermistors, so it is better suited for observing the fine structure (Fig. 4-3A). The SCAMP profiles show step-like layering as a warmer diurnal surface layer forms very near the surface (11:13, Fig. 4-3A), then deepens (13:34, Fig. 4-3A).

4.1.2 January 2008 experiment: Strong salt stratification and internal seiching

The experiment of 07 January 2008 to 24 January 2008 occurred at the height of the rainy season; although only 3.6 cm of rain fell during the experiment, nearly 7 cm rain fell in the four days immediately preceding the experiment. Because of this wet weather, there were large freshwater flows into the lagoon from the watershed (Fig. 4-4). These freshwater inputs,

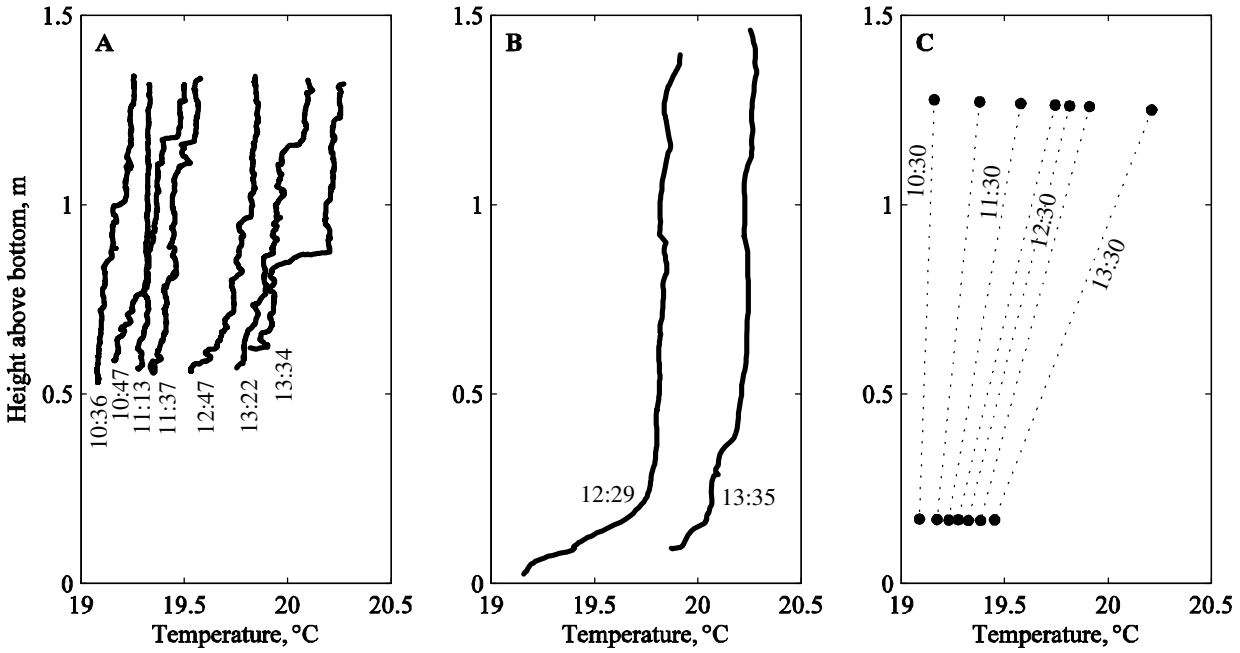

Fig. 4-3. Temperature profiles collected 18 July 2007 in Rodeo Lagoon. Data sources include (**A**) a microstructure profiler with a resolution of ~1 mm dropped from the water surface, (**B**) a traditional profiling CTD with a resolution ~1 cm dropped from the surface, and (**C**) a pair of moored CTDs near the surface and bed. The time stamps indicate when the various profiles were collected at the lagoon center station.

combined with high ocean wave conditions capable of building a high beach berm, led to the flooding shown in Fig. 4-5 and the peak lagoon volume observed over the period of December 2005 – June 2008 (Fig 2-5).

Throughout the January 2008 experiment, the outlet intermittently opened and closed in response to the strong forcing on both sides. On 11 January 2008, the lagoon broke through the beach berm and rapidly drained about 40% of its volume, though very little of the bottom salty water was flushed out during this process (Fig. 4-6). In fact, despite significant freshwater flow through the lagoon and several windy days, there was very little diapycnal mixing observed over the period of 13–23 January, as evidenced by salinity time series data from the center of the lagoon and longitudinal cross sections collected five days apart (Figs. 4-6, 4-7). Furthermore,

Fig. 4-4. The photo on the left from 11 January 2008 shows the lagoon outlet in its open state. The fresh footprints are evidence of a recent exchange between the the ocean to the lagoon. The outlet periodically opened and closed throughout the January 2008 experiment. The photo on the right from 28 January 2008 shows that freshwater inputs from the watershed were quite high due to the wet winter climate.

Fig. 4-5. Rodeo Lagoon was deeper than usual in this picture taken 09 January 2008, flooding the pedestrian bridge to Rodeo Beach. The yellow booms are a response to the Cosco Busan oil spill of 07 November 2007, which reached Rodeo Beach.

since the outlet was open, additional salt water may have flowed from the ocean into the lagoon during the January 2008 experiment, though Fig. 4-6 suggests that such inflows were minimal. The combination of very low diapycnal mixing rates and saltwater inflows precludes the possibility of performing mixing efficiency calculations for the January 2008 experiment.

An extremely sharp density interface was present during most of the January 2008 experiment (Figs. 4-7, 4-8). The sharp interface appears in profiles collected with both SCAMP and Sea-Bird, but the location of the pycnocline was considerably more variable in the Sea-Bird profiles; by comparison, the SCAMP profiles showed close agreement with one another. The difference in vertical position is likely due to SCAMP pressure sensor offset error and a time lag error in the Sea-Bird, which pumps the water through the instrument. Regardless, peak values of N^2 at the pycnocline exceeded 0.1 s^{-2} on all the days of profiling in January 2008 (Fig. 4-26B). Such values of N^2 are comparable to values seen in other salt-wedge estuaries (Geyer et al. 2008) or man-made systems like mining waste pit lakes (e.g., Stevens et al. 2005). Unlike salt-wedge estuaries, of course, Rodeo Lagoon lacks tidal energy.

The pycnocline responded to wind forcing by tilting and seiching. For example, the cross-sections of 16 January 2008 (Fig. 4-7A) captured tilting of the pycnocline in response to wind forcing. Wind speeds on 16 January were quite high, with a mean wind speed of 4.0 m s^{-1} at the lagoon weather station; by comparison, tilting was not observed in the cross section collected on the much calmer day of 21 January, when the mean wind speed was only 1.8 m s^{-1}. The wind on

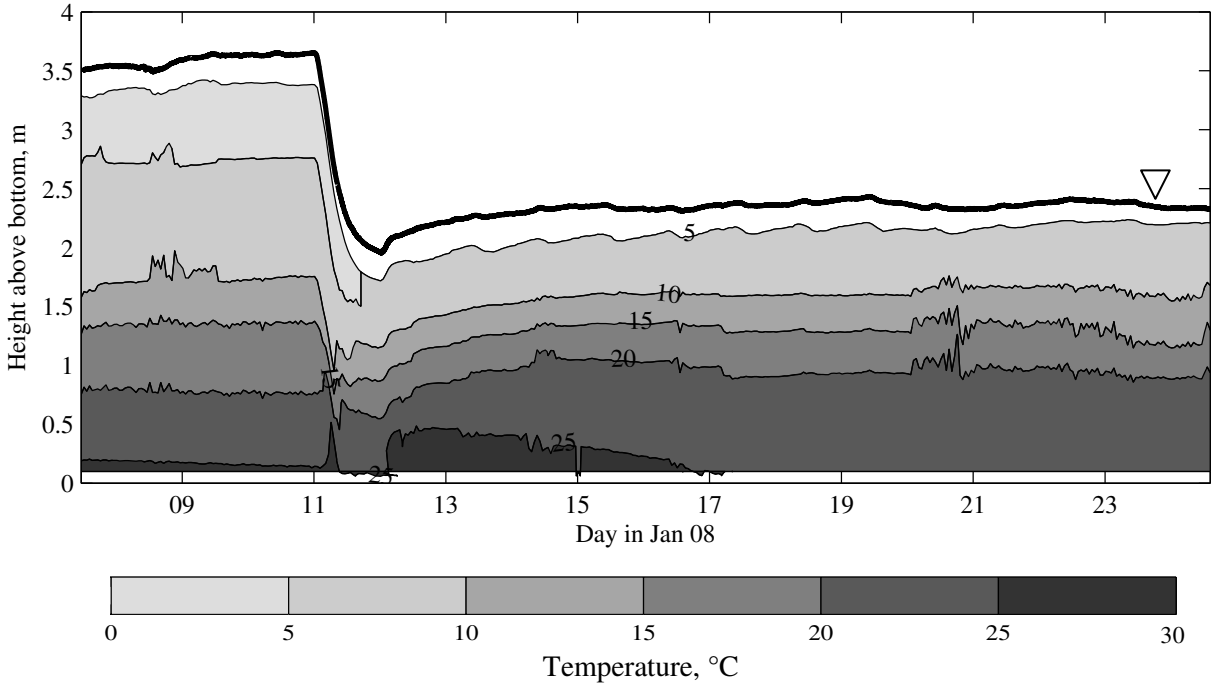

Fig. 4-6. Time evolution of salinity structure in January 2008. Data are hourly averages from a vertical array of four CTDs floating from a surface buoy and two CTDs moored at the bottom. The pycnocline appears to be more gradual than in Fig. 4-7 or Fig 4-8 because of the coarse vertical resolution of the CTDs. The water surface is indicated by the thick black line at 2.5–3.5 m above the bed. White regions beneath the surface are an indication of no data.

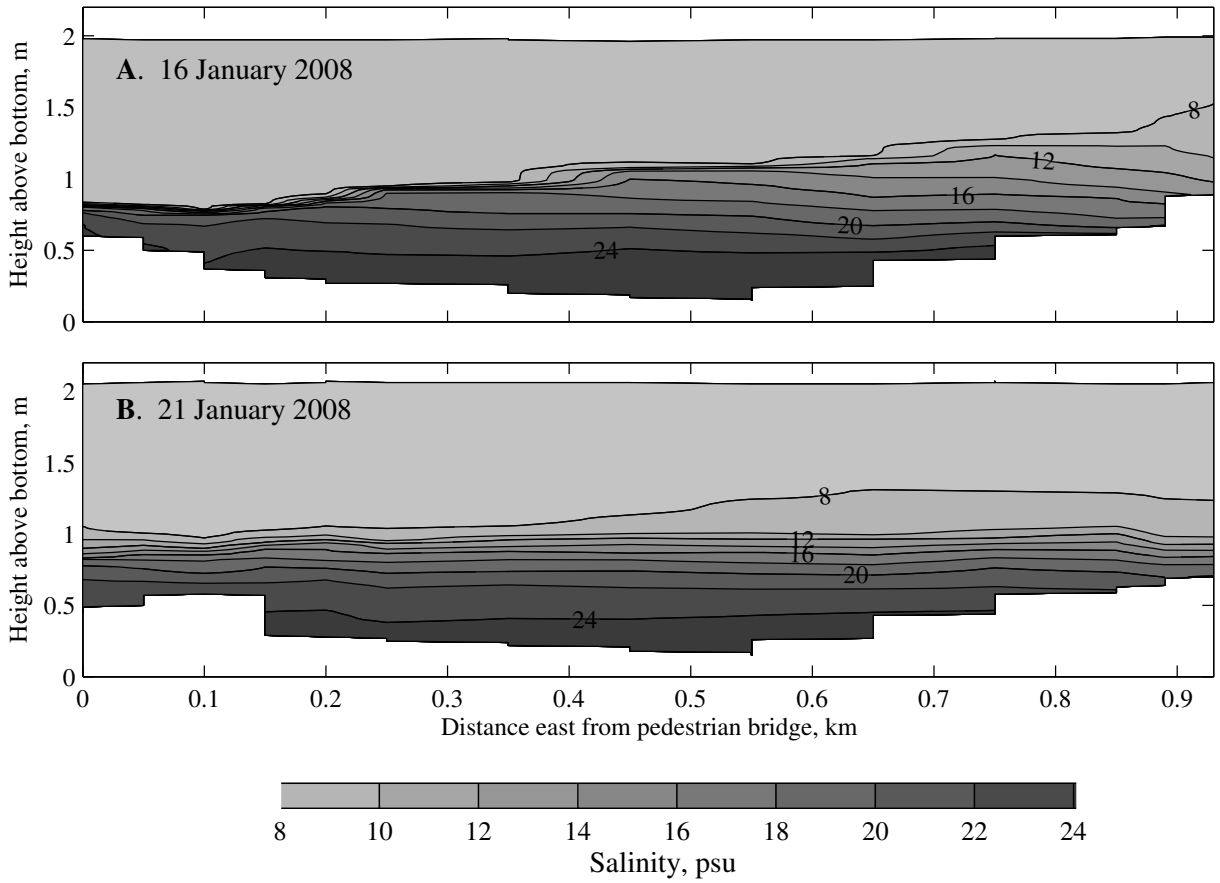

Fig. 4-7. Two longitudinal transects of salinity as collected with the microstructure profiler in January 2008 show strong vertical density stratification. The alignment of the longitudinal transect is shown in Fig. 2-2.

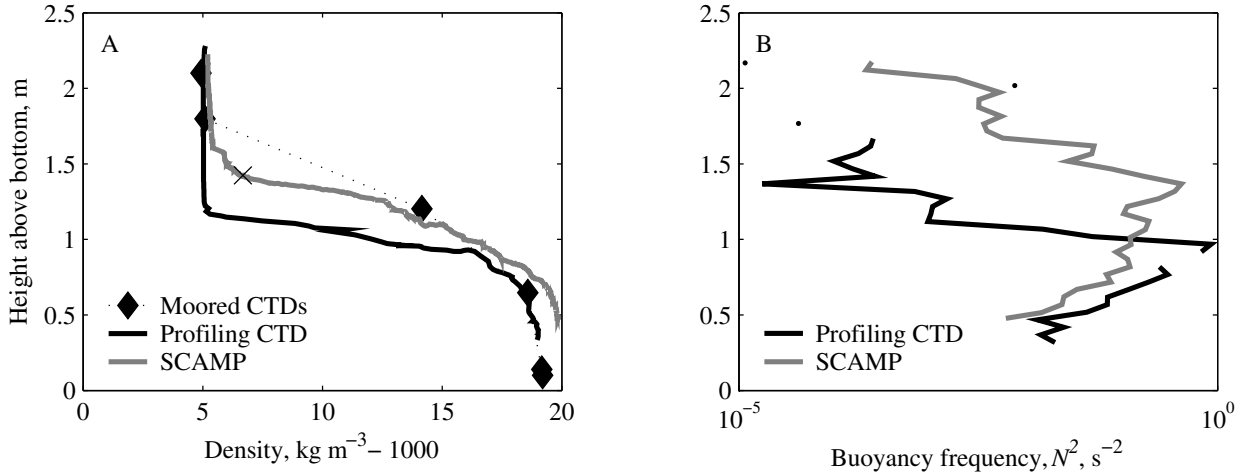

Fig. 4-8. (**A**) Density profiles collected with three different types of sensors on 15 January 2008: moored CTDs (Sea-Bird SBE 37 and RBR XR-420), a traditional pumped profiling CTD (Sea-Bird SBE 19+), and a temperature microstructure profiler with salinity channel (SCAMP). × marks the location of the pycnocline as defined for SCAMP segmentation. (**B**) Buoyancy frequency, N^2, calculated from 5-cm bins of the data shown in (**A**).

16 January was from the north east, so it makes sense that there should be downwelling on the west side (Fig. 4-7A, left side) and upwelling on the east (right side). The appearance of upwelling is probably enhanced by the freshwater inflows at the eastern end. The Wedderburn number (eq. 1-2) remains greater than 1, typically ranging between about 5 and 15 in January 2008, so this upwelling probably did not reach the surface; even on 16 January, the Wedderburn number had a minimum value of 3.

The windiest period of the experiment was 20 January 2008, when wind speeds reached 6 m s^{-1} (Fig. 2-3B). On that day, the pycnocline showed oscillations that are consistent with seiching

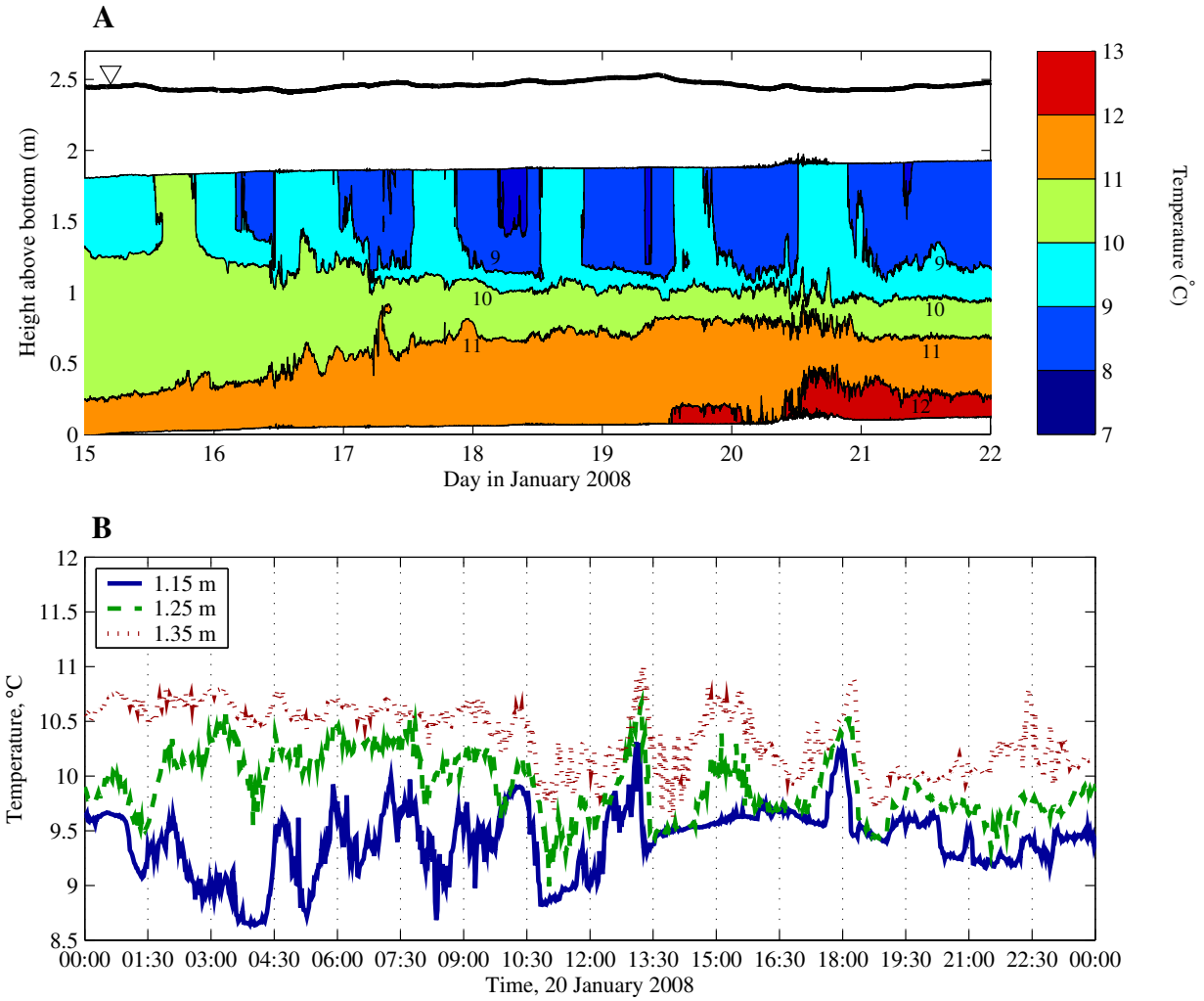

Fig. 4-9. (**A**) Time evolution of temperature structure from a string of thermistors in January 2008. Data are from a vertical array of 15 thermistors moored at the lagoon center station and sampling every 90 seconds. In the top panel, the water surface is indicated by the thick black line at approximately 2.5 m above the bed; white regions beneath the surface are an indication of no data. The top of the pycnocline was located about 1 m above the bottom during the period shown (Fig. 4-7). (**B**) Temperature record on 20 January 2008 from three thermistors located in the pycnocline (1.15 m, 1.25 m, and 1.35 m below the surface). Variability at 90 minutes and 180 minutes is evident, consistent with seiching at those frequencies.

(Fig.4-9A, 10º and 11º isotherms, and 4-9B). The expected period for the first mode of oscillation in a two-layer, two-dimensional system (Kalff 2002) is

$$T = \frac{2L}{\sqrt{\frac{g(\rho_1 - \rho_2)}{\frac{\rho_1}{h_1} + \frac{\rho_2}{h_2}}}} \qquad (4\text{-}1)$$

where L is the length of the basin, ρ_1 and h_1 the density and depth of the lower layer, and ρ_2 and h_2 the density and depth of the upper layer. Applying values from January 2008 ($h_1 = h_2 = 1$ m, L = 750 m, $\rho_1 = 1017$ kg m^{-3}, and $\rho_2 = 1005$ kg m^{-3}), the expected period is about 100 minutes. The observed period is about 90 minutes, very close to this expected value; oscillations at 180 minutes are also evident (Fig. 4-9B).

4.1.3 April 2008 experiment: Mixing and potential energy

The experiment of 01 April 2008 to 21 April 2008 took place during the transition from the wet season, when saltwater inflows also tend to occur, into the dry season. No rain fell during the experiment, and the preceding month was also quite dry, with less than 1 cm of rain. The outlet was closed for the duration of the experiment, and inflows were relatively low (Fig. 4-10). However, significant inflows of salt water apparently occurred in the two months preceding the experiment, leading to conditions perfectly suited for observing the nearly conservative mixing of fresh and salty water in the lagoon.

The density structure in April 2008 was almost completely controlled by salinity. At the beginning of the experiment (prior to 14 April), salt-based stratification was equivalent to a density difference of $\Delta\rho \sim 8$–12 kg m^{-3} over less than 25 cm (Fig. 4-11D). This strong stratification allowed inverse temperature stratification to develop that was equivalent to $\Delta\rho \sim -1$ kg m^{-3} (Fig. 4-11B). By the end of the experiment, however, the lagoon was well-mixed in terms of both salt and temperature.

Fig. 4-10. The photo on the left shows the outlet in its closed state, while the photo on the right shows that inflows from weir spillage were low during the April 2008 experiment. Both photos are from 14 April 2008.

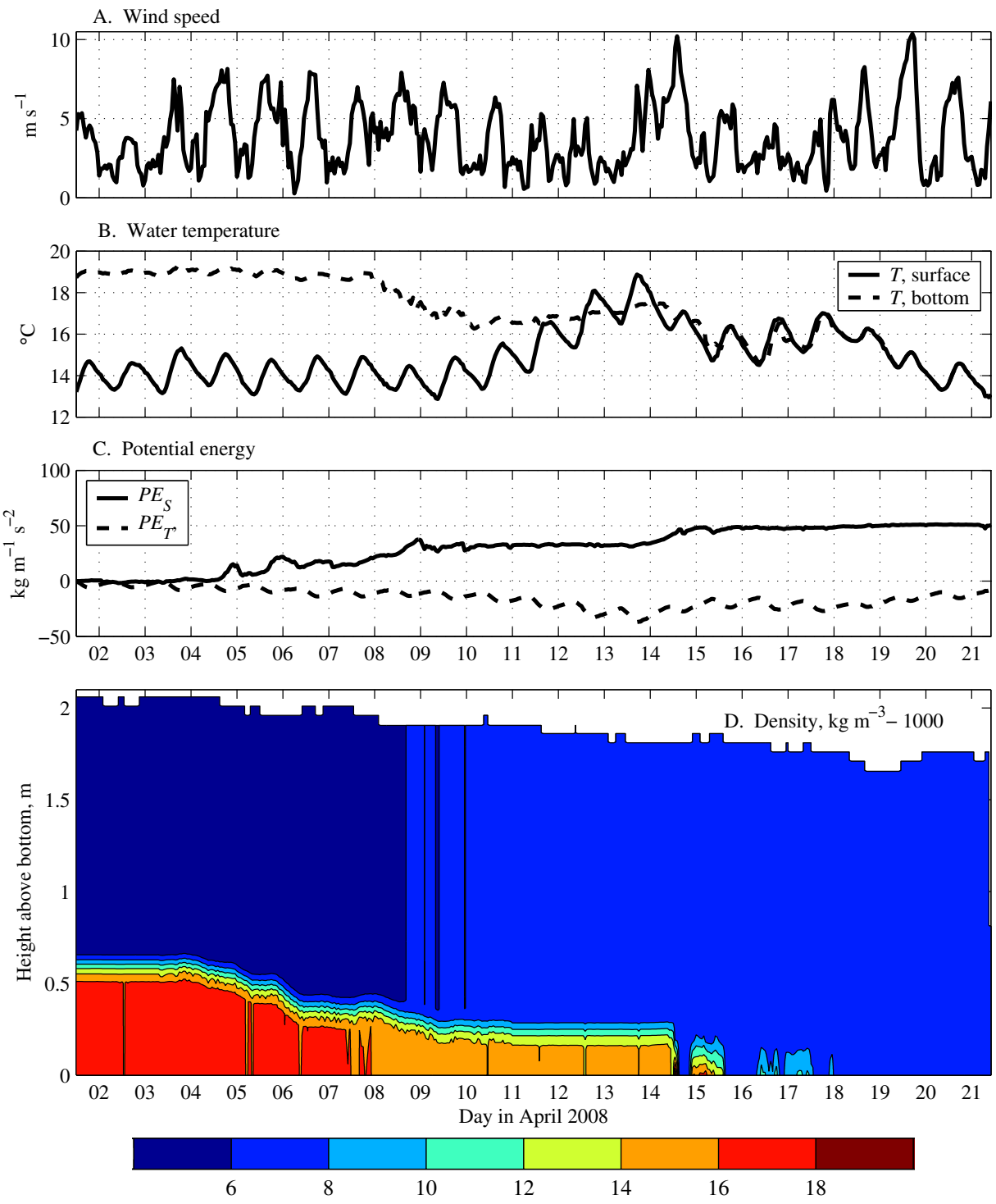

Fig. 4-11. (**A**) Hourly wind speed (m s^{-1}) in April 2008, calculated from eq. 2-3. (**B**) Temperature (°C) during the April 2008 experiment. Data are from moored CTDs (RBR XR-420) near the surface and bottom of the lagoon. (**C**) The portions of potential energy due to salinity, PE_S, and temperature, PE_T (eq. 2-19), less their initial values. (**D**) Time evolution of the vertical density profile, $\rho(z,t)$ (kg m^{-3}- 1000, color bar), inferred from moored CTDs and SCAMP profiles. Temperature variability is not included in this version of $\rho(z,t)$.

One way to quantify changes in vertical density structure is via the potential energy, *PE* (eq. 2-19). The change in total potential energy over time is mostly a result of changes in water column depth, because the lagoon lost about 13% of its volume over the course of the April 2008 experiment. However, due to the bathymetric hump at the outlet, this outflow had very little effect on the vertical density structure except to make the surface layer gradually less deep. More important than the change in depth, then, is the variability in *PE* due to changes in salinity (PE_S, Fig. 4-11C, solid line) and temperature (PE_T, Fig. 4-11C, dashed line). Although PE_T shows considerable diurnal variability, the heat exchanges involved do not significantly contribute to irreversible mixing of the salty layer (see §4.5.2). Therefore, PE_S is of greater relevance here. The record of PE_S shows three major jumps reflecting irreversible mixing on 04–06, 07–08, and 14 April 2008 (Fig. 4-11C, solid line). After 14 April, the salinity is more or less evenly distributed, so additionally energy inputs cannot produce any change in PE_S. As discussed in greater detail in §4.5.1, the time rate of change of PE_S and mixing efficiency are linked to the wind forcing.

The salty layer was also subject to displacement by the wind, a process which occurs in tandem with irreversible mixing. As winds approached 10 m s^{-1} on 14 April 2008 (Fig. 4-11A), salinity in the comparatively well-mixed surface layer ($N^2 < 1\times10^{-4}$, Fig. 4-26G) gradually increased from 9.2 to 10 psu. Meanwhile, salinity at the bottom of the lagoon rapidly decreased over 2 hours from 20 to 10 psu (Fig. 4-11D), reflecting a combination of mixing of the brackish layer past the point of the moored CTD and downwind displacement of that layer. Salinities suddenly rebounded on the evening of 14 April 2008, 6 hours after the peak winds occurred at 14:00 h, which may represent a gravity current of brackish water returning after wind setup relaxes. An approximate travel time for a shallow-water gravity current (Shin et al. 2004) is

$$T = \frac{\mathrm{L}}{\sqrt{\mathrm{g\,h}\,\Delta\rho\,(1-\mathrm{h/H})/\rho_0}} \qquad (4\text{-}2)$$

where L is the distance traveled, H is the total depth, h is the depth of the gravity current, and $\Delta\rho$ the density difference between the two layers. Applying values from 14 April 2008 (H = 2 m, $\Delta\rho$ = 6 kg m^{-3}, h ~ 0.1 m, L ~ 300 m), the front travel time estimate is 1.1 hrs. This suggests that if a gravity current of displaced brackish water is responsible for the rebound in salinity, it did not begin to move for several hours after wind speed peaked. Such a lag is consistent with the ADCP current speeds, which do not fall below 0.05 m s^{-1} until around the time salinity rebounds. On 15-16 April 2008, a similar decrease and rebound of salinity occurred, except this time the rebound took nearly 10 hours after the peak wind speed passed. Although $\Delta\rho$ is smaller in this case ($\Delta\rho$ = 2.3 kg m^{-3}), the predicted travel time is only on the order of about 2 hours. In this instance, a fast-moving gravity current is not a good explanation for the observations; instead, the rebound was associated with a reversal of wind direction, which produced a change in the bottom current direction of about 100°. In summary, the salinity contour plot of Fig. 4-11D, which appears to show a physically impossible increase in bottom salinity on 14 and 16 April, makes sense if pockets of salty water were temporarily stored in the lagoon away from the center station where salinity was monitored, then subsequently redistributed by currents.

4.1.4 Summary – density structure

Despite being small and shallow, Rodeo Lagoon exhibits many of the density dynamics that were originally recognized in much larger lakes, and can be analyzed within a similar conceptual framework. These dynamics include diurnal heating and cooling, diurnal temperature stratification (§4.1.1, Fig. 4-3), seiching of the pycnocline (§4.1.2, Fig. 4-9), and wind-driven diapycnal mixing (§4.1.3., Fig. 4-11). The primary difference from lake physics is that here the seasonal stratification is caused by salt rather than temperature, producing a density structure that is vertically condensed and has steeper gradients than in a lake. Also, the seasonality is reversed, with the strongest stratification in winter rather than summer.

4.2 Currents, stresses and shear

4.2.1 ADV results: Currents and stresses at the bed

Mean horizontal near-bed velocities in Rodeo Lagoon were quite low (Fig. 4-12, Table 4-1). Burst-averaged horizontal ADV velocities 20 cm from the bed were typically less than 0.02 m s^{-1}, while vertical velocities were always at least an order of magnitude lower than the horizontal velocities. Velocities at the ADV located 10 cm from the bed (not shown) were of similar magnitude. The mean velocities frequently flip direction, even after rotation into principal axes; this is most noticeable in the January 2008 data, which also saw the most pronounced reversal of wind speeds (Fig. 2-3).

Experiment Date	$\overline{\lvert U \rvert}$, **m s^{-1}**	$\overline{\lvert V \rvert}$, **m s^{-1}**	$\overline{\lvert W \rvert}$, **m s^{-1}**	**Dominant variability**
July 2007	1.1×10^{-2}	5.3×10^{-3}	8.6×10^{-4}	Diurnal
Jan 2008	0.8×10^{-2}	2.4×10^{-3}	3.5×10^{-4}	Seiche
Apr 2008	0.4×10^{-2}	2.3×10^{-3}	3.8×10^{-4}	Extreme winds / synoptic

Table 4-1: Summary of near-bed velocity components in the two horizontal directions, U and V, and the vertical direction, W, expressed as an average of the absolute value during each experiment. The dominant mode of variability expressed in Fig. 4-13 is also noted.

Near-bed velocities exhibited different dominant frequencies under the different experimental conditions of the July 2007, January 2008, and April 2008 experiment (Fig. 4-13, Table 4-1). This is illustrated in the spectral power distribution for the detrended, hourly averages of the horizontal velocity U, Reynolds stress component $\langle u'w' \rangle$, and wind speed from the three experiments (Fig. 4-13). Under well-mixed conditions in July 2007, there is a broad peak in spectral power at the diurnal frequency in all three quantities, indicating that both mean currents and turbulent mixing at the bed are varying on the time scale of the daily sea breeze (f=1/day $=1.16\times10^{-5}$ Hz, solid line, Fig. 4-13A). Weak temperature stratification, which could modulate the effect of wind forcing on currents and mixing, also varies on a diurnal time scale.

Under salt-stratified conditions in January 2008 there is evidence for motion at shorter time scales that could be seiche harmonics (3.5-7 hours, shaded region, Fig. 4-13B). The expected period for the first mode of an internal seiche is 90-100 minutes (eq. 4-1), which is a higher frequency than those resolved in Fig. 4-13 because of the one-hour sampling frequency. The diurnal peak is not evident in any of the January 2008 spectra. In April 2008, when the lagoon

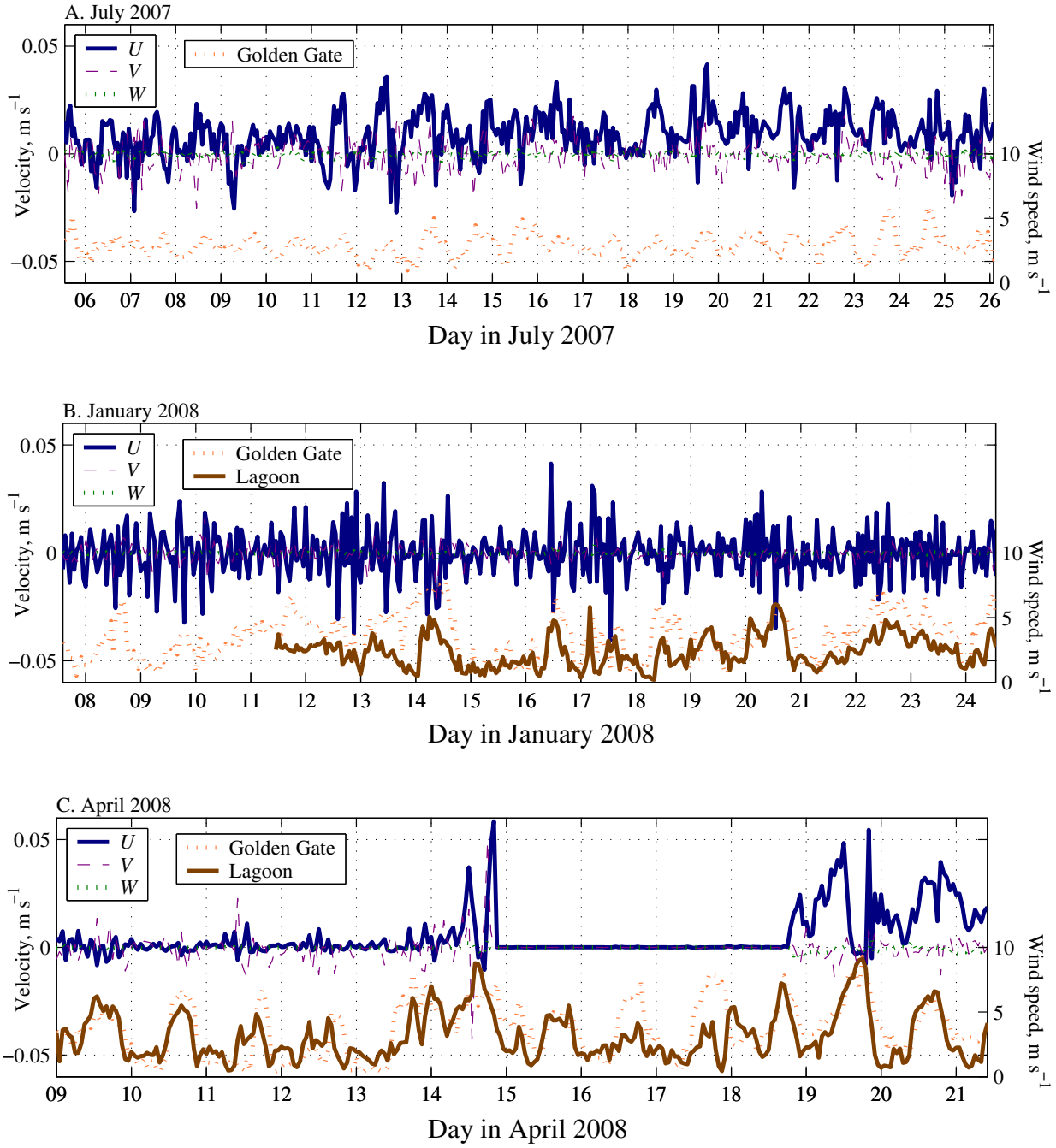

Fig. 4-12. Burst-averaged mean velocities from an ADV located 20 cm from the bed in (**A**) July 2007, when the lagoon had a uniform salinity distribution; (**B**) January 2008, when it was stratified by salt; and (**C**) April 2008, when the lagoon transitioned from stratified to well-mixed around 14 April. Velocities in the two horizontal directions (*U*, solid blue line and *V*, dashed purple line) and vertical (*W*, dotted green line) are indicated on the left axis, while wind speeds at the Golden Gate weather station (dotted orange line) and lagoon weather station (solid brown line) are indicated on the right axis.

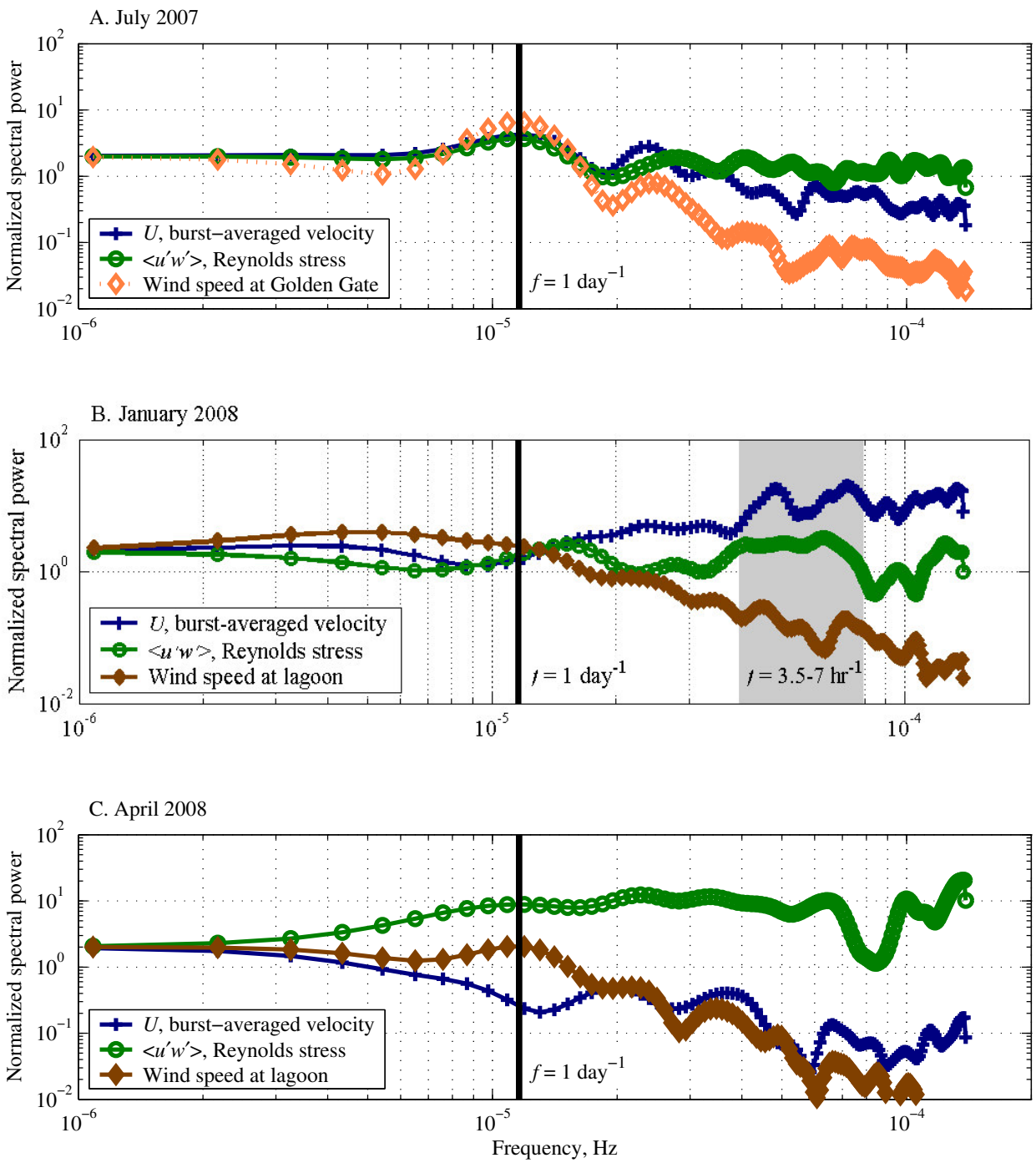

Fig. 4-13. Normalized spectral density from an ADV located 20 cm from the bed in (**A**) July 2007; (**B**) January 2008; and (**C**) April 2008. Spectral density was calculated on detrended data and smoothed with a Hamming window with a block size of 64 data points (~2.7 days). The results were then normalized by dividing by the spectral power at $f = 0$. Shown are spectral densities for the burst-averaged velocity along the primary horizontal axis, U (blue pluses and squares), the Reynolds stress component $\langle u'w' \rangle$ (green circles), and wind speeds at the Golden Gate weather station (open orange diamonds) or lagoon weather station (solid brown diamonds).

transitioned from stratified to well-mixed, most of the variability in the average velocity U is at longer time scales, so the spectral peak for U is at the minimum resolved value of f (Fig. 4-13C). This is consistent with the very strong wind forcing and fast velocities observed on just two days (14 and 19 April), with weak winds and slow velocities during the remainder of the experiment (Fig. 4-12C). A diurnal peak is evident in the April 2008 wind data, but not in the Reynolds stresses or U. The lack of a diurnal signal in January and April 2008 is probably because of two factors: (a) the physical forcing, including inflow and wind, was operating on a synoptic rather than diurnal time scale, corresponding to the passing of winter low pressure systems, and (b) the lagoon was strongly stratified, so any surface-driven forcing was be transmitted to the bed less effectively.

Bed stresses can be quantified several ways: using the root-mean-square of two components of the Reynolds stresses ($u*_{bed}^2$, eq. 2-11), using the wave-debiased estimator of Shaw and Trowbridge ($u*_{cov}^2$, eq. 2-12), or using dissipation ($u*_{dissipation}^2$, eq. 2-15), all of which are shown in Fig. 4-14. The dissipation-based estimates show a much larger range than the other two estimates, which is a reflection of the way this method of calculation substantially differs from the other two (see §2.2.1). The wave-debiased estimates do not differ significantly from the Reynolds stresses (green and blue lines, Fig. 4-14), indicating that wind wave contamination is not a major problem. All three types of bed stress estimates show similar variability with respect to wind forcing, though the type of response varied by experiment, as discussed below.

The best agreement between wind forcing and bed stresses was under well-mixed conditions in July 2007. There is a positive correlation, albeit a weak one, between wind stress, $u*_{wind}$, and the shear velocity calculated from the Reynolds stresses at 20 cm above the bed, $u*_{bed}$ ($r^2 = 0.16$, Fig. 4-15A). Also, as shown in Fig. 4-13A and Fig 4-14A, mean velocities from the July 2007 experiment showed a diurnal variability that is clearly a reflection of diurnal variations in the local sea breeze. Similarly, bed stresses appear much higher under windy conditions in April 2008 (compare Fig. 4-12C to Fig. 4-14C), although on an hourly basis the correlation between $u*_{bed}$ and $u*_{wind}$ is very weak ($r^2 < 0.01$, not shown). The poor correlation is a result of the nonlinear response of bed stresses to wind speeds, particularly the time lag between peak wind speeds and peak bed stresses.

Stratification, whether weak temperature stratification or strong salt stratification, clearly reduces the coupling between wind stress and bed stress. For example, when the lagoon is salt-stratified, as in January 2008, Reynolds stresses near the bed are much lower for a given wind stress compared to when the lagoon is well-mixed (Fig. 4-15). Also, the relationship between the two variables is extremely weak ($r^2 = 0.05$ for January 2008, Fig. 4-15B).

Density stratification can reduce the effect of wind stress on turbulent mixing on the time scale of days, not merely on a seasonal basis. In each of the July 2007 and April 2008 experiments (but not in the January 2008 experiment), N^2 varied considerably over the deployment. In July 2007, weak temperature stratification was present, reaching peak values of $N^2 \sim 10^{-3}$ s^{-2} on warm, sunny days (Fig. 3-7). In April 2008, density stratification was more dependent on salinity gradients, ranging from $N^2 \sim 5\times10^{-2}$ s^{-2} at the start of the deployment to $N^2 < 10^{-5}$ s^{-2} at the end (Fig. 4-11D). To assess variability among u^*_{bed}, u^*_{wind} and N^2 beyond the diurnal time scale, I averaged their values over a 24-hour window beginning and ending at 06:00 h, which

corresponds to a minimum in the observed diurnal variability of the wind. This aggregation over a day is useful because there is a time lag between peak winds and turbulent mixing. The exact duration of this lag is unknown and presumably varies with each wind event.

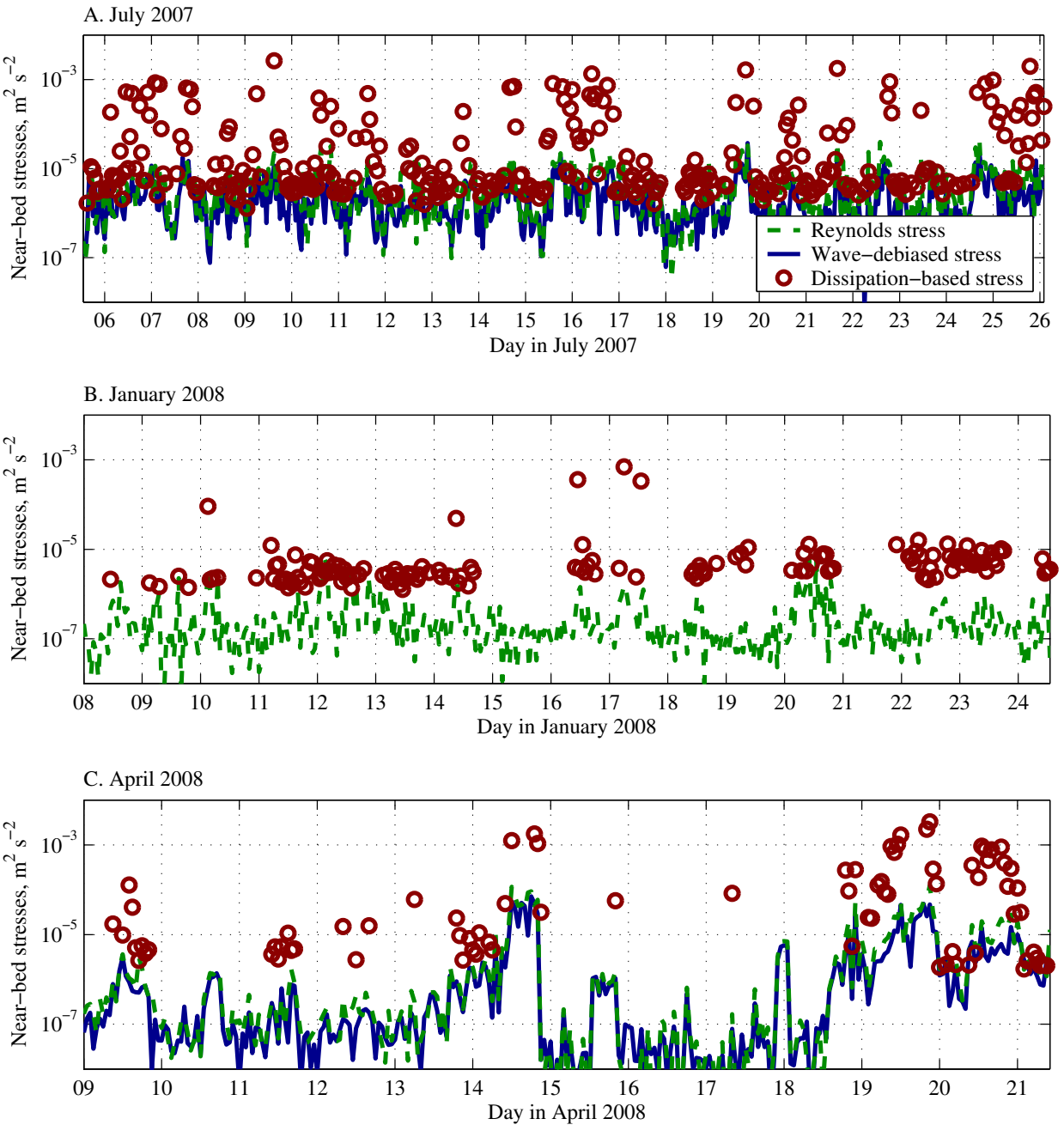

Fig. 4-14. Near-bed stresses calculated three ways: Reynolds stresses (square of eq. 2-11, solid blue line), a wave-debiased estimate from the method of Shaw and Trowbridge (2001) (eq. 2-12, dashed green line), and from dissipation (eq. 2-15, red circles). No wave debiased stress is available in January 2008 due to an instrument malfunction.

The relationship between bottom stress and wind stress is most simply expressed by the ratio of the shear velocity and surface wind friction velocity, u^*_{bed}/u^*_{wind}. There is significant negative correlation between this ratio and the buoyancy frequency as represented by $\log_{10} N^2$ (Fig. 4-16, $r^2 = 0.43$ for July 2007; $r^2 = 0.42$ for April 2008). The results of Fig. 4-16 are an indication that as stratification strengthens, wind stresses imposed at the surface are transferred less efficiently to the bottom boundary layer.

Tidal energy does not propagate into the lagoon except as a slow-moving influx of salt water during high tide or wave conditions, and energy from freshwater inflow is mostly dissipated by large boulders around the inlet structure. The dominant local tidal period is 12.4 hours (M2), but I could detect no evidence of variability at this frequency in the near-bed velocity data from the three experiments or in the depth gage data, which spans several years.

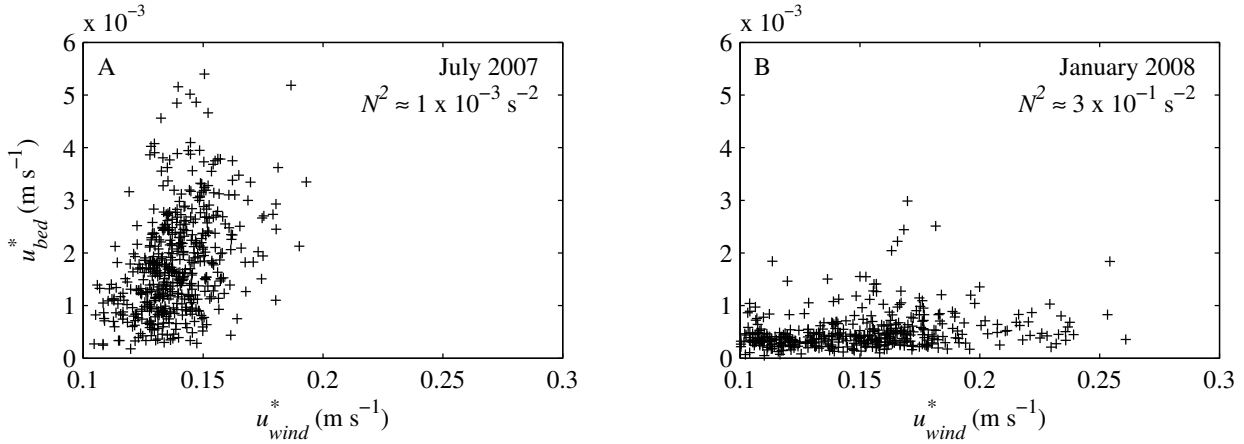

Fig. 4-15. Shear velocity u^*_{bed} (m s^{-1}) 20 cm above the bed vs. surface wind friction velocity u^*_{wind} (m s^{-1}). Shear velocities are hourly averages from ADV deployments in (**A**) July 2007 and (**B**) January 2008. Values of u^*_{wind} are derived from the Golden Gate weather station. N^2 values are representative maximums from each deployment.

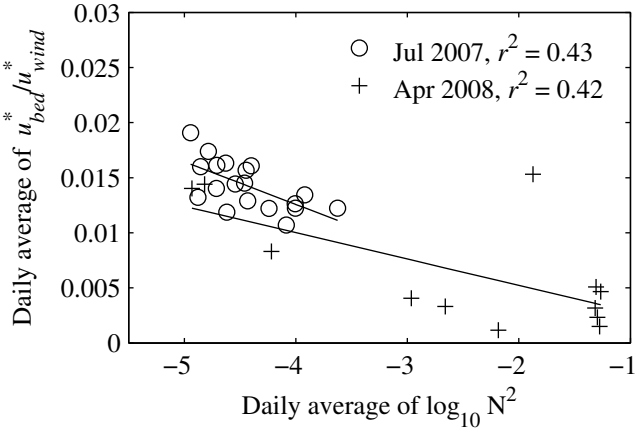

Fig. 4-16. Variability in the daily average of $\log_{10} N^2$ with the ratio of bed shear velocity to surface wind friction velocity, u^*_{bed}/u^*_{wind}. Values of u^*_{bed} and u^*_{wind} are also daily averages. Data are from moored deployments of CTDs and an ADV in July 2007 (circles) and April 2007 (crosses). Values of u^*_{wind} are derived from the Golden Gate weather station.

4.2.2 ADCP results: Current profiles and shear

In shallow lakes, surface currents in the main basin are typically aligned with the wind, or rotated to the right of the wind when Coriolis effects are significant (George 1981; Kalff 2002). Return flows are confined to the edges and highly dependent on bathymetry. This general pattern lies in contrast to large deep lakes, where the currents in the shallows are aligned with the wind while the deeper middle has return flows (Csanady 1978). Density stratification can enhance return flow currents in a layer just above the pycnocline (Kalff 2002), but currents in the hypolimnion itself are typically much slower than surface currents. Currents rotate increasingly to the right away from the surface as an Ekman spiral if Coriolis forcing is significant, which is more likely in slower flows. This conceptual framework gives some basis for understanding the observations in April 2008, the only time period for which current profiles and shear are available.

During the April 2008 experiment, the predominant feature of the mean velocity profiles was a two-layered structure, with very low velocity below the pycnocline when the lagoon is salt-stratified, compared with much higher velocities in the upper mixed layer (Fig. 4-17, solid red lines). Mean currents in the lagoon during the deployment ranged from as low as 0.005 m/s below the pycnocline to about 0.15 m/s in the upper mixed layer under steady winds (> 5 m/s) (Fig. 4-17). The difference in mean velocities produces shear at the pycnocline (Fig. 4-18A), which is a potential source of turbulence, as discussed below. This observation is consistent with low velocities in the hypolimnia of other stratified lakes, at least in the absence of energetic bottom boundary currents.

The direction of mean surface currents appears to be fairly consistently towards the north or slightly northwest (300–360° East of North). Given the consistency of the westerly winds and the observation of Langmuir cells, which typically indicate that waves and surface currents are aligned (Langmuir 1938; Leibovich 1983), surface currents towards the east or south (90-180° E of N) were expected. Thus, the northerly currents are a surprising result and may point to a compass offset error, although no such error could be reproduced in the laboratory. The velocities in the upper and lower layers were often in opposing directions, with velocities near the bed as much as 100 degrees different from the surface (e.g., afternoon of 02 April 2008, solid red line, Fig. 4-17B). Once the lagoon was well-mixed, this difference in direction naturally disappeared (Fig. 4-17, dotted blue line). At low velocities there was also a pattern of gradual rotation to the right away from the surface by up to 100° over 1.5 m, independent of any rotation at the pycnocline, which looks like a surface Ekman spiral and signifies that the Coriolis effect is significant.

Wind was clearly a driver for surface currents (Fig. 4-19), even though wind speed and average surface currents showed only a weak linear correlation (r^2=0.03, not shown). Peak currents in the upper mixed layer often occurred when the wind had no diurnal relaxation and instead maintained its direction over more than a day, as occurred from 07 to 09 April 2008. Peak currents often lagged peak wind speeds, as in the case of 04, 05, and 14 April 2008 (Fig. 4-19). Surface currents in shallow water driven directly by the wind tend to decay quickly when wind forcing is reduced (Csanady 1983), so one possible explanation for this observation is that the currents were associated with baroclinic pressure gradients that form under wind-induced mixing. The wind preferentially mixes the downwind side, which under a sea breeze is the

eastern and shallower side of the lagoon. When the wind relaxes, circulation like the baroclinic pumping described by Rueda et al. (2003) would result.

Reynolds stresses calculated from the ADCP data reveal when and where the vertical transfer of momentum is occurring. Reynolds stress values that have a negative sign indicate transport of momentum down-gradient, the expected direction (Fig. 4-18B,C), while positive values (not shown) are an indication of momentum moving up-gradient. The results were mostly but not uniformly negative, with positive values often found when wind forcing was low, indicating noise or stresses indistinguishable from zero under these conditions. The negative Reynolds

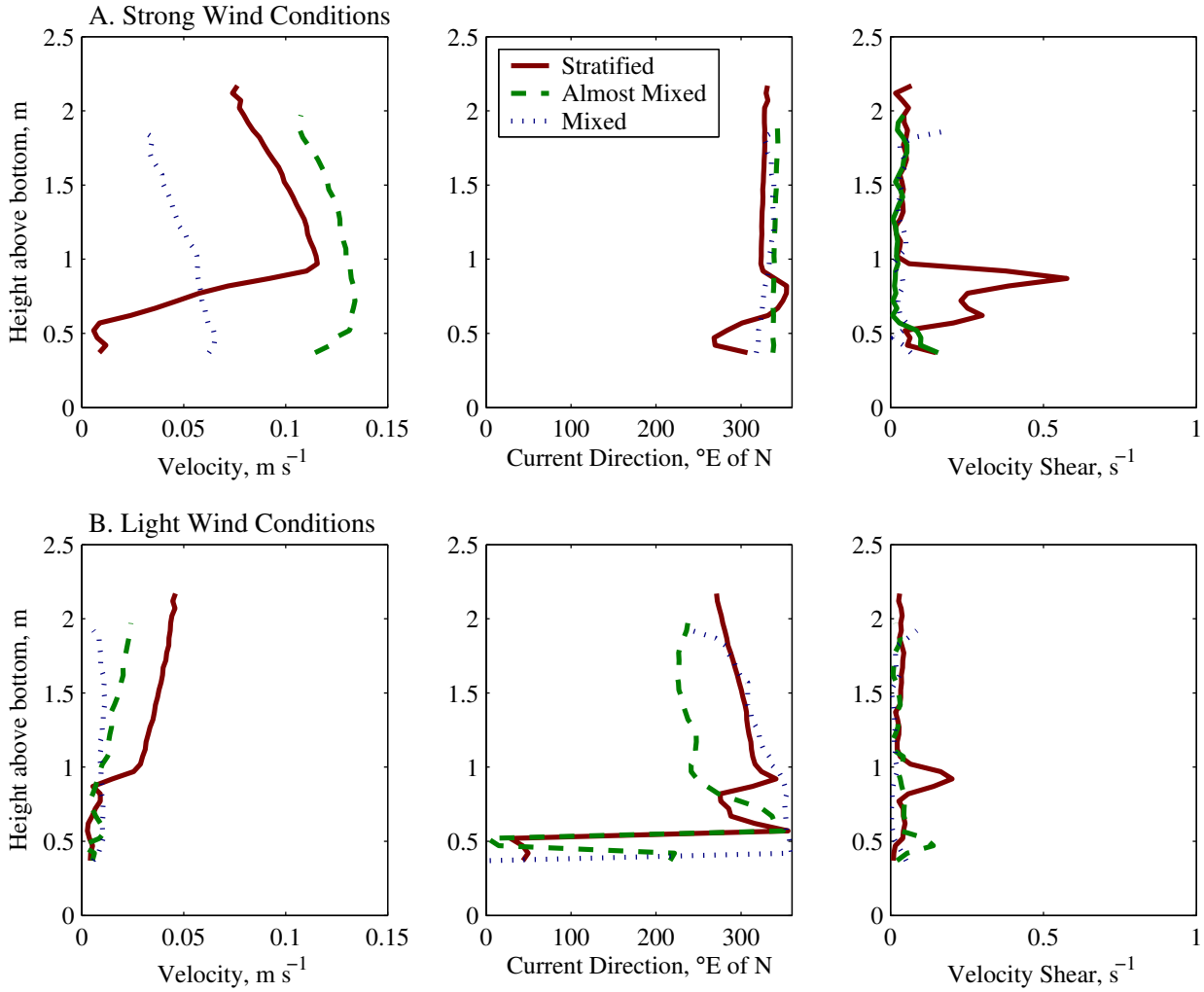

Fig. 4-17. Vertical profiles of water velocity (m s^{-1}), current direction (°E of N), and velocity shear (s^{-1}) at the lagoon under six different forcing conditions. (**A**) The response of the velocity profiles to **strong winds** under stratified conditions (04 April 18:00, U_{wind} = 6.4 m s^{-1} 279°E of N), almost mixed (14 April 10:00, U_{wind} = 5.6 m s^{-1} 282°E of N), and completely mixed conditions (19 April 18:00, U_{wind} = 8.8 m s^{-1} 279°E of N). (**B**) The response to **light winds** under stratified conditions (02 April 18:00, U_{wind} = 1.8 m s^{-1} 110°E of N), almost mixed (13 April 10:00, U_{wind} = 1.4 m s^{-1} 91°E of N), and completely mixed conditions (20 April 18:00, U_{wind} = 1.7 m s^{-1} 296°E of N).

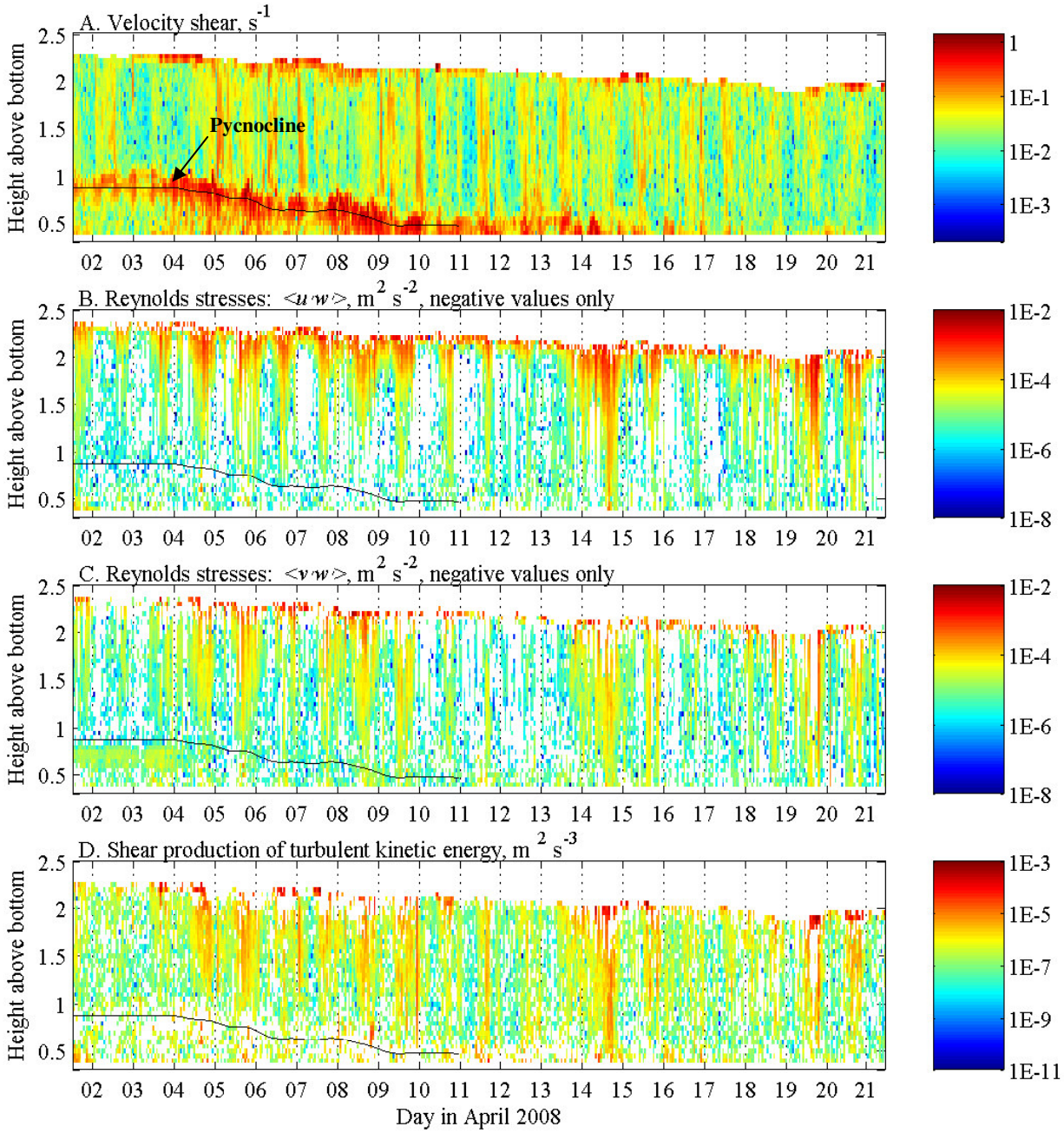

Fig. 4-18. ADCP data from April 2008. (**A**) Velocity shear (s^{-1}) defined using the vertical gradient of the mean velocity, $\partial U/\partial z$. (**B, C**) Reynolds stresses in two directions, $\langle u'w' \rangle$ and $\langle v'w' \rangle$ ($m^2\ s^{-2}$). Only the negative values relevant to down-gradient transfer of momentum are shown. (**D**) Shear production of turbulent kinetic energy ($m^2\ s^{-3}$). For reference, the inferred location of the pycnocline is also shown in each figure. All quantities are on a log scale.

stresses, log-averaged over the upper mixed layer, show a fairly tight coupling with wind stress ($r^2 = 0.63$, Fig. 4-20A). However, the relationship appears to have an upper threshold value of about 1×10^{-4} m^2 s^{-2} at high wind speeds, with Reynolds stresses increasing quickly under low winds until this threshold is reached. Reynolds stresses in and below the pycnocline were typically either positive, or very small and negative, making it reasonable to conclude that there was very little energetic motion in this area. However, there may have been some bottom boundary mixing, as seen in the first few days of the $\langle v'w' \rangle$ signal (Fig. 4-18C, lower left).

Even though the strongest shear was clearly at the pycnocline (Fig. 4-18A), production of turbulent kinetic energy (TKE) did not appear to be large in this region since the stresses were small or poorly defined (i.e., positive). Instead, TKE production was largest near the surface

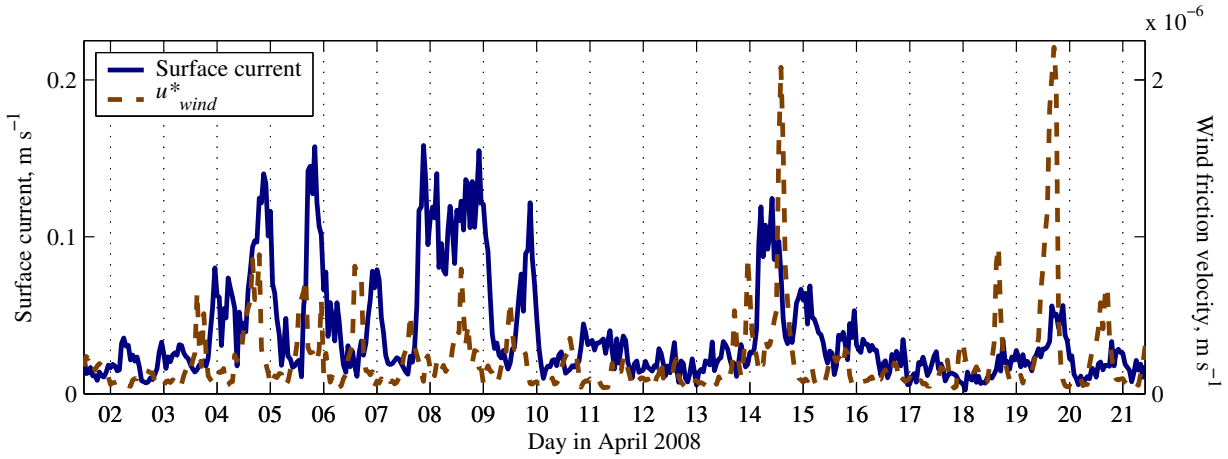

Fig. 4-19. Average surface currents in the upper water column, above the pycnocline, as measured by the bottom-mounted ADCP in April 2008 (m s^{-1}, left axis, blue line). Also shown for comparison is the wind friction velocity, u^*_{wind} (m s^{-1}, right axis, dashed brown line).

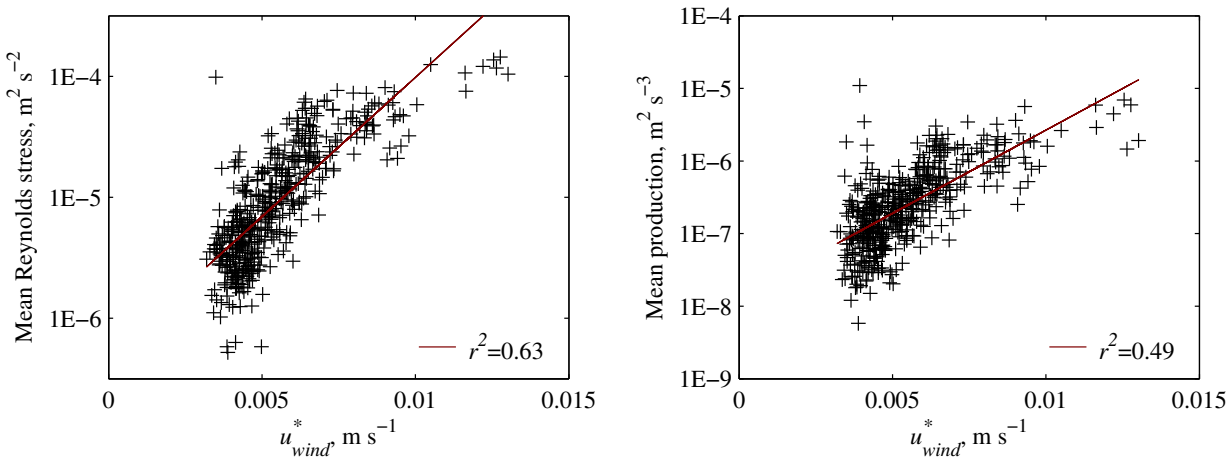

Fig. 4-20. (**A**) Mean Reynolds stress in the surface layer, calculated as a log average of $\langle u'w' \rangle$ and $\langle v'w' \rangle$ (m^2 s^{-2}), as a function of the surface wind friction velocity u^*_{wind}. (**B**) Mean production of turbulent kinetic energy in the surface layer, calculated as a log average, as a function of the surface wind friction velocity u^*_{wind}.

(Fig. 4-18D). Also, the magnitude of TKE production in the surface layer shows a significant relationship with wind stress (r^2= 0.49, Fig. 4-20B). Based on this spatial distribution of TKE production and its temporal relationship with wind, mixing must have been driven from the top down by surface winds, rather than by shear at the pycnocline.

4.3 Wind waves

The local wind direction is usually a sea breeze aligned with the long axis of the Rodeo Lagoon, resulting in co-aligned surface currents and waves that easily produce Langmuir circulation patterns on the water surface, as shown in Fig. 4-21 and as previously recognized at this site by Szeri (1996). Other than contributing to surface windrows, though, how important are wind *waves* themselves, as separate from the wind *stress* discussed in the previous section? In this section, I present evidence that wind waves are predominantly a surface feature, and correspondingly have very little impact on fluid, nutrient, or sediment fluxes near the bed.

Wind waves at Rodeo Lagoon are produced locally, so there was a single, well-defined wind wave frequency that varied from about f = 0.5 to 1.0 Hz (a period of 1–2 seconds), depending on wind conditions. This wind wave frequency appears as a single broad peak in the spectral power distribution, as prototyped in Fig. 4-22; unlike open estuaries or large lakes, there are not additional wave frequencies from wind waves or swell propagating from further afield (e.g., Schwab et al. 1984; Talke and Stacey 2003). In the ADCP data, the wind wave band is defined as all frequencies greater than 0.4 Hz; the ADCP itself samples at 2.5 Hz, so the high-frequency end of the spectrum is truncated. In the ADV data, which is collected at 16 Hz, the wind wave band is defined somewhat more narrowly as 0.6 Hz to 1.3 Hz; perhaps because the ADV samples at a single location rather than over the entire water column, the wind wave peak is narrower in this data set. For either data set, the task of separating out wind waves from other motions is fairly straightforward, as detailed in §2.2.1 and §2.2.2.

Spectral analysis of ADCP velocity data indicates that wind waves were confined to the well-mixed surface layer, usually within 1 m of the surface. As Fig. 4-23A shows, the spectral power distribution for ADCP data does not show a peak in the wind wave band (f > 0.4 Hz) below the

Fig. 4-21. Surface windrows from presumed Langmuir circulation. Photo taken 08 May 2006.

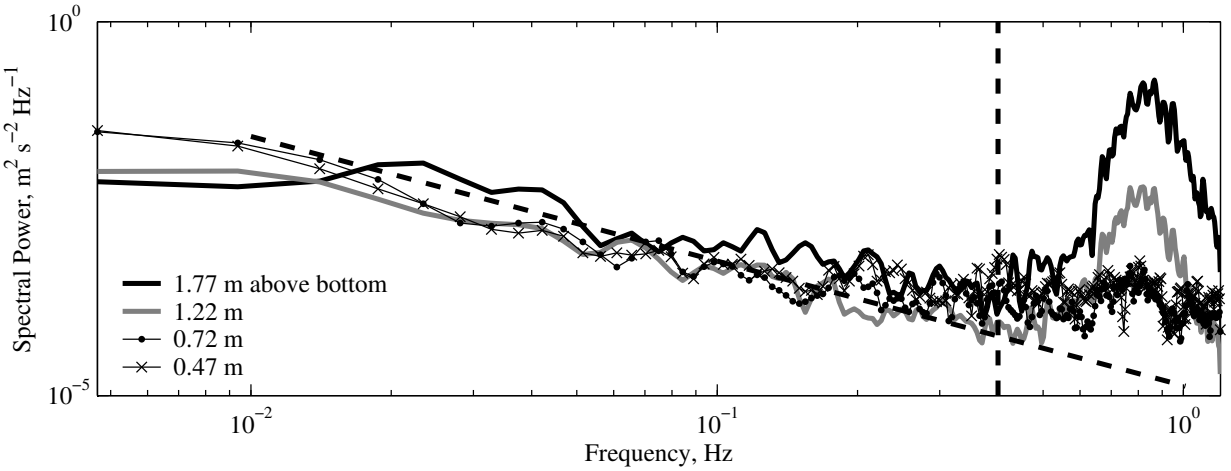

Fig. 4-22. Power spectral density (m^2 s^{-2} Hz^{-1}) as a function of frequency f (Hz) for ADCP velocities in bins 1.77 m, 1.22 m, 0.72 m, and 0.47 m above the bed. The wind wave band lies to the right of $f = 0.4$ Hz (vertical dashed black line). The inclined dashed line has a slope of -5/3, typical of the inertial subrange (see eq. 2-13).

pycnocline. Instead, the spectral evidence of wind waves declines dramatically with depth, only clearly reaching the bottom on 14 and 19 April once the salty layer has been mixed. Conversely, the velocity signal that has been filtered to remove wind waves **does** show increased variance in the region below the pycnocline (Fig. 4-23B). These peaks correspond to windy afternoons, but the spectral power from the filtered signal is heightened due to turbulence, not wind waves.

A closer look at the period of 13 to 18 April 2008 (Fig. 4-24) also shows confinement of wind waves to the near-surface. For velocity from the bin closest to the surface (black solid line), nearly all of its variability is found in the wind wave band ($f > 0.4$ Hz). But closer to the bed, a maximum of only about 10% of the spectral power is found in the wind wave band, even during one of the windiest times of the experiment when rapid mixing was occurring (14 April). The vast majority of the signal is due to turbulence and larger-scale motions; as Fig. 4-22 shows, a -5/3 slope fits reasonably well with that portion of the spectrum that is not wind waves ($f < 0.4$ Hz), indicating well-developed turbulence. Furthermore, for many of the times when the fraction of the total spectral power in the wind wave band appears high near the bed (e.g., the early morning of 13 April), it is actually because there is very little signal of any kind. In such cases, a -5/3 slope does not fit the spectral energy distribution of the velocity data; there is no turbulence to be contaminated by a wave signal.

The ADVs, from their position near the bed, tell a similar story. Fig. 4-25 shows the fraction of total power in the u' signal that is explained by frequencies in the wind wave band of 0.6-1.3 Hz. In most cases, this fraction is less than 0.05. The few bursts where this is not true tend to be very low-energy bursts to begin with, and do not show a wind wave peak. Two important exceptions are 14 and 19 April 2008, when the fraction of total power outside the wind wave band peaks during two strong wind events. The wave orbital velocities exceeded 0.01 m s^{-1} under these conditions, and velocities were not well-resolved.

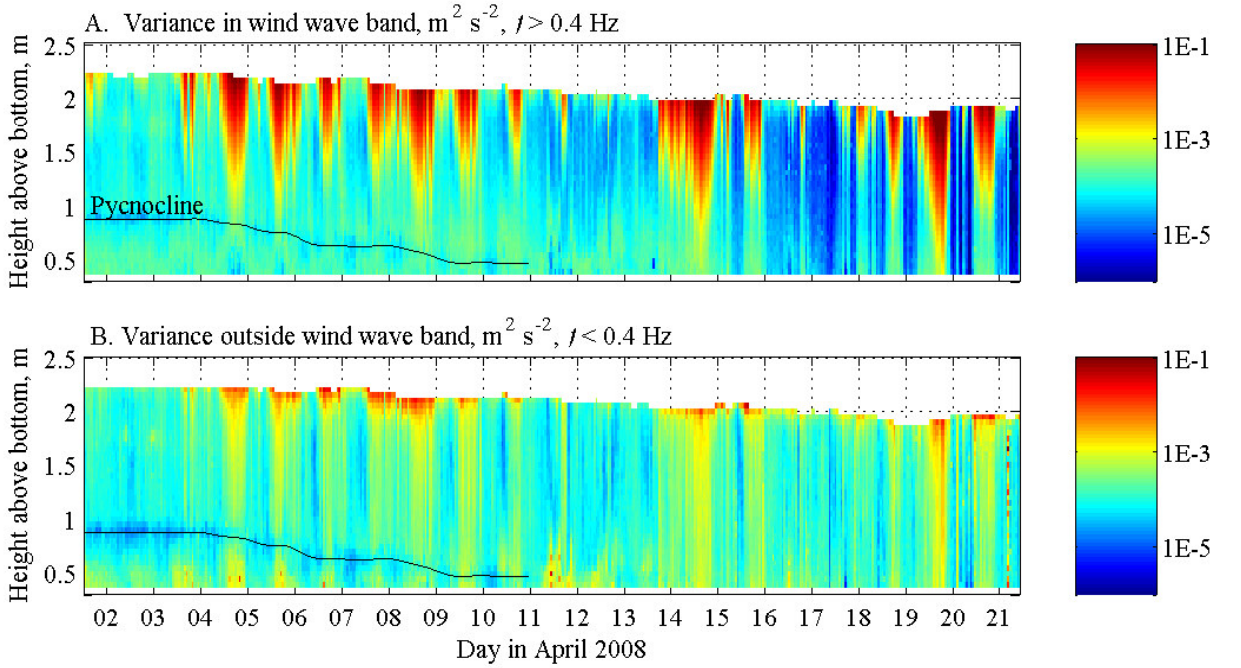

Fig. 4-23. Variance (m^2 s^{-2}, log scale) in the velocity signal measured by the ADCP in April 2008. (**A**) Variance in the wind wave band, which is $f > 0.4$ Hz. (**B**) Variance outside of the wind wave band, $f < 0.4$ Hz.

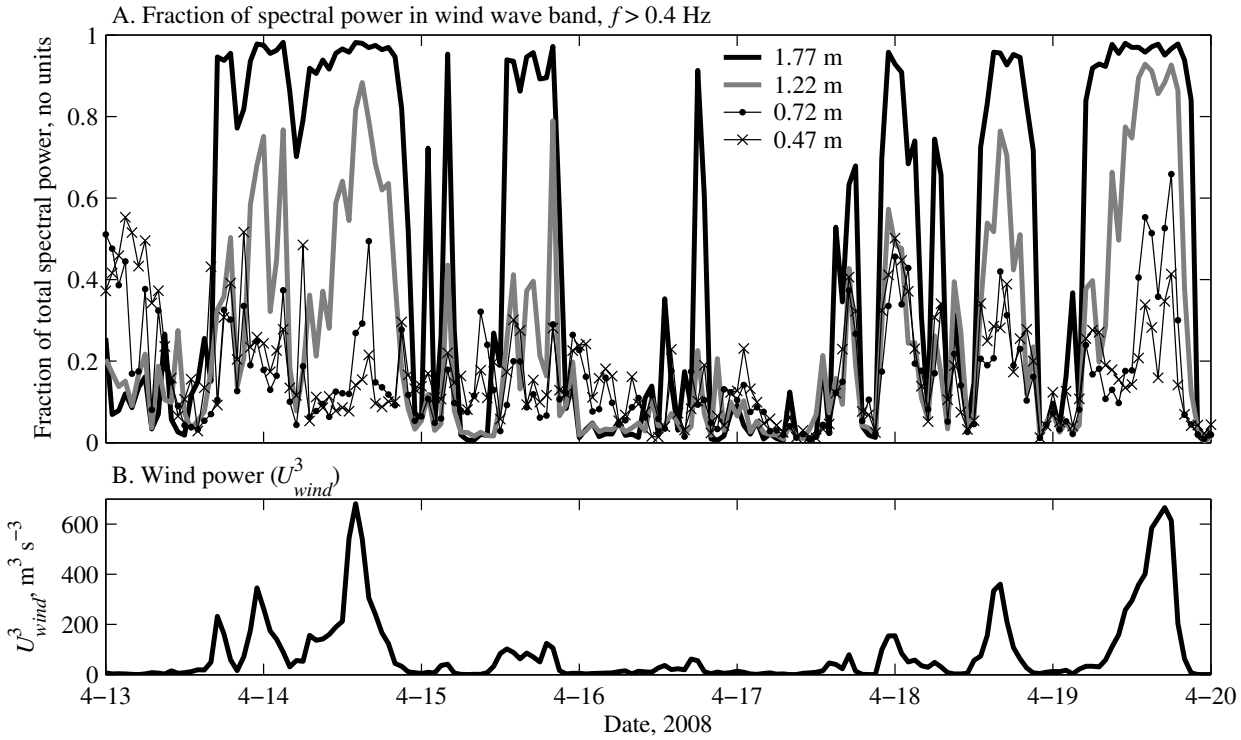

Fig. 4-24. (**A**) The fraction of spectral power in the ADCP velocity signal at frequencies faster than 0.4 Hz in bins 1.77 m, 1.22 m, 0.72 m, and 0.47 m above the bottom, which is presumed to reflect the presence of wind waves. (**B**) Wind power, shown as the the quantity U_{wind}^3 (m^3 s^{-3}).

A frequent concern with shear stress estimates in wave-dominated flows is that the Reynolds stress can become biased by wave motions (Trowbridge 1998). Fortunately, the ADCP was mounted in a nearly flat position (pitch = 1.0–1.1°), so the bias introduced by wind waves should be relatively small (Rippeth et al. 2003). Likewise in the ADV data set, bias does not appear to be major problem. As discussed above, although wind wave spectral peaks are evident in a few of the burst cospectra of u' and w' and in the spectra of u' alone, these wave peaks make up a small percentage of the overall power in the spectra and cospectra. Furthermore, the Reynolds and wave-debiased bed stresses match fairly well (Fig. 4-14).

One possible explanation for the fact that wind waves did not penetrate very far into the water column, despite having been a dominant surface feature, is that wave orbital velocities were low due to fetch limitations on wave height. The expected significant wave height $H_{1/3}$ and frequency ω for fetch-limited wind waves are:

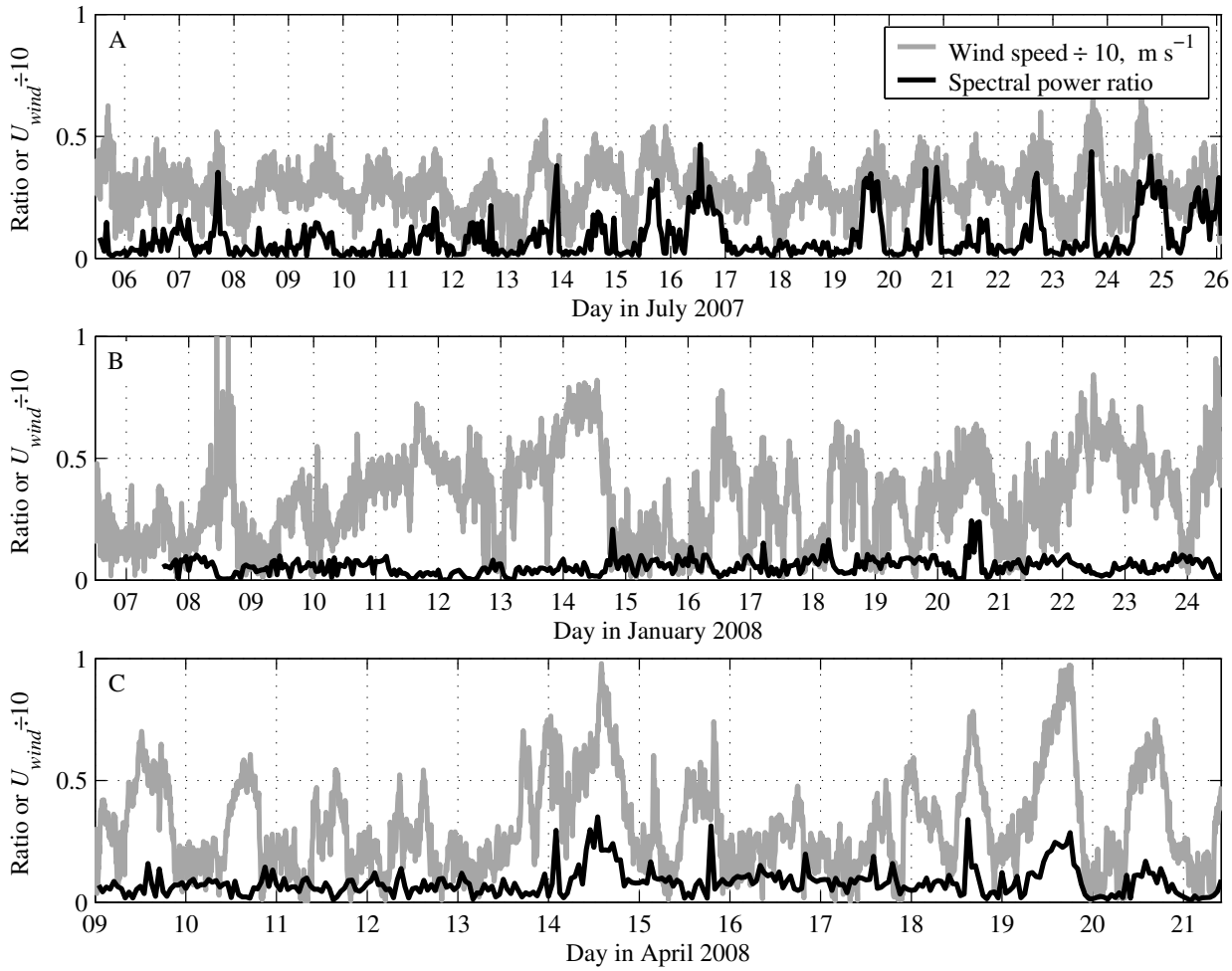

Fig. 4-25. The fraction of spectral power of the ADV velocity signal in the wind wave band $0.6 < f < 1.3$ Hz (black line, unitless) in (**A**) July 2007, (**B**) January 2008, and (**C**) April 2008. Wind speed (gray line, m s^{-1} ÷ 10) is also shown for reference.

$$H_{1/3} = 0.051(u*_{wind}{}^2 \, X/g)^{1/2} \quad (4\text{-}3)$$

$$\omega = 7.1(g/u*_{wind})(gX/w_*{}^2)^{-1/3} \quad (4\text{-}4)$$

where X is the fetch (m) (Hasselmann et al. 1973; Csanady 2001; Wüest and Lorke 2003). For a wind speed U_{wind} of 4 m s^{-1}, $H_{1/3}$ at 1000 m downwind of the beach is only 8 cm; for U_{wind} = 8 m s^{-1}, $H_{1/3}$ is 14 cm. With a water depth of only 1.5 m, as observed in the July 2007 experiment, the resulting waves behave as deep water waves and should theoretically produce maximum wave orbital velocities 20 cm from the bed of 3×10^{-3} m s^{-1} when U_{wind} = 4 m s^{-1} and 2×10^{-2} m s^{-1} when U_{wind} = 8 m s^{-1}. The observed wave orbital motions roughly match these predictions, and for the typical case of light winds, no wave orbital motions were detectable.

The presence of density stratification also helped to isolate the bed from the effects of wind waves. For example, the fraction of spectral power in the wind wave band for ADV velocities is significantly lower under salt-stratified conditions (all of January 2008, Fig. 4-25B and 09 to 14 April 2008, Fig. 4-25C) than under well-mixed conditions (remainder of Fig. 4-25). Also, wind waves reach slightly further down into the water column after it becomes well-mixed in April 2008 (e.g., 19 April, Fig. 4-23A, 4-24).

To conclude, wind waves in this small, fetch-limited lagoon that are produced by light winds are clearly separable from turbulence and mixing. They do not reach the bed, and apparently do little more than organize themselves into Langmuir cells and send surface accumulations of algal mats to wash up at the one end. One the other hand, the less common extreme high-wind events, which may occur on the order of a few dozen times a year, do reach the bottom – especially when the lagoon is not stratified. In those instances, they are difficult to separate out from the turbulence, and may indirectly contribute to mixing.

4.4 Turbulence

Since advection is quite weak in and below the pycnocline, a characteristic that Rodeo Lagoon shares with many larger lakes, turbulent mixing is presumed to be the main transport mechanism for scalars like salt, nutrients, and phytoplankton in this region (Powell and Jassby 1974). This makes an estimate of the vertical turbulent scalar diffusivity critical for understanding and predicting such mixing. In this section, I describe how I arrived at estimates for this quantity under various seasonal forcings and using different types of field instruments. The April 2008 experiment is a particular focus due to the increased availability of data and because turbulent mixing transformed the water column from salt-stratified to well-mixed over a short period.

4.4.1 Analytical methods

The ADCP and temperature microstructure data provide information that can be used to estimate turbulent mixing rates via several different methods, each of which is described below.

4.4.1.1 Simple physical scaling

The simplest parameterization for scalar diffusivity is a parabolic physical scaling based solely on surface wind forcing and distance away from boundaries (Fischer et al. 1979):

$$K_z(z) = \kappa u^*_{wind} \Delta h_{mix}(z/\Delta h_{mix})(1\text{-}z/\Delta h_{mix}) \quad (4\text{-}5)$$

κ is the von Karman constant ($\kappa = 0.4$) and u^*_{wind} is calculated as in eq. 2-1. This formula for the mixed layer makes no allowance for stratification – mixing is assumed to be negligible below the pycnocline – so z is the distance above the pycnocline. The formula is not used below the pycnocline.

4.4.1.2 Turbulent kinetic energy budget

Following the method of Stacey et al. (1999b), I assumed a local turbulent kinetic energy (TKE) balance to transform raw ADCP data into estimates of scalar turbulent diffusivity. The simplified turbulent kinetic energy (TKE) budget for a steady, locally homogeneous stratified shear flow reduces to the following balance:

Shear-induced production (P) = buoyancy flux (b) + dissipation (ε) (4-6a)

The terms in (4-6a) are defined as follows, where u_3 is the vertical velocity:

$$-\overline{u_i' u_j'}\frac{\partial \overline{u_i}}{\partial x_j} = \frac{g}{\rho_0}\overline{u_3'\rho'} - \nu\overline{u_i'\nabla^2 u_i'} \quad (4\text{-}6b)$$

Due the dimensions of the lagoon (length >> depth and flat bathymetry), the mean vertical velocity and its derivatives should be negligible compared to mean horizontal velocities away from the boundaries ($U,V >> W$), while the horizontal derivatives should be small ($\partial/\partial x$, $\partial/\partial y \sim 0$). These assumptions further reduce the production term to the balance shown below:

$$-\overline{u'w'}\frac{\partial U}{\partial z} - \overline{v'w'}\frac{\partial V}{\partial z} = \frac{g}{\rho_0}\overline{u_3'\rho'} + \varepsilon \quad (4\text{-}7)$$

In the absence of direct, co-located measurements of ρ' and u_3' to calculate the instantaneous buoyancy flux, some additional assumptions are required to estimate scalar diffusivity using the TKE balance (Osborn 1980). The first step is to combine the definition of turbulent viscosity with a definition of the turbulent Prandtl number, Pr_T, to define the scalar diffusivity:

$$\nu_T = \frac{P}{\left(\frac{\partial \overline{u_i}}{\partial x_j}\right)^2} = P/S^2 \quad \text{and} \quad \mathrm{Pr}_T = \frac{\nu_T}{K_\rho} \quad \text{so} \quad K_\rho = \frac{\nu_T}{\mathrm{Pr}_T} \quad (4\text{-}8)$$

As a first-order estimate for K_ρ, I assume that $\mathrm{Pr}_T = 1$. This means momentum and temperature have the same turbulent mixing rate, since technically speaking the turbulent Prandtl number refers to the ratio of turbulent viscosity to turbulent temperature diffusivity. However, I further assume that the Schmidt number (ν_T/K_ρ) and Prandtl number are equivalent, so that if $\mathrm{Pr}_T = 1$ then the ratio of *any* scalar diffusivity to viscosity is 1. This assumption, which is applied throughout this section, is called the *Reynolds analogy* (Tennekes and Lumley 1972). It is well established that $\mathrm{Pr}_T > 1$ in stably stratified flows, and this assumption has the benefit of producing

an estimate of K_ρ with no further knowledge required about N^2 or the state of the turbulence and its efficiency.

For a better estimate of the scalar diffusivity K_ρ, one needs to know something about the scalar field and mixing efficiency. Pr_T, rather than being constant, is theorized to depend on the ratio of the local gradient Richardson number, Ri_g, and the flux Richardson number, R_f, so that $\mathrm{Pr}_T = Ri_g/R_f$. The following definitions apply:

$$Ri_g = \frac{N^2}{S^2} = \frac{N^2}{\left((\mathrm{d}U/\mathrm{d}z)^2 + (\mathrm{d}V/\mathrm{d}z)^2\right)^{1/2}} \tag{4-9}$$

$$R_f = b/P \tag{4-10}$$

Making a series of substitutions with eqs. 4-9 and 4-10, eq. 4-8 becomes:

$$K_\rho = \frac{P}{\mathrm{Pr}_T\, S^2} = \frac{R_f}{Ri_g}\frac{P}{S^2} = \frac{R_f S^2}{N^2}\frac{P}{S^2} = \frac{R_f P}{N^2} \tag{4-11}$$

Substituting eq. 4-10 into eq. 4-6 gives $\varepsilon = P(1-R_f)$, so that another way of writing eq. 4-11 follows Osborn (1980):

$$K_\rho = \frac{R_f \varepsilon}{(1-R_f)N^2} = \Gamma\frac{\varepsilon}{N^2} \tag{4-12}$$

The ADCP in this experiment provides an estimate of production, not dissipation, so the natural fit is to use eq. 4-11, not eq. 4-12. With either approach, an estimate of R_f or its Γ equivalent is required.

The challenge of estimating R_f has been approached by many different researchers (Ivey et al. 2008), a few of whose methods will be used here. The theory of Osborn (1980), based on observational work, holds that $R_f \leq 0.15$ or $\Gamma \leq 0.2$. This maximal value of R_f has been validated by field studies in energetic environments, at least in the average sense (e.g., Moum 1996), and is sometimes used in the absence of any other information. This is despite the fact that laboratory studies (e.g., Rohr and Van Atta 1987), field studies (e.g., Etemad-Shahidi and Imberger 2001) and numerical simulations (e.g., Itsweire et al. 1993) have found evidence that the assumption is not valid under conditions where the stratification strongly dampens the turbulence. Taking this into account, (Ivey and Imberger 1991) proposed the following functional form for R_f:

$$R_f = \frac{1}{1+3Fr_T^{\,2}} \qquad \text{for } \mathrm{Fr}_T > 1.2 \tag{4-13a}$$

$$R_f = a + b\,\mathrm{Fr}_T + c(\mathrm{Fr}_T)^2 \qquad \text{for } \mathrm{Fr}_T < 1.2 \tag{4-13b}$$

where $a = 0.49 + 1.44c$,
$b = -0.25 - 2.4c$,
$c = (0.25\alpha - 0.49)/(\alpha^2 - 2.4\alpha + 1.44)$, and
$\alpha = 3.9\ \mathrm{Re}_T^{-1/2}$.

For the ADCP data, the following definitions from Stacey et al. (1999b) for the turbulent Reynolds number Re_T and turbulent Froude number Fr_T apply:

$$\mathrm{Re}_T = 4.3\frac{P}{\nu S^2} \quad \text{and} \quad \mathrm{Fr}_T = 0.48 Ri_g^{-1/2} \tag{4-14}$$

Applying eq. 4-13 to observations from Rodeo Lagoon, about half of which are in the region $\mathrm{Fr}_T < 1.2$, produces peak values of about $R_f = 0.235$, or $\Gamma = 0.31$. These large R_f values may be produced because the values of Re_T used by Ivey and Imberger (1991) to develop eq. 4-13 were around 40, whereas those here are considerably larger (~1000), reflecting the field rather than laboratory conditions.

Ivey et al. (2008) proposed an alternate functional form for R_f that depends on the product $\mathrm{Re}_T\ \mathrm{Fr}_T^2$, which is equivalent to $\varepsilon/\nu N^2$. For the versions of Re_T and Fr_T in eq. 4-14 above, which imply the assumption that $P = \varepsilon$:

$$R_f = 0.17 \qquad \text{for } 7 < \varepsilon/\nu N^2 < 100 \tag{4-15a}$$

$$R_f = \frac{2}{\mathrm{Re}_T^{1/2}\,\mathrm{Fr}_T} = \frac{2}{(P/\nu N^2)^{1/2}} \qquad \text{for } \varepsilon/\nu N^2 > 100 \tag{4-15b}$$

Shear production of TKE, P, is calculated from ADCP data using the product of Reynolds stresses and velocity shear, as shown in eq. 2-18. In the calculations of K_ρ presented below, I compare results using R_f values from eq. 4-13 with those from eq. 4-15.

4.4.1.3 Temperature microstructure

I used two slightly different methods, each described below, to transform the raw SCAMP data into estimates of turbulent scalar diffusivity: the "Osborn method," named for the formulation by Osborn (1980), and the "Osborn-Cox method," creatively named for the formulation by Osborn and Cox (1972).

Initial data processing was the same for both methods. I first divided each vertical profile into non-overlapping segments of 128 data points, which corresponds to about 13 cm. A very small number of profile segments with an instrument profile speed less than 5 cm s^{-1} were excluded from further analysis. For the January 2008 data, I aligned the segments with the top of the pycnocline, defined for segmentation purposes as the point corresponding to 10% of the total density jump across the pycnocline as measured from the surface (Fig. 4-8A). In April 2008, the pycnocline was located very close to the bottom; to avoid discarding valuable information at the bottom of the profile, the segments were aligned with the bottom. Stationarity as described by Imberger and Ivey (1991) was not necessary as a criterion for segmentation; in fact, a test using this criterion revealed that most segments near the pycnocline would *not* be stationary.

However, most non-stationary segments also had poor Batchelor fits (see below), making the additional criteria of stationarity unnecessary.

Both methods rely on the Taylor frozen turbulence hypothesis, which allows conversion of thermistor data from the frequency to wavenumber domain. Both methods also make use of the dissipation of temperature variance, χ, which is defined as $\chi = 6\,\mathrm{D_T}\left\langle \frac{\partial \mathrm{T}'}{\partial \mathrm{z}} \frac{\partial \mathrm{T}'}{\partial \mathrm{z}} \right\rangle$ where D_T is the molecular diffusivity of temperature, $\partial T'/\partial \mathrm{z}$ is the vertical gradient in the temperature perturbations measured by the SCAMP's fast thermistors, and brackets indicate a segment average.

Osborn-Cox method
Assuming a local balance of production and dissipation in the temperature variance budget (Osborn and Cox 1972), χ and the mean vertical temperature gradient $\partial \overline{T} / \partial \mathrm{z}$ can be used to estimate the turbulent heat flux $\overline{w'T'}$ and thus the turbulent temperature diffusivity K_T:

$$K_T = \frac{\chi}{2(\partial \overline{T}/\partial z)^2} \qquad (4\text{-}16)$$

Values of $\partial \overline{T} / \partial z$ were calculated using the density-sorted temperature record for each segment (Nash and Moum 2002). The estimate of χ was improved by following the methods of Ruddick et al. (2000) and Steinbuck et al. (2009), which filter instrument noise and re-create portions of χ lost in high or low wavenumber regions of Batchelor spectra.

By applying the Osborn-Cox method, I assume that K_T is a representative diffusivity for other scalars of interest, like salt and dissolved nutrients. However, K_T is really a turbulent *temperature* diffusivity, and it is not necessarily meant to be equal to other scalar diffusivities such as K_ρ. Indeed, in cases where the flow is not truly turbulent, these diffusivities should diverge, since the molecular diffusivity of temperature greatly exceeds that of salt.

Osborn method
At the heart of Osborn method for calculating diffusivity are fits of the Batchelor spectrum to temperature microstructure data to produce an estimate of the turbulent kinetic energy dissipation, ε. Then, the method proceeds much as in the TKE budget method above, using eq. 4-12. I followed the standard methods of Luketina and Imberger (2001) and Ruddick et al. (2000) to calculate ε. To improve handling of noise contamination during Batchelor curve-fitting, the calculation method for χ and ε followed the modifications suggested by Steinbuck et al. (2009). Poor Batchelor fits were identified using the spectral fit criteria of Ruddick et al. (2000):

$$R = [\text{variance}\{(\text{observed Batchelor spectra})(\text{theoretical spectra})^{-1}\} \cdot (\text{degrees of freedom})]^{1/2} \qquad (4\text{-}17)$$

Values of ε from those fits with an R-value above a threshold of 2.0 (July 2007 data) or 2.5 (all 2008 data) were rejected, with the criteria based on a visual inspection of the Batchelor fits.

2008 data generally had better Batchelor fits due to greater temperature variability in the water column. By contrast, values of χ from all segments were used.

For the calculation of R_f using eq. 4-13 above, the method of Ivey and Imberger (1991) provides the following definitions of Re_T and Fr_T. These definitions are conceptually similar to the definitions in eq. 4-14 for use with the ADCP, but use the data more readily available from the SCAMP:

$$\mathrm{Re}_T = \frac{\varepsilon^{1/3} \mathrm{L_{th}}^{4/3}}{\nu} \qquad \mathrm{Fr}_T = \left(\frac{\varepsilon}{N^3 \mathrm{L_{th}}^2} \right)^{1/3} \tag{4-18}$$

Thorpe displacements are identified by subtracting the density-sorted profile from the original profile; each Thorpe displacement is calculated as the vertical distance a point measurement must be moved during density sorting (Dillon 1982). The Thorpe scale, $\mathrm{L_{th}}$, is then defined as the root mean square of Thorpe displacements within each segment. Though a measured quantity, the Thorpe scale is typically of comparable magnitude to the more theoretical Ozmidov scale (Thorpe 1977; Dillon 1982). In calculating $\mathrm{L_{th}}$, I excluded all Thorpe displacements smaller than the resolution of the instrument, 1 mm. Per Ivey and Imberger (1991), R_f was set to zero for segments where $\mathrm{Re}_T < 14.8$ or where the equations above produced a negative value of R_f. For these segments, no values of K_ρ, Re_T, or Fr_T were included in the profile averages or attached plots.

Averaging of SCAMP results
The reported profiles of N^2 were calculated using the density-sorted profile for each segment; the individual segment N^2 values were then averaged over all instrument drops from each day into 0.05 m depth bins. This averaging implicitly assumes that conditions were steady in time over several hours. Values of K_T, K_ρ, Re_T, and Fr_T were log-averaged within 0.1 m depth bins. Data from each segment were assigned to a depth bin based on the average depth of the segment. Log-averaging within depth bins is the last step in the calculation of K_T, which is first calculated using individual segment values of χ and $\partial\overline{\mathrm{T}}/\partial \mathrm{z}$, not bin averages of those variables. For the comparison of wind forcing with the buoyancy flux, defined as $K_T \cdot N^2$, I present the log-averaged value over the entire water column.

4.4.2 Vertical turbulent diffusivity

4.4.2.1 Estimates of diffusivity by various methods

Temperature microstructure
The SCAMP temperature microstructure data, processed via the Osborn or Osborn-Cox method, provide the only means of estimating K for all three experiments. The Osborn-Cox method, which produces the estimate K_T, provides the more robust estimate of K because it assumes less about the shape of the Batchelor spectra and uses fewer empirical parameters. Nonetheless, I will also discuss the estimates K_ρ from the Osborn method, as it provides an interesting comparison and also allows comparison with work by others on the state of turbulent mixing as represented by the parameters Re_T and Fr_T.

The turbulent scalar diffusivities K_T (Osborn-Cox method) and K_ρ (Osborn method) were affected similarly in time and space by salt stratification, though K_T reacted more sensitively to the physical forcing. K_T was reduced directly below the pycnocline by more than two orders of magnitude, while the reduction in K_ρ was more than one order of magnitude (Fig. 4-26). In extreme cases, the decline in K_T was as much as three orders of magnitude over less than 1 m (Fig. 4-26E,H), or for K_ρ as much as two orders of magnitude (Fig. 4-26F,J). By contrast, when the lagoon was relatively well-mixed in summer, the variation in K_T from its mean was less than

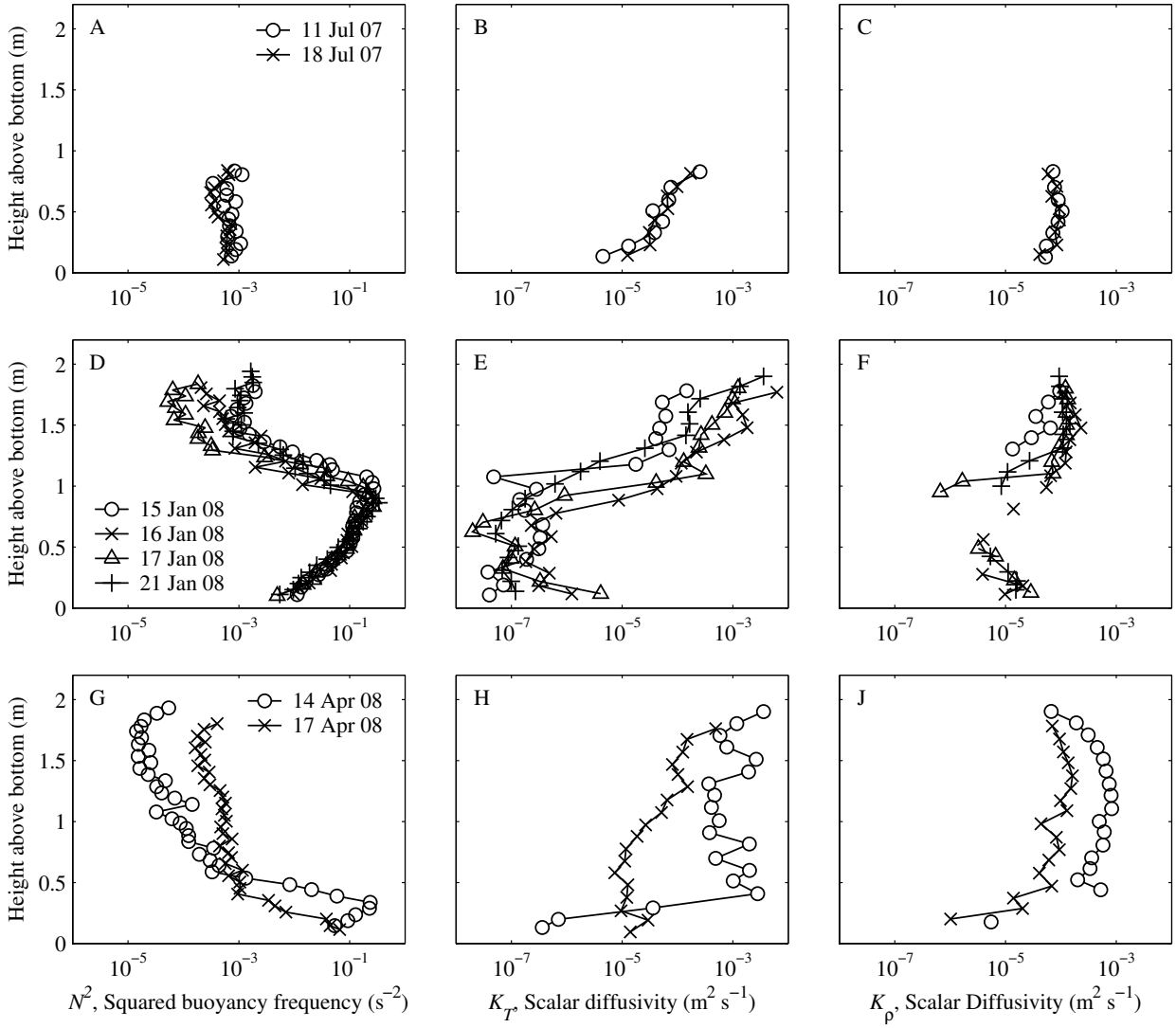

Fig. 4-26. (**A, D, G**) Squared buoyancy frequency, N^2 (s^{-2}); (**B, E, H**) Vertical turbulent scalar diffusivity K_T ($m^2\ s^{-1}$) from the Osborn-Cox method (eq. 4-16); and (**C, F, J**) vertical turbulent scalar diffusivity K_ρ ($m^2\ s^{-1}$) from the Osborn method (eqs. 4-12, 4-13). All quantities are from segments of 128 data points (approx. 13 cm) collected in (**A, B, C**) July 2007, (**D, E, F**) January 2008, and (**G, H, J**) April 2008. Data are binned log averages of many ($n \geq 30$) profiles from each day of SCAMP observations.

1 order of magnitude (Fig. 4-26B), while K_ρ was nearly constant (Fig. 4-26C). Similarly, in the better-mixed region above the pycnocline the variation in K_T was less pronounced among sampling days, varying between about 10^{-4} and 10^{-3} m^2 s^{-1} regardless of the stratification conditions below. K_ρ showed even less variation in the well-mixed pycnocline, and had significantly smaller values than K_T; except for the very windy day of 14 April 2008, all the values are between 0.5–1.0×10^{-4} m^2 s^{-1}.

Below the pycnocline, turbulence was damped by stratification to the extent that motions were typically wave-dominated in this region rather than displaying active turbulence. In a plot of Re_T and Fr_T in a turbulence phase diagram with regions of active turbulence, buoyancy-affected turbulence, and waves demarcated after Ivey and Imberger (1991) (Fig. 4-27), most data points in the "active turbulence" region (A), are above the pycnocline. Very few points lie in the region of most efficient turbulent mixing, where the flux Richardson number R_f exceeds 0.15. Furthermore, there are relatively few points in the buoyancy-affected region, probably because the pycnocline, if present, is so sharp that very few data points exist in this part of the vertical

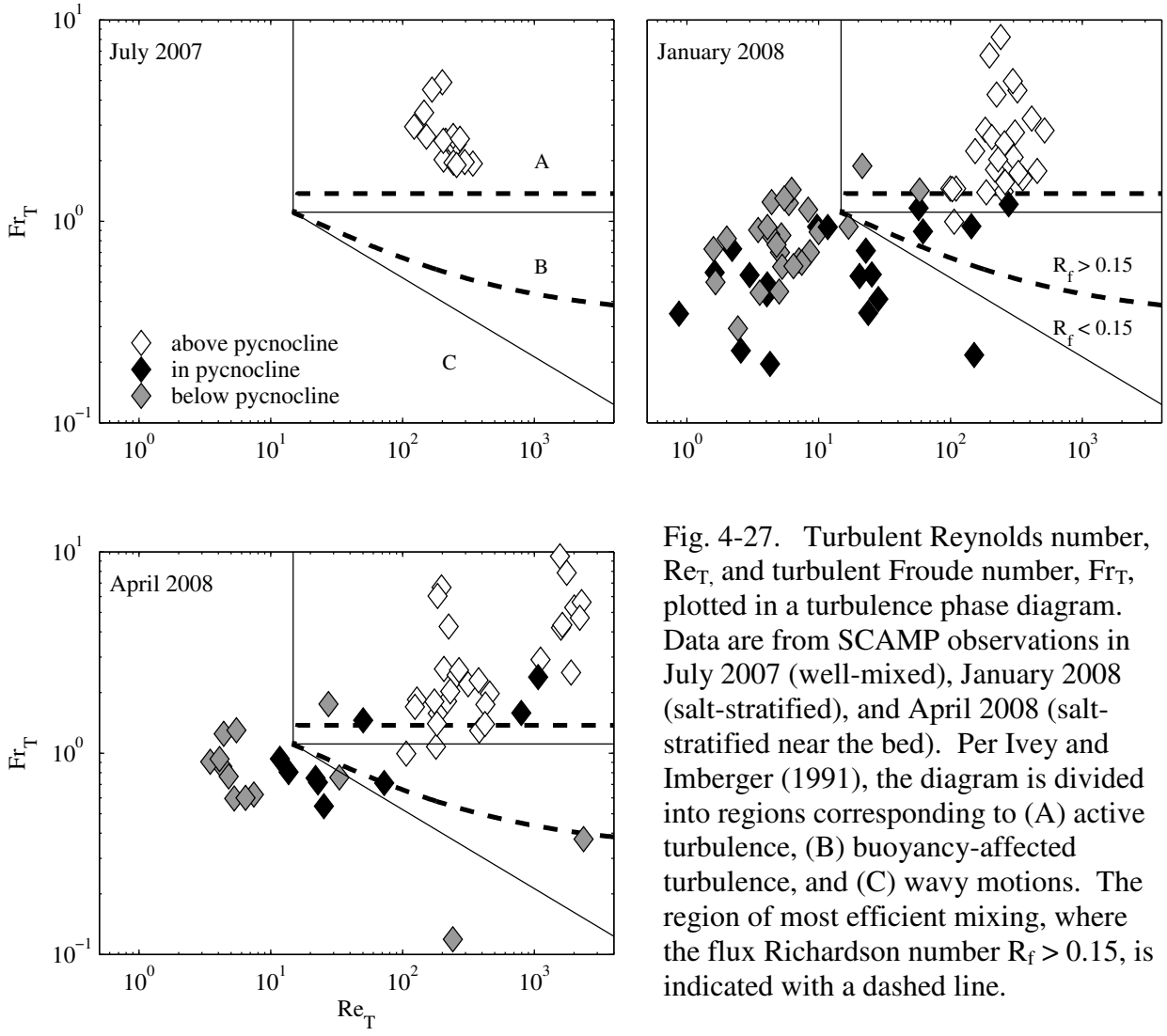

Fig. 4-27. Turbulent Reynolds number, Re_T, and turbulent Froude number, Fr_T, plotted in a turbulence phase diagram. Data are from SCAMP observations in July 2007 (well-mixed), January 2008 (salt-stratified), and April 2008 (salt-stratified near the bed). Per Ivey and Imberger (1991), the diagram is divided into regions corresponding to (A) active turbulence, (B) buoyancy-affected turbulence, and (C) wavy motions. The region of most efficient mixing, where the flux Richardson number $R_f > 0.15$, is indicated with a dashed line.

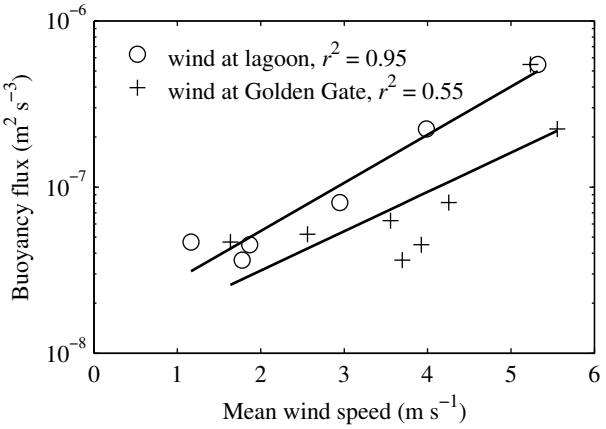

Fig. 4-28. Buoyancy flux $K_T \cdot N^2$ (m^2 s^{-3}) as a water column average calculated with SCAMP data, and its log-linear correlation with wind speed. Wind speed data are available from the Golden Gate weather station for all 8 days of diffusivity measurements (crosses), but from the lagoon weather station for only 6 of those days (circles). Local wind speeds are slower because the anemometer was closer to the water surface.

profile. Most points in and below the pycnocline are near the "waves" region (C), but with lower Re_T and higher Fr_T values than are typically observed for wavy flows. This unusual trend is due to the extremely low values (< 1 cm) of L_{th} found in and below the very strong pycnocline. In this region, vertical diffusivity was close to its molecular value (Fig. 4-26E,H). By contrast, in portions of the water column that were comparatively well-mixed, Re_T and Fr_T values are consistent with active turbulence.

Turbulent mixing rates depended on wind, which is an expected result. Specifically, the buoyancy flux $K_T \cdot N^2$ shows a fairly strong log-linear correlation with wind speed (Fig. 4-28). This is true whether wind speed is measured 2 m above the water surface at the field site (r^2=0.95) or 10 m above the water surface at the more distant Golden Gate weather station (r^2 = 0.55). The poorer fit at the Golden Gate station is primarily due to the higher wind speeds reported at the Golden Gate station, which can be blocked by topography at Rodeo Lagoon.

Methods using the TKE budget

Estimates of K from the TKE budget method for ADCP data (see §4.4.1.2) are available for each hourly burst of the April 2008 experiment. For the two days that SCAMP data are available, the very windy day of 14 April 2008 (Fig. 4-29A) and the less windy day of 17 April 2008 (Fig. 4-29B), it is therefore possible to compare the multitude of approaches. Compared to K_T and K_ρ from the SCAMP results (filled squares and circles, Fig. 4-29), the other methods performed as follows:

- Parabolic profile from the simple parameterization of eq. 4-5, $K_\rho \sim \kappa u^*_{wind} \Delta h_{mix}$ (dashed line, Fig. 4-29): Considering the sparse amount of data used for this estimate, this method performs surprisingly well in the upper water column, but there is still much room for improvement. The estimates for 17 April 2008 (Fig. 4-29B) are too high by about an order of magnitude. There is insufficient variability in the estimates of K_ρ between the two days, since u^*_{wind} only changes by a factor of 1.5. Also, there is no reduction of K_ρ in the pycnocline, as this method has no way of accounting for the effects of stratification.

- Results using the assumption that $K_\rho = \nu_T$, eq. 4-8 with $Pr_T = 1$ (green triangles, Fig. 4-29): Most of the results from this method are within an order of magnitude of the SCAMP values,

at least above the pycnocline. Once again, there is no reduction of K_ρ in the pycnocline, so this can only be considered an estimate for the upper water column. There is considerable scatter in the estimates compared to the other methods, particularly for 17 April 2008, which has estimates for K_ρ above the pycnocline spread over two orders of magnitude.

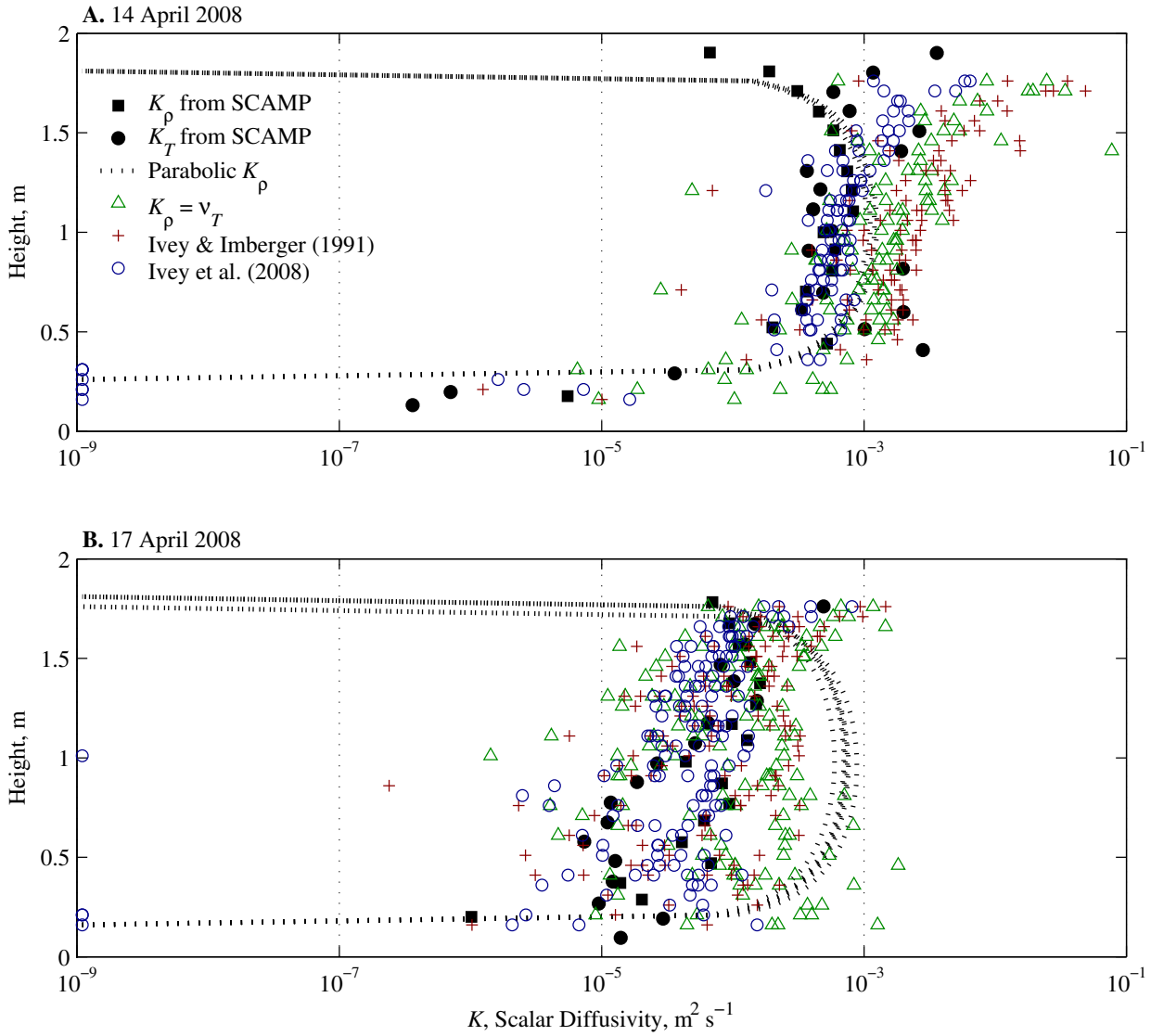

Fig. 4-29. Various estimates of the scalar diffusivity $K(z)$ (m^2 s^{-1}) during the times when SCAMP data was collected: (**A**) 10:00-11:00 on 14 April 2008 and (**B**) 10:00-13:00 on 17 April 2008. K_ρ (filled black squares) and K_T (filled black circles) from SCAMP are shown for reference. Results from the parabolic estimate $K_\rho = f(u^*_{wind}, h_{mix}, z)$ from eq. 4-5 are shown as dotted lines. Results using the assumption $K_\rho = \nu_T = P/S^2$ (i.e., $Pr_T = 1$) from equation 4-8 are shown in green triangles. Results for K_ρ from the method of Ivey and Imberger (1991) using eqs. 4-11 and 4-13 are shown as red crosses. Results for K_ρ from the method of Ivey et al. (2008) using eqs. 4-11 and 4-15 are shown as open blue circles.

- Results from the method of Ivey and Imberger (1991), eq. 4-11 with R_f from eq. 4-13 (red crosses, Fig. 4-29): For the two dates shown here, the results from this method do not differ significantly from the method that assumes $Pr_T = 1$ (green triangles). However, the results are an improvement since K_ρ is much reduced in and below the pycnocline, which is not shown here but is relevant earlier in the experiment when the salty layer was thicker. There is still considerable spread in the estimates for 17 April 2008 (Fig. 4-29B). The results from 14 April 2008 are too high, especially in the upper water column (Fig. 4-29A).

- Results from the method of Ivey et al. (2008), eq. 4-11 with R_f from eq. 4-15 (open blue circles): This method shows much better agreement with the SCAMP results than the other methods considered above. There is less spread in the estimates than the methods above, and the shape of the profiles roughly matches that in the SCAMP results.

The instantaneous profiles of $K_\rho(z)$ from Ivey and Imberger (1991) and Ivey et al. (2008) are quite sensitive to the input values of N^2, which are both large and uncertain in the region above the pycnocline. The method of Ivey and Imberger (1991) (red crosses, Fig. 4-29) holds that $K \sim N^{-2}$, while the method of Ivey et al. (2008) (open blue circles, Fig. 4-29) holds that $K \sim N^{-1}$. Since the method of Ivey et al. (2008) has N^2 raised to a small power than the method of Ivey and Imberger (½ instead of 1), the results are less sensitive to potential errors in N^2. This may contribute to the better agreement of this method with the SCAMP results.

4.4.2.2 Evolution of salt field – model vs. observations

I used the estimates of K_ρ as input for a 1-D numerical model of the salt field $C(z,t)$ that uses the observed salt profile $C(z)$ from 02 April 2008 as its initial condition, then explicitly solves the equation

$$\frac{\partial C}{\partial t} = K_\rho \frac{\partial^2 C}{\partial z} \qquad (4\text{-}19)$$

with a time step of 60 seconds and a spatial resolution of $\Delta z = 0.01$ m. The model input parameter K_ρ changes hourly. I compared model output with the observation evolution of the salt field in April 2008 (Fig. 4-11D).

The algorithm of Ivey et al. (2008) represented by eqs. 4-11 and 4-15 produced a salt field that best matched the observed $C(z,t)$ (Fig. 4-30). This is because the numerical model is highly sensitive to K_ρ values in the pycnocline, which for this method are set to $K_{molecular}$ (1.1×10^{-9} for salt) when the quantity $(P/\nu N^2)$ is small. Patches where this restriction applied appear as dark blue in Fig. 4-30A. In fact, even using a $K_{molecular}$ for temperature ($K_T = 1.4\times10^{-7}$) results in predicted mixing that is faster than observed. The uncertainty of the value of N^2 in the upper water column makes very little difference here, because in fact the value of K_ρ in the upper water column makes very little difference in the evolution of $C(z,t)$.

In conclusion, among the diffusivity estimates that do not rely on temperature microstructure data, the method of Ivey et al. (2008) seems to perform the best in Rodeo Lagoon. The main reasons for the method's success appear to be its lower sensitivity to N^2, and its explicit reversion to $K = K_{molecular}$ in non-turbulent patches.

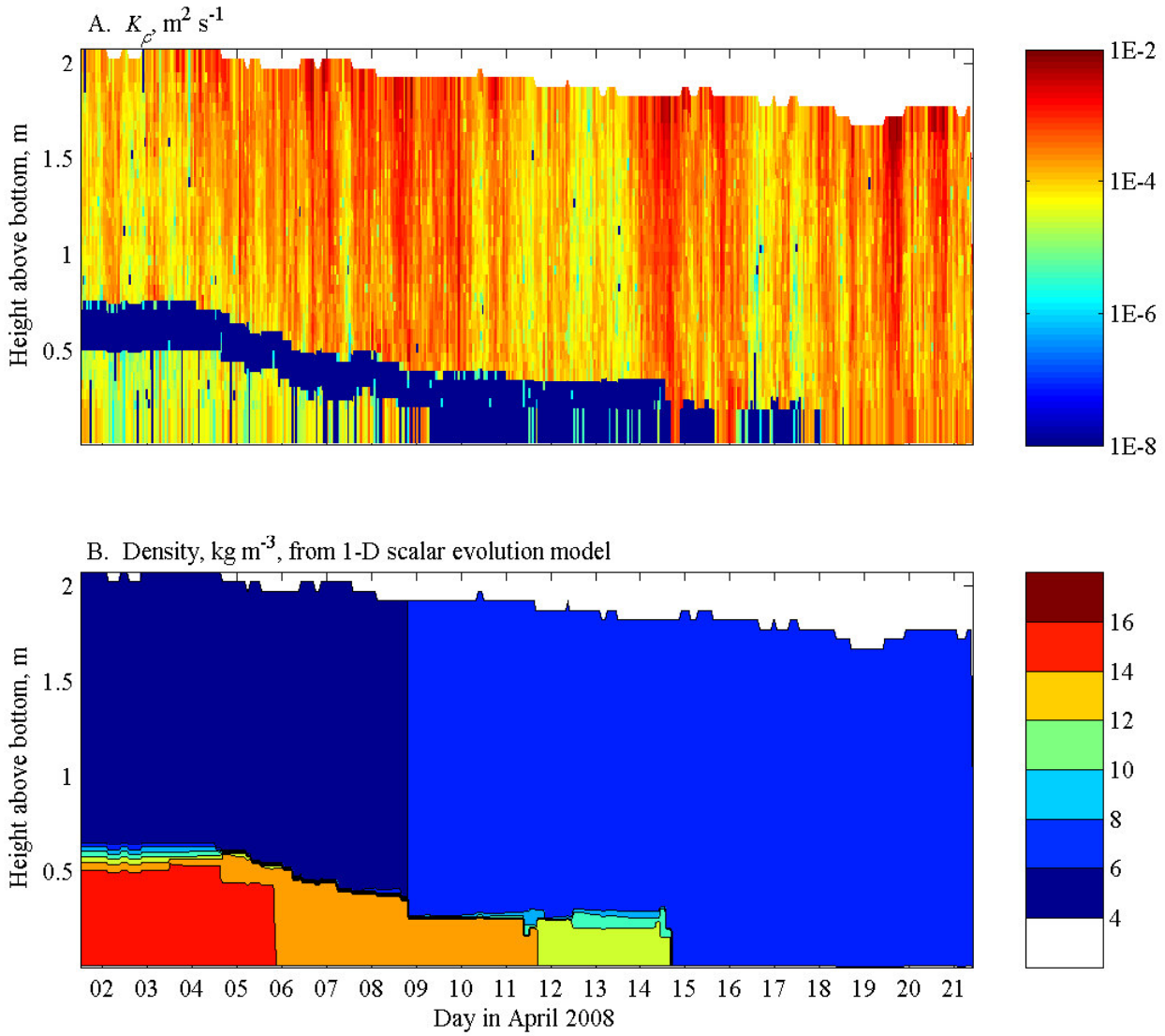

Fig. 4-30. (**A**) K_ρ as calculated from the method of Ivey et al. (2008) using eqs. 4-11 and 4-15, with K_ρ set to $K_{molecular}$ when $\varepsilon/\nu N^2 < 7$ (eq. 4-15a) or when ε was undefined due to positive Reynolds stresses. (**B**) The modeled evolution of $\rho(z,t)$ in sigma units (ρ-1000, kg m^{-3}) using values of K_ρ from panel (A). For comparison with the observed evolution of $\rho(z,t)$, see Fig. 4-11D.

4.4.3 Turbulent mixing efficiency

The turbulent mixing efficiency, Γ, represents the conversion of turbulent kinetic energy to potential energy via irreversible mixing. A value of Γ was implied in the calculations of K_ρ in the previous section, since $\Gamma = R_f/(1-R_f)$, but in this section I will test those assumptions by calculating a rough estimate of Γ in April 2008 using estimates of the change in potential energy over time. The equation for mixing efficiency is:

$$\Gamma = \frac{Energy\,used\ for\,mixing}{Total\ energy\ dissipated} = \frac{\mathrm{d}\,PE_S\,/\mathrm{d}\,t \cdot A}{\rho_w \varepsilon V} \cong \frac{\mathrm{d}\,PE_S\,/\,\mathrm{d}\,t}{\rho_w \varepsilon H} \qquad (4\text{-}20)$$

dPE_S/dt is defined as the first term in eq. 2-21 using the time rate of change of density due to the change in salinity, $\partial\rho/\partial t\,|_S$. The dissipation of turbulent kinetic energy ε in the denominator of eq. 4-20 was not measured directly, so I estimated ε by assuming a local turbulent energy balance (ε=P-B). Production P is defined in eq. 2-18, and buoyancy flux B in eq. 2-22. The hourly values of B are highly variable and include negative values, so I used a 12-hour windowed definition of P-B that is consistent with the windowed definition of dPE_S/dt. B is much smaller than P in most cases, so to first order eq. 4-20 reduces to $\Gamma \sim B/P$.

The estimated values of Γ over 12-hour windows range from negative values to 0.5, with a mean value of 0.11 over the period that salt stratification was present (Fig. 4-31). The negative values are the result of contamination of the input variables B and dPE_S/dt by data that is probably advection rather than reversible mixing of salt. The peak value of Γ corresponds to a period of persistent winds, rather than the time of the peak wind speed. A relationship of some kind between Γ and wind is expected, since Γ is a ratio of observed mixing to variables that I have already established are dependent on wind (namely, P). Additionally, the occurrence of peak Γ during persistent winds is consistent with the idea that the wind drag coefficient should be higher for winds of longer duration (Imberger and Patterson 1990), a concept which was not previously incorporated here.

The estimates of Γ compare favorably with estimates from other field studies. As discussed in §4.4.1.2, a typical assumption is that $\Gamma \leq 0.2$. Though it is impossible to summarize all the literature here, the reported values range widely, from as low as 0 to as high as 0.7. Beginning at the low end, Etemad-Shahidi and Imberger (2002) found an average value of $\Gamma = 0.04$ in a very strongly stratified estuary, while they found $\Gamma = 0$ in a study of two thermally stratified lakes (Etemad-Shahidi and Imberger 2001). From a study of temperature-stratified lakes, Wüest et al. (2000) report an average value of $\Gamma = 0.15$. Geyer et al. (2008) report that $\Gamma > 0.2$ for about half of their observations in a strongly stratified estuary, and attribute the higher-than-expected result

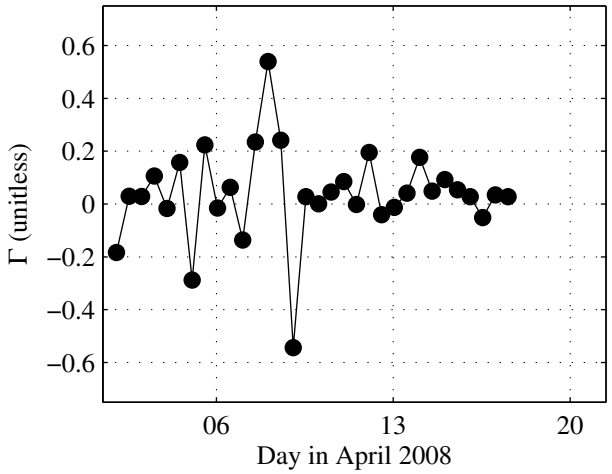

Fig. 4-31. Estimates of the turbulent mixing efficiency, Γ, calculated over 12-hour windows in April 2008 using eq. 4-20.

to shear instabilities. Gargett and Moum (1995) found an even larger value, $\Gamma \sim 0.7$, and concluded that despite possible deficiencies in their method, the stratified tidal fronts that they studied do have highly efficient turbulent mixing.

Efficiency must drop as density gradients weaken, so by definition $\Gamma = 0$ in an unstratified water body. It is therefore not surprising that strongly stratified estuaries exhibit higher values of Γ than weakly stratified lakes. Rodeo Lagoon shows mixing efficiencies that are occasionally high, which is possible since there is strong stratification. However, the mean mixing efficiency is moderately low, since true turbulent mixing is only intermittent.

4.5 Diapycnal mixing

4.5.1 Wind mixing efficiency

The relationships between wind stress and Reynolds stress discussed above in §4.2.1 indicate that wind is the dominant source of mixing in Rodeo Lagoon. Taking the analysis one step further, the detailed observations of April 2008 provide the means to estimate the efficiency of this process. I will use the term "wind mixing efficiency," or m, to refer to the ratio of the increase in potential energy due to mixing ($\mathrm{d}PE_S/\mathrm{d}t$) to the turbulent energy flux at 10 m above the water level (P_{10}):

$$m = \frac{\mathrm{d}PE_S / \mathrm{d}t}{\rho_{air} C_D U_{wind}^{\ 3}} = \frac{\mathrm{d}PE_S / \mathrm{d}t}{P_{10}} \tag{4-21}$$

The notation $P_{10} = \tau U_{wind} = \rho_{air} C_D U_{wind}^{\ 3}$ for the denominator is from Wüest et al. (2000). The concept that the ratio m may be a universal constant, one curiously independent of the surface mixed layer depth or the density jump across the interface, was put forth by Kato and Philips (1969) and Turner (1969). The value of the constant, may, however, depend on the factors that one typically finds affecting C_D – boundary layer stability, wave climate, and so on – and its estimation is the subject of much of the literature on mixed layer entrainment. With these factors taken into consideration, the wind mixing efficiency m is far from universal, and in fact the estimated value varies considerably, as shown in Table 4-1. The numerator must be an actual observed change in potential energy, not the so-called "energy available for mixing" as in Lombardo and Gregg (1989), which is more similar to the denominator of the turbulent mixing efficiency described in the previous section.

A related but slightly different framework for evaluating the contribution of various forcing mechanisms to diapycnal mixing is that of the potential energy anomaly, ϕ, an approach recently reviewed by Burchard and Hofmeister (2008). This approach has been extensively used in estuaries, but of particular note here are studies that explore the dependence of the potential energy anomaly's time derivative, $\mathrm{d}\phi/\mathrm{d}t$, on wind and thermal forcing. For example, Ranasinghe and Pattiaratchi (1999) and Gale et al. (2006) related ϕ to mixing from wind, heating and cooling, and precipitation in a water body that shared many features with Rodeo Lagoon, namely salt stratification in a shallow, intermittently closed and open lagoon. Both used the following definitions for the dependence of $\mathrm{d}\phi/\mathrm{d}t$ on wind:

Source	System	Notation	m $\times 10^{-3}$	C_D $\times 10^{-3}$	mC_D $\times 10^{-6}$
Nunes and Lennon (1987)	Shallow semi-enclosed sea	$h\,\mathrm{d}\phi/\mathrm{d}t/(\rho_a C_D W^3) = \delta k_s/C_D$ δ from Simpson and Bowers (1981) for tidal stirring	0.11*	2.0	0.22
Ranasinghe and Pattiaratchi (1999)	Seasonally open estuary	$\delta k_s/C_D$ from Nunes and Lennon (1987)	0.11	2.0	0.22
Gale et al. (2006)	Seasonally open estuary	$\delta k_s/C_D$ from Nunes and Lennon (1987)	0.11	2.0	0.22
Wüest et al. (2000)	Lake (review of seven)	P_{pot}/P_{10}	0.38* ± 0.17	~1	~0.38
This study	**Coastal lagoon**	$(\mathrm{d}PE_S/\mathrm{d}t)/P_{10}$	**0.46**	**1.0**	**0.46**
Wüest et al. (2000)	Lake	P_{pot}/P_{10}	0.61*	0.9	0.55
Simpson and Bowers (1981)	Tidal estuary	$\mathrm{d}V/\mathrm{d}t\,/(\rho_s C_D W^3) = \delta k_s/C_D$	0.69*	2.0	1.4
Wiles et al. (2006)	Microtidal basin	$h\,\mathrm{d}\phi/\mathrm{d}t/(\rho_a C_D W^3) = \delta\gamma$ $\delta\gamma$ values from Simpson and Bowers (1981)	0.69	2.0	1.4
Fischer et al. (1979)	Lakes	$0.5\eta^3(C_D\rho_a/\rho_w)^{1/2}$ η=1.23	1.0	1.0	1.0
Kato and Phillips (1969)	Laboratory	$1.25(C_D\rho_a/\rho_w)^{1/2}$	1.4*		

Table 4-2. Values of wind mixing efficiency m *and drag coefficient* C_D *reported in previous field and laboratory studies and listed in order of increasing* m*. Only in the studies marked with a star (*) is the value of* m *calculated anew rather than assumed.*

$$\mathrm{d}\phi/\mathrm{d}t = \delta k_s \rho_{air} U_{wind}^3/h \qquad (4\text{-}22)$$

where $\delta = .0037$ and $k_s = 6.4\times10^{-5}$, which theoretically represents $C_D \cdot U_{surface\ current}/U_{wind}$ as originally formulated by Simpson et al. (1978) and Simpson and Bowers (1981). Simpson et al. (1978) actually calculated $\delta = 0.023$ for wind mixing, with $\delta = .0037$ for tidal stirring. The use of $\delta = .0037$ by Ranasinghe and Pattiaratchi (1999) is based on Nunes and Lennon (1987), who justified using the value because their thermocline was much deeper, it was more convenient computationally, and they believed that tidal stirring and wind mixing should be equally efficient. Not surprisingly, Ranasinghe and Pattiaratchi (1999) therefore predict that wind should be about two orders of magnitude less important than convection, yet in their own observations strong winds were capable of mixing the water column.

Wiles et al. (2006) also used the equivalent of eq. 4-22 in a shallow (< 5 m), stratified, microtidal basin, and noted that with values of $\delta = 0.023$ and $k_s = 6.4\times10^{-5}$ the predicted value of $\mathrm{d}\phi/\mathrm{d}t$ was unreasonably small. They attributed the difference between their system and the Simpson and Bowers (1981) shelf sea, where the δ was originally calculated, to the fact the pycnocline was much shallower than in a shelf sea, so wind mixing should have been concomitantly stronger. Noting that wind waves can originate outside the immediate area, they therefore added a "wave stirring" parameter. Although the notion that wind waves rather than the wind itself contributes to mixing makes a certain amount of physical sense, in fact waves and turbulence are usually

envisioned as separate processes; additionally, Rodeo Lagoon is not connected to any other water body, so all the wind waves have to be generated by the same wind that is acting directly on the water. In other words, wind stirring and wind waves in Rodeo Lagoon are not independent, as they could have been in Wiles et al. (2006).

The variability of m in Table 4-2 is about an order of magnitude ($0.11–1.4\times10^{-3}$), while the variability in mC_D is slightly less ($0.22–1.4\times10^{-3}$). The value of m or mC_D from this study of Rodeo Lagoon falls in the low-to-middle part of the observed range, which is not surprising given the relatively small size of this system (< 1 km fetch). Indeed, modeling studies suggest that in larger water bodies, a larger fraction of the energy imparted by the wind can be used for diapycnal mixing (e.g., Rueda and Schladow 2009). Twelve-hour windows of the ratio m vary considerably in the April 2008 data, from ~0 (actually slightly negative) to 1.1×10^{-3} depending on the wind event (Fig. 4-32). More energy is transferred to mixing when the wind is faster and when the stratification is stronger, which corresponds to earlier in the experiment when the stratification was closer to the surface. Even the highest 12-hour value of m falls within the range of values reported in Table 4-2. It is not surprising that the values of m and mC_D are smaller than that reported by Simpson and Bowers (1981), since others (e.g., Wiles et al. 2006), have also found their estimate to be too small.

4.5.2 Convective mixing

The discussion of wind mixing efficiency in §4.5.1 is founded on the assumption that wind is the only source of mixing, whether through surface stirring or shear production. However, convective cooling is another potential source of mixing, and it is important to understand its relative contribution to mixing. Unlike wind, which acts *indirectly* to increase PE through the creation of turbulent kinetic energy, heat transfer *directly* changes PE and ϕ by modifying density through the equation of state, with no need for an "efficiency" term in the equation (Simpson and Hunter 1974):

$$d\phi/dt = \alpha g H_{net}/(2C_p) \qquad (4\text{-}23)$$

where H_{net} is the net heat transfer rate, α is the thermal expansion coefficient (~$1.5–2\times10^{-4}$ °C^{-1}),

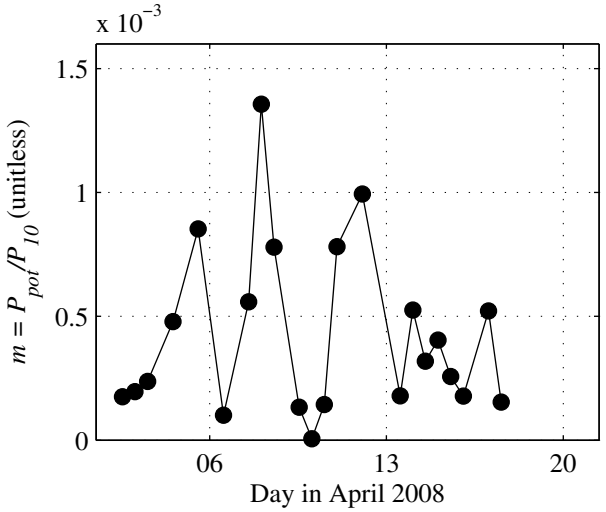

Fig. 4-32. Estimates of the wind mixing efficiency, m, calculated over 12-hour windows in April 2008 using eq. 4-21.

and C_p is the specific heat of water (4.1×10^3 J kg^{-1} °C^{-1}). During cooling, PE and ϕ decrease. However, as discussed below, this does not necessarily mean that irreversible diapycnal mixing is occurring – the density structure must be re-arranged, rather than simply increasing or decreasing in its average value (Winters et al. 1995).

Estimating the relative contributions of wind and convective cooling requires an assumption about the efficiency of wind mixing. Fig. 4-33 shows estimated values of dPE/dt or h dϕ/dt for some of the assumed efficiencies m in Table 4-2 – those from Wüest et al. (2000), Fischer et al. (1979), and Simpson and Bowers (1981). Convective cooling was comparable to wind-driven mixing only on very calm days, such as 16 April (Fig. 4-33). On windier days like 14 April and 18 April, convective cooling made a much smaller contribution to mixing than wind – and these windy days are when nearly all the observed irreversible mixing took place.

Wind and convection can affect both the temperature and salinity distributions, and therefore dPE_S/dt and dPE_T/dt. A regression on the 12-hour windowed values of dPE_S/dt on wind and convective cooling shows that while wind forcing explains a fairly high amount of the variation in dPE_S/dt (r^2 = 0.54), adding convective cooling does not improve the correlation (r^2 = 0.54). The relationship between convective cooling alone and dPE_S/dt is weak (r^2 = 0.10), and adding the contribution of heating does not improve the situation much (r^2= 0.12). However, as expected from the validation of the heat budget, cooling and heating do provide the forcing for dPE_T/dt (r^2 = 0.85 for hourly values). It therefore seems possible to separate out wind, which intermittently eroded the salinity structure, from heating and cooling, which diurnally impacted the temperature structure alone.

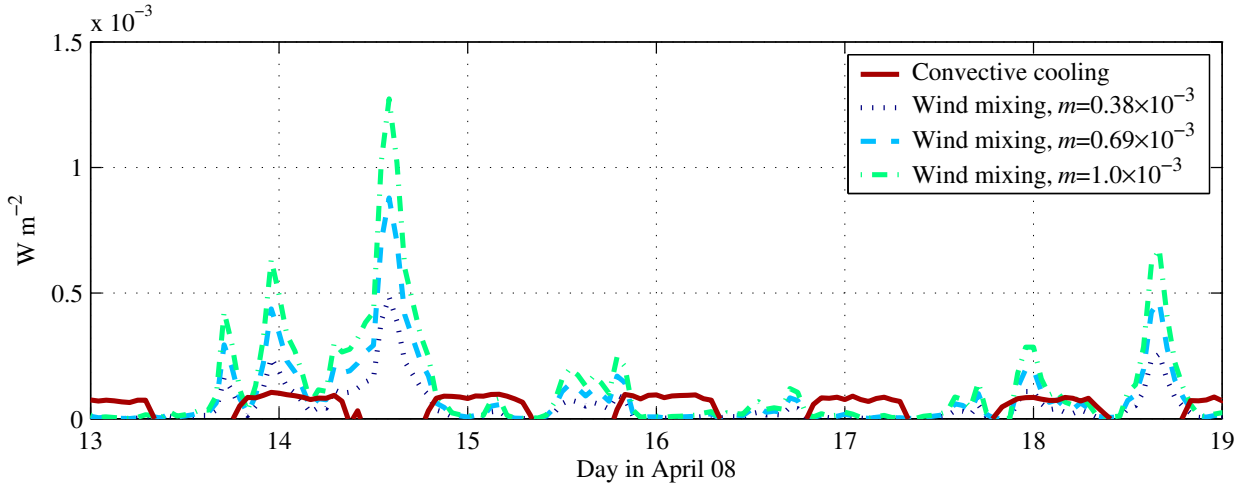

Fig. 4-33. Wind-driven mixing (solid red line), quantified as ($h\, d\phi/dt$) or dPE/dt (W m^{-2}), compared with the contribution of convective cooling (blue and green broken lines). Estimates for the contribution of wind-driven mixing require an assumption about efficiency m. Shown here are three values from the literature: m=0.38×10^{-3} from Wüest et al. (2000), m=0.69×10^{-3} from Simpson and Bowers (1981), and m=1.0×10^{-3} from Fischer et al. (1979).

4.6 Summary of hydrodynamics observations

Wind stress produces waves and currents, and ultimately drives mixing in Rodeo Lagoon. Other sources of mixing energy, like creek inflows and convective cooling, play a relatively minor role compared to wind. Tidal forcing is absent altogether.

Equally important to wind in lagoon hydrodynamics is the seasonal density stratification that results from inflows of salt water from the ocean. This density stratification is ultimately erased by wind-driven mixing, but while it is present, it has a major effect on bottom stresses, currents, and turbulence. Strong wind forcing also occasionally energizes the pycnocline at a larger scale, resulting in seiching. In fact, only unusually strong, persistent winds are capable of efficiently mixing this density stratification. The light, diurnal sea breeze that is more commonplace at the site creates windrows characteristic of Langmuir circulation, but otherwise does very little to generate mixing or seiching. The small size of the lagoon, which results in fetch limitations on wind wave development and wind stress, is a partial explanation for this result. However, averaging over several weeks, both the efficiency in the conversion of wind stress to irreversible vertical mixing of salt, m, and the efficiency in the conversion of turbulence to irreversible vertical mixing, Γ, are in line with observations from other lakes and estuaries.

Though wind waves only reach the bottom under strong winds, energy from wind stress does ultimately reach the bottom of the lagoon under well-mixed conditions, when there is a positive correlation between wind stress and bottom stress. Salt-based density stratification nearly removes this coupling, as wind-generated turbulence has difficulty energizing the brackish layer, though it certainly energizes the overlying surface layer. Stratification also leads to a pronounced suppression of turbulence below the pycnocline. In and below the sharp pycnocline, both ADCP and temperature microstructure data indicate that the flow field is frequently more consistent with wave-type motions than active turbulence. As a result, it appears that the vertical diffusivity is close to molecular values in these patches. As further evidence, a numerical model for the evolution of the salt field in April 2008 agrees best with observations when diffusivity is at molecular values for salt (1.1×10^{-9} m^2 s^{-1}) within the pycnocline.

Wind generates mixing of the pycnocline by entrainment from the surface layer. The alternative is for mixing to result from the shear production of turbulent kinetic energy at the pycnocline; this mechanism is commonly found in more energetic and less strongly stratified conditions, and is invoked almost universally in numerical models of mixing. Although there is strong shear in the velocity profile near the pycnocline, density stratification prevents energetic turbulent motions from developing; production of turbulent kinetic energy was low at the interface in April 2008.

Chapter 5

Linkages between hydrodynamics and water quality

By altering hydrodynamics, a topic discussed in the previous chapter, density stratification has a deleterious impact on water quality in Rodeo Lagoon. This impact is both immediate, operating at a time scale of days to weeks when stratification is present, and longer-term, acting in a cumulative way over many years. In this chapter, I first summarize the observations that link hydrodynamics and water quality at short time scales. In the second part, I present data in support of the argument that recurring density stratification contributes to nutrient retention in the lagoon over a time scale of multiple years.

5.1 Immediate effects of density stratification

The presence of salt-based density stratification has a significant impact on other water quality variables like dissolved oxygen, temperature, and ammonium concentration, as discussed in Chapter 3. This is because the weakened turbulence in and below the pycnocline prevents scalar fluxes between the two layers, as demonstrated in Chapter 4. Each specific type of water quality impact is discussed below.

5.1.1 Nutrient enrichment and phytoplankton

During salt stratification, the bottom layer had concentrations of ammonium and orthophosphate that were orders of magnitude higher than those seen in the surface layer (Table 3-2). These elevated nutrient concentrations were presumably the result of benthic fluxes that were trapped near the bed by the near-elimination of turbulent mixing within the pycnocline. Ammonium concentrations were high enough to exceed the federal criteria for total ammonia in saltwater, which is based on chronic toxicity to aquatic organisms and ranges from 82–376 μMol L^{-1} (see §3.8.3.2, US EPA 1989).

Strong density stratification in winter led to the temporary retention of phytoplankton in and below the pycnocline due to gravitational settling (e.g., December 2006 through March 2007, Fig. 3-9). However, these thin layers of elevated Chl *a* were observed at a time of relatively low biomass, several months before the summer peaks in phytoplankton biomass. The linkage between the two types of biomass peaks, one in time and one space, is in the retention of nutrients for use later in summer due to settling and subsequent trapping in the lower layer.

5.1.2 Hypoxia

When the lagoon is salt-stratified, the bottom layer typically becomes depleted in dissolved oxygen. More specifically, about three-quarters of the lagoon cross-sections collected under salt-stratified conditions had a hypoxic bottom layer. The severity of the oxygen deficit was variable,

with conditions worsening when the salty layer was thicker and when phytoplankton were not present in sufficient density to compensate for the benthic oxygen demand. Another major factor governing the presence of hypoxia is the residence time of the salt water (Ishikawa et al. 2004); as I discuss in §5.2.1, the residence time of the salty layer is quite long, on the order of months. Rodeo Lagoon appears to be typical of productive, salt-stratified coastal lagoons, since hypoxia caused by the isolation of bottom waters has also been reported in similar systems (e.g., Sharples et al. 2003, Gale et al. 2006). The problem is exacerbated by the higher temperature of the salty layer, which increases microbial respiration rates while reducing oxygen solubility.

In summer, diurnal temperature stratification may also reduce re-aeration, but the impact is mitigated by the fact that the stratification and photosynthetic oxygen production both peak around mid-day. The worst impacts would come when temperature stratification persists over several days, as happens occasionally during the sunniest periods (e.g., 04–05 July 2007 in Fig. 3-7). Unfortunately, temperature stratification coincides with the some of the highest water temperatures of the year, which sharply reduces oxygen solubility and multiplies the harmful effect on fish.

5.1.3 Light climate

In winter and spring, stratification reduces the depth of the surface mixed layer by a modest amount (~25%), which means that surface phytoplankton are exposed to higher average light levels as they are retained in the mixed layer. This seasonality is the reverse of the typical Sverdrup (1953) model, and it occurs when water temperatures, solar radiation, and nutrient concentrations are at seasonal lows in the surface layer. Nonetheless, phytoplankton were abundant in spring 2007, as surface Chl *a* concentrations reached 49 μg L^{-1} before the water column completely mixed in early April. Although this value is low for Rodeo Lagoon, it is high by almost any other standard. At a minimum, the spring stratification by salt may assist the phytoplankton in getting established earlier in the season, as Chl *a* concentrations exceeded 400 μg L^{-1} by the end of April.

5.1.4 Summary of immediate ecological impacts

On short time scales, salt-based stratification has an impact on water quality beyond the obvious increase in salinity. By reducing mixing near the bed and allowing detritus to accumulate near the sediment-water interface, it leads to much lower dissolved oxygen and much higher nutrient concentrations. Both of these effects are potentially harmful to fish, but fish kills in Rodeo Lagoon are actually more common in late summer and fall, so they do not appear to be linked to the localized hypoxia and elevated ammonia caused by salt stratification in winter. Presumably this is because the well-oxygenated and fresher surface layer provides ample refugia from the poor water quality conditions below. The more harmful effect of stratification on fish is therefore via the indirect route of encouraging potentially harmful algae blooms, as discussed in the sections below.

5.2 Long-term effects of density stratification

Density stratification can cause a short term deterioration in water quality, but its more significant impact may be its contribution to the gradual retention of nutrients in the lagoon. In this section, I explain how stratification lengthens the water residence time of the lower layer, thereby enhancing the capture of nutrients stored in organic detritus and sediments.

5.2.1 Residence times

Flushing time (T_f) and mean residence time (τ) are closely related parameters that measure the amount of time that water or scalars spend in a water body. Both measures are related to productivity in aquatic systems by way of their respective relationships with the supply of water and nutrients, the time available for settling, and the time available for phytoplankton communities to grow (Kalff 2001). In estuaries, these two characteristic times typically have slightly different definitions from one another; flushing time is a bulk parameter for the entire water body, whereas residence time is specific to a particular water parcel and may vary throughout an estuary due to spatial variability in flushing (Geyer et al. 2000; Monsen et al. 2002). In limnology, where spatial variability is less of a concern, flushing time and mean residence time are considered equivalent measures due to the longer time scales (~years) typically involved (Kalff 2001). In Rodeo Lagoon, flushing and mean residence times will be about the same under well-mixed conditions, since the lagoon is fairly small and horizontally homogeneous. However, under salt-stratified conditions, mean residence time will differ from flushing time, with different residence times for the two layers. For simplicity in the discussion below, residence time τ refers to a mean residence time.

Freshwater inflow during the wet season is almost exclusively responsible for flushing the lagoon, with large swings in water volume occurring as the outlet intermittently opens and closes. To calculate flushing time in winter, an adaptation of the tidal prism method for the case of no return flow (Monsen et al. 2002) was applied:

$$T_{f,freshwater} = V_{avg} T \Big/ \Delta V \qquad (5\text{-}1)$$

where V_{avg} is the mean basin volume, T is the duration of the fill-drain period, and ΔV is the volume difference between high and low water.

Using the time record of lagoon volume, I identified 18 events during the winters of 2006, 2007, and 2008 during which the lagoon rose rapidly, overtopped the beach, cut an outlet channel, and then drained (Fig. 5-1). The three winters differed dramatically from one another, with the rainy winter of 2006 (0.87 m precipitation) experiencing many more fill-drain events than the dry winters of 2007 and 2008 (0.43 and 0.44 m precipitation, respectively). The average flushing time during the three wet seasons was 23 days.

This estimate of $T_{f,freshwater}$ assumes that the entire lagoon volume is actively mixed, when in fact the lagoon is density-stratified by salt water. The presence of two layers means the fresher water has a shorter residence time as it short-circuits across the top of the lagoon, while the brackish layer has a much longer residence time. Salty water can fill up to a maximum of half the lagoon volume, which means the residence time for freshwater could be up to half as long as the whole-lagoon flushing time of 23 days calculated above.

I assumed that the residence time of brackish water depends entirely on turbulent mixing into the overlying water column, since bathymetric restrictions typically prevent it from directly exiting the lagoon via the outlet channel. A rough estimate of the residence time is as follows:

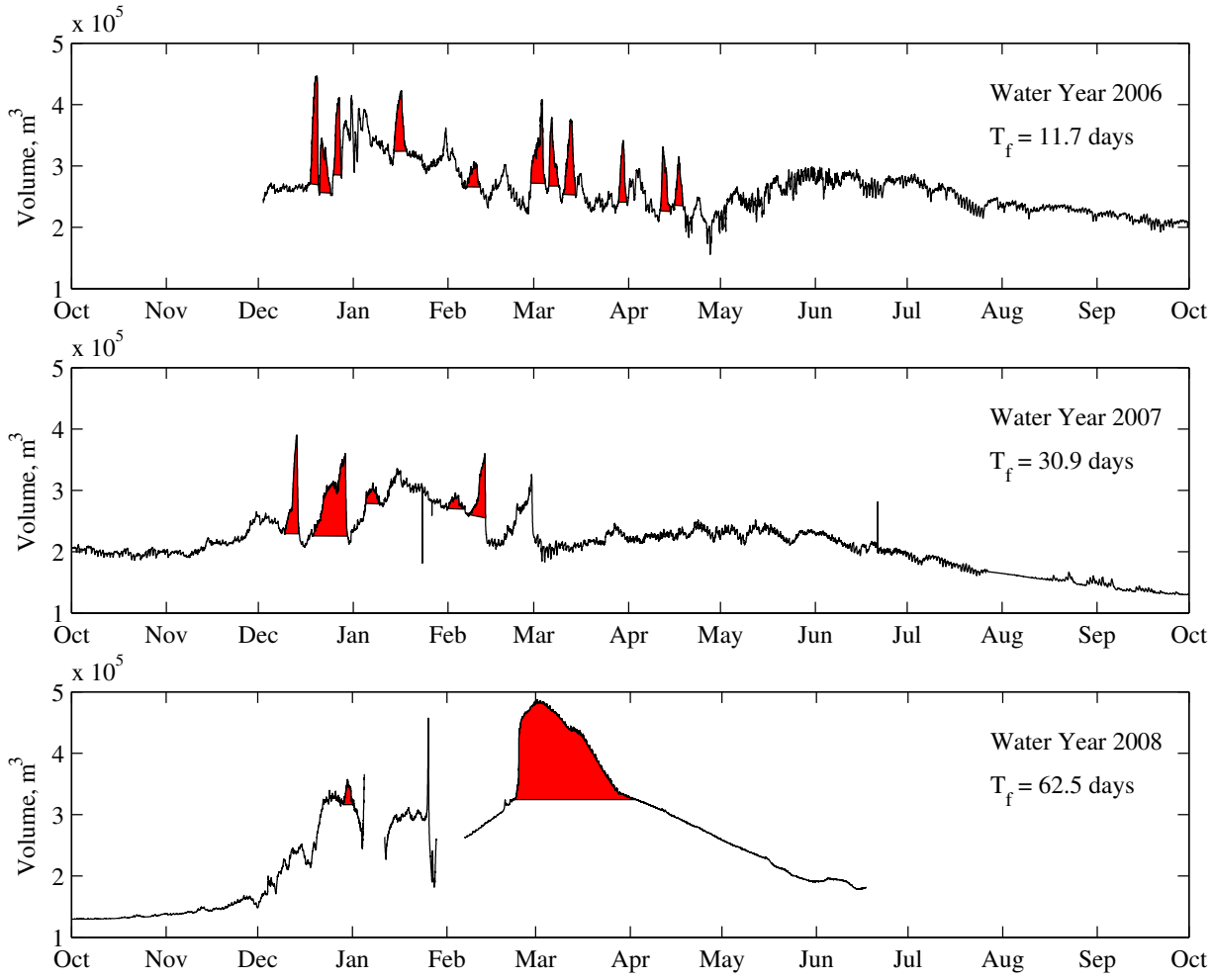

Fig. 5-1. Fill-drain events (red) used to calculate flushing time.

$$\tau_{\text{brackish}} = \frac{\text{M}_{\text{brackish water}}}{K_T \frac{\partial \rho}{\partial z} A} \qquad (5\text{-}2)$$

where $\text{M}_{\text{brackish water}}$ is the mass of salty water below the pycnocline, K_T is the vertical turbulent scalar diffusivity, $\partial\rho/\partial z$ is the vertical density gradient, and A is the surface area of the pycnocline. The mass of salty water was calculated with lagoon bathymetry taken into account. Fig. 5-2 shows the two density profiles used in this calculation, which were collected with the SCAMP on 16 January 2008 and 14 April 2008. In the January profile, salty water fills much of the water column, whereas in April it is confined to the very bottom of the lagoon. The density gradient $\partial\rho/\partial z$ was defined using the peak value from the binned SCAMP segments (Fig. 4-26A,D,G). To represent the salt flux across the pycnocline, values of K_T for each day are the log-average of SCAMP profile segments collected within 0.1 m of the peak value of $\partial\rho/\partial z$. Table 5-1 lists the inputs into the calculation of residence time for the salty layer.

	Jan 2008	Apr 2008
$M_{saltwater}$, mass of salty water (kg)	6.3×10^{9}	3.9×10^{8}
K_T, vertical diffusivity ($m^2\ s^{-1}$)	4.5×10^{-6}	1.6×10^{-4}
$\partial\rho/\partial z$, density gradient ($kg\ m^{-4}$)	24	24
A, area of interface (m^2)	1.4×10^{5}	9.8×10^{4}
τ, mean residence time (d)	4700	12

Table 5-1. Residence time for salty layer.

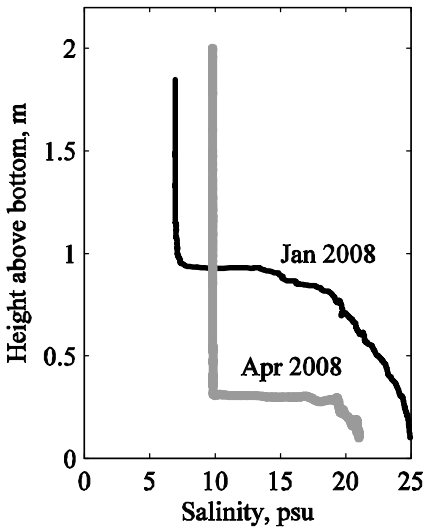

Fig. 5-2 (right). Salinity profiles used for residence time calculations.

The January estimate of 4700 days is clearly an upper bound on the true value of the residence time, since it assumes constant mixing when in fact mixing rates vary temporally based on wind speed, and because some salty water found mid-water column may have flowed out when the outlet was open in January or March 2008.

The estimates for residence time of the salty water show a large range (12 to 4700 days) because of the different conditions present in the lagoon when the two profiles were collected. In January, a large volume of salty water was present, while in April much less salt remained. Also, in April, higher wind speeds resulted in an elevated value of K_T compared to January. In fact, the salty layer mixed out completely over the ensuing days after this density profile was collected (Fig. 4-11), corroborating the estimate above. Likewise, a salty layer was observed in the lagoon throughout the spring of 2008, consistent with the longer estimate of τ for January.

In summer, the lagoon's water balance is dominated by a small freshwater inflow ($< 5\ L\ s^{-1}$) and evaporation; outflow is only possible as slow seepage through the beach berm. Because the basin acts like a closed system for scalars like salt and sediment, which have no large sources or sinks in summer, the concept of "flushing time" breaks down. For example, between 01 June and 01 October 2007, when no rainfall occurred and the lagoon outlet was closed, salinity increased by 44% (Fig. 3-3), while volume decreased by 43%. The net effect is only an 18% loss of salt mass over four months, which is most likely due to seepage losses towards the beginning of the summer when the water surface elevation is higher than mean sea level. No appreciable flushing occurs in summer; the residence time can effectively be defined as the period between breaches of the lagoon outlet, which typically is on the order of five to seven months (D. Fong pers. comm.)

To summarize, Rodeo Lagoon is rapidly flushed by inflow from the watershed during the wet season. The average surface layer residence time during winter is less than a month. By contrast, the residence time for the lower brackish layer is much larger, on the order of a few months, due to bathymetric trapping and limited mixing with the surface layer. In summer, when no appreciable scalar flushing occurs, the residence time is on the order of six months.

5.2.2 Nutrient retention and release

Winter stratification by brackish water has important implications for nutrient retention in the lagoon. Density stratification apparently confines nutrients released from the sediment into the lower layer, which has a long residence time of up to several months compared to the rapidly flushed surface layer. Water short-circuits across the top of the lagoon in its transit from creek inflow to ocean outflow, as quantified by the shorter residence time of the surface layer and by velocity profiles collected under stratified conditions, which show significantly faster flows in the surface layer than in the comparatively stagnant lower layer (Fig. 4-17). Rather than flushing out nutrients, the fresh water is simply flowing across the denser, nutrient-rich lower layer.

Meanwhile, the lower layer has elevated nutrient concentrations (Table 3-2), particularly of ammonium, due to its contact with the bed, which contains the particulate remnants of the previous summer's phytoplankton and macrophyte growth. Storage of nutrients in the solid phase – whether as algal detritus or sorbed to inorganic particles – is the main mechanism by which nutrients are retained (Thornton et al. 1995), which is why the longer residence times and reduced bed stresses in the lower layer have an impact on nutrient retention. In the absence of salt stratification, the large freshwater flows in winter would flush out some of this material.

Similar trends linking nutrient storage to residence time have been observed across the spectrum of aquatic systems that Rodeo Lagoon resembles. For example, wetlands also export fewer nutrients as residence time increases, and detritus is major sink for both N and P (Howard-Williams 1985; Reddy et al. 1999). Nixon et al. (1996) found that N and P retention in estuaries was correlated with residence time, though for N the retention is typically followed by removal by denitrification. In lakes, longer water residence times are also associated with increased P retention and increased loss of N through denitrification (Kalff 2002). However, as previously noted in §3.7.3.1, denitrification rates are lower in eutrophic marine systems due to sulfide inhibition, so that loss pathway for N will be relatively less important here.

Since density stratification limits turbulent scouring of the bed, not only is net nutrient accumulation by detrital algae and macrophytes possible, but so is reseeding of certain phytoplankton populations from resting spores remaining in the bottom sediments. For example, potentially viable *N. spumigena* resting spores (akinetes) were found to a depth of 20 cm in Rodeo Lagoon sediments (Cousins et al. 2010). As indicated by the reduced shear stresses and scalar diffusivity near the bed, the rapidly flushed freshwater layer has a limited ability to mobilize organic sediments or dissolved nutrients found at the sediment-water interface. Without a full-scale flushing of the lagoon, both these nutrients and phytoplankton live cells and spores remain in the bed.

Salinity stratification is a major reason why it has become difficult to flush algal detritus from the lagoon, but admittedly other factors also contribute. The macrophytes fringing the lagoon can store nutrients in their roots and rhizomes (Reddy et al. 1999), as well as reduce turbulent bed stresses (James and Barko 1994). Finally, the microbial biofilm at the sediment-water interface may also temporarily store nitrogen (Graco et al. 2001) and reduce sediment mobility (Decho 2000).

The timing of wind-driven destratification in late spring and early summer is important: it typically occurs *after* the outlet channel has closed for the season, which inhibits any further export out of the lagoon of material previously found in the nutrient-enriched bottom layer.

Phytoplankton growth in summer is fueled by a combination of long residence times and plentiful nutrients. Due to the pronounced dry season and loss of connectivity with the ocean, the water residence time in summer is on the order of several months. Phytoplankton are not exported out of the system due to negligible outflows, so abundance can increase more easily; the maximum specific growth rate of most cyanobacteria is about 0.4-2.0 d^{-1} (Oliver and Ganf 2000), compared to a residence time of 100 days or more. Furthermore, in summer internal loading of nutrients from the sediment can serve as an important factor in sustaining phytoplankton populations; any nutrients released from the sediment can be used and recycled multiple times. The well-mixed water column facilitates redistribution and recycling of nutrients from the sediments into the photic zone.

5.3 Management implications

If salinity stratification and internal nutrient loading are contributing to the deteriorated water quality of Rodeo Lagoon, what management approaches could be used to correct the problem? The low salinity of the lagoon is clearly an integral part of its ecological niche; for example, the tidewater goby is most commonly found in waters with a salinity around 10–12 psu (2008). Therefore, converting the lagoon to freshwater habitat by completely eliminating salt water inflows would not be an attractive option. Similarly, dredging the bottom sediments of the lagoon would reduce internal nutrient loading, but could present a major disruption to the bottom-burrowing tidewater goby (2008). In lieu of these more drastic approaches, the goal should be to export as much detritus and sediment out of the lagoon in winter as possible using "natural" flushing, while allowing enough salt water back in to maintain the brackish conditions.

Several options are available to boost the export of nutrients and sediment. One approach would be to artificially destratify the lagoon in winter, thereby redistributing some dissolved nutrients, detritus, and sediment towards the surface where they could be flushed out. This would be somewhat analogous to the artificial destratification of eutrophic, temperature-stratified lakes, where the approach can improve water quality by cooling and deepening the surface mixed layer. In these lakes, destratification is typically achieved by adding mechanical energy via engineered solutions such as pumps or air bubblers. Although such an approach could be used to destratify the lagoon in winter, it bears repeating that summer-time thermal stratification, although occasionally present on a diurnal basis, is not central to the eutrophication problem. This is because the peak algal blooms do **not** co-occur with the much stronger salt-based stratification; the two are separated in time by several months. Instead, the goal would be to achieve a modest increase in the export of nutrients in dissolved and detrital form that would otherwise be confined near the bed. This approach is based on the observation that turbulent bed stresses are higher when the lagoon is not stratified, which should encourage the resuspension of detritus and sediments. A permanently installed array of salinity sensors near the middle of the lagoon would assist such efforts, as the density stratification cannot be clearly observed from more convenient sampling locations like the shoreline, the west end at the pedestrian bridge, or the east end at the Bunker Road bridge.

Another option would be to artificially breach the outlet channel to allow salt water to drain, although currently a bathymetric hump between the center of the lagoon and the outlet would prevent this approach from being very effective. The practice of artificially opening and closing the lagoon was formerly common when the lagoon and its watershed were managed by the military (Striplen et al. 2004), but in this case the goal would be to prevent water quality problems, rather than to drain the lagoon once water quality had already deteriorated. In a similar approach, the outlet channel could be increased in size or dredged to allow swifter flows near the bed. It is possible, though purely speculative, that the outlet channel has become artificially stabilized by some combination of invasive vegetation, including ice plant, and the adjacent structures, which include a pedestrian bridge, road, and parking lot.

Modifying the lagoon inlet from the creek holds less promise. The installation of the weir between the lake and lagoon probably reduced peak inflow rates compared to their historic values, thereby reducing the flushing and scouring these peak flows could have produced. However, the fact the lake is acting as a primary settling basin for the lagoon makes it a net benefit, so modifications at this point would not necessarily improve lagoon water quality.

To summarize, Rodeo Lagoon differs from eutrophic, stratified freshwater lakes in that density stratification contributes to the problem in a more indirect way. In freshwater lakes, the formation of a summer mixed layer has a direct effect on the resident phytoplankton by improving the light climate. By contrast, stratification is problematic in Rodeo Lagoon because it reduces the export of nutrients over time, not because it immediately alters the phytoplankton growth climate. Any management approaches should keep in mind this important distinction.

References

2009. Endangered and threatened wildlife and plants; removal of the brown pelican (*Pelecanus occidentalis*) from the federal list of endangered and threatened wildlife; final rule. *Federal Register* **74**: 59443-59472.

2008. Endangered and threatened wildlife and plants; revised designation of critical habitat for the tidewater goby (*Eucyclogobius newberryi*); Final Rule. *Federal Register* **73**: 5920-6006.

An, S., and Gardner, W.S. 2002. Dissimilatory nitrate reduction to ammonium (DNRA) as a nitrogen link, versus denitrification as a sink in a shallow estuary (Laguna Madre/Baffin Bay, Texas). *Mar Ecol-Prog Ser* **237**: 41–50.

Arar, E. 1997. *Method 446.0 - In vitro determination of chlorophylls* a*,* b*,* c1 + c2 *and pheopigments in marine and freshwater algae by visible spectrophotometry*. United States Environmental Protection Agency, National Exposure Research Laboratory, Office of Research and Development, Cincinnati, Ohio.

Arar, E., and Collins, G. 1997. *Method 445.0 - In vitro determination of chlorophyll* a *and pheophytin a in marine and freshwater algae by fluorescence*. United States Environmental Protection Agency, National Exposure Research Laboratory, Office of Research and Development, Cincinnati, Ohio.

Badosa, A., Boix, D., Brucet, S., Lopez-Flores, R., and Quintana, X. 2006. Nutrients and zooplankton composition and dynamics in relation to the hydrological pattern in a confined Mediterranean salt marsh (NE Iberian Peninsula). *Estuar Coast Shelf S* **66**: 513-522.

Barica, J., and Mur, L. 1980. *Hypertrophic ecosystems*. Dr. W. Junk bv Publishers, The Hague.

Barry, M., Ivey, G., Winters, K., and Imberger, J. 2001. Measurements of diapycnal diffusivities in stratified fluids. *J Fluid Mech* **442**: 267-291.

Beutel, M. 1998. *Golden Gate National Recreation Area storm water monitoring program 1997/1998: Final report*. Beutel Environmental.

BioSystems Analysis, I. 1993. Rodeo Lagoon nutrient analysis: sediment and water sampling,

November 1992, prepared for National Park Service, Golden Gate National Recreation Area.

Bird, E. 1994. Physical setting and geomorphology of coastal lagoons. In *Coastal lagoon processes* (ed. B. Kjerfve), *Elsevier Oceanography Series*, pp. 9-40, Elsevier, Amsterdam.

Booth, B. 1993. Estimating cell concentrations and biomass of autotrophic plankton using microscopy. In *Handbook of methods in aquatic microbial ecology* (eds. P. Kemp, B. Sherr, E. Sherr, and J. Cole), pp. 199-206, Lewis Publishers, Boca Raton, Fla.

Bormans, M., Ford, P., Fabbro, L., and Hancock, G. 2004. Onset and persistence of cyanobacterial blooms in a large impounded tropical river, Australia. *Mar Freshwater Res* **55**: 1-15.

Bormans, M., Sherman, B., and Webster, I. 1999. Is buoyancy regulation in cyanobacteria an adaptation to exploit separation of light and nutrients? *Mar Freshwater Res* **50**: 897-906.

Boström, B., Andersen, J., Fleischer, S., and Jansson, M. 1988. Exchange of phosphorus across the sediment - water interface. *Hydrobiologia* **170**: 229-244.

Branco, B., and Torgersen, T. 2009. Predicting the onset of thermal stratification in shallow inland waterbodies. *Aquat Sci* **71**: 65-79.

Bricker, S., Longstaf, B., Dennison, W., Jones, A., Boicourt, K., Wicks, C., and Woerner, J. 2008. Effects of nutrient enrichment in the nation's estuaries: A decade of change. *Harmful Algae* **8**: 21-32.

Buck, E.H., and Folger, P. 2009. *Ocean Acidification*. Congressional Research Service, Washington, D.C.

Burchard, H. et al. 2008. Observational and numerical modeling methods for quantifying coastal ocean turbulence and mixing. *Progress in Oceanography* **76**: 399-442.

Burchard, H., and Hofmeister, R. 2008. A dynamic equation for the potential energy anomaly for analysing mixing and stratification in estuaries and coastal seas. *Estuar Coast Shelf S* **77**: 679–687.

Burns, N.M., and Rosa, F. 1980. In situ measurement of the settling velocity of organic carbon particles and 10 species of phytoplankton. *Limnol Oceanogr* **25**: 855–864.

Carstensen, J., Henriksen, P., and Heiskanen, A. 2007. Summer algal blooms in shallow estuaries: Definition, mechanisms, and link to eutrophication. *Limnol Oceanogr* **52**: 370-384.

Chapra, S. 1997. *Surface water-quality modeling*. McGraw-Hill, New York.

Chorus, I., and Bartram, J. 1999. *Toxic cyanobacteria in water: a guide to their public health consequences, monitoring, and management*. E & FN Spon, London.

Chubarenko, B., Koutitonsky, V., Neves, R., and Umgiesser, G. 2005. Modeling concepts. In *Coastal lagoons: ecosystem processes and modeling for sustainable use and development* (eds. I. Gönenç and J. Wolflin), pp. 231-306, CRC Press, Boca Raton, Fla.

Cioffi, F., Dieugenio, A., and Gallerano, F. 1995. A new representation of anoxic crises in hypertrophic lagoons. *Appl Math Model* **19**: 685-695.

Cloern, J. 1991. Tidal stirring and phytoplankton bloom dynamics in an estuary. *J Mar Res* **49**: 203-221.

Cloern, J. 1987. Turbidity as a control on phytoplankton biomass and productivity in estuaries. *Cont Shelf Res* **7**: 1367-1381.

Codemo, C., Podlech, M., Brown, R., and Jordan, W. 1996. *Characterization of phytoplankton in Rodeo Lagoon and Rodeo Lake, GGNRA, during August 1996. Prepared for the National Park Service, Golden Gate National Recreation Area*. Institute of Chemical Biology, University of San Francisco, San Francisco, Calif.

Condie, S., and Bormans, M. 1997. The influence of density stratification on particle settling, dispersion and population growth. *J Theor Biol* **187**: 65-75.

Condie, S., and Webster, I. 2002. Stratification and circulation in a shallow turbid waterbody. *Environ Fluid Mech* **2**: 177-196.

Conley, D., Carstensen, J., Vaquer-Sunyer, R., and Duarte, C. 2009. Ecosystem thresholds with hypoxia. *Hydrobiologia* **629**: 21-29.

Cousins, M., Stacey, M., and Drake, J.L. 2010. Effects of seasonal stratification on turbulent mixing in a hypereutrophic coastal lagoon. *Limnol Oceanogr* **55**: 172–186.

Csanady, G. 2001. *Air-sea interaction: Laws and mechanisms*. Cambridge University Press, Cambridge.

Csanady, G. 1978. Water circulation and dispersal mechanisms. In *Lakes: Chemistry, geology and physics* (ed. A. Lerman), pp. 21–64, Springer-Verlag, New York.

Davis, J., and Koop, K. 2006. Eutrophication in Australian rivers, reservoirs and estuaries - a southern hemisphere perspective on the science and its implications. *Hydrobiologia* **559**: 23-76.

Decho, A.W. 2000. Microbial biofilms in intertidal systems: an overview. *Cont Shelf Res* **20**: 1257-1273.

Dillon, T. 1982. Vertical overturns: A comparison of Thorpe and Ozmidov length scales. *J Geophys Res-Oc Atm* **87**: 9601-9613.

Drake, J.L. 2008. Community structure and dynamics of phytoplankton blooms in Rodeo Lagoon (Golden Gate National Recreation Area). Master's thesis. San Francisco State University, Biology, San Francisco, Calif.

Drake, J.L., Carpenter, E.J., Cousins, M., Nelson, K., Guido Zarate, A., and Loftin, K. *In press*. Effects of light and nutrients on seasonal phytoplankton succession in a temperate eutrophic coastal lagoon. *Hydrobiologia*.

Elder, W. 2001. Geology of the Golden Gate Headlands. In *Geology and natural history of the San Francisco Bay Area: a field-trip guidebook* (eds. P. Stoffer and L. Gordon), pp. 61-86, U.S. Geological Survey, Menlo Park, Calif. http://geopubs.wr.usgs.gov/bulletin/b2188/.

Elwany, M., Flick, R., and Aijaz, S. 1998. Opening and closure of a marginal southern California lagoon inlet. *Estuaries* **21**: 246-254.

Emery, W., and Thomson, R. 2001. *Data analysis methods in physical oceanography*. 2nd ed. Elsevier Science B.V., Amsterdam.

Eppley, R.W., Holmes, R.W., and Strickland, J.D. 1967. Sinking rates of marine phytoplankton measured with a fluorometer. *J Exp Mar Biol Ecol* **1**: 191–208.

Etemad-Shahidi, A., and Imberger, J. 2002. Anatomy of turbulence in a narrow and strongly stratified estuary. *J Geophys Res-Oceans* **107**: 3070.

Etemad-Shahidi, A., and Imberger, J. 2001. Anatomy of turbulence in thermally stratified lakes. *Limnol Oceanogr* **46**: 1158–1170.

Farmer, D., and Smith, J. 1980. Tidal interaction of stratified flow with a sill in Knight Inlet. *Deep-Sea Res* **27A**: 239-254.

Fischer, H., List, E., Koh, R., Imberger, J., and Brooks, N. 1979. *Mixing in inland and coastal waters*. Academic Press, San Diego, Calif.

Fong, D. 1997. 1996 fall fish kill evaluation for Rodeo Lagoon, Golden Gate National Recreation Area, Marin Co.

Frascari, F., Matteucci, G., and Giordano, P. 2002. Evaluation of a eutrophic coastal lagoon ecosystem from the study of bottom sediments. *Hydrobiologia* **475**: 387-401.

Friehe, C., and Schmitt, K. 1976. Parameterization of air-sea interface fluxes of sensible heat and moisture by bulk aerodynamic formulas. *J Phys Oceanogr* **6**: 801-809.

Fugate, D., and Chant, R. 2005. Near-bottom shear stresses in a small, highly stratified estuary. *J Geophys Res-Oceans* **110**: 3022.

Gale, E., Pattiaratchi, C., and Ranasinghe, R. 2006. Vertical mixing processes in Intermittently Closed and Open Lakes and Lagoons, and the dissolved oxygen response. *Estuar Coast Shelf S* **69**: 205-216.

Ganf, G., and Oliver, R. 1982. Vertical separation of light and available nutrients as a factor causing replacement of green algae by blue-green algae in the plankton of a stratified lake. *J Ecol* **70**: 829-844.

Gargett, A., and Moum, J. 1995. Mixing efficiencies in turbulent tidal fronts: Results from direct and indirect measurements of density flux. *J Phys Oceanogr* **25**: 2583-2608.

George, D. 1981. Wind-induced water movements in the South Basin of Windermere. *Freshwater Biol* **11**: 37-60.

Geyer, W., Scully, M., and Ralston, D. 2008. Quantifying vertical mixing in estuaries. *Environ Fluid Mech* **8**: 495-509.

Golden Gate National Recreation Area, ed. 1992. Rodeo Lagoon protection and enhancement plan - Draft.

Gomez, E., Fillit, M., Ximenes, M., and Picot, B. 1998. Phosphate mobility at the sediment-water interface of a Mediterranean lagoon (etang du Mejean), seasonal phosphate variation. *Hydrobiologia* **374**: 203-216.

Graco, M., Farias, L., Molina, V., Gutierrez, D., and Nielsen, L. 2001. Massive developments of microbial mats following phytoplankton blooms in a naturally eutrophic bay: Implications for nitrogen cycling. *Limnol Oceanogr* **46**: 821-832.

Haines, P. 2008. *ICOLL management: strategies for a sustainable future*. BMT WBM Pty Limited, Broadmeadow, NSW, Australia.

Haines, P., Tomlinson, R., and Thom, B. 2006. Morphometric assessment of intermittently open/closed coastal lagoons in New South Wales, Australia. *Estuar Coast Shelf S* **67**: 321-332.

Hambrook Berkman, J., and Canova, M. 2007. Algal biomass indicators (ver. 1.0). In *Techniques of Water-Resources Investigations, Chapter A7, Biological Indicators*, U.S. Geological Survey http://pubs.water.usgs.gov/twri9A/.

Hansen, D., and Rattray, M. 1965. Gravitational circulation in straits and estuaries. *J Mar Res* **23**: 104–122.

Harris, G. 1999. Comparison of the biogeochemistry of lakes and estuaries: ecosystem processes, functional groups, hysteresis effects and interactions between macro- and microbiology. *Mar Freshwater Res* **50**: 791-811.

Hartzell, J.L., Jordan, T.E., and Cornwell, J.C. 2010. Phosphorus burial in sediments along the salinity gradient of the Patuxent River, a subestuary of the Chesapeake Bay (USA). *Estuaries and Coasts* **33**: 92–106.

Harzallah, A., and Chapelle, A. 2002. Contribution of climate variability to occurrences of anoxic crises 'malaigues' in the Thau lagoon (southern France). *Oceanol Acta* **25**: 79-86.

Hasselmann, K. et al. 1973. *Measurements of wind wave growth and swell decay during the Joint North Sea Wave Project (JONSWAP)*. Deutsches Hydrographisches Institut, Hamburg.

Head, M. 1983. The use of miniature four-electrode conductivity probes for high resolution measurement of turbulent density or temperature variations in salt-stratified water flows. Ph.D. thesis. University of California, San Diego, San Diego, Calif.

Hearn, C., and Robson, B. 2001. Inter-annual variability of bottom hypoxia in shallow Mediterranean estuaries. *Estuar Coast Shelf S* **52**: 643-657.

Henderson-Sellers, B. 1986. Calculating the surface-energy balance for lake and reservoir modeling: A review. *Rev Geophys* **24**: 625-649.

Hill, M. 1970. Barrier beach. *Mineral information service, California Division of Mines and Geology* **23**: 231-237.

Holm-Hansen, O., and Riemann, B. 1978. Chlorophyll a determination: improvements in methodology. *Oikos* **30**: 438-447.

Howard-Williams, C. 1985. Cycling and retention of nitrogen and phosphorus in wetlands: a theoretical and applied perspective. *Freshwater Biol* **15**: 391-431.

Huisman, J., Matthijs, H., and Visser, P., eds. 2005. *Harmful cyanobacteria.* Springer, Dordrecht, The Netherlands.

Ibelings, B., Mur, L., and Walsby, A. 1991. Diurnal changes in buoyancy and vertical distribution in populations of *Microcystis* in two shallow Lakes. *J Plankton Res* **13**: 419-436.

Imberger, J. 1985. The diurnal mixed layer. *Limnol Oceanogr* **30**: 737-770.

Imberger, J., and Ivey, G. 1991. On the nature of turbulence in a stratified fluid. Part 2: Application to lakes. *J Phys Oceanogr* **21**: 659-680.

Imberger, J., and Patterson, J.C. 1990. Physical limnology. *Advances in Applied Mechanics* **27**: 303-475.

Ingall, E., and Jahnke, R. 1994. Evidence for enhanced phosphorus regeneration from marine sediments overlain by oxygen depleted waters. *Geochim Cosmochim Ac* **58**: 2571-2575.

Ishikawa, T., Suzuki, T., and Qian, X. 2004. Hydraulic study of the onset of hypoxia in the Tone River estuary. *J Environ Eng-ASCE* **130**: 551-561.

Itsweire, E., Koseff, J., Briggs, D., and Ferziger, J. 1993. Turbulence in stratified shear flows: Implications for interpreting shear-induced mixing in the ocean. *J Phys Oceanogr* **23**: 1508-1522.

Ivey, G., and Imberger, J. 1991. On the nature of turbulence in a stratified fluid. Part 1: The energetics of mixing. *J Phys Oceanogr* **21**: 650-658.

Ivey, G., Winters, K., and Koseff, J. 2008. Density stratification, turbulence, but how much mixing? *Annu Rev Fluid Mech* **40**: 169-184.

James, W.F., and Barko, J.W. 1994. Macrophyte influences on sediment resuspension and export in a shallow impoundment. *Lake and Reservoir Management* **10**: 95-102.

Jonas, T., Stips, A., Eugster, W., and Wüest, A. 2003. Observations of a quasi shear-free lacustrine convective boundary layer: Stratification and its implications on turbulence. *J Geophys Res* **108**: 3328.

Joye, S.B., and Hollibaugh, J.T. 1995. Influence of sulfide inhibition of nitrification on nitrogen regeneration in sediments. *Science* **270**: 623-625.

Kalff, J. 2002. *Limnology: inland water ecosystems*. Prentice Hall, Upper Saddle River, N.J.

Kanoshina, I., Lips, U., and Leppanen, J. 2003. The influence of weather conditions (temperature and wind) on cyanobacterial bloom development in the Gulf of Finland (Baltic Sea). *Harmful Algae* **2**: 29-41.

Kato, H., and Phillips, O. 1969. On the penetration of a turbulent layer into stratified fluid. *J Fluid Mech* **37**: 643-655.

Kawanisi, K., and Yokosi, S. 1997. Characteristics of suspended sediment and turbulence in a tidal boundary layer. *Cont Shelf Res* **17**: 859–875.

Kirk, J. 1983. *Light and photosynthesis in aquatic ecosystems*. Cambridge University Press, Cambridge.

Kjerfve, B., and Magill, K. 1989. Geographic and hydrodynamic characteristics of shallow coastal lagoons. *Mar Geol* **88**: 187-199.

Kundu, P. 1990. *Fluid mechanics*. Academic Press, San Diego.

Langmuir, I. 1938. Surface motion of water induced by wind. *Science* **87**: 119–123.

Lavery, A.C., and Ross, T. 2007. Acoustic scattering from double-diffusive microstructure. *J Acoust Soc Am* **122**: 1449-1462.

Leach, P.S., Podlech, M., and Brown, R. 1997. *Rodeo Valley / Tennesse Valley / Redwood Creek water quality monitoring report, October 1996 - March 1997*. Institute of Chemical Biology, University of San Francisco, San Francisco, Calif.

Leibovich, S. 1983. The form and dynamics of Langmuir circulations. *Annu Rev Fluid Mech* **15**: 391–427.

Lombardo, C., and Gregg, M. 1989. Similarity scaling of viscous and thermal dissipation in a convection surface boundary layer. *J Geophys Res-Oceans* **94**: 6273-6284.

Long, S.P., Humphries, S., and Falkowski, P.G. 1994. Photoinhibition of photosynthesis in nature. *Annual Review of Plant Biology* **45**: 633–662.

Luketina, D., and Imberger, J. 2001. Determining turbulent kinetic energy dissipation from Batchelor curve fitting. *J Atmos Ocean Tech* **18**: 100-113.

MacIntyre, S., Alldredge, A., and Gotschalk, C. 1995. Accumulation of marine snow at density discontinuities in the water column. *Limnol Oceanogr* **40**: 449-468.

Madej, M.A. 1989. Analysis of USGS water quality data for Marin Headlands 1986-1988, Golden Gate National Recreation Area.

Martin, B., Saiki, M., and Fong, D. 2007. Relation between mortality of prickly sculpin and diurnal extremes in water quality at Rodeo Lagoon, Marin County, California. *Calif Fish Game* **93**: 214-223.

May, C., Koseff, J., Lucas, L., Cloern, J., and Schoellhamer, D. 2003. Effects of spatial and temporal variability of turbidity on phytoplankton blooms. *Mar Ecol-Prog Ser* **254**: 111-128.

McComb, A., ed. 1995. *Eutrophic shallow estuaries and lagoons*. CRC Press, Boca Raton, Fla.

Møller, J.S. 1996. Water masses, stratification and circulation. In *Eutrophication in coastal marine ecosystems* (eds. B.B. Jørgensen and K. Richardson), *Coastal and estuarine studies*, American Geophysical Union, Washington, D.C.

Moum, J., Farmer, D., Smyth, W., Armi, L., and Vagle, S. 2003. Structure and generation of turbulence at interfaces strained by internal solitary waves propagating shoreward over

the continental shelf. *J Phys Oceanogr* **33**: 2093-2112.

Nash, J., and Moum, J. 2002. Microstructure estimates of turbulent salinity flux and the dissipation spectrum of salinity. *J Phys Oceanogr* **32**: 2312-2333.

Nelson, K., and Jiménez, B. 2000. Sludge accumulation, properties and degradation in a waste stabilization pond in Mexico. *Water Sci Technol* **42**: 231-236.

Nezu, I., and Nakagawa, H. 1993. *Turbulence in open-channel flows*. A.A. Balkema, Rotterdam.

Nixon, S. et al. 1996. The fate of nitrogen and phosphorus at the land sea margin of the North Atlantic Ocean. *Biogeochemistry* **35**: 141-180.

Nunes, R., and Lennon, G. 1987. Episodic stratification and gravity currents in a marine environment of modulated turbulence. *J Geophys Res-Oceans* **92**: 5465-5480.

O'Brien, M.P. 1952. Salinity currents in estuaries. *Trans Amer Geophys Union* **33**: 520-522.

Oliver, R., and Ganf, G. 2000. Freshwater blooms. In *The ecology of cyanobacteria: their diversity in time and space* (eds. B. Whitton and M. Potts), pp. 149-194, Kluwer Academic Publishers, Hingham, Mass.

Osborn, T. 1980. Estimates of the local rate of vertical diffusion from dissipation measurements. *J Phys Oceanogr* **10**: 83-89.

Osborn, T., and Cox, C. 1972. Oceanic fine structure. *Geophys Astro Fluid* **3**: 321 - 345.

Passow, U. 1991. Species-specific sedimentation and sinking velocities of diatoms. *Mar Biol* **108**: 449–455.

Peters, H. 1997. Observations of stratified turbulent mixing in an estuary: Neap-to-spring variations during high river flow. *Estuar Coast Shelf S* **45**: 69-88.

Pilkaityte, R., and Razinkovas, A. 2006. Factors controlling phytoplankton blooms in a temperate estuary: nutrient limitation and physical forcing. *Hydrobiologia* **555**: 41-48.

Podlech, M., Codemo, C., Brown, R., and Jordan, W. 1993. *Some physical, chemical, and biological characteristics of Rodeo Lagoon, Rodeo Lake, and Rodeo Creek: Initial study, summer 1993*. Institute of Chemical Biology, University of San Francisco, San Francisco, Calif.

Powell, T., and Jassby, A. 1974. The estimation of vertical eddy diffusivities below the thermocline in lakes. *Water Resour Res* **10**: 191–198.

Ranasinghe, R., and Pattiaratchi, C. 1999. Circulation and mixing characteristics of a seasonally open tidal inlet: a field study. *Mar Freshwater Res* **50**: 281-290.

Razinkovas, A., Gasiūnaitė, Z., Viaroli, P., and Zaldívar, J. 2008. Preface: European lagoons—need for further comparison across spatial and temporal scales. *Hydrobiologia* **611**: 1-4.

Reddy, K., Kadlec, R., Flaig, E., and Gale, P. 1999. Phosphorus retention in streams and wetlands: A review. *Crit Rev Env Sci Tec* **29**: 83-146.

Reynolds, C., Oliver, R., and Walsby, A. 1987. Cyanobacterial dominance: The role of buoyancy regulation in dynamic lake environments. *New Zeal J Mar Fresh* **21**: 379-390.

Reynolds-Fleming, J., and Luettich, R. 2004. Wind-driven lateral variability in a partially mixed estuary. *Estuar Coast Shelf S* **60**: 395-407.

Rippeth, T.P., Simpson, J., Williams, E., and Inall, M.E. 2003. Measurement of the rates of production and dissipation of turbulent kinetic energy in an energetic tidal flow: Red Wharf Bay revisited. *J Phys Oceanogr* **33**: 1889–1901.

Robson, B., and Hamilton, D. 2003. Summer flow event induces a cyanobacterial bloom in a seasonal Western Australian estuary. *Mar Freshwater Res* **54**: 139–151.

Rohr, J., and Van Atta, C. 1987. Mixing efficiency in stably stratified growing turbulence. *J Geophys Res-Oceans* **92**: 5481-5488.

Roy, P. et al. 2001. Structure and function of south-east Australian estuaries. *Estuar Coast Shelf S* **53**: 351-384.

Rozan, T., Taillefert, M., Trouwborst, R., Glazer, B., Ma, S., Herszage, J., Valdes, L., Price, K., and Luther, G. 2002. Iron-sulfur-phosphorus cycling in the sediments of a shallow coastal bay: Implications for sediment nutrient release and benthic macroalgal blooms. *Limnol Oceanogr* **47**: 1346-1354.

Ruddick, B., Anis, A., and Thompson, K. 2000. Maximum likelihood spectral fitting: The Batchelor spectrum. *J Atmos Ocean Tech* **17**: 1541-1555.

Rueda, F., and Schladow, S. 2009. Mixing and stratification in lakes of varying horizontal length scales: Scaling arguments and energy partitioning. *Limnol Oceanogr* **54**: 2003–2017.

Rueda, F., Schladow, S., Monismith, S., and Stacey, M. 2003. Dynamics of large polymictic lake. I: Field observations. *J Hydraul Eng-ASCE* **129**: 82-91.

Saggio, A., and Imberger, J. 2001. Mixing and turbulent fluxes in the metalimnion of a stratified lake. *Limnol Oceanogr* **46**: 392-409.

Scheffer, M., Rinaldi, S., Gragnani, A., Mur, L., and van Nes, E. 1997. On the dominance of filamentous cyanobacteria in shallow, turbid lakes. *Ecology* **78**: 272-282.

Schubert, H., Schlüter, L., and Feuerpfeil, P. 1996. The ecophysiological consequences of the underwater light climate in a shallow Baltic estuary. In *Proceedings Baltic Science Marine Conference*, pp. 29-37, Rønne, Denmark.

Schwab, D., Bennett, J., Liu, P., and Donelan, M. 1984. Application of a simple numerical wave prediction model to Lake Erie. *J Geophys Res* **89**: 3586–3592.

SFBRWQCB. 2008. *Water quality monitoring and bioassessment in selected San Francisco Bay region watersheds in 2004-2006*. Surface Water Ambient Monitoring Program, San Francisco Bay Regional Water Quality Control Board, Oakland, Calif.

Sharples, J., Coates, M., and Sherwood, J. 2003. Quantifying turbulent mixing and oxygen fluxes in a Mediterranean-type, microtidal estuary. *Ocean Dynamics* **53**: 126-136.

Shaw, S.D. 2005. Wetland processes and restoration opportunities in the Rodeo Lagoon watershed. M.L.A. professional report. University of California, Berkeley, Landscape Architecture and Environmental Planning, Berkeley, Calif.

Shaw, W., and Trowbridge, J. 2001. The direct estimation of near-bottom turbulent fluxes in the presence of energetic wave motions. *J Atmos Ocean Tech* **18**: 1540-1557.

Sherman, B., and Webster, I. 1994. A model for the light-limited growth of buoyant phytoplankton in a shallow, turbid waterbody. *Australian Journal of Marine and Freshwater Research* **45**: 847-862.

Sherman, B., Webster, I., Jones, G., and Oliver, R. 1998. Transitions between *Aulacoseira* and *Anabaena* dominance in a turbid river Weir pool. *Limnol Oceanogr* **43**: 1902-1915.

Shin, J., Dalziel, S., and Linden, P. 2004. Gravity currents produced by lock exchange. *J Fluid Mech* **521**: 1-34.

Silkie, S. 2008. Use of host-specific molecular markers in fecal source tracking. Ph.D. thesis. University of California, Berkeley, Civil and Environmental Engineering, Berkeley, Calif.

Simpson, J., Allen, C., and Morris, N. 1978. Fronts on the continental shelf. *J Geophys Res-Oc Atm* **83**: 4607-4614.

Simpson, J., and Bowers, D. 1981. Models of stratification and frontal movement in shelf seas. *Deep-Sea Res* **28**: 727-738.

Simpson, J., and Hunter, J. 1974. Fronts in the Irish Sea. *Nature* **250**: 404-406.

Sloth, N.P., Blackburn, H., Hansen, L.S., Risgaard-Petersen, N., and Lomstein, B.A. 1995. Nitrogen cycling in sediments with different organic loading. *Mar Ecol-Prog Ser* **116**: 163–170.

Smith, N. 1994. Water, salt, and heat balances of coastal lagoons. In *Coastal lagoon processes* (ed. B. Kjerfve), *Elsevier Oceanography Series*, pp. 69-101, Elsevier, Amsterdam.

Smith, V. 1983. Low nitrogen to phosphorus ratios favor dominance by blue-green algae in lake phytoplankton. *Science* **221**: 669-671.

Solorzano, L. 1969. Determination of ammonia in natural waters by phenolhypochlorite method. *Limnol Oceanogr* **14**: 799-801.

Søndergaard, M., Jensen, J.P., and Jeppesen, E. 2003. Role of sediment and internal loading of phosphorus in shallow lakes. *Hydrobiologia* **506**: 135-145.

Søndergaard, M., Kristensen, P., and Jeppesen, E. 1992. Phosphorus release from resuspended sediment in the shallow and wind-exposed Lake Arresø, Denmark. *Geochim Cosmochim Ac* **228**: 91-99.

Spooner, D. 2005. Nutrient, organic carbon and suspended solid loadings in two ICOLLs, NSW Australia – biogeochemical responses. Ph.D. thesis. University of Canberra, Applied Science, Canberra ACT, Australia.

Stacey, M., Monismith, S.G., and Burau, J.R. 1999a. Measurements of Reynolds stress profiles in unstratified tidal flow. *J Geophys Res-Oceans* **104**: 10933-10949.

Stacey, M., Monismith, S.G., and Burau, J.R. 1999b. Observations of turbulence in a partially stratified estuary. *J Phys Oceanogr* **29**: 1950–1970.

Steinbuck, J., Stacey, M., and Monismith, S. 2009. An evaluation of χ_T estimation techniques: Implications for Batchelor fitting and ε. *J Atmos Ocean Tech* **26**: 1652-1662.

Stevens, C. 2003. Turbulence in an estuarine embayment: Observations from Beatrix Bay, New Zealand. *J Geophys Res-Oceans* **108**: 3030.

Stevens, C., Fisher, T., and Lawrence, G. 2005. Turbulent layering beneath the pycnocline in a strongly stratified pit lake. *Limnol Oceanogr* **50**: 197-206.

Striplen, C., Grossinger, R., and Collins, J. 2004. *Wetland habitat changes in the Rodeo Lagoon watershed, Marin County, CA*. San Francisco Estuary Institute, Oakland, Calif.

Sverdrup, H.U. 1953. On conditions for the vernal blooming of phytoplankton. *ICES Journal of Marine Science* **18**: 287.

Swenson, R.O. 1994. A study of the tidewater goby (*Eucyclogobius newberryi*) at Rodeo Lagoon, Marin County, California.

Szeri, A. 1996. Langmuir circulations in Rodeo Lagoon. *Mon Weather Rev* **124**: 341-342.

Talke, S. 2005. An investigation on the hydrodynamics and sediment dynamics on an intertidal mudflat in Central San Francisco Bay. Ph.D. thesis. University of California, Berkeley, Civil and Environmental Engineering, Berkeley, Calif.

Talke, S., and Stacey, M. 2003. The influence of oceanic swell on flows over an estuarine intertidal mudflat in San Francisco Bay. *Estuar Coast Shelf S* **58**: 541-554.

Talling, J.F. 1971. The underwater light climate as a controlling factor in the production ecology of freshwater phytoplankton. *Mitt Internat Verein Limnol* **19**: 214–243.

Tennekes, H., and Lumley, J. 1972. *A first course in turbulence*. MIT Press, Cambridge, Mass.

Tennessee Valley Authority (TVA), D. 1972. *Heat and mass transfer between a water surface and the atmosphere. Report no. 0-6803.* Tennessee Valley Authority, Norris, Tenn.

Thompson, E.N. 1979. *Forts Baker, Barry, Cronkhite of Golden Gate National Recreation Area, California*. National Park Service, United States Dept. of the Interior, Denver.

Thompson, R., and Imberger, J. 1980. Response of a numerical model of a stratified lake to wind stress. In *International Symposium of Stratified Flows*, Vol. 1 of, pp. 562-570, Tapir, Trondheim, Norway.

Thornton, J., McComb, A., and Ryding, S. 1995. The role of the sediments. In *Eutrophic shallow estuaries and lagoons*, CRC Press, Boca Raton, Fla.

Thorpe, S. 1977. Turbulence and mixing in a Scottish loch. *Philos T Roy Soc A* **286**: 125-181.

Trowbridge, J. 1998. On a technique for measurement of turbulent shear stress in the presence of surface waves. *J Atmos Ocean Tech* **15**: 290-298.

Turner Designs. 2004. *Self-contained underwater fluorescence apparatus: User's manual*. Turner Designs, Sunnyvale, Calif.

Turner, J. 1969. A note on wind mixing at the seasonal thermocline. *Deep-Sea Res* **16S**: 297-300.

United States Environmental Protection Agency (US EPA). 1989. *Ambient water quality criteria for ammonia (saltwater). EPA/440/5-86-004*. Office of Water Regulation and Standards, Criteria and Standards Division, Washington, D.C.

United States Environmental Protection Agency (US EPA). 2009. *Aquatic life ambient water quality criteria for ammonia - freshwater. Draft 2009 update.* Office of Water, Office of Science and Technology, Washington, D.C.

United States Geological Survey (USGS). 2010. *Hypoxia definition page.* http://toxics.usgs.gov/definitions/hypoxia.html.

Valle-Levinson, A., Jara, F., Molinet, C., and Soto, D. 2001. Observations of intratidal variability of flows over a sill/contraction combination in a Chilean fjord. *J Geophys Res-Oceans* **106**: 7051-7064.

Van Duin, E., Blom, G., Los, F., Maffione, R., Zimmerman, R., Cerco, C., Dortch, M., and Best, E. 2001. Modeling underwater light climate in relation to sedimentation, resuspension, water quality and autotrophic growth. *Hydrobiologia* **444**: 25-42.

Vincent, W., Neale, P., and Richerson, P. 1984. Photoinhibition: Algal responses to bright light during diel stratification and mixing in a tropical alpine lake. *J Phycol* **20**: 201-211.

Vollenweider, R.A., and Kerekes, J. 1982. *Eutrophication of waters: monitoring, assessment and control*. Organisation for Economic Co-operation and Development, Paris.

Wakeley, J. 1970. The unique beach sand at Rodeo cove. *Mineral information service, California Division of Mines and Geology* **23**: 238-241.

Waljeski, C., and Williams, J. 2004. *Spatial distribution and possible sources of saline waters in Rodeo Lagoon, Golden Gate National Recreation Area, Marin County, California, 2004*. http://repositories.cdlib.org/wrca/restoration/waljeski/.

Wang, J. 1983. *Ecology of fishes in Rodeo Lagoon and Rodeo Lake of the Golden Gate National Recreation Area, California, with special emphasis on the Tidewater* goby Eucyclogobius newberryii *(Girard) and the Yellowfin goby* Acanthogobius flavimanus *(Temminck and Schlegel)*. Clayton, Calif.

Watson, E.B. 2006. Rodeo Lagoon Survey.

Webster, I., and Harris, G. 2004. Anthropogenic impacts on the ecosystems of coastal lagoons: modelling fundamental biogeochemical processes and management implications. *Mar Freshwater Res* **55**: 67-78.

Wetzel, R. 1983. *Limnology*. 2nd ed. Saunders College Publishing, Philadelphia.

Whitledge, T., Malloy, S., Patton, C., and Wirick, C. 1981. *Automated nutrient analyses in seawater. Formal Report 51398*. Oceanographic Sciences Division, Department of Energy and Environment, Brookhaven National Laboratory, Upton, N.Y.

Wiles, P., van Duren, L., Hase, C., Larsen, J., and Simpson, J. 2006. Stratification and mixing in the Limfjorden in relation to mussel culture. *J Marine Syst* **60**: 129-143.

Wilkerson, F., Dugdale, R., Marchi, A., and Collins, C. 2002. Hydrography, nutrients and chlorophyll during El Niño and La Niña 1997-99 winters in the Gulf of the Farallones, California. *Progress in Oceanography* **54**: 293-310.

Wilson, J. 2008. Preface. *Hydrobiologia* **608**: 1-2.

Winters, K., Lombard, P., Riley, J., and D'Asaro, E. 1995. Available potential energy and mixing in density-stratified fluids. *J Fluid Mech* **289**: 115–128.

Wüest, A., and Lorke, A. 2003. Small-scale hydrodynamics in lakes. *Annu Rev Fluid Mech* **35**: 373-412.

Wüest, A., Piepke, G., and Van Senden, D. 2000. Turbulent kinetic energy balance as a tool for estimating vertical diffusivity in wind-forced stratified waters. *Limnol Oceanogr* **45**: 1388-1400.

Yelland, M., and Taylor, P. 1996. Wind stress measurements from the open ocean. *J Phys Oceanogr* **26**: 541-558.

Zembsch, S. 1993. *Bathymetric survey of Rodeo Lagoon, Golden Gate National Recreation Area, Ft. Cronkhite*. Watershed Science.

Appendix A

Water Quality Database

Explanation of fields and abbreviations in Appendix A

For additional details about methods, see §2.1.2.

Stations	A = west side of lagoon (pedestrian bridge) B = center of lagoon C = east side of lagoon (Bunker Rd. bridge) D = Rodeo Lake weir into lagoon
Depth, m	Depth at which the sample was collected, measured from the surface.
Depth category	S = surface M = middle of water column B = bottom P = pore water
pH, Lab	Analysis performed by J. Drake at Romberg Tiburon Center
pH, Field	Analysis performed in field with Oakton pHTestr 2
Salinity, Lab	Analysis performed by J. Drake at Romberg Tiburon Center
Salinity, Field **Temperature** **[DO], % saturation** **[DO], mg/L**	Analysis performed in field with YSI-85
Spec. Cond.	Analysis of specific conductance performed in field with YSI-85
Nitrate	$[NO_3] + [NO_2]$. Analysis performed by A. Marchi at Romberg Tiburon Center.
Ammonium	$[NH_3] + [NH_4^+]$. Analysis performed by J. Drake and A. Marchi at Romberg Tiburon Center.
Orthophosphate	Analysis performed by A. Marchi at Romberg Tiburon Center.
Notes	s### = sample ID numbers from S. Silkie database A = Salinity, temperature, and [DO] are from Seabird 19+ CTD profile B = Lab pH measured using pH strips C = Salinity for pore water samples is from YSI-85 readings at the bed D = Salinity readings on YSI-85 were highly variable

ND = Not detected. "-" indicates no measurement was taken.

ID	Date	Station	Depth, m	Depth category	Local Time	pH, Lab	pH, Field	Salinity, psu, Lab	Salinity, psu, Field	Temperature, °C	[DO], % Saturation	[DO], mg/L	Spec. Cond., mS/cm	Nitrate, µM	Orthophosphate, µM	Ammonium, µM	Notes
1	1/23/06	D	0	S	11:50	-	-	-	-	11.9	-	-	-	-	-	-	s010
2	1/30/06	D	0	S	14:20	-	-	-	0.1	10.4	65	7.2	0.1	-	-	-	s015
3	2/6/06	B	0	S		-	-	-	-	-	-	-	-	-	-	-	s040
4	2/6/06	A	0	S	10:22	-	-	-	-	10.8	-	-	-	-	-	-	s042
5	2/6/06	D	0	S	11:45	-	7.4	-	0.1	10.7	88	9.7	0.2	-	-	-	s039
6	2/13/06	A	0	S	13:15	-	8.6	-	1.3	15.7	85	8.3	2.5	-	-	-	s071
7	2/13/06	D	0	S	12:05	-	7.7	-	0.1	11.5	62	6.7	0.2	-	-	-	s067
8	2/20/06	B	0	S		-	-	-	1.5	9.1	64	7.3	2.0	-	-	-	s086
9	2/20/06	A	0	S	11:35	-	8.3	-	1.8	9.1	83	9.4	3.4	-	-	-	s087
10	2/20/06	D	0	S	14:55	-	7.4	-	0.1	9.1	55	6.6	0.2	-	-	-	s083
11	2/27/06	A	0	S	13:35	-	7.8	-	1.8	12	91	9.8	3.4	-	-	-	s102a
12	2/27/06	A	0	S		-	-	-	-	-	-	-	-	1.39	3.16	22.86	s102b
13	2/27/06	D	0	S	12:42	-	7.1	-	0.1	10.2	46	5.2	0.2	-	-	-	s099
14	3/6/06	B	0	S	10:45	-	7.6	-	1.1	12.7	99	10.3	2.2	-	-	-	s118
15	3/6/06	A	0	S	10:45	-	7.6	-	0.9	13.3	92	10.1	1.7	-	-	-	s119
16	3/6/06	D	0	S	10:45	-	7.2	-	0.1	10	76	8.6	0.1	-	-	-	s114
17	3/13/06	B	0	S		-	-	-	-	-	-	-	-	-	-	-	s133
18	3/13/06	A	0	S	11:30	-	7.8	-	1.3	10.2	85	9.3	2.4	-	-	-	s134
19	3/13/06	D	0	S	11:00	-	7.5	-	0.1	8.1	84	9.8	0.1	-	-	-	s124
20	3/20/06	A	0	S	9:00	-	7.7	-	1.1	12.2	84	8.8	2.1	-	-	-	s151
21	3/20/06	D	0	S		-	7.2	-	0.1	9.8	46	5.2	0.2	-	-	-	s148
22	3/27/06	B	0	S	12:10	-	-	-	0.9	13.7	103	10.5	1.7	-	-	-	s168
23	3/27/06	B	1.65	B	11:55	-	-	-	13.4	13.3	5	0.4	21.9	-	-	-	s171
24	3/27/06	B	1	M	12:15	-	-	-	1	13.6	102	10.5	1.9	-	-	-	s169
25	3/27/06	B	1.5	M		-	-	-	13.2	13.2	2	0.1	-	-	-	-	s170
26	3/27/06	B	1.6	B		-	-	-	12.2	13.4	3	0.0	20.2	-	-	-	s167
27	3/27/06	B	0	S	12:55	-	-	-	0.8	13.6	102	10.3	1.6	-	-	-	s164
28	3/27/06	B	1	M	13:00	-	-	-	0.9	13.5	102	10.3	1.7	-	-	-	s165
29	3/27/06	B	1.5	B		-	-	-	1.9	13.4	78	8.9	3.2	-	-	-	s166
30	3/27/06	A	0	S	14:40	-	8.1	-	1	13.4	95	10.1	1.9	-	-	-	s172
31	3/27/06	D	0	S	15:55	-	7.5	-	0.1	11	69	7.6	0.2	-	-	-	s161
32	4/13/06	A	0	S	10:45	-	7.7	-	0.3	13.5	85	8.9	0.6	-	-	-	s196
33	4/13/06	D	0	S	10:15	-	7.4	-	0.1	12.4	66	7.0	0.1	-	-	-	s193
34	4/14/06	B	1.5	B		-	-	-	-	-	-	-	-	-	-	-	s591
35	4/14/06	B	0	S		-	-	-	-	-	-	-	-	-	-	-	s197
36	4/14/06	B	1	M		-	-	-	-	-	-	-	-	-	-	-	s198
37	4/14/06	B	1.7	B		-	-	-	-	-	-	-	-	-	-	-	s199
38	4/14/06	A	0	S		-	-	-	-	-	-	-	-	-	-	-	s590
39	4/27/06	A	0	S	16:50	-	-	-	1.2	16.9	98	9.5	2.4	-	-	-	s206
40	4/27/06	A	1.5	B	16:52	-	-	-	1.9	15.9	25	2.6	3.7	-	-	-	s208
41	4/27/06	D	0	S	16:15	-	-	-	0.1	14.6	53	5.3	0.2	-	-	-	s207
42	5/3/06	B	1.5	B		-	-	-	-	-	-	-	-	-	-	-	s210
43	5/3/06	B	0	S		-	-	-	-	-	-	-	-	-	-	-	s211
44	5/3/06	B	1.5	B		-	-	-	-	-	-	-	-	-	-	-	s212
45	5/3/06	B	0	S		-	-	-	-	-	-	-	-	-	-	-	s213

ID	Date	Station	Depth, m	Depth category	Local Time	pH, Lab	pH, Field	Salinity, psu, Lab	Salinity, psu, Field	Temperature, °C	[DO], % Saturation	[DO], mg/L	Spec. Cond., mS/cm	Nitrate, µM	Orthophosphate, µM	Ammonium, µM	Notes
46	5/3/06	C	1.5	B		-	-	-	-	-	-	-	-	-	-	-	s214
47	5/3/06	C	0	S		-	-	-	-	-	-	-	-	-	-	-	s215
48	5/3/06	A	1.5	B		-	-	-	-	-	-	-	-	-	-	-	s217
49	5/3/06	A	0	S		-	-	-	-	-	-	-	-	-	-	-	s218
50	5/8/06	A	0	S	12:40	-	8.8	-	1.5	17.1	118	11.2	2.9	-	-	-	s224
51	5/8/06	A	1.5	B	12:42	-	-	-	4.9	16.2	1	0.1	8.4	-	-	-	s234
52	5/8/06	D	0	S	12:06	-	7.2	-	0.1	14.5	41	4.1	0.2	-	-	-	s233
53	5/26/06	A	0	S	12:15	-	9.3	-	2.2	18.3	94	8.6	4.2	-	-	-	s246
54	5/26/06	A	1.5	B	12:20	-	-	-	13.7	16.9	5	0.4	22.6	-	-	-	s247
55	5/26/06	D	0	S	11:15	-	7.2	-	0.1	15.3	33	3.2	0.2	-	-	-	s242
56	6/9/06	B	0	S		-	-	-	-	-	-	-	-	-	-	-	s588
57	6/9/06	B	0.6	M		-	-	-	-	-	-	-	-	-	-	-	s632
58	6/9/06	B	1.1	M		-	-	-	-	-	-	-	-	-	-	-	s633
59	6/9/06	B	1.6	M		-	-	-	-	-	-	-	-	-	-	-	s634
60	6/9/06	B	1.75	B		-	-	-	-	-	-	-	-	-	-	-	s589
61	6/9/06	A	0	S	12:30	-	9.3	-	2	19.3	81	7.1	3.8	-	-	-	s261
62	6/9/06	A	1.5	S	12:40	-	-	-	2.1	18.2	6	0.5	3.9	-	-	-	s263
63	6/9/06	A	1.5	S	12:35	-	9.4	-	2	18.4	54	5.0	3.9	-	-	-	s262
64	6/9/06	D	0	S	11:20	-	6.9	-	0.1	14.6	16	1.6	0.2	-	-	-	s257
65	6/15/06	B	0	S		-	-	-	-	-	-	-	-	-	-	-	s265
66	6/15/06	B	0.6	M		-	-	-	-	-	-	-	-	-	-	-	s266
67	6/15/06	B	1.1	M		-	-	-	-	-	-	-	-	-	-	-	s267
68	6/15/06	B	1.6	M		-	-	-	-	-	-	-	-	-	-	-	s268
69	6/15/06	B	1.75	B		-	-	-	-	-	-	-	-	-	-	-	s269
70	6/21/06	B	2	B		-	-	-	2.5	20.6	80	7.1	-	-	-	-	s284
71	6/21/06	B	0	S		-	-	-	-	21.2	77	-	-	-	-	-	s285
72	6/21/06	B	0.6	M		-	-	-	2.1	21.2	76	6.8	-	-	-	-	s286
73	6/21/06	B	1.1	M		-	-	-	2.1	21.2	95	6.6	-	-	-	-	s287
74	6/21/06	B	1.6	M		-	-	-	2.1	20.9	97	8.4	-	-	-	-	s288
75	6/21/06	B	1.75	B		-	-	-	2.1	20.7	80	8.6	-	-	-	-	s289
76	6/21/06	A	0	S	12:38	-	-	-	2	21.6	95	8.2	3.9	-	-	-	s282
77	6/21/06	A	1.5	B	12:40	-	-	-	2.1	20	56	5.0	4.0	-	-	-	s283
78	6/21/06	D	0	S	11:55	-	--	-	0.1	15.4	12	1.3	0.2	-	-	-	s278
79	7/5/06	A	0	S	11:30	-	-	-	2.3	17.8	80	7.5	4.3	-	2.79	-	s298
80	7/5/06	A	1.5	B	11:32	-	-	-	2.3	17.4	56	5.7	4.3	-	1.79	5.71	s299
81	7/5/06	D	0	S	11:10	-	--	-	0.1	14.6	8	0.8	0.2	-	1.16	15.71	s294
82	7/17/06	B	0	S		-	-	-	-	-	-	-	-	-	-	-	s305
83	7/17/06	B	0.5	M		-	-	-	-	-	-	-	-	-	-	-	s306
84	7/17/06	B	1	M		-	-	-	-	-	-	-	-	-	-	-	s307
85	7/17/06	B	1.5	M		-	-	-	-	-	-	-	-	-	-	-	s308
86	7/17/06	B	2	B		-	-	-	-	-	-	-	-	-	-	-	s309
87	7/18/06	B	0	S		-	-	-	-	-	-	-	-	-	0.74	5.71	s318
88	7/18/06	A	0	S	13:10	-	-	-	2.3	21.6	115	10.0	4.3	2.79	5.79	13.57	s319
89	7/18/06	A	1.5	B	13:15	-	-	-	2.3	19.2	11	0.9	4.3	-	-	-	s320
90	7/18/06	A	1	M	13:20	-	-	-	2.3	19.7	66	5.8	4.3	-	-	-	s321

ID	Date	Station	Depth, m	Depth category	Local Time	pH, Lab	pH, Field	Salinity, psu, Lab	Salinity, psu, Field	Temperature, °C	[DO], % Saturation	[DO], mg/L	Spec. Cond., mS/cm	Nitrate, µM	Orthophosphate, µM	Ammonium, µM	Notes
91	7/18/06	D	0	S	12:30	-	-	-	-	16.3	5	0.5	0.2	-	1.16	16.43	s314
92	8/2/06	A	0	S	12:34	-	9.6	-	2.3	18.5	109	9.9	4.3	1.39	-	4.29	s334
93	8/2/06	D	0	S	11:50	-	6.8	-	-	15.2	4	0.4	0.2	-	1.05	6.43	s330
94	8/17/06	B	0	S		-	-	-	2.7	-	-	-	-	-	1.89	10.71	s346
95	8/17/06	B	0.5	M		-	-	-	2.7	-	-	-	-	-	0.95	8.57	s347
96	8/17/06	B	1	M		-	-	-	2.7	-	-	-	-	-	1.79	10.00	s348
97	8/17/06	B	1.5	M		-	-	-	2.7	-	-	-	-	-	2.21	13.57	s349
98	8/17/06	B	1.65	B		-	-	-	2.7	-	-	-	-	2.79	2.53	11.43	s350
99	8/17/06	A	0	S	12:45	-	9.1	-	2.7	18.9	107	9.4	5.0	9.75	2.63	11.43	s351
100	8/17/06	A	1.5	B	12:50	-	-	-	2.7	17.8	3	0.3	5.0	-	-	-	s352
101	8/17/06	D	0	S	11:55	-	6.7	-	-	15.9	6	0.6	0.3	-	1.05	12.86	s342
102	8/28/06	A	0	S	11:50	-	9.2	-	2.7	15.9	55	5.6	5.0	-	1.68	6.43	s368
103	8/28/06	A	1.5	B	11:55	-	-	-	2.7	15.9	3	0.3	5.0	-	-	-	s369
104	8/28/06	D	0	S	11:20	-	6.8	-	-	14.5	5	0.5	0.3	-	1.16	35.71	s364
105	9/6/06	B	0	S		-	-	-	2.6	16.7	66	6.1	4.8	-	1.19	9.29	s378
106	9/6/06	B	0.5	M		-	-	-	2.6	17.4	60	5.7	4.8	-	1.11	8.93	s379
107	9/6/06	B	1	M		-	-	-	2.6	17.2	58	5.4	4.8	-	1.00	7.76	s380
108	9/6/06	B	1.5	M		-	-	-	2.6	17	57	5.3	4.8	-	1.05	7.76	s381
109	9/6/06	B	1.8	B		-	-	-	2.6	16.8	57	5.4	1.8	-	1.00	11.43	s382
110	9/12/06	A	0	S	12:20	-	9.6	-	2.6	17.8	111	10.3	4.9	-	2.11	-	s398
111	9/12/06	A	1.5	B	12:15	-	-	-	2.6	16	46	4.4	4.9	-	-	16.43	s389
112	9/12/06	D	0	S	14:00	-	6.8	-	-	15.4	4	0.3	0.2	-	2.32	-	s395
113	10/3/06	A	0	S	14:20	-	9.5	-	2.6	15.2	76	7.5	4.9	-	1.05	7.86	s410
114	10/3/06	D	0	S	13:17	-	6.8	-	-	13.5	5	0.5	0.3	-	-	20.71	s407
115	10/5/06	D	0	S	12:00	-	7.0	-	-	13.3	3	0.3	0.2	-	-	-	s418
116	10/18/06	A	0	S	13:35	-	9.6	-	2.6	15.2	101	10.1	4.8	-	-	-	s433
117	10/18/06	D	0	S	12:55	-	6.8	-	-	13.1	4	0.4	0.3	-	-	-	s430
118	11/1/06	B	0	S		-	-	-	2.7	-	-	-	-	-	2.11	2.86	s592
119	11/1/06	B	0.5	M		-	-	-	2.7	-	-	-	-	-	1.16	4.29	s593
120	11/1/06	B	1.5	B		-	-	-	2.7	-	-	-	-	-	1.53	5.00	s594
121	11/1/06	A	0	S	11:55	-	9.5	-	2.6	13.7	97	9.8	4.8	-	1.42	7.86	s446
122	11/1/06	D	0	S	11:25	-	7.1	-	-	13.2	21	2.2	0.3	-	0.58	5.00	s443
123	11/27/06	A	0	S	11:15	-	8.0	-	2	11.2	79	8.6	3.7	-	1.89	12.86	s467
124	11/27/06	A	1.5	B	11:15	-	8.0	-	2	11.2	79	8.6	3.7	-	-	-	s468
125	11/27/06	D	0	S	10:40	-	6.9	-	-	9.8	16	1.8	0.3	-	2.53	9.29	s463
126	12/1/06	B	0	S	10:00	-	-	-	1.9	9.2	108	13.3	3.6	-	-	-	s474
127	12/1/06	B	0.5	M	10:00	-	-	-	1.9	9.3	104	11.6	3.6	-	-	-	s475
128	12/1/06	B	1	M	10:00	-	-	-	1.9	8.9	99	12.2	3.6	-	-	-	s476
129	12/1/06	B	1.5	M	10:00	-	-	-	1.9	9	102	12.0	3.6	-	-	-	s477
130	12/1/06	B	1.8	B	10:00	-	-	-	1.9	8.8	100	12.2	3.7	-	-	-	s478
131	12/9/06	A	0	S	16:45	-	8.9	-	2.1	11.1	123	11.1	3.9	-	-	-	s533
132	12/10/06	D	0	S	0:07	-	6.9	-	-	9.9	33	-	0.2	-	-	-	s530
133	12/26/06	A	0	S	16:45	-	-	-	1.4	10.3	103	11.4	2.8	-	-	-	s561
134	12/26/06	A	1.5	B	16:50	-	-	-	20.7	10.7	60	5.7	33.1	-	-	-	s562
135	12/26/06	D	0	S	14:50	-	6.7	-	-	9.4	38	4.5	0.2	-	-	-	s558

ID	Date	Station	Depth, m	Depth category	Local Time	pH, Lab	pH, Field	Salinity, psu, Lab	Salinity, psu, Field	Temperature, °C	[DO], % Saturation	[DO], mg/L	Spec. Cond., mS/cm	Nitrate, µM	Orthophosphate, µM	Ammonium, µM	Notes
136	1/8/07	A	0	S	13:50	-	9.0	-	3.3	9.9	125	13.9	6.0	-	-	-	s576
137	1/8/07	A	1.5	B	13:55	-	-	-	17.1	11	13	1.3	27.8	-	-	-	s578
138	1/8/07	D	0	S	13:17	-	7.1	-	-	8.8	83	9.7	0.2	-	-	-	s570
139	1/9/07	B	0	S		-	-	-	2.9	9.4	121	13.6	5.3	-	0.74	-	s583
140	1/9/07	B	0.5	M		-	-	-	2.9	10	125	13.3	5.3	ND	0.13	0.77	
141	1/9/07	B	1	M		-	-	-	3	9.9	123	13.5	5.4	ND	0.06	0.50	
142	1/9/07	B	1.5	M		-	-	-	11.7	10.4	35	3.6	20.1	ND	4.12	25.34	
143	1/9/07	B	2	B		-	-	-	15.8	11.2	40	3.8	25.9	-	23.68	264.29	s585
144	1/22/07	B	0	S	11:15	-	-	-	5.3	7.2	128	15.1	9.5	-	0.74	-	s623
145	1/22/07	B	0.5	M	11:15	-	-	-	5.3	7.7	118	13.6	9.5				
146	1/22/07	B	1	M	11:15	-	-	-	5.3	7.4	112	13.6	9.5				
147	1/22/07	B	1.5	M	11:15	-	-	-	5.6	7.4	123	14.0	10.0				
148	1/22/07	B	2.05	B	11:15	-	-	-	18.4	10.2	38	3.7	29.8	-	17.84	-	s626
149	2/15/07	B	0	S		-	-	2.9	-	-	-	-	-	-	-	-	
150	2/15/07	B	1.3	B		-	-	-	-	-	-	-	-	-	-	-	
151	2/15/07	C	0	S		-	-	2.7	-	-	-	-	-	-	-	-	
152	2/15/07	A	0	S		-	-	3.1	-	-	-	-	-	-	-	-	
153	2/16/07	B	0	S	11:00	-	-	-	2.5	12.3	112	11.6	4.6	1.25	0.33	1.76	
154	2/16/07	B	1.3	B	11:00	-	-	-	16.7	12.9	26	2.3	27.1	ND	24.51	178.90	
155	2/16/07	D	0	S		-	-	-	0.1	-	-	-	-	2.64	0.11	1.08	
156	2/22/07	B	0	S		8.0	-	3.5	-	-	-	-	-	-	-	-	
157	2/22/07	B	1.4	B		-	-	13.1	-	-	-	-	-	-	-	-	
158	2/22/07	C	0	S		-	-	0.3	-	-	-	-	-	-	-	-	
159	2/22/07	A	0	S		-	-	4.3	-	-	-	-	-	-	-	-	
160	3/7/07	B	0	S		-	-	-	-	-	-	-	-	-	-	-	
161	3/7/07	B	1.4	B		-	-	-	-	-	-	-	-	-	-	-	
162	3/7/07	C	0	S		-	-	0.2	-	-	-	-	-	-	-	-	
163	3/7/07	A	0	S		-	-	2.8	-	-	-	-	-	-	-	-	
164	3/14/07	B	0	S		9.0	-	2.4	2.3	15.6	124	11.9	4.2	0.87	0.44	0.33	
165	3/14/07	B	0	S		9.0	-	2.4	2.3	15.6	124	11.9	4.2	ND	0.02	0.30	
166	3/14/07	B	1.4	B	11:00	7.7	-	8	15.2	16	26	2.2	24.9	ND	24.44	140.61	
167	3/14/07	C	0	S		7.3	-	0.3	1.2	14.3	95	9.9	-	0.01	0.40	0.40	
168	3/14/07	A	0	S		8.9	-	2.5	2.53	14.5	95	9.6	-	0.25	0.30	0.97	
169	3/14/07	D	0	S	13:30	-	-	-	0.1	12.9	71	7.5	0.2	-	-	-	
170	3/21/07	B	0	S		7.9	-	3.2	-	-	-	-	-	-	-	0.27	
171	3/21/07	B	1.5	B		7.6	-	4.1	-	-	-	-	-	-	-	-	
172	3/21/07	C	0	S		7.2	-	-	-	-	-	-	-	-	-	0.68	
173	3/21/07	A	0	S		8.0	-	3.3	-	-	-	-	-	-	-	0.18	
174	3/29/07	B	0	S		8.1	-	4.2	-	-	-	-	-	ND	0.27	0.12	
175	3/29/07	B	1.4	B		8.0	-	4.2	-	-	-	-	-	-	-	-	
176	3/29/07	C	0	S		7.6	-	1.9	-	-	-	-	-	ND	0.39	0.50	
177	3/29/07	A	0	S		8.1	-	4.3	-	-	-	-	-	ND	0.21	0.24	
178	4/5/07	B	0	S		8.4	-	4.4	-	-	-	-	-	ND	0.25	ND	
179	4/5/07	B	1.35	B		7.8	-	4.4	-	-	-	-	-	-	-	-	
180	4/5/07	C	0	S		7.5	-	2.3	-	-	-	-	-	ND	0.32	0.48	

ID	Date	Station	Depth, m	Depth category	Local Time	pH, Lab	pH, Field	Salinity, psu, Lab	Salinity, psu, Field	Temperature, °C	[DO], % Saturation	[DO], mg/L	Spec. Cond., mS/cm	Nitrate, µM	Orthophosphate, µM	Ammonium, µM	Notes
181	4/5/07	A	0	S		8.5	-	4.4	-	-	-	-	-	ND	0.22	0.33	
182	4/12/07	B	0	S		9.5	-	4.4	-	-	-	-	-	-	-	0.28	
183	4/12/07	B	1.35	B		9.3	-	4.4	-	-	-	-	-	-	-	-	
184	4/12/07	C	0	S		7.6	-	1	-	-	-	-	-	0.46	0.39	1.73	
185	4/12/07	A	0	S		9.6	-	4.6	-	-	-	-	-	ND	0.18	0.27	
186	4/16/07	B	0	S	10:45	-	-	-	4.3	15.7	138	13.9	7.7	0.01	0.16	0.59	
187	4/16/07	B	1.6	B	10:45	-	-	-	4.3	15.4	128	12.6	7.8	-	-	-	
188	4/16/07	D	0	S	12:00	-	-	-	0.1	13.3	71	7.5	0.2	-	-	-	
189	4/19/07	B	0	S		10.1	-	4.5	-	-	-	-	-	-	-	-	
190	4/19/07	B	1.3	B		9.9	-	4.5	-	-	-	-	-	-	-	-	
191	4/19/07	C	0	S		9.2	-	2.5	-	-	-	-	-	0.08	0.31	0.53	
192	4/19/07	A	0	S		10.3	-	4.5	-	-	-	-	-	ND	0.07	0.24	
193	4/26/07	B	0	S		-	10.3	-	4.5	16.5	-	13.0	7.7	-	-	0.27	
194	4/26/07	B	0	S		-	10.3	-	4.5	16.5	-	13.0	7.7	ND	0.03	0.88	
195	4/26/07	B	1.45	B		-	9.9	-	4.4	-	-	-	-	ND	0.12	-	
196	4/26/07	C	0	S		-	8.9	-	2.2	-	-	-	-	ND	0.27	0.36	
197	4/26/07	A	0	S		-	10.2	-	4.5	-	-	-	-	ND	0.18	0.18	
198	4/26/07	D	0	S	12:00	-	-	-	0.1	11.8	44	4.7	0.2	ND	0.34	1.00	
199	5/3/07	B	0	S		10.0	-	4.3	4.2	16.1	102	10.0	7.5	0.01	0.23	0.27	
200	5/3/07	B	1.45	B		9.9	-	4.3	4.2	16.1	100	9.7	7.5	-	-	-	
201	5/3/07	C	0	S		8.1	-	1.9	-	-	-	-	-	0.10	0.31	0.71	
202	5/3/07	A	0	S		10.2	-	4.4	-	-	-	-	-	ND	0.10	0.24	
203	5/9/07	D	0	S		-	-	-	0.1	-	-	-	-	ND	ND	0.94	
204	5/10/07	B	0	S		9.7	-	4.3	-	-	-	-	-	ND	0.18	3.17	
205	5/10/07	B	1.45	B		9.2	-	4.3	-	-	-	-	-	-	-	-	
206	5/10/07	C	0	S		7.3	-	0.9	-	-	-	-	-	0.40	0.23	3.87	
207	5/10/07	A	0	S		9.5	-	4.3	-	-	-	-	-	ND	0.20	10.90	
208	5/15/07	B	0	S		9.5	-	4.3	4.1	14.7	102	10.0	7.4	0.12	0.29	0.53	
209	5/15/07	B	0	S		9.5	-	4.3	4.1	14.7	102	10.0	7.4	ND	0.07	0.27	
210	5/15/07	B	1.45	B		9.4	-	4.3	4.1	14.5	93	9.1	7.4	-	-	-	
211	5/15/07	C	0	S		7.6	-	1.3	-	-	-	-	-	1.29	0.27	3.05	
212	5/15/07	A	0	S		9.4	-	4.3	4.3	14.1	81	8.3	-	0.37	0.28	2.15	A
213	5/24/07	B	0	S		9.3	-	4.3	-	-	-	-	-	-	-	11.14	
214	5/24/07	B	1.4	B		9.3	-	4.3	-	-	-	-	-	-	-	-	
215	5/24/07	C	0	S		10.5	-	2	-	-	-	-	-	ND	0.37	22.05	
216	5/24/07	A	0	S		10.3	-	4.3	-	-	-	-	-	0.56	0.32	14.39	
217	5/31/07	B	0	S		9.6	-	4.4	4.2	14.1	115	11.4	-	3.63	0.22	5.70	
218	5/31/07	B	1.4	B		9.4	-	4.3	4.2	-	101	11.0	-	0.83	0.05	8.23	
219	5/31/07	C	0	S		7.5	-	1.1	-	-	-	-	-	-	-	7.28	
220	5/31/07	A	0	S		9.6	-	4.3	-	-	98	9.5	-	3.89	0.13	13.34	
221	5/31/07	D	0	S		-	-	-	0.1	-	-	-	-	ND	ND	3.87	
222	6/7/07	B	0	S		10.3	-	4.3	4.2	17.3	137	12.6	7.5	0.96	ND	0.37	
223	6/7/07	B	1.4	B		9.7	10.2	4.3	4.2	17.4	105	9.5	7.5	-	-	-	
224	6/7/07	C	0	S		8.1	7.6	2.3	2.2	16.1	73	7.0	4.2	-	-	-	
225	6/7/07	A	0	S		10.3	10.1	4.3	4.2	18.2	110	9.6	7.6	-	-	0.36	

ID	Date	Station	Depth, m	Depth category	Local Time	pH, Lab	pH, Field	Salinity, psu, Lab	Salinity, psu, Field	Temperature, °C	[DO], % Saturation	[DO], mg/L	Spec. Cond., mS/cm	Nitrate, µM	Orthophosphate, µM	Ammonium, µM	Notes
226	6/14/07	B	0	S		9.9	-	4.4	4.4	20.6	89	7.8	-	-	-	0.41	A
227	6/14/07	B	1.3	B		8.5	-	4.4	4.5	20.6	96	8.4	-	-	-	-	A
228	6/14/07	C	0	S		8.0	9.1	3	2.9	-	63	5.7	-	-	-	12.42	
229	6/14/07	A	0	S		9.0	9.9	4.4	-	20.4	134	11.3	-	-	-	2.93	
230	6/21/07	B	0	S		-	9.4	4.7	4.4	-	94	8.8	-	1.08	0.34	0.61	
231	6/21/07	B	0	S		-	9.4	4.7	4.4	-	94	8.8	-	1.33	0.44	2.03	
232	6/21/07	B	1.25	B		-	-	4.6	4.6	-	83	7.3	-	0.24	0.17	13.82	
233	6/21/07	C	0	S		-	8.5	3.6	-	18.7	80	7.4	5.4	-	-	-	
234	6/21/07	A	0	S		-	9.4	4.7	4.4	-	88	8.3	-	1.36	0.49	3.61	
235	6/21/07	D	0	S		-	6.9	-	0.1	15	9	0.7	0.2	ND	ND	0.87	
236	6/28/07	B	0	S	10:00	10.0	9.4	4.8	4.6	18.4	64	5.7	8.3	ND	1.12	1.18	B
237	6/28/07	B	1.2	B	10:00	9.0	-	4.8	4.6	18.3	65	5.9	8.2	-	-	-	B
238	6/28/07	C	0	S		7.0	-	2.3	-	-	-	-	-	-	-	5.08	B
239	6/28/07	A	0	S	10:45	10.0	9.4	4.8	4.6	18.1	60	5.3	8.3	-	-	0.51	B
240	6/28/07	D	0	S	11:00	-	7.3	-	0.1	15.3	11	1.2	0.2	-	-	-	
241	7/5/07	B	0	S		9.0	9.2	4.9	4.7	21.7	70	5.9	8.4	-	-	1.28	B
242	7/5/07	B	1.1	B		8.0	-	4.9	-	-	-	-	-	-	-	-	B
243	7/5/07	C	0	S		7.0	-	3.2	-	-	-	-	-	-	-	12.03	B
244	7/5/07	A	0	S		8.0	-	4.9	-	-	-	-	-	-	-	0.61	B
245	7/12/07	B	0	S	9:40	9.0	9.1	5	4.8	19.0	140	12.5	8.5	-	-	1.00	B
246	7/12/07	B	0	S	10:30	-	-	-	4.6	19.3	160	14.7	8.2	-	-	-	
247	7/12/07	B	0.5	M	10:30	-	-	-	4.6	19.2	152	13.8	8.2	-	-	-	
248	7/12/07	B	1	M	10:30	-	-	-	4.7	18.5	119	11.6	8.4	-	-	-	
249	7/12/07	B	1.1	B		-	-	5	-	-	-	-	-	-	-	-	
250	7/12/07	B	1.35	B	10:30	-	-	-	4.7	18.4	73	5.0	8.3	-	-	-	
251	7/12/07	C	0	S	11:40	6.0	7.6	2.8	1.3	18.7	122	11.9	2.7	0.09	0.07	4.20	B
252	7/12/07	A	0	S	11:00	8.0	9.1	5	4.9	19.4	150	12.7	8.7	0.45	0.17	2.28	B
253	7/12/07	D	0	S	12:00	-	-	-	0.1	16.5	13	1.0	0.3	ND	ND	1.00	
254	7/19/07	B	0	S		9.0	-	5.1	-	-	-	-	-	-	-	0.39	B
255	7/19/07	B	0.7	B		9.0	-	5.1	-	-	-	-	-	-	-	-	B
256	7/19/07	C	0	S		7.0	-	1.4	-	-	-	-	-	-	-	3.37	B
257	7/19/07	A	0	S		10.0	-	5.1	-	-	-	-	-	-	-	0.53	B
258	7/26/07	B	0	S		8.0	7.6	5.3	5.0	18.0	43	3.9	8.9	ND	0.15	20.96	B
259	7/26/07	B	0	S		-	-	-	5.0	18.0	51	4.4	8.9	ND	ND	11.85	
260	7/26/07	B	0.5	M		-	-	-	5.0	18.2	41	3.8	8.9	ND	0.10	14.44	
261	7/26/07	B	1	M		-	-	-	5.0	18.1	41	3.5	8.9	0.06	0.18	15.97	
262	7/26/07	B	1.1	B		8.0	-	5.3	-	-	32	2.9	-	-	-	-	B
263	7/26/07	B	1.25	B		-	-	-	5.0	18.1	35	2.7	8.9	ND	0.02	18.43	
264	7/26/07	B	-	P		-	-	-	5.0	-	-	-	-	ND	39.94	-	C
265	7/26/07	B	-	P		-	-	-	5.0	-	-	-	-	0.06	60.43	-	C
266	7/26/07	B	-	P		-	-	-	5.0	-	-	-	-	ND	94.67	-	C
267	7/26/07	C	0	S		6.0	7.8	2	1.8	16.7	39	3.9	3.4	ND	0.15	10.07	B
268	7/26/07	A	0	S		8.0	7.5	5.3	-	18.0	24	2.2	-	ND	0.40	26.91	B
269	7/26/07	D	0	S		-	7.1	-	0.1	16.0	6	0.6	0.3	ND	0.02	1.26	
270	8/2/07	B	0	S		9.0	-	5.4	-	-	101	10.3	-	ND	0.36	0.41	B

ID	Date	Station	Depth, m	Depth category	Local Time	pH, Lab	pH, Field	Salinity, psu, Lab	Salinity, psu, Field	Temperature, °C	[DO], % Saturation	[DO], mg/L	Spec. Cond., mS/cm	Nitrate, µM	Orthophosphate, µM	Ammonium, µM	Notes
271	8/2/07	B	0.8	B		8.0	-	5.4	-	-	69	7.0	-	-	-	-	B
272	8/2/07	C	0	S		7.0	-	1.3	-	-	-	-	-	-	-	5.69	B
273	8/2/07	A	0	S		9.0	-	5.4	-	-	58	5.1	-	ND	0.70	5.10	B
274	8/9/07	B	0	S		9.0	8.5	5.5	-	16.3	62	6.0	-	ND	1.46	-	B
275	8/9/07	B	1	B		8.0	-	5.5	5.0	16.2	43	4.0	8.8	-	-	-	B
276	8/9/07	C	0	S		6.0	7.1	0.8	-	16.1	62	6.9	-	ND	0.26	6.70	B
277	8/9/07	A	0	S		9.0	8.5	5.4	-	15.9	60	5.7	-	-	-	3.08	B
278	8/9/07	D	0	S	14:00	-	6.9	-	0.2	15.1	5	0.4	0.3	-	-	-	
279	8/16/07	B	0	S		9.0	-	5.6	-	-	64	9.9	-	-	-	1.10	B
280	8/16/07	B	0.9	B		8.0	-	5.5	-	-	47	5.1	-	-	-	-	B
281	8/16/07	C	0	S		7.0	-	3.6	-	-	-	-	-	-	-	1.07	B
282	8/16/07	A	0	S		9.0	-	5.5	-	-	-	-	-	-	-	0.77	B
283	8/23/07	B	0	S		9.0	8.3	5.6	5.4	19.9	77	4.1	9.5	-	-	0.98	B
284	8/23/07	B	0	S		9.0	8.3	5.6	5.4	19.9	77	4.1	9.5	ND	1.32	1.31	B
285	8/23/07	B	0.9	B		9.0	8.4	5.6	5.4	19.7	3	0.2	9.6	ND	1.34	1.47	B
286	8/23/07	C	0	S		7.0	8.2	2.6	3.5	19.3	100	9.0	6.4	-	-	-	B
287	8/23/07	A	0	S		9.0	8.6	5.6	5.4	18.9	82	7.3	9.7	-	-	-	B
288	8/23/07	D	0	S	11:30	-	7.2	-	0.1	17.5	33	4.0	0.3	ND	0.28	1.12	
289	8/28/07	B	0	S		8.0	-	5.8	-	-	42	4.2	-	ND	1.02	-	B
290	8/28/07	B	0.85	B		8.0	-	5.7	-	-	26	3.8	-	-	-	-	B
291	8/28/07	C	0	S		7.0	-	3.4	-	-	-	-	-	ND	0.95	4.82	B
292	8/28/07	A	0	S		8.0	-	5.7	-	-	33	3.0	-	ND	1.16	19.02	B
293	9/4/07	B	0	S		8.0	-	5.9	-	-	52	4.6	-	-	-	36.65	B
294	9/4/07	B	0.85	B		8.0	-	5.9	-	-	42	4.0	-	-	-	-	B
295	9/4/07	C	0	S		7.0	-	2.9	-	-	-	-	-	-	-	25.55	B
296	9/4/07	A	0	S		9.0	-	5.9	-	-	-	-	-	-	-	41.33	B
297	9/6/07	B	0	S		-	8.3	-	5.7	20.3	67	5.8	10.0	-	-	-	
298	9/6/07	C	0	S		-	8.7	-	5.3	20.2	123	10.8	9.5	-	-	-	
299	9/6/07	A	0	S		-	8.1	-	5.7	18.9	73	6.5	10.0	-	-	-	
300	9/6/07	D	0	S		-	7.2	-	0.2	16.3	16	1.6	0.3	-	-	-	
301	9/11/07	B	0	S		8.0	-	6	-	-	59	5.3	-	-	-	67.73	B
302	9/11/07	B	0.85	B		9.0	-	6	-	-	41	4.1	-	-	-	-	B
303	9/11/07	C	0	S		7.0	-	0.7	-	-	52	4.8	-	ND	0.28	14.56	B
304	9/11/07	A	0	S		9.0	-	6	-	-	59	4.8	-	-	-	74.14	B
305	9/18/07	B	0	S	10:00	8.0	8.0	6.2	5.8	18.8	47	7.2	10.3	ND	0.55	33.71	B
306	9/18/07	B	0.8	B	10:00	8.0	8.1	6.1	5.6	18.7	6	0.6	10.0	-	-	-	B
307	9/18/07	C	0	S		7.0	-	4.1	4.4	18.1	60	5.4	8.0	-	-	69.77	B
308	9/18/07	A	0	S	10:00	9.0	8.0	6.2	5.9	18.2	52	4.6	10.4	-	-	107.02	B
309	9/18/07	D	0	S		-	7.1	-	0.2	16.1	12	1.0	0.3	-	-	-	
310	9/25/07	B	0	S		8.0	7.2	6.3	5.8	17.1	24	2.4	10.2	ND	0.51	95.77	B
311	9/25/07	B	0.75	B		8.0	7.5	6.2	5.9	16.0	8	0.7	10.3	ND	0.43	104.59	B
312	9/25/07	C	0	S		7.0	7.2	3.2	1.4	16.5	55	5.6	2.8	ND	0.33	101.64	B
313	9/25/07	A	0	S		9.0	7.7	6.2	6.0	17.0	38	3.5	10.5	0.05	0.86	164.94	B
314	9/25/07	D	0	S		-	7.1	-	0.2	15.8	11	1.0	0.4	ND	0.04	2.11	
315	10/2/07	B	0	S		8.0	8.0	6.4	5.9	16.4	58	5.5	10.4	-	-	190.66	B

ID	Date	Station	Depth, m	Depth category	Local Time	pH, Lab	pH, Field	Salinity, psu, Lab	Salinity, psu, Field	Temperature, °C	[DO], % Saturation	[DO], mg/L	Spec. Cond., mS/cm	Nitrate, µM	Orthophosphate, µM	Ammonium, µM	Notes
316	10/2/07	B	0	S		8.0	8.0	6.4	5.9	16.4	58	5.5	10.4	0.97	0.38	128.09	B
317	10/2/07	B	0.75	B		8.0	7.9	6.2	6.1	16.4	34	3.2	10.6	-	-	-	B
318	10/2/07	C	0	S		8.0	7.7	1.7	1.4	14.0	35	3.5	1.2	0.02	0.24	63.06	B, D
319	10/2/07	A	0	S		8.0	7.9	6.4	6.1	16.6	43	4.0	10.7	1.86	0.65	192.49	B
320	10/2/07	D	0	S		-	7.6	-	0.2	12.4	5	0.4	0.3	-	-	-	
321	10/9/07	B	0	S	10:00	8.0	8.0	6.5	6.2	16.0	106	10.1	10.9	2.74	0.57	194.24	
322	10/9/07	B	0	S	10:00	8.0	8.0	6.5	6.2	16.0	106	10.1	10.9	0.44	0.31	123.68	
323	10/9/07	B	0.75	B		8.0	-	6.5	6.2	15.8	70	6.7	10.9	-	-	-	
324	10/9/07	C	0	S		7.0	7.5	1.8	4.8	14.9	93	9.4	3.0	1.88	0.25	64.12	B, D
325	10/9/07	A	0	S		8.0	8.0	6.3	6.2	15.5	89	8.5	10.9	2.51	0.60	191.04	
326	10/9/07	D	0	S	13:00	-	7.1	-	0.2	14.4	44	4.2	0.3	-	-	-	
327	10/15/07	B	0	S		-	8.0	6.2	-	-	108	10.8	10.4	5.50	0.42	178.90	
328	10/15/07	B	0.7	B		-	8.0	6.2	-	-	-	-	-	-	-	-	
329	10/15/07	C	0	S		-	7.7	3.4	-	-	68	7.1	5.8	5.08	0.34	106.61	
330	10/15/07	A	0	S		-	8.0	6.2	-	-	100	9.4	10.4	5.38	0.49	178.91	
331	10/23/07	B	0	S		-	7.7	-	5.8	15.2	75	7.2	10.2	2.91	0.46	116.01	
332	10/23/07	B	0.85	B		-	8.3	-	5.8	15.2	64	6.1	10.2	6.57	0.52	83.45	
333	10/23/07	C	0	S		-	7.4	-	4.7	16	50	5.6	8.4	6.06	0.57	170.32	
334	10/23/07	A	0	S		-	7.8	-	5.8	15.4	79	7.6	10.3	9.88	0.58	178.15	
335	10/23/07	D	0	S		-	7.1	-	0.1	13	24	2.5	0.3	ND	0.12	0.64	
336	10/30/07	B	0	S		-	8.1	-	5.8	14.7	91	8.9	10.1	6.65	0.21	105.30	
337	10/30/07	B	0.8	B		-	8.1	-	5.7	14.8	17	1.6	10.1	-	-	-	
338	10/30/07	C	0	S		-	7.4	-	0.9	13	71	7.3	1.3	-	-	28.41	
339	10/30/07	A	0	S		-	8.0	-	5.9	14.3	83	8.2	10.3	-	-	180.65	
340	10/30/07	D	0	S		-	7.1	-	0.1	12.4	25	2.6	0.3	-	-	-	
341	11/6/07	B	0	S		-	8.0	-	5.8	13.9	106	10.6	10.2	12.38	0.31	107.54	
342	11/6/07	B	0.8	B		-	7.9	-	5.8	13.9	74	7.4	10.3	-	-	-	
343	11/6/07	C	0	S		-	7.3	-	0.7	12.6	83	8.8	1.2	-	-	47.12	
344	11/6/07	A	0	S		-	7.9	-	5.9	13.5	87	8.6	10.4	-	-	176.01	
345	11/6/07	D	0	S		-	6.9	-	0.1	12.3	32	3.4	0.3	-	-	-	
346	11/13/07	B	0	S		-	8.2	-	5	14.9	139	13.5	8.9	13.20	0.12	84.62	
347	11/13/07	B	0.9	B		-	8.1	-	5.2	14.6	18	1.7	9.3	-	-	-	
348	11/13/07	C	0	S		-	7.2	-	0.3	13	76	7.8	0.6	-	-	9.82	
349	11/13/07	A	0	S		-	8.3	-	5.1	14.8	124	12.0	9.2	-	-	152.78	
350	11/13/07	D	0	S		-	6.9	-	0.1	12.1	21	2.3	0.3	-	-	-	
351	11/20/07	B	0	S		-	8.6	-	5	13.2	136	13.9	8.9	-	-	86.54	
352	11/20/07	B	0	S		-	8.6	-	5	13.2	136	13.9	8.9	15.04	ND	63.29	
353	11/20/07	B	1	B		-	8.6	-	5.2	13.2	104	10.4	9.2	12.44	ND	41.10	
354	11/20/07	C	0	S		-	7.7	-	3.4	13.6	109	11.1	6.2	17.60	0.16	51.05	
355	11/20/07	A	0	S		-	8.6	-	5.2	12.6	118	12.1	9.3	23.73	0.06	89.28	
356	11/20/07	D	0	S		-	7.1	-	0.1	11.3	20	2.1	0.3	ND	0.05	3.52	
357	11/27/07	B	0	S	9:45	-	9.1	-	5.3	9.8	133	14.6	9.4	18.63	ND	24.00	
358	11/27/07	B	1	B	9:45	-	-	-	5.3	9.9	119	12.4	9.4	-	-	-	
359	11/27/07	C	0	S	11:10	-	8.9	-	4.3	10.7	115	12.2	7.8	-	-	-	
360	11/27/07	A	0	S	10:00	-	9.1	-	5.3	10	135	14.7	9.4	-	-	-	

ID	Date	Station	Depth, m	Depth category	Local Time	pH, Lab	pH, Field	Salinity, psu, Lab	Salinity, psu, Field	Temperature, °C	[DO], % Saturation	[DO], mg/L	Spec. Cond., mS/cm	Nitrate, µM	Orthophosphate, µM	Ammonium, µM	Notes
361	11/27/07	D	0	S	11:20	-	7.1	-	0.1	9.5	25	2.9	0.3	-	-	-	
362	12/4/07	B	0	S	10:20	-	9.0	-	5.3	11.6	132	13.8	9.4	20.78	ND	-	
363	12/4/07	B	0	S	10:10	-	-	-	5.4	11.4	139	14.6	9.6	-	-	-	
364	12/4/07	B	0.5	M	10:20	-	-	-	5.3	11.6	-	-	9.4	-	-	-	
365	12/4/07	B	0.5	M	10:10	-	-	-	5.4	11.4	-	-	9.6	-	-	-	
366	12/4/07	B	1	M	10:10	-	-	-	14.8	11.6	-	-	23.3	-	-	-	
367	12/4/07	B	1.1	B	10:20	-	-	-	17.1	11.6	14	1.3	27.7	-	-	-	
368	12/4/07	B	1.3	B	10:10	-	-	-	23	12	-	-	33.4	-	-	-	
369	12/4/07	C	0	S	11:15	-	-	-	2.8	12.2	96	9.4	5.2	-	-	-	
370	12/4/07	A	0	S	9:55	-	-	-	4.9	11.8	138	14.5	8.8	-	-	-	
371	12/4/07	A	0.5	M	9:55	-	-	-	5.3	11.7	-	-	10.6	-	-	-	
372	12/4/07	A	1	M	9:55	-	-	-	16.8	12	119	-	27.0	-	-	-	
373	12/4/07	D	0	S	11:20	-	7.3	-	0.1	12.1	80	8.2	0.3	-	-	-	
374	12/11/07	B	0	S	10:00	-	9.1	-	6.1	8.3	109	12.5	10.8	40.11	ND	28.14	
375	12/11/07	B	1.35	B	10:00	-	-	-	18.5	11.2	48	4.6	30.3	20.51	0.03	80.08	
376	12/11/07	C	0	S		-	-	-	6.7	8.7	125	13.9	11.4	25.30	0.12	17.71	
377	12/11/07	A	0	S	11:45	-	9.1	-	6	9.3	97	10.8	10.6	40.47	0.05	22.85	
378	12/11/07	D	0	S	12:30	-	7.1	-	0.1	8.8	51	5.8	0.3	ND	0.31	1.91	
379	12/18/07	C	0	S		-	-	-	-	-	-	-	-	20.36	0.18	ND	
380	12/18/07	A	0	S		-	-	-	-	-	-	-	-	38.18	0.05	11.34	
381	1/11/08	B	0	S	11:30	-	-	-	5	10.3	93	10.1	8.9	6.63	0.11	12.18	
382	1/11/08	B	0.5	M	11:35	-	-	-	4.8	10.4	88	9.3	8.6	8.42	0.04	6.67	
383	1/11/08	B	1	M	11:40	-	-	-	11.1	10.4	79	7.9	8.8	14.39	ND	18.63	
384	1/11/08	B	1.5	M	11:45	-	-	-	18.2	10.8	68	6.4	29.5	18.95	0.36	25.66	
385	1/11/08	B	2	M	11:50	-	-	-	18.6	10.9	49	4.9	30.1	14.57	0.25	32.40	
386	1/11/08	D	0	S	13:15	-	-	-	0.4	11.8	70	7.3	0.9	4.30	0.15	4.41	
387	1/17/08	B	-	P		-	-	-	20.6	-	-	-	-	1.43	ND	18.62	C
388	1/17/08	B	-	P		-	-	-	20.6	-	-	-	-	ND	16.20	121.31	C
389	1/17/08	B	-	P		-	-	-	20.6	-	-	-	-	0.29	40.87	-	C
390	1/17/08	B	-	P		-	-	-	20.6	-	-	-	-	ND	32.86	-	C
391	1/17/08	B	0	S	11:15	-	7.9	-	6.7	9.2	94	10.1	11.7	6.82	ND	2.51	
392	1/17/08	B	0.5	M	11:20	-	-	-	6.7	10.3	67	7.1	11.7	10.15	0.04	-	
393	1/17/08	B	1	M	11:25	-	-	-	6.8	10.1	67	7.2	11.8	4.66	ND	-	
394	1/17/08	B	1.2	M	11:30	-	-	-	11.5	10.7	66	6.7	19.3	13.25	0.12	-	
395	1/17/08	B	1.4	M	11:35	-	-	-	13.7	11	64	6.4	22.6	5.73	ND	-	
396	1/17/08	B	1.6	M	11:40	-	-	-	18.5	11.2	60	5.6	29.7	7.56	ND	-	
397	1/17/08	B	1.8	M	11:45	-	-	-	18.9	11.4	52	4.8	30.5	10.41	0.02	-	
398	1/17/08	B	2	B	11:50	-	-	-	22.4	11.8	38	3.3	35.6	6.88	0.06	79.41	
399	1/17/08	B	0	S	12:30	-	7.9	-	6.7	9.7	85	9.3	11.8	-	-	-	
400	1/17/08	B	0.5	M	12:35	-	-	-	6.8	10	79	8.6	11.8	-	-	-	
401	1/17/08	B	1	M	12:40	-	-	-	6.7	9.6	78	8.3	11.8	-	-	-	
402	1/17/08	B	1.2	M	12:45	-	-	-	12.4	10.4	70	6.5	15.2	-	-	-	
403	1/17/08	B	1.4	M	12:50	-	-	-	16.1	10.9	63	6.1	26.6	-	-	-	
404	1/17/08	B	1.6	M	12:55	-	-	-	17.8	10.9	57	5.3	29.5	-	-	-	
405	1/17/08	B	1.8	M	1:00	-	-	-	19.3	11.4	47	4.4	31.1	-	-	-	

ID	Date	Station	Depth, m	Depth category	Local Time	pH, Lab	pH, Field	Salinity, psu, Lab	Salinity, psu, Field	Temperature, °C	[DO], % Saturation	[DO], mg/L	Spec. Cond., mS/cm	Nitrate, µM	Orthophosphate, µM	Ammonium, µM	Notes
406	1/17/08	B	2	B	1:05	-	7.5	-	20.6	11.2	40	3.5	32.8	-	-	-	
407	2/14/08	B	0	S		-	-	-	3.7	11.2	81	-	-	0.10	0.45	1.45	A
408	2/14/08	B	1	M		-	-	-	3.7	11.2	80	-	-	5.72	0.25	10.07	A
409	2/14/08	B	1.5	B		-	-	-	21.8	11.7	90	-	-	4.31	0.24	53.18	A
410	2/14/08	D	0	S	10:20	-	7.6	-	0.1	10.2	69	7.7	0.2	0.78	0.34	2.58	